Structure and Bonding 180
Series Editor: D.M.P. Mingos

Jean-François Halet *Editor*

Ligated Transition Metal Clusters in Solid-State Chemistry

The Legacy of Marcel Sergent

Springer

180
Structure and Bonding

Aims and Scope

Structure and Bonding is a publication which uniquely bridges the journal and book format. Organized into topical volumes, the series publishes in depth and critical reviews on all topics concerning structure and bonding. With over 50 years of history, the series has developed from covering theoretical methods for simple molecules to more complex systems.

Topics addressed in the series now include the design and engineering of molecular solids such as molecular machines, surfaces, two dimensional materials, metal clusters and supramolecular species based either on complementary hydrogen bonding networks or metal coordination centers in metal-organic framework materials (MOFs). Also of interest is the study of reaction coordinates of organometallic transformations and catalytic processes, and the electronic properties of metal ions involved in important biochemical enzymatic reactions.

Volumes on physical and spectroscopic techniques used to provide insights into structural and bonding problems, as well as experimental studies associated with the development of bonding models, reactivity pathways and rates of chemical processes are also relevant for the series.

Structure and Bonding is able to contribute to the challenges of communicating the enormous amount of data now produced in contemporary research by producing volumes which summarize important developments in selected areas of current interest and provide the conceptual framework necessary to use and interpret mega-databases.

We welcome proposals for volumes in the series within the scope mentioned above. Structure and Bonding offers our authors and readers:

- OnlineFirst publication. Each chapter is published online as it is finished, ahead of the print volume
- Wide dissemination. The chapters and the volume will be available on our platform SpringerLink, one of the largest collections of scholarly content in the world. SpringerLink attracts more than 50 million users at 15.000 institutions worldwide.
- Easy manuscript preparation. Authors do not have to spend their valuable time on the layout of their contribution. Springer will take care of all the layout related issues and will provide support throughout the complete process.

More information about this series at http://www.springer.com/series/430

Jean-François Halet
Editor

Ligated Transition Metal Clusters in Solid-State Chemistry

The Legacy of Marcel Sergent

With contributions by

R. Arratia-Perez · C. Candolfi · R. Chevrel · S. Cordier · A. Dauscher · V. E. Fedorov · P. Gall · P. Gougeon · J.-F. Halet · P. Lemoine · B. Lenoir · A. Muñoz-Castro · N. G. Naumov · D. Paez-Hernandez · A. Perrin · C. Perrin · M. Potel · E. Soto · L. F. Szczepura

Springer

Editor
Jean-François Halet
Institut des Sciences Chimiques de
Rennes – UMR 6226
Univ Rennes, CNRS
Rennes, France

ISSN 0081-5993 ISSN 1616-8550 (electronic)
Structure and Bonding
ISBN 978-3-030-25123-9 ISBN 978-3-030-25124-6 (eBook)
https://doi.org/10.1007/978-3-030-25124-6

This Springer imprint is published by the registered company Springer Nature Switzerland AG.
The registered company address is: Gewerbestrasse 11, 6330 Cham, Switzerland

Preface

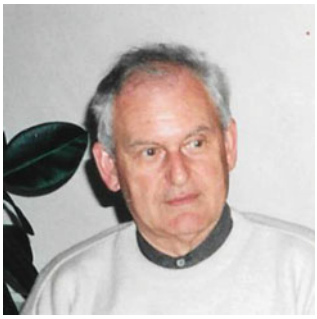

This volume, which deals with ligated transition-metal clusters in solid-state chemistry, is dedicated to the memory of Professor Marcel Sergent who devoted his professional life to this area of chemistry. Marcel was born in Douarnenez, a fishing port located in the extreme West of Brittany, France, an area that he loved and never forgot throughout his life. Indeed, he spoke the Breton (Celtic) language fluently in his childhood, a local language which was still widely used in Brittany when he was a boy. Marcel Sergent graduated in chemistry from the University of Rennes and started his Thesis of *Doctorat ès Sciences Physiques* under the supervision of Prof. Jacques Prigent in the *Laboratoire de Chimie Minérale B*. Subsequently he was appointed by the CNRS from 1964 until his retirement in 1999 with the first class degree of Directeur de Recherches. Very regrettably, he passed away very suddenly in 2015.

He earned his doctoral degree in 1969. The topic of his dissertation research was the study of alkaline thiochromites, thiomolybdites and thiotungstites obtained by sulphidation/reduction of the double oxides under a CS_2 stream at quite low temperatures. He had very early in his research the intuition that direct reduction of MoS_2 by elemental Mo (eventually in the presence of a second metallic element) could be possible and lead to some interesting compounds. For this purpose he

developed, in Rennes, the method of high-temperature syntheses using sealed evacuated silica tubes. This approach turned out to be extremely productive as it allowed the development in his laboratory of the very rich and varied chemistry of transition element ligated clusters.

In the early 1970s, with his PhD student Roger Chevrel, he discovered the first ternary molybdenum chalcogenides, based on the Mo_6 octahedral metal-metal bonded clusters, e.g. $PbMo_6S_8$, which exhibits exceptional superconducting properties, with the highest critical temperatures and critical magnetic fields at that time. This class contained numerous and related compounds, now well-known as "Chevrel phases". They were extensively studied all around the world. As a result Marcel Sergent established a number of collaborations not only in France but also in many foreign countries. The most prominent were with Profs. Jean Rossat-Mignot and Robert Tournier in CRTBT (Grenoble) and Prof. Østein Fischer in DPMC of Geneva University. Indeed, Marcel Sergent had very early appreciated the great importance of close collaborations with solid-state physics laboratories.

Following these outstanding results on ternary molybdenum chalcogenides, Marcel Sergent was the advisor of a large number of students and/or co-workers who extended the chemistry to halides, chalcogenides and chalcohalides built around tetrahedral, octahedral and condensed clusters of niobium, tantalum, molybdenum, tungsten and rhenium. In parallel, he supervised very original research on transition metal compounds of phosphides and arsenides with metal-metal bonds. Later, he also became involved in studies of high critical temperature superconducting cuprates.

Marcel Sergent understood very early the potential in solid-state chemistry of X-ray diffraction analyses. His rigor in the complete interpretation of any powder X-ray diffraction patterns was at the basis of the discovery of a number of original phases. According to him, a new compound was fully characterized only if, at least (at this pioneering period), the unit-cell parameters and space group were determined by single-crystal X-ray diffraction techniques. For this reason he put considerable efforts to provide his laboratory with Weissenberg and Buerger cameras, which led to the first Chevrel-phase structure determinations. Later, with the arrival of Prof. Daniel Grandjean, a crystallographer, this structural approach tended to become systematic, at a time where the automatic diffractometers still did not exist.

Having always in mind the importance of mastering the crystallization of the compounds, synthesized by his group, he developed in Rennes various methods of crystal growth and stimulated the emergence of a thin films growth and characterization research group. Also he was strongly involved in the processing of Chevrel-phase wires (Eureka Program from EU) and the synthesis of catalysts by the impregnation approach.

Marcel Sergent was the author and co-author of about 400 scientific publications, mainly in international journals, and a dozen patents. He was the leader of a number of national and international research programmes, mainly devoted to the study and applications of Chevrel phases and related cluster compounds. He was also an able

administrator, being Deputy Director, then Director of the CNRS Laboratory of Solid State and Molecular Inorganic Chemistry (1981–1992) at the University of Rennes, member of the CNRS National Committee (1983–1987) and *Chargé de Mission* of the CNRS for the scientific research in the Brittany region. His achievements have been recognized by the French Chemical Society award (1981), the French Academy of Sciences A. Guye award (1981), and the Silver Medal of CNRS, shared with R. Chevrel (1981).

Beyond these prominent scientific skills Marcel Sergent is remembered by all his students and co-workers for his exceptional enthusiasm, dynamism and tenacity, and most of all for his great creativity. Indeed he worked non-stop in order to check any of his hypotheses about the formation of new compounds and/or their structural determination. To all of them he passed on his rigor and scientific honesty as well as his unusual humility, receptiveness and kindness to his French colleagues and foreign collaborators. All these qualities mark his most important legacy for those that worked with him. Everyone who knew Marcel Sergent will have pleasant memories of his kind, reliable and straightforward personality.

Through this collection of chapters, colleagues and friends gratefully acknowledge his diverse and outstanding contributions to ligated transition-metal clusters in solid-state chemistry. This volume opens with a historical overview of the Chevrel phases. André Perrin, Christiane Perrin and Roger Chevrel recount the impact of the seminal discovery of the Chevrel phases in the early 1970s and the subsequent developments in the field to this day. The following chapters provide contemporary accounts of a variety of experimental and theoretical studies in this fascinating area of chemistry. Examples include the chemistry of molybdenum and rhenium octahedral chalcogenide cluster compounds carried out at the Nikolaev Institute of Inorganic Chemistry (Vladimir Fedorov and Nikolay Naumov), and that of niobium and tantalum octahedral cluster halide compounds with three-dimensional frameworks (Pierric Lemoine, Jean-François Halet, Stéphane Cordier). The chapter by Lisa Szczepura and Ernesto Soto explores the breadth of terminal ligands incorporated into molybdenum halide and rhenium chalcogenide cluster complexes. In a subsequent chapter, Alvaro Muñoz-Castro, Dayan Paez-Hernandez and Ramiro Arratia-Perez describe the bonding, optical, magnetic, redox and biological properties of rhenium hexanuclear clusters. Finally, Christophe Candolfi and his co-authors give a detailed account on the thermoelectric properties of ternary and quaternary molybdenum-based selenide clusters in their chapter. Readers will realize that almost 50 years after their discovery, the Chevrel phases and their derivatives continue to represent a vital research area, which attracts chemists, physicists and material scientists.

I warmly thank all of the authors for their timely contributions to this volume and hope that their efforts will stimulate younger chemists to join the field of ligated transition-metal clusters in solid-state chemistry and thereby keep it and the memory of Marcel Sergent alive. I am also grateful to Christiane and André Perrin – they were among the first actors in the field of Chevrel phases – and kindly provided me

with important details about Marcel Sergent's scientific career. Finally, my thanks go to Mike Mingos, Series Editor of *Structure and Bonding*, who had greatly admired Marcel's research on clusters and suggested the topic of this volume during a short visit to Rennes in 2016.

Rennes, France Jean-François Halet
May 2019

Contents

Struct Bond (2019) 180: 1–30
DOI: 10.1007/430_2019_35

Published online: 11 May 2019

Chevrel Phases: Genesis and Developments

André Perrin, Christiane Perrin, and Roger Chevrel

Contents

Abstract This chapter summarizes the important role played by Marcel Sergent in the discovery in the Rennes Laboratory of the Chevrel Phases, which stimulated considerable interest in the international solid-state chemistry community, because of their remarkable superconducting properties. After a brief general introduction to this topic, the seminal discoveries associated with these phases between 1970 and 1990 are described. After that their initial synthesis and structural determination was discovered, it was necessary to establish their critical superconducting transition temperature, the critical magnetic field, and the critical current density in wires, single crystals, and thin films. More recently their applications as battery materials, in catalysis, and their thermoelectric properties have been studied and are briefly described. These phases opened up the way not only to a rich solid-state chemistry

A. Perrin (✉), C. Perrin, and R. Chevrel
Institut des Sciences Chimiques de Rennes, UMR CNRS 6226, Université de Rennes 1, Rennes, France
e-mail: andre.perrin@univ-rennes1.fr

but also to a rich solution chemistry, which complemented the classical field of transition metal carbonyl clusters. The basic cluster units of the Chevrel Phases continue to be studied in the Rennes Laboratory by the heirs of Marcel Sergent and more widely in the international community.

Keywords Chevrel Phases · Hydrodesulfurization · Marcel Sergent · Molybdenum clusters · Rhenium clusters · Secondary batteries · Superconductivity · Ternary molybdenum sulfide · Thermoelectricity

1 Introduction

The aim of this chapter dedicated to the memory of Dr. Marcel Sergent is to relate his outstanding contribution to the discovery of the so-called Chevrel Phases, their developments, and the way they have paved the way to a large and important area of cluster chemistry. Although many people consider now that very old papers are obsolete, we have chosen to systematically refer here to original papers in order to get a memory of them, because they are often forgotten by the computer-assisted bibliographic tools and their users: "if nobody remembers something, it did not ever exist" [1]. This chapter does not provide an up-to-date and comprehensive review of this area but a historical account of the scientific contribution of Marcel Sergent to this area and its subsequent development. Consequently, the bibliography concentrates on the literature from 1970 to 1990, for which many details are covered in reference [2], and a more comprehensive review of this area is to be found in a recent paper by O. Peña [3].

2 The Early Beginnings

The Thesis Dissertation [4] of Marcel Sergent, defended in 1969, was devoted to the synthesis of new "Alkaline thiomolybdites, thiotungstites and thiochromites." This topic was chosen because the head of the Laboratory, Prof. J. Prigent, was a specialist of uranium chemistry and decided to extend the study of uranates and thiouranates to molybdenum and tungsten analogues. The experimental solid-state route for these syntheses was the sulfuration of the metallate by CS_2 transported by N_2 at around 300–400°C (Fig. 1). The resulting thiometallates were subsequently reduced under H_2 in the range 500–700°C. This approach was chosen because the alkaline metals are too reducing and the handling of alkaline sulfides was problematic.

The study of molybdenum and tungsten led to a number of new compounds of general formula $MMeS_2$ (M = alkaline metal, Me = Mo or W) where the Me metal has the formal oxidation state of +3 [5]. Conductivity measurements showed that they were semiconducting, and the magnetic measurements suggested the presence

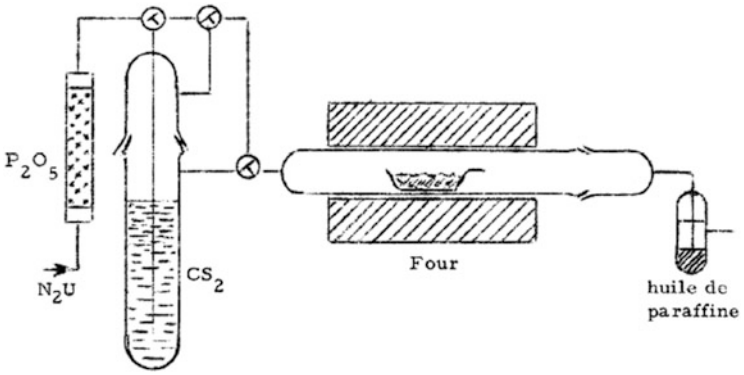

Fig. 1 The setup used by Marcel Sergent in his Thesis for the sulfuration experiments [4]

of metal-metal bonds. A further reduction under H_2 of the thiotungstites produces metallic W at temperature as low as 850°C. In contrast, thiomolybdites are reduced near 900°C to the new compounds of divalent molybdenum: $M_2Mo_5S_6$ (M = K, Rb, Cs) and $M_2Mo_2S_3$ (M = Li, Na) [4]. The XRD patterns of the latter were very similar to the one reported just previously by Espelund for "$SnMo_6S_7$," the pattern of which was tentatively indexed with a pseudocubic unit cell with $a = 6.53$ Å [6]. Remembering that $SnMo_6S_8$ was later shown to have a trigonal *R*-3 unit cell with $a = 6.52$ Å and $\alpha = 89.73°$, it becomes clear now that these compounds were in fact the first examples of the Chevrel Phases (hereafter abbreviated as CPs).

It is noteworthy to mention the Conclusions of the Thesis of Marcel Sergent, relative to these thio compounds of Mo(II): "[they] form a very original series, owing to their electrical and magnetic properties, very different from the ones of chromium and other transition elements. These compounds are actually characteristic of the low valency chemistry of molybdenum, tungsten, niobium, and rhenium, based on Me-Me chains or polymers." We can guess that the last word in this sentence would refer in his mind to "$MoCl_2$" derivatives that were already known since the 1940s to have structures based on octahedral Mo_6 units with strong Mo-Mo bonds [7, 8].

3 The Discovery of Chevrel Phases

As he developed an independent research program, Marcel Sergent decided to pursue this interesting emerging chemistry of ternary molybdenum(II) sulfides. Indeed, Marcel Sergent and his student Roger Chevrel intuitively felt that it may be possible to reduce MoS_2 by Mo and a third metallic element, using high-temperature direct solid-state syntheses in evacuated sealed silica tubes (as was done by Espelund), a method that was not well-developed at that time in the solid-state community. They implemented it in the laboratory, enabling syntheses up to about 1,200°C. Indeed, this approach was very fruitful and gave opportunity to

develop in Rennes the transition element cluster chemistry of the early transition metals. It remains, 50 years on, very commonly used in solid-state laboratories worldwide for high-temperature solid-state syntheses.

3.1 Syntheses of the First Thio Compounds

The first attempts were carried out within the framework of the M.Sc. Diploma (unpublished) of his student Roger Chevrel, which described the exploration of the Fe-Mo-S system. Two new phases were detected: $FeMo(II)_3S_4$ which was later identified and assigned to the so-called Chevrel Phases (CPs) and also $FeMo(III)_2S_4$. These synthetic procedures were extended to a number of ternary sulfides and reported in the Thesis of R. Chevrel [9]. The overall approach was to explore the range of compositions $M_2(I)S$-$Mo(II)S$ and $M(II)S$-$Mo(II)S$, targeting formulas $M_2(I)Mo_nS_{n+1}$ and $M(II)Mo_nS_{n+1}$. Following several oral communications in scientific meetings in the 1968–1970, the results were first published (in French; see Fig. 2) in 1971 in the seminal paper titled "On New Molybdenum Ternary Sulfides Phases" [10] and summarized in Table 1.

Stoichiometric compounds were obtained when M was a large cation, namely, Ag, Sn, Pb, Sr, and Ba. From Weissenberg and Buerger X-ray photographs, it was shown that they crystallize in the trigonal system, *R*3 or *R*-3 space groups (SG). The unit-cell constants, refined from X-ray diffraction powder data, are all close to $a = 6.5$ Å and $\alpha = 90°$: for instance, in the example of the Pb compound, they are $a = 6.54$ Å and $\alpha = 89°28'$.

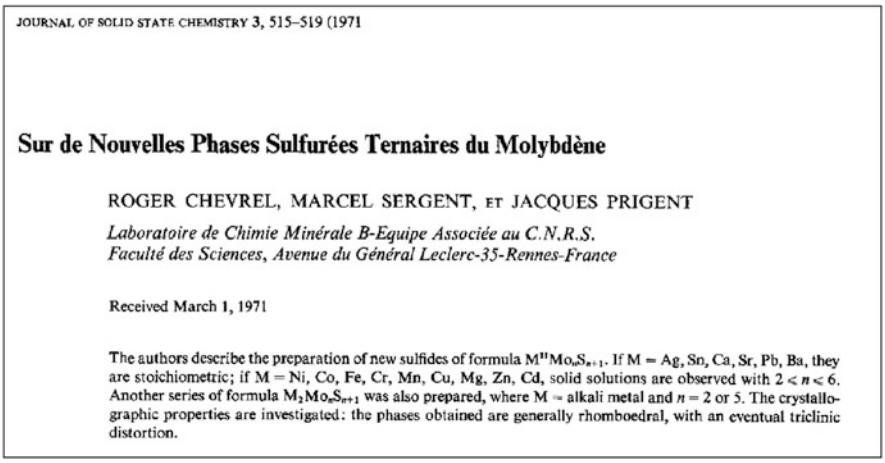

JOURNAL OF SOLID STATE CHEMISTRY 3, 515–519 (1971

Sur de Nouvelles Phases Sulfurées Ternaires du Molybdène

ROGER CHEVREL, MARCEL SERGENT, ET JACQUES PRIGENT

Laboratoire de Chimie Minérale B-Equipe Associée au C.N.R.S.
Faculté des Sciences, Avenue du Général Leclerc-35-Rennes-France

Received March 1, 1971

The authors describe the preparation of new sulfides of formula $M^{II}Mo_nS_{n+1}$. If M = Ag, Sn, Ca, Sr, Pb, Ba, they are stoichiometric; if M = Ni, Co, Fe, Cr, Mn, Cu, Mg, Zn, Cd, solid solutions are observed with $2 < n < 6$. Another series of formula $M_2Mo_nS_{n+1}$ was also prepared, where M = alkali metal and $n = 2$ or 5. The crystallographic properties are investigated: the phases obtained are generally rhomboedral, with an eventual triclinic distortion.

Fig. 2 A partial facsimile of the first report on Chevrel Phases [10] (reproduced from J. Solid State Chem., with permission)

Table 1 $M_2(I)Mo_nS_{n+1}$ and $M(II)Mo_nS_{n+1}$ compounds reported in the first paper published by R. Chevrel, M. Sergent, and J. Prigent [10]

Cation	n value or range	Comment
Ag	4	Stoichiometric compounds (trigonal)
Sn	5	
Pb	6	
Sr	6	
Ba	7	
Ni	3–5	Solid solutions (trigonal)
Co	3–5	
Fe	2–5	
Mn	2–6	
Cr	2–3	Triclinic
Cu_x	3–4 and $x = 1$–2	Double solid solution
Mg	2–6	Trigonal→triclinic transition depending upon stoichiometry
Zn	3–6	
Cd	3–5	
Li or Na	2	Trigonal

Solid solutions, with a large variability in cation concentration, were obtained with smaller cations, Ni, Co, Fe, and Mn. They also crystallize in the *R*3 or *R*-3 SG, with similar unit-cell constants, but α is now slightly larger than 90°. The Cr solid solution in contrast showed a triclinic distortion although the unit cell remains very close to the trigonal parent, while Mg, Zn, and Cd solid solutions undergo a trigonal to triclinic transition for high concentrations of the cations. A special mention concerns the copper compounds as they were apparently characterized by a double nonstoichiometry. In fact, it was found later that the solid solution $Cu_xMo_6S_8$ extended from $x = 1.6$ to $x = 4$.

Finally, the paper mentioned some alkaline thiomolybdites that present a trigonal unit cell similar to the abovementioned ones (for Li, Na), while $M_2Mo_5S_6$ (M = K, Rb, Cs) are quadratic.

An important conclusion of this paper, drawn from both the chemical properties and magnetic measurements, was that the molybdenum had a formal oxidation state of +2 and the d^4 configuration was capable of establishing Mo-Mo bonds, and the authors restated a visionary hypothesis of the formation of "metal clusters" (defined by Cotton as "a finite group of metal atoms held together mainly or at least to a significant extent, by bonds directly between the metal atoms, even though some non-metal atoms may also be intimately associated with the cluster" [11]) in such compounds, similar to that reported for $MoCl_2$ [7, 8].

3.2 Syntheses of the First Seleno and Telluro Compounds

For the synthesis of such compounds, a valuable advantage of the sealed tubes method is the use of elemental Se (Te), avoiding the need to handle the very harmful H_2Se (H_2Te). Consequently, many ternary molybdenum(II) selenides were published in the next few years. O. Bars et al. reported in a short paper the synthesis and unit cells of Mo_3Se_4 and the solid solutions $M_xMo_3Se_4$ (M = Fe, Co, Ni) as early as 1970 [12]. As all these compounds appeared to be isostructural, it was suggested that the binary product would act as a host structure for counter-cations, leading to the ternary chalcogenides. Some time later, R. Chevrel and M. Sergent extended and completed this work [13]. It is noteworthy that in the meantime the crystal structure of Mo_3Se_4 was solved (see Sect. 4), giving unambiguous structural evidence for Mo_6 octahedral cluster-based Mo_6Se_8 units. In their second full paper, Chevrel and Sergent used the notation "$M_xMo_3Se_4$," but finally, after structural determinations, it became evident that the use of the $M_xMo_6Q_8$ (Q = chalcogen) formula was more accurate and established that the common basic unit was the rigid Mo_6Q_8 entity, for all the CPs (see Sect. 4).

As previously, large cations led to definite compounds $M_xMo_3Se_4$ where M was Zn, Ag, Cd, Sn, and Pb with x close to 0.6. They crystallize as above in the trigonal $R3$ or $R\text{-}3$ SG, the unit-cell volume increasing monotonically with the radius of M. For M = Fe, Mn, Cr, V, and Ti, a triclinic solid solution is observed ($0.5 < x < 0.7$). For Cu and Co, the trigonal solid solution extends from $x = 0$ (i.e., Mo_3Se_4) to $x = 1.4$ and 0.7, respectively. In the example of $Ni_xMo_3Se_4$, the trigonal solid solution extends in the ranges $0 < x < 0.3$ and $0.6 < x < 0.8$, while in-between is observed a triclinic distortion.

3.3 Subsequent Synthetic Studies

This pioneering work resulted in an incredible blooming of new compounds during the 1970s. Besides the main group and transition elements, they included rare-earth [14] and actinide counter-cations [15, 16]. For example, in the late 1970s, more than 80 CP compounds were identified and characterized [2, 17]. Also it should be mentioned that the substitution of some of the chalcogens by halogens could be achieved and some of the molybdenum atoms could be replaced by Re or Ru. This opened up the way to very important series of new cluster-based chalcohalides, as discussed in more detail in Sect. 7.

4 The Crystal Structures of Chevrel Phases

The first pertinent work related to CPs was the structure determination in 1973 of the binary Mo_6Se_8 by O. Bars et al. [18]. Indeed, this compound was synthesized some years before by decomposition at 1180°C of $MoSe_2$ under a vacuum [19], but only the full solid-state approach afforded single crystals easily obtained and suitable for an X-ray diffraction analysis. This pioneering structural work established the presence of slightly distorted octahedral Mo_6 groups, based on octahedral metal "clusters," and M. Sergent realized that they were similar to those present in $MoCl_2$ (see Fig. 3). Within the cluster, the Mo-Mo distances are 2.68 and 2.83 Å, consistent with the presence of strong metal-metal bonds. In molybdenum metal, the Mo-Mo distance is 2.73 Å [20]. The Mo_6 clusters are inscribed in a Se_8 pseudo-cube, leading to the Mo_6Se_8 units, which are the structural basis of all of the CPs. In addition, there are six longer intercluster Mo-Mo contacts of 3.26 Å. Of special interest in this paper is another illustration of the unit-cell stacking: the small arrows in Fig. 3 represent Mo-Se interunit bonds and evidence the fact that a selenium atom lies on each "apical" position of the Mo_6 octahedron (i.e., on the pseudo-quaternary axis), exactly like some of the halogen atoms in $MoCl_2$. The correct description of the three-dimensional structure is based on the three-dimensional stacking of $Mo_6[Se_2{}^{i}Se_{6/2}{}^{i\text{-}a}]Se_{6/2}{}^{a\text{-}i}$, where the symbols

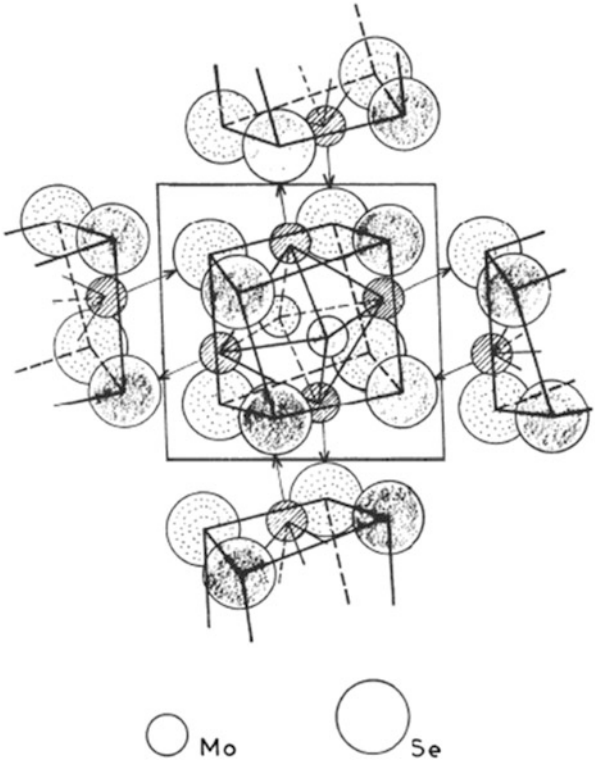

Fig. 3 The first representation of a Chevrel Phase structure: the empty Mo_6Se_8 binary host [18]

a and *i* act as "apical" and "inner" (i.e., belonging to the Se_8 pseudo-cube), according to the Schäfer notation [21]. This structure forms some channels and cavities, especially at the origin of the unit cell, and the assumption was made in the paper that it acted as a host structure in the ternary CPs.

Indeed, this work was followed very soon by the determination of the structures of ternary phases: $Ni_{0.66}Mo_6Se_8$ [22] and $Ni_2Mo_6S_8$ [23] and many others. The structure of $PbMo_6S_8$ [24, 25] was particularly noteworthy, because it is considered as the prototype of CPs with a large cation, as well as the structure of the very extended solid solution $Cu_xMo_6S_8$ ($1.6 < x < 4$) [26]. In the first case, Pb^{2+} counter-cations are located at the origin ("site 1"), while in the second one, the Cu^+ counter-cations are statistically distributed in a puckered hexagon around this same site 1 and on another one denoted as "site 2." Simultaneously, the structure of the selenide $PbMo_6Se_8$ was also reported [25].

In the following years, many of these structures were accurately refined, giving evidence for some additional nonstoichiometries: as an example, "$PbMo_6S_8$" was actually $PbMo_{6.35}S_8$ [15]. However, for reasons of clarity, we will use the simplified formulae hereafter.

5 The Electronic Structure of Chevrel Phases

Well before the discovery of CPs, the isolated cluster unit $[Mo_6Cl_8]^{4+}$ was studied by several authors [27–29] using a simple molecular orbital (MO) approach. Although the precise ordering of the MO levels was uncertain at this stage (it was precisely established some years later as a_{1g}, t_{1u}, t_{2g}, t_{2u}, and e_g, from the bottom to the top [30]), the important point was the evidence of the formation of 12 metal-metal bonds involving 24 electrons on the metal cluster, a magic number called valence electron count (VEC) [31]. This corresponds obviously to the establishment of single bonds with a bond order of 1, as formalized by J. D. Corbett [32].

In the late 1970s and early 1980s, such calculations were extended to the newly discovered CPs [33–36]. The pedagogic report of T. Hughbanks and R. Hoffmann [37] was particularly noteworthy since their calculations emphasized the crucial role of apical $S^{a\text{-}i}$ ligands. This point of view agrees closely with the previous statement of Corbett that "a maxim of cluster chemistry is that the outer or exo [i.e., 'apical' in the Schäfer notation used here] positions are strongly bonding and are always occupied by some basic group" [32]. Indeed, this is this feature that imposes a rotation of about 25° (as seen in Fig. 3) of the cluster unit inside the counter-cation pseudo-cube, in order to put a sulfur atom of a surrounding cluster unit in front of each molybdenum of a given (Mo_6S_8) cluster unit. These additional sulfur atoms lie onto the pseudo-quaternary axes of the octahedron. Introducing these apical sulfur ligands in the calculation, instead of restricting to the (Mo_6S_8) cluster unit, actually opens a gap above the e_g MO, the top-most level of the Mo-*d* group, as illustrated in Fig. 4. As the e_g levels are fully occupied for a VEC = 24, this explains why a

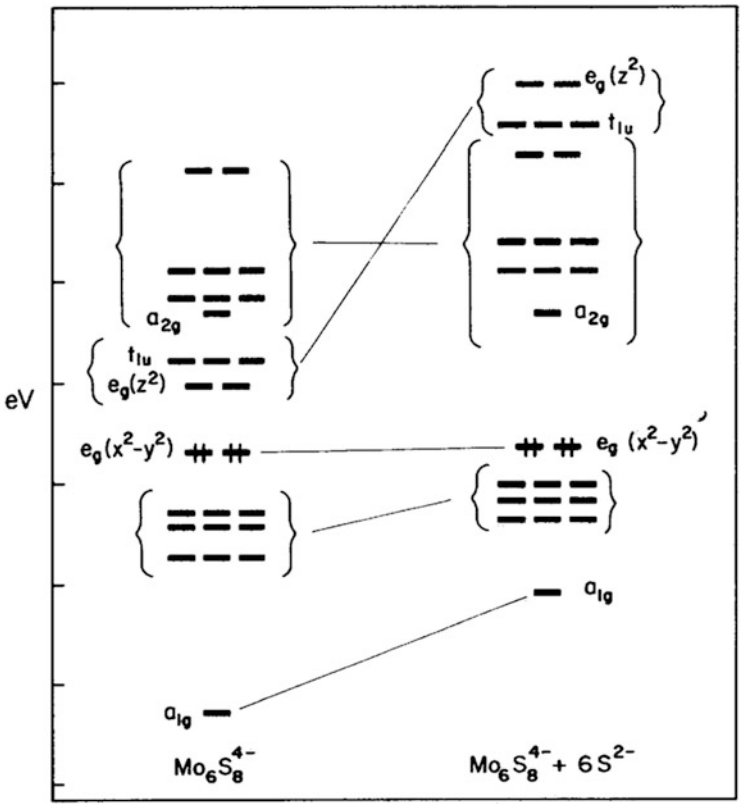

Fig. 4 Molecular orbital diagram of Chevrel Phases, illustrating the perturbation of the $Mo_6S_8^{4-}$ levels by six apical S^{2-} ions, consequently opening the gap [37]

compound like $Mo_2Re_4Se_8$, strictly isostructural with Mo_6Se_8, turns out to be a semiconductor, as it accommodates exactly 24 e^-/cluster (see Sect. 7).

Similar results were reported simultaneously and independently by the team of R. Lissillour in Rennes [38]. They extended the calculations to a number of $M_6L_8L'_6$ cluster-based compounds (M = Mo, Re; L and L′ = halogen or chalcogen; see Sect. 7) and formalized their results within their so-called three-band model, where from the bottom to top lies a band mainly composed of *p* L ligand orbitals and the second is made of 12 *d* M metallic orbitals (bonding) and the third, separated by the gap, of 18 *d* M metallic orbitals (antibonding) [39].

6 The Golden Age of Chevrel Phases

6.1 Superconductivity

6.1.1 Critical Temperature

A very short time after the publication of the paper of R. Chevrel, M. Sergent, and J. Prigent on ternary molybdenum sulfides, the group of B. T. Matthias discovered a superconducting behavior in several of them and published in *Science* a short paper entitled "High-Temperature Superconductors: The First Ternary System" [40]. For the Cd, Mg, Zn, Cu, Sn, and Pb compounds, critical temperatures (T_c) of 2.3, 2.4, 2.7, 10.8, 10.9, and 12.5 K, respectively, were reported. Such a discovery initiated immediately an intense international research on the superconductivity of CPs, promoting in particular a very long-lasting and fruitful collaboration between the groups of M. Sergent in Rennes and Ø. Fischer in Geneva. As reported in reference [17], the T_c of more than 80 compounds was measured in 1978. Figure 5 illustrates an example of resistive transitions reported early [41].

The effect of doping by a fourth (metal) element suggested that the nature of the counter-cations between the Mo_6S_8 units plays an important role on the value of the critical temperature [42]. However, the subsequent report that $Mo_6S_6Br_2$ exhibits a T_c as high as that in $PbMo_6S_8$ (see Sect. 7) does not support this assertion. From a

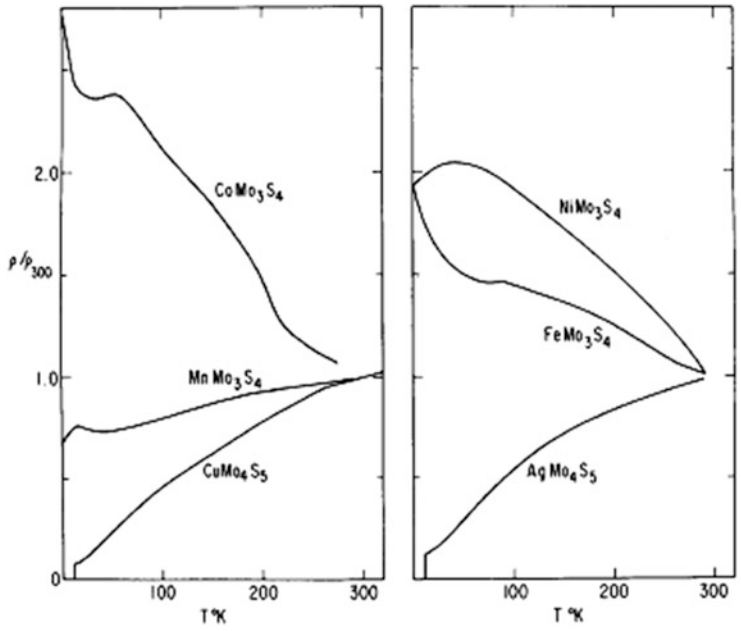

Fig. 5 Early reported resistivity curves of several Chevrel Phases, illustrating the superconducting transitions for the copper and silver compounds [41]

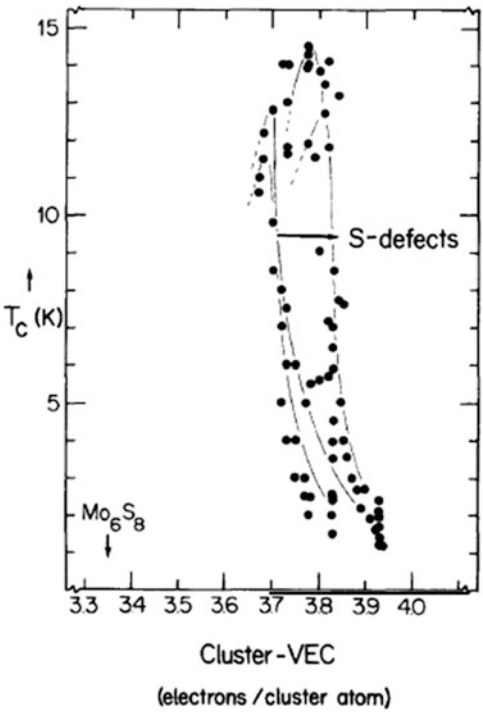

Fig. 6 A correlation between the critical temperature and the VEC (here relative to one molybdenum atom) for a number of superconducting Chevrel Phases [31]

study of the effect of the (partial) substitution of S by Se or Te in $PbMo_6S_8$ and Mo_6S_8, it was concluded that correlations between T_c and both the rhombohedral angle α and the intercluster Mo-Mo distance [43] existed. Further research showed no direct correlation between the superconductivity and the nature of the ternary element M, suggesting that the 4*d* electrons of Mo were essentially responsible for the superconducting properties [14]. This was confirmed some years later by theoretical calculations. In contrast, a clear correlation of T_c and the VEC was established [31]. Figure 6 shows a maximum of T_c around a value of 3.7–3.8 electrons/Mo, i.e., around 22 electrons/Mo_6 cluster, again in accordance with a maximum of the density of states near this value.

6.1.2 Critical Magnetic Field

Another striking characteristic of superconducting CPs is their extraordinary high critical magnetic field, which was only exceeded by the so-called HCTS cuprates discovered in 1986. Indeed, the Fischer group reported in 1974 the first measurements, using a pulsed magnetic field limited to 350 kG. For some samples they could not reach the critical magnetic field H_{c2} but deduced from a model values up to about 450 and 550 kG for $PbMo_6S_8$ and Al-doped $SnMo_6S_8$, respectively [44]. The same year, using a new coil delivering up to 510 kG, they obtained at 4 K a critical field

estimated to 560 kG (for full destruction of superconductivity), meaning more than 600 kG at 0 K, for a slightly Gd-doped $PbMo_6S_8$ sample [45]. Finally, the following year, H_{c2} was increased to 580 kG at 4 K and more than 600 kG at 2 K for a sample doped with both Gd and Eu, implying that a magnetic field above 700 kG would be necessary to make it entirely normal [46]. As CPs are not cubic, experiments were carried out on oriented single crystals. An anisotropy of about 20% was measured for all three representative $PbMo_6S_8$, $PbMo_6Se_8$, and $SnMo_6Se_8$, with the maximum of H_{c2} obtained when H is perpendicular to the ternary axis [47].

6.1.3 Coexistence of Magnetism and Superconductivity

Finally, the discovery of the coexistence of magnetism and superconductivity in the $(RE)Mo_6S_8$ systems should be mentioned. Indeed, it was shown that a partial substitution of Pb or Sn in $PbMo_6S_8$ or $SnMo_6S_8$ by magnetic rare-earth ions did not destroy the superconductivity [14, 48] (see Fig. 7 [14]). A subsequent study, involving all RE ions series, was carried out, and most of the $(RE)Mo_6S_8$ are superconducting above 1.1 K. It was the first time that a system containing a regular lattice of magnetic ions was superconducting. It was concluded that the exchange interaction between the superconducting electrons and the RE ions was very weak, because the latter are located at the origin site, far away from the Mo_6 cluster [14]. This situation contrasts with the case of small magnetic transition elements of the first group like Fe, where these ions are delocalized around several sites and are then closer to the cluster, fully destroying the superconductivity, as expected. Very unusual behavior was reported for some $(RE)Mo_6S_8$. For instance, $HoMo_6S_8$ is superconducting at 1.2 K but becomes normal again below 0.65 K where a magnetic

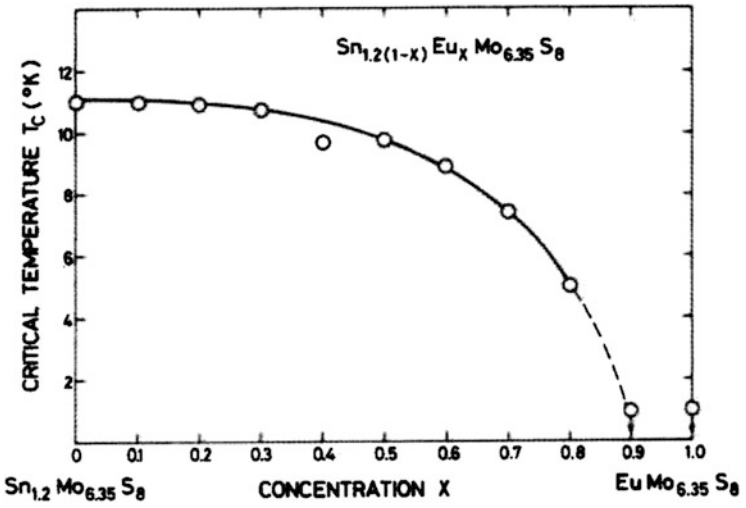

Fig. 7 Critical temperature versus concentration x of europium ions in $Sn_{1.2(1-x)}Eu_xMo_{6.35}S_8$ [14]

transition occurs [49]; this particular state was called "reentrant superconductivity" [50]. On the other hand, $EuHoMo_6S_8$ exhibits a phenomenon of magnetic field-induced superconductivity: at $T < 1$ K, superconductivity is destroyed in a low field (about 10 kG), reappears at 80 kG, and finally disappears only above 200 kG [51]. Interested readers could find more detail in [3] and references therein.

6.1.4 Processing Chevrel Phases

Figure 8 illustrates clearly the superiority of $PbMo_6S_8$ with respect to technical superconductors Nb-Ti, Nb_3Sn, and even Nb_3Ge in terms of critical field [17]. Indeed, a considerable effort was made to produce wires of CP, because they appear to be excellent candidates to build coils able to sustain higher magnetic fields. For this purpose, they have to be processed in the form of wires, additionally able to support high current density. The main drawback arises from the fact that CPs are very brittle materials (as Nb_3Sn and Nb_3Ge, while in contrast Nb-Ti is a ductile

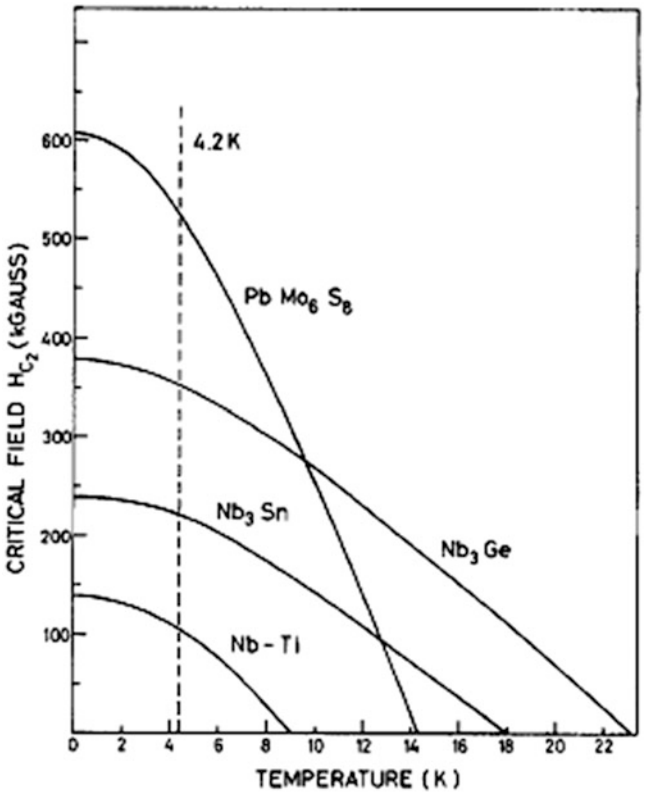

Fig. 8 Comparison between the critical fields of $PbMo_6S_8$, Nb_3Ge, Nb_3Sn, and the Nb-Ti alloy [17]

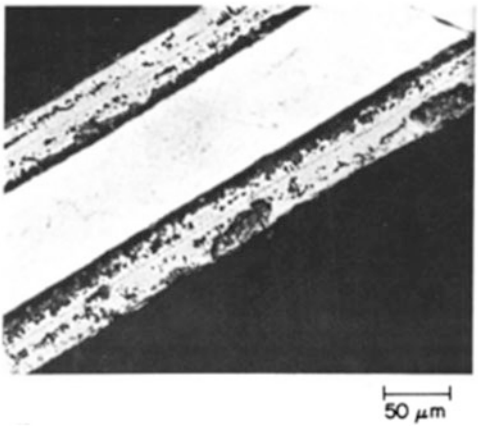

Fig. 9 A cut along the axis of a $PbMo_6S_8$ wire grown on the surface of a molybdenum wire [52]

alloy). One of the first attempts was based on the sulfidation of a molybdenum wire, followed by a heat treatment under Pb vapor (see Fig. 9) [52]. The current density was quite modest, 2 10^7A/m^2 in a field of 40 kG [52]. In the following years, the technology of powder metallurgy was developed, implying in most cases the help of specialized factories. Then several consortiums were established, for instance, in France, University of Rennes with CGE Marcoussis, CEN Saclay and Grenoble, and SNCI Grenoble, and in Europe, Universities of Rennes, Geneva, and Nijmegen with Plansee, Spectrospin, and Promogap (European Union Program Eureka 96). Briefly, the CP (pre-reacted [53] or its precursors [54]) is compacted in a copper tube ("billet") that is extruded and then drawn as a long monofilament wire. In further improvements, sections of such wires were assembled in bundles and again extruded and drawn to produce multifilament wires as shown in Fig. 10 [50, 54]. In order to avoid any contamination of $PbMo_6S_8$ by Cu, an anti-diffusion barrier (mainly Nb and in some cases Mo) was inserted [50, 53, 54]. Whatever the route used, the critical current density was in the range 1–2 10^8 A/m^2 at 200 kG and 4.2 K [55]. Values of 5.4 10^8 and 3.1 10^8 A/m^2 were further reached at 1.9 K for fields as high as 200 kG and 240 kG, respectively [56]. Figure 11 shows that CP wires overpassed any technical superconductors above 170 kG [57].

Thin films are the ideal form for some physical measurements, such as critical current density and the development of superconducting junctions. The first attempt used RF sputtering from a composite target to grow CPs with Cu, Ag, Sn, and Pb, deposited onto Mo substrates [58]. The films were either grown in situ on heated substrates (750–900°C) or deposited at room temperature and subsequently annealed in silica tube sealed under vacuum. Critical temperatures close to the one of bulk material were achieved. Such films exhibited J_c as high as 10^9 A/m^2 at zero field [59] and were later used to produce superconducting tunneling junctions based on CPs [60]. In the following years, reactive physical vapor deposition was proposed [61], but other groups used sputtering, with different variants [62, 63]. During this period, M. Sergent decided to provide his laboratory with a miniaturized sputtering device, and T_c = 13 K and J_c = 3.10^7 A/m^2 were achieved for $PbMo_6S_8$ with this very

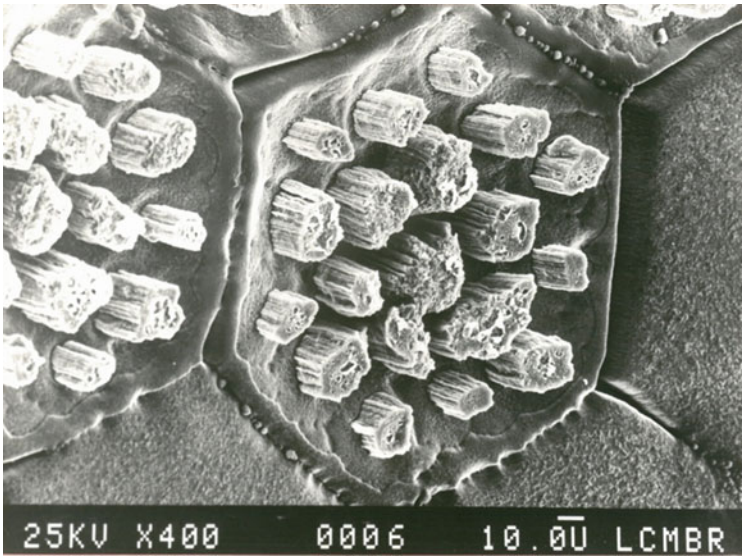

Fig. 10 A scanning electron micrograph of a Chevrel Phase multifilament wire in copper matrix. © A. Perrin LCMBR

simple apparatus [64, 65]. When pulsed laser deposition became popular, this method was applied to the in situ growth of $Cu_xMo_6S_8$, and epitaxial thin films of CPs were obtained for the first time [66]. More recently, films of $Cu_2Mo_6S_8$ were synthesized by chemical solution deposition, based on the use of a polymeric precursor: the coatings were first calcined and then sulfided under a H_2/H_2S flow and finally reduced under H_2 [67]. On the other hand, the preparation of a thick film (17 μm) of $Cu_xMo_6S_8$ was done by a chemical transport technique [68], similar to the method used to process wires reported in [52].

Single crystals are obviously of great importance for many physical measurements. Indeed, crystals suitable for structure determination were in most cases picked from the powders resulting from the synthetic procedures. Chemical transport reactions were carried out for $Co_2Mo_6S_8$ [9] and $PbMo_6S_8$ [69, 70], giving isolated well-formed crystals, but the latter were still too small for physical measurements. Crystallization from melt is difficult, because many of CPs undergo incongruent melting. In addition, it is necessary to take into account the sensitivity to oxidation, the high melting temperature, and the high chemical reactivity [71]. Then, welded Mo crucibles [72], or high Ar or He counterpressure [73, 74] or liquid-encapsulated melting [75], were proposed, especially in the examples of ternary sulfides with Pb, Sn, or Cu. Obviously, much efforts were done for rare-earth ternary sulfides, because of their outstanding properties. Sealed Mo crucibles [76], often associated with an Al_2O_3 liner and an excess of RE sulfide [71], were used. A very complete study of the kinetics of the crystal growth of $REMo_6S_8$ was carried out [77]. It established the possibility of working in open crucibles under argon at atmospheric pressure, as long

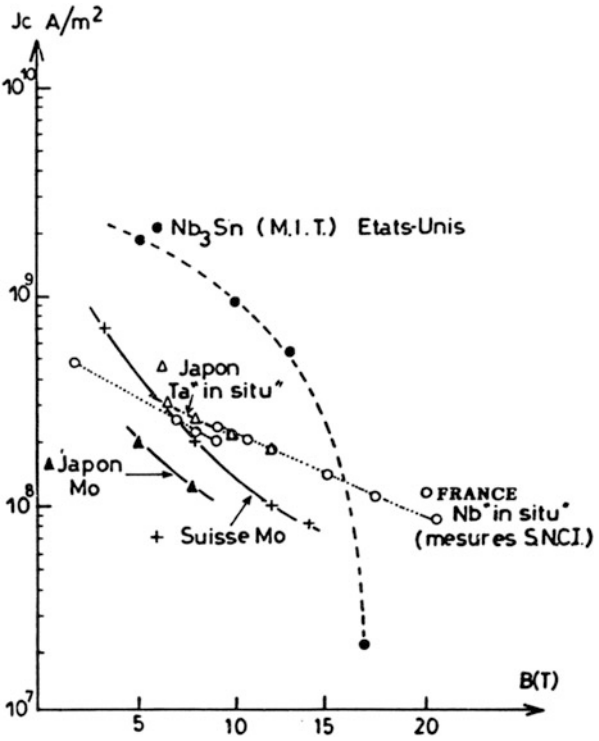

Fig. 11 A graph of the best critical current densities as a function of applied magnetic field for single-wire Chevrel Phases obtained in various laboratories, compared to the classical Nb_3Sn superconductor [57]

as the initial charge was sufficiently shifted in composition. A general survey including details about the physical properties measured on $REMo_6S_8$ crystals is given in [78]. The reader is also referred to a recent review [3]. Finally, the systematic study of the crystal growth of the selenides $REMo_6Se_8$ was carried out more recently [79].

6.2 Other Properties and Potentialities

As outlined in the previous section, CPs have been studied in detail for their outstanding superconducting behavior. In addition, this series of compounds exhibits several other striking properties, which are summarized below.

6.2.1 Electrodes for Secondary Batteries

As mentioned above, the structure of CPs provides an open framework with three-dimensional channels, where delocalized small counter-cations are accommodated. These metal ions are mobile within these channels. Indeed, Chevrel and Sergent

removed the counter-cations from some small-cation CPs (e.g., copper and nickel), by leaching them with a dilute inorganic acid and then giving access to the metastable Mo_6S_8 binary compound [80]. The reaction is reversible, and ternary representatives can again be obtained using soft conditions. In addition, the process is topotactic in character, and the authors were able to determine and refine the crystal structure of Mo_6S_8 [80]. Soon after, Schöllhorn et al. succeeded in intercalation-deintercalation reactions using an electrochemical approach. In their studies, both transition metal CPs were removed with aqueous electrolyte and alkaline CPs with an organic one [81]. These results opened the way to the study of CPs as cathode materials for rechargeable batteries. Most work was devoted to the Cu-, Fe-, Ni-, and Cr-based CPs associated with lithium and organic electrolyte [82–86]. Thick [87] and thin films [88, 89] were also studied. More recently, the group of D. Aurbach highlighted the potential interest of Mg/CP batteries [89] because Mg is eco-friendly, nontoxic, abundant in the earth crust, and divalent and gives fast and reversible intercalation in CP. These CPs have been claimed to be the currently best available model cathode for Mg batteries, as practical energy densities of 60 W h kg^{-1} (about half of the Li-ion battery) with excellent cyclability (>3,000 cycles) were reported [90]. For a recent, complete, and critical review, see reference [91]. As a final remark, it is clear that CPs have a limited intrinsic massic capacity, due to their quite high molecular weight. However, they could be very attractive for land-based stationary battery systems, in relation to the need for the storage of intermittent renewable energy sources like wind or sun.

6.2.2 Catalysis

In 1984, McCarty and Schräder compared the ability of several CPs as catalysts for hydrodesulfurization of crude oils versus both classical unpromoted and Co-promoted MoS_2 (usually labeled "CoMoS") catalysts [92]. They found that all CPs tested had efficiencies comparable and even better than the standard model catalysts, on the basis of catalyst surface area. In addition, they showed that CPs had a higher selectivity and stability. Their long-term activity was also better than those of classical model catalysts. However, samples were synthesized by the standard high-temperature solid-state route, resulting in low specific surface area, about 1 m^2/g. Obviously, improved efficiency of the catalytic process depends strongly on the specific area of the material used. Then, M. Sergent and his group launched a program devoted to increasing the surface areas of the CPs. The work drew on a previous result in his Thesis [4] that the hydrogen reduction of alkaline thiomolybdites affords new compounds that turned out to be in fact CPs. The first approach was to reduce mixtures of ammonium thiomolybdates and, for instance, copper salts. The CP $Cu_xMo_6S_8$ was obtained at temperature as low as 600°C, with an intermediate step involving a mixture of MoS_2 and Cu [93]. Subsequently, samples of $Cu_xMo_6S_8$ supported on alumina were prepared by impregnation with an ammonia solution of ammonium heptamolybdate and copper nitrate, followed by air calcination, sulfuration under a H_2S flow, and finally reduction by hydrogen

[94]. The crystallites were so small that the CP could not be characterized by X-ray diffraction, only by EXAFS. Also, searching for a preindustrial route for CP preparation, finely grained $Ni_xMo_6S_8$ powders (0.5–1 μm) were prepared by bubbling H_2S in an aqueous solution of heptamolybdate and Ni nitrate. The coprecipitate was dried and H_2 treated as previously [95]. Finally, an indirect route to prepare supported Ni-CP catalyst was to start from a commercial Ni-Mo catalyst precursor; to sulfide it until the early formed "NiMoS" was fully dissociated in MoS_2 and Ni particles, as mentioned above in the example of copper; and to react and reduce them under hydrogen in order to synthesize the CP [96]. Catalytic activity measurements were used to optimize the reduction treatment. It should be noticed that $Cu_xMo_6S_8$ was recently evaluated also as a catalyst for the ring opening of tetrahydrofuran [97] and for hydrogenation, dehydrogenation, and hydrogenolysis reactions, similar to those commonly catalyzed by platinum group metals [98].

6.2.3 Thermoelectricity

The figure of merit of a thermoelectric material, that is a measure of its efficiency at a temperature T, is given by $ZT = \alpha^2 T/\rho\lambda$, where α is the Seebeck coefficient, ρ the electrical resistivity, and λ the thermal conductivity (both electronic and of the lattice). The latter should be minimized, and, in this respect, compounds with heavy constituent masses and open structures hosting mobile atoms that act as good scattering centers for phonon are good candidates [99]. This is the case of CPs where the counter-cations have large thermal factors, especially for smaller ones, which are strongly delocalized and are able to "rattle" inside their cage-like site. In addition, partial substitutions are possible both on the chalcogen positions and even on the cluster itself, increasing the local disorder. Finally, the electrical resistivity can be tuned, by varying the VEC. Although first evaluations of Seebeck coefficients of *metallic* CPs were published quite early [100, 101], it is only in the late 1990s that theoretical calculations were carried out for the search of CP-based thermoelectric materials [102, 103]. The same year, T. Caillat et al. studied the *semiconducting* mixed-cluster pseudo-binary (see Sect. 7) $Mo_2Re_4Se_8$ [104], followed by the obtention of a ZT value of 0.6 at 1150 K for $Cu_{1.38}Fe_{0.66}Mo_6Se_8$ [105]. This value is very encouraging, because it is comparable to that of Si-Ge alloy in the same temperature range and to the state-of-art thermoelectric materials ($ZT \approx 1$ for most of them) and it was not yet overpassed for any MMo_6Q_8 true CP, in spite of subsequent attempts. In contrast, higher value was recently reported for the condensed cluster (see Sect. 7) compound $Ag_{3.8}Mo_9Se_{11}$ with $ZT \approx 0.7$ at 800 K only, about twice the value calculated for $Cu_{1.38}Fe_{0.66}Mo_6Se_8$ at the same temperature [106]. The thermoelectric properties of this very rich series of condensed clusters materials are still the subject of extensive studies within the framework of a close French collaboration between the Institut des Sciences Chimiques de Rennes and the Institut Jean Lamour in Nancy ([107] and references therein). Interested readers could also refer to the chapter of this volume entitled *Thermoelectric Properties of Ternary and Quaternary Mo_6 and Mo_9 Cluster Selenides*.

7 The Legacy of Chevrel Phases

Soon after the discovery of CPs and the understanding that they displayed outstanding properties, considerable synthetic works were made in Rennes, under the supervision of Marcel Sergent. These new approaches involved changing the conditions for the synthetic procedures and thereby providing opportunities for fine-tuning their properties. These developments are summarized below.

7.1 Condensed Clusters

In 1979 M. Sergent and R. Chevrel, working with indium counter-cation, reported the first example of a condensed cluster based on CPs [108]. It was based on the Mo_9Se_{11} unit built from two octahedral Mo_6 clusters sharing a common Mo_3 face perpendicular to the ternary axis, as displayed in Fig. 12a. This topic was extended with M. Potel and P. Gougeon. Indeed, in the same year, the Mo_{12} cluster (Fig. 12b) was discovered as well as the infinite chain $(Mo_{6/2})_{\infty}$, based on the stacking of Mo_3Q_3 triangular groups staggered along a ternary axis in the structure of $K_2Mo_6S_6$ [109]. Intermediates in this series were discovered when the giant clusters Mo_{18}, Mo_{24}, and Mo_{30} [110, 111] were synthesized and characterized. All these cluster units can be written by the general formula $Mo_{3n}Q_{3n+2}$ ($n \geq 2$). Note that in many

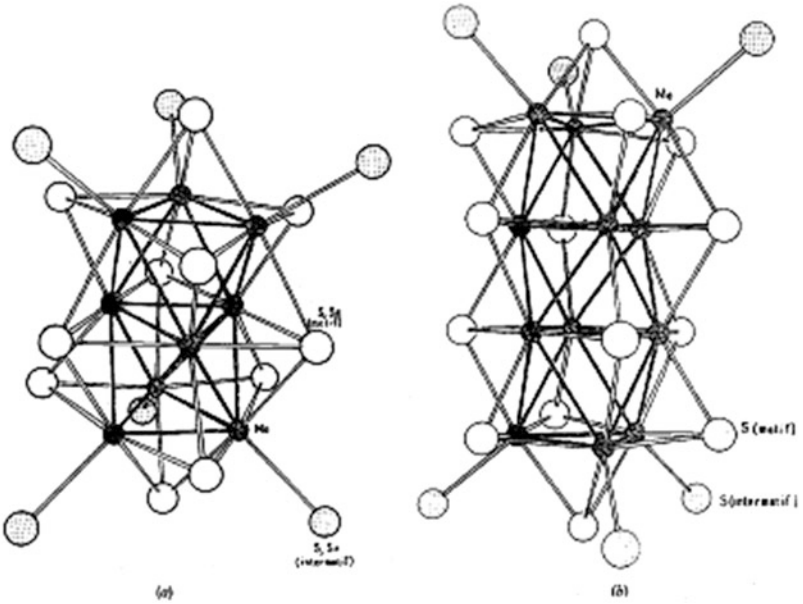

Fig. 12 The Mo_9S_{11} unit in $K_2Mo_{15}S_{19}$ (**a**) and the $Mo_{12}S_{14}$ (**b**) unit in $K_2Mo_9S_{11}$ [109]

cases, the condensed clusters coexist in the structure with the octahedral one: for instance, the compound $K_2Mo_{15}S_{19}$ corresponds to the developed formula $K_2(Mo_6S_8)(Mo_9S_{11})$ [109], and, in contrast, Mo_9Se_{11} alone was found in the structures of $Ag_xMo_9Se_{11}$ ($x = 3.6$ and $x \approx 4$) [112]. Many compounds based on such high-nuclearity clusters were synthesized and structurally characterized in the following years. They included the giant cluster $(Mo_{36}S_{38})^{10-}$ [113], as well as the $(Mo_{15}Se_{17})^{3-}$ [114] and $(Mo_{21}Se_{23})^{5-}$ ones [115], the latter having an odd number of molybdenum atoms. A theoretical study of Mo_9Q_{11}, $Mo_{12}Q_{14}$, and $(Mo_3Q_3)_\infty$ was performed in the early stage [37], followed by a more extensive DFT calculations, which interrelated to the whole series $Mo_{3n}Q_{3n+2}$ ($n = 3$–8 and 10) [116]. The filling of all bonding orbitals leads to an optimal VEC of $(13n - 2)$ for even n (refer to the value of 24 for CP, with $n = 2$) and $(13n - 3)$ for odd n. Also, a large HOMO-LUMO gap is maintained in all these compounds [116, 117]. Then, depending on the filling of the MOs, i.e., the counter-cation stoichiometry, semimetallic [112] and semiconducting [107] behaviors were reported. As mentioned above, the latter compounds are subject of intensive research as thermoelectric materials. $InMo_9Se_{11}$ and $In_xMo_{15}Se_{19}$ ($x = 2$–3) were also evaluated for catalysis [118]. Many of these condensed cluster compounds exhibit superconductivity with T_c in the range 1.7–4 K [110]. In the example of $Tl_2Mo_6Se_6$ ($T_c = 2.2$ K), a very high anisotropy of the critical field was reported [119], as expected from its strongly anisotropic structure. Finally, some of these infinite chain-containing compounds $M_xMo_6Q_6$ (Q = Se, Te) were dispersed in polar solvents. The pristine material was recovered after evaporation, giving access to highly oriented films by brushing a thin layer of the solution in one direction onto a substrate: the longitudinal conductivity was five times larger than the transverse one [120].

Finally, it is noteworthy that Marcel Sergent also initiated with P. Gougeon the study of another type of condensed clusters, present in low-valence molybdenum oxides, where Mo_6 octahedra share their edges [121]. This family is very rich, and its development is still being pursued in Rennes [122].

7.2 *Mo_6 and Re_6 Cluster Compounds Derived from Chevrel Phases*

The Mo_6S_8 Chevrel Phase with 20 electrons per Mo_6 cluster is not stable and decomposes at 470°C [80]. Its stabilization can be obtained by adding up to 24 electrons to the Mo *4d* band, corresponding to the filling of the energy bands near the Fermi level. This can be achieved by substituting sulfur ligands by halogen ones in Mo_6S_8 or by replacing molybdenum atoms of the Mo_6 cluster by other atoms richer in valence electrons. M. Sergent developed this topic with C. Perrin and A. Perrin. More details are given in previous review papers [123, 124].

7.2.1 Mo_6 Cluster Chalcohalides

A consequence of the replacement of chalcogen by halogen in CPs, performed at high temperature (1,000–1,200°C), resulted in new stable Mo_6 chalcohalides where the VEC values ranged from 20 to 24. The first discovered and structurally characterized of these Mo_6 chalcohalides were $Mo_6Q_{8-x}X_x$ (X = halogen, Q = chalcogen, $0 < x \leq 2$) isostructural to Mo_6Q_8 [125]. In these chalcohalides, the cluster units are interconnected in the same way as in CPs by inner-apical chalcogen double bridges ($Q^{i\text{-}a}/Q^{a\text{-}i}$), while inner halogens lie on the 2*c* site located on the threefold axis of the unit. The channels that develop in the three directions of the lattice are empty [126]. When Q = S, definite compounds have been obtained with $x = 2$, namely, $Mo_6S_6Br_2$ and $Mo_6S_6I_2$. They are superconducting at $T_c \approx 14$ K, exactly like $PbMo_6S_8$, while Mo_6S_8 is superconducting only at a very low temperature. A previous ^{119}Sn Mössbauer study on $SnMo_6S_8$ ($T_c = 11$ K) suggested that the high T_c of CPs could be due in large part to the additional soft lattice mode associated with Sn in $SnMo_6S_8$ [127]. However, the high T_c reached by $Mo_6S_6Br_2$ and $Mo_6S_6I_2$ without any counter-cation in the channels ruled out this assertion. Finally it was assumed that it is essential that the halogen ligands occupy the 2*c* sites on the ternary axis in order to maintain the symmetry and then to maintain the twofold degeneracy of the *Eg*-band at the Fermi level [125]. In addition, these two chalcohalides have a VEC value of 22 as in $PbMo_6S_8$ ($T_c = 14$ K), confirming the importance of the VEC for the superconducting properties. As discussed by theoreticians, the 22 VEC value corresponds to a maximum of the density of states near the Fermi level [17].

When Q = Se or Te, solid solutions $Mo_6Q_{8-x}X_x$ were obtained with X = Cl, Br, I and $0 \leq x \leq 2$. T_c increases correlatively with the VEC value up to 7.0, 7.1, and 7.6 K for Q = Se and X = Cl, Br, and I, respectively (Fig. 13). Mo_6Te_8, not superconducting above 1 K, becomes superconducting after iodine substitution with a maximum $T_c = 2.6$ K for $Mo_6Te_6I_2$ [125].

Note that these compounds constituted the first molybdenum chalcohalides obtained at high temperatures, in contrast to the previous ones synthesized around 500°C, like MoS_2Cl_2, MoS_2Cl_3, $Mo_2Cl_5S_3$, or $Mo_3S_7Cl_4$ [128–130], where molybdenum has a higher oxidation state. These results opened the way to new families of stable, high-temperature Mo_6 chalcohalides, in which the 24 VEC Mo_6L_{14} (L = halogen or chalcogen) units are interconnected by shared inner and/or apical ligands as in the following examples. The three-dimensional $Mo_6X_{10}Q$ (X = Cl, Br and Q = S, Se, Te; X = I and Q = Se, Te), with $X^{a\text{-}a}$ interunit connections developing in the three directions of the space [131], are insulating and exhibit dielectric relaxations [132]. The one-dimensional $Mo_6X_8Q_2$ (X = Br and Q = S; X = I and Q = S, Se) develops infinite chains of units via $Q^{i\text{-}i}$ and $X^{a\text{-}a}$ bridges [133, 134]. They are insulating and exhibit as expected a dielectric anisotropy [132]. The semiconducting two-dimensional $Mo_6Br_6S_3$ is built up from chains similar to the ones observed in $Mo_6X_8Q_2$, but here the units are slightly tilted in the chains to establish interchain connections in the second direction of the space via inner-apical ligands ($S^{i\text{-}a}/S^{a\text{-}i}$) [135].

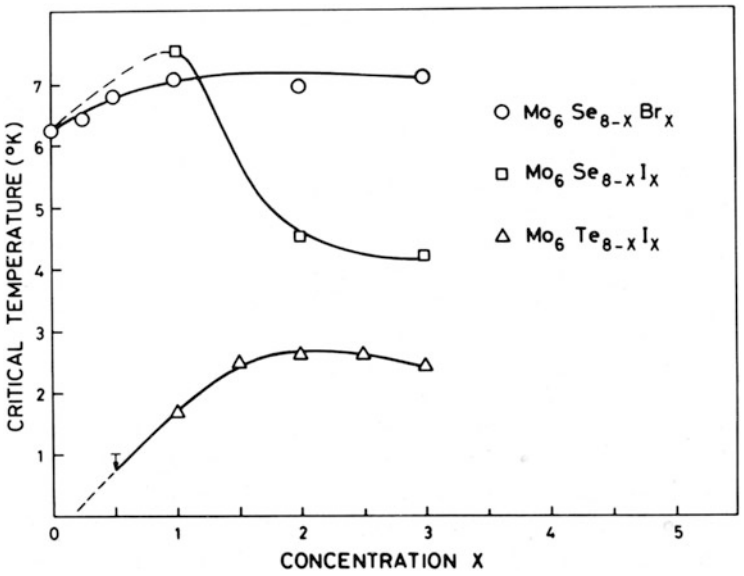

Fig. 13 Critical temperature T_c as a function of halogen concentration x for the solid solutions $Mo_6Se_{8-x}Br_x$, $Mo_6Se_{8-x}I_x$, and $Mo_6Te_{8-x}I_x$ [125]

7.2.2 Re_6 Cluster Chalcogenides and Chalcohalides

A second way to tune the VEC in CPs was to substitute (at least in part) Mo by a metal richer in electrons, such as Re [136] or either Ru or Rh [137]. All the compounds synthesized are isostructural with Mo_6Se_8. As selected examples, the solid solutions $Mo_2Re_4S_{8-x}Se_x$ ($0 \leq x \leq 8$) and $Mo_2Re_4Se_{8-x}Te_x$ ($0 \leq x \leq 1.2$) turned out to be a rare example of truly semiconducting CP, owing to the filling of energy band near the Fermi level by 24 valence electrons (Fig. 14) [136]. In the case of Te, the synthesis of $Mo_2Re_4Te_8$ failed, and in place, the diamagnetic $Mo_4Re_2Te_8$ was obtained. With a VEC of 22, it is a superconductor with $T_c = 3.55$ K (Fig. 14) and an initial slope of the upper critical field comparable to that of Mo_6Se_8 [136]. $Mo_4Re_2Te_8$ is – with the above-mentioned $Mo_6Te_6I_2$ – a rare example of a superconducting telluride Chevrel Phase. Note that a mixed cluster compound was also obtained with ruthenium: the 24 VEC semiconducting $Mo_4Ru_2Se_8$ [137]. Any attempt to obtain purely Re_6-based CP structure is of course unattainable because it would imply a VEC value higher than 24, corresponding to the filling of antibonding metal-metal orbitals.

Indeed, these results prompted M. Sergent and A. Perrin to start a systematic search for Re_6 chalcohalides built from Re_6L_{14} (L = halogen/chalcogen) units with various halogen/chalcogen ratios, with a VEC = 24. At the beginning, the system Re-Se-Cl was chosen, because it was particularly suitable for X-ray contrast of ligands. The first isolated compound was the lamellar $Re_6Se_8Cl_2$ where adjacent units are connected in a plane by four inner-apical ($Se^{i\text{-}a}/Se^{a\text{-}i}$) double bridges,

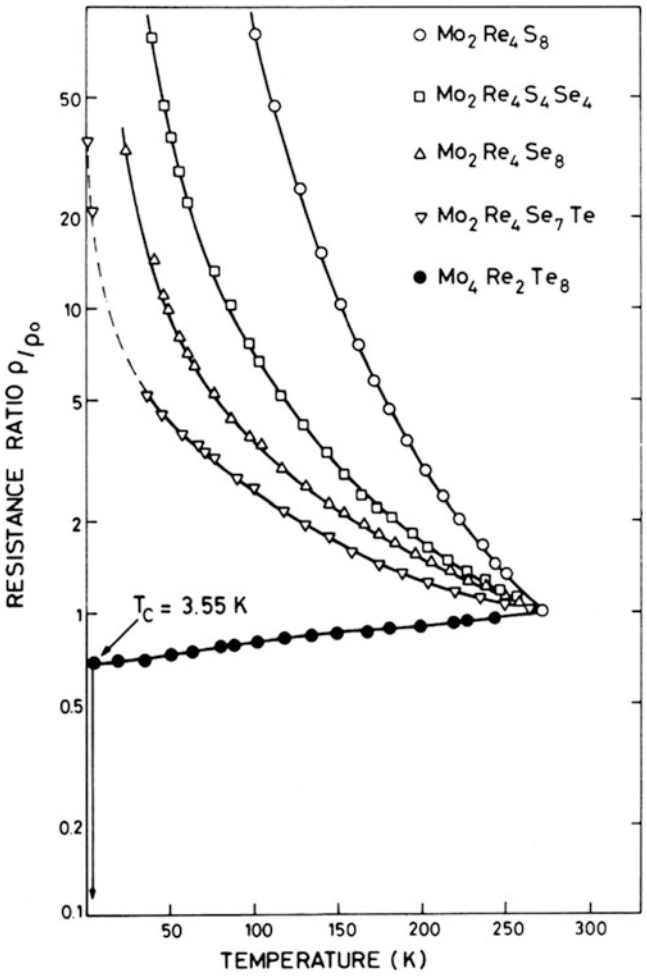

Fig. 14 Temperature dependence of the resistance ratio of the semiconducting $Mo_2Re_4S_8$, $Mo_2Re_4S_4Se_4$, $Mo_2Re_4Se_8$, and $Mo_2Re_4Se_7Te$ and the superconducting $Mo_4Re_2Te_8$ compounds [136]

exactly as in CPs, while in the third direction are terminal Cl^a ligands [138, 139]. It is a semiconductor with a resistivity ratio up to 10^2 at room temperature [140] and a bandgap of 1.42 eV [141]. Its discovery was followed by the series of definite compounds $Re_6Se_{8-n}Cl_{2+2n}$ ($n = 1$, 2, and 3) where the cluster units are linked by $Cl^{a\text{-}a}$ halogen bridges extending along 3, 2, and 1 direction, respectively. 0-D compounds were also obtained, namely, the neutral $Re_6Se_4Cl_{10}$ (i.e., $n = 4$) and the ionic compound $KRe_6Se_5Cl_9$ [139]. All these compounds are dielectrics [132], and some of them are isostructural with molybdenum analogues, while others display original structures.

This work was subsequently extended to brominated compounds, and a number of new structures were reported, for instance, $KRe_6S_5Br_9$ [142] or $Cs_4KRe_6S_8Br_7$ [143], if we restrict ourselves to the first reports. Many original arrangements were subsequently published, the detail of which can be found in review articles [123, 124, 144, 145]. Note that some ionic compounds with large counter-cations (viz., cesium) are readily soluble in various solvents [144] and then could act as starting materials for solution chemistry (see below). A review of the photoluminescent properties of Re_6 cluster-based compounds, in relation with theoretical calculations, is reported in the chapter of this volume entitled *Renium Hexanuclear Clusters: Bonding, Spectroscopy, and Applications of Molecular Chevrel Phases*.

7.3 The Beginning of Solution Chemistry of Octahedral Clusters

The CPs are obviously insoluble in any solvent, due to the strong intercluster bridging ligands. This is also the case of most of the cluster-based chalcohalides mentioned above. In contrast, several Mo_6 chalcohalides built from discrete Mo_6L_{14} units are slightly soluble [146], while the molybdenum halides $Cs_2Mo_6X_{14}$ (X = Br, I) appear as efficient precursors for solution chemistry [147]. The ionic $K_2Re_6Se_5Cl_9$ chalcohalide was reported to be slightly soluble in ethanol [148], but not enough to be effective synthetic reagent. Several approaches were proposed to improve the solubility of chalcohalides, in order to have available molecular precursors suitable for developing novel solution chemistry:

- Replace the inorganic counter-cation by an organic one, like tetrabutylammonium, via a metathesis reaction; this pioneering approach was used for the electro-crystallization of tetrathiafulvalene derivatives [149, 150].
- Replace the terminal ligands, either starting from an ionic compound or using an excision reaction; prominent examples include pyridines [151]; phosphines [152]; cyano [153–155], hydroxo [156, 157], or aquo groups [157, 158]; and dendrimers [159].

The availability of these precursors led to an intensive research program for making new hybrid compounds. Novel coordination compounds and self-organized structures resulted (refer, for instance, to the reviews [123, 124, 144, 155, 157]). Further examples can be found in the chapters of this volume entitled *Octahedral Chalcogenide Rhenium Clusters: From Solids to Isolated Cluster Complexes* and *Exploring the Breath of Terminal Ligands in* $[Mo_6X_8]^{4+}$ *and* $[Re_6Q_8]^{2+}$ *Based Cluster Complexes*.

8 Conclusion

In this chapter we summarized and highlighted the essential role of Marcel Sergent in the discovery and the development of what are now commonly described as the Chevrel Phases and the more general cluster chemistry he and his research group in Rennes developed after this discovery. Marcel Sergent received well-deserved and worldwide recognition for his outstanding initiation and participation in this research area. However, we should mention that this topic was only a small part of his scientific activities. For instance, he found another series of ternary molybdenum chalcogenides, namely, MMo_2Q_4, characterized by the presence of zigzag chains of molybdenum [160] and series of compounds based on tetrahedral clusters, like $Mo_4S_4Br_4$ [161] and MMe_4Q_8 (M = Al, Ga; Me = Mo, Nb, Ta, V, Re) [162, 163]. The work on Mo_6L_{14} and Re_6L_{14} clusters was completed by studies devoted to the Nb_6L_{18} and Ta_6L_{18} ones (see the chapter of this volume: *Inorganic Niobium and Tantalum Octahedral Cluster Halide Compounds with Three-dimensional Frameworks: A Review on their Crystallographic and Electronic Structures*). He started the study of Mo_6 edge-sharing condensed clusters, present in low-valence molybdenum oxides, as mentioned above [121]. He also initiated a research program on ternary phosphides and arsenides with metal chains and diamond-shaped clusters [164]. Last but not least, he was strongly involved in the study of high-T_c superconducting cuprates, taking advantage from the specific equipment he had previously implemented for the study of Chevrel Phases. The scientific inheritance of Marcel Sergent endures even after several decades. He paved the way for the present research, outside [165–171] and more especially in his original laboratory [122, 172–178], where his heirs have built new developments from his initial outstanding contributions to Chevrel Phases and, more generally, to cluster chemistry.

Marcel Sergent was a very effective research advisor, and we consider as a rare privilege to have worked with him during years. We are confident that all his past students and coworkers, in Rennes and outside, have the same feeling. We will keep in our mind the memory of this exceptional researcher and vey kind man. Finally, we would like to associate with this tribute to Marcel Sergent his close coworker and very good friend Ø. Fisher (1942–2013). The emergence of the Chevrel Phases was, in a large part, the fruit of their intense and non-lasting collaboration and friendship.

Acknowledgments The authors are very grateful to Marie-Jeanne Sergent, spouse of Marcel, and to Prof. Odile Sergent, his daughter, for giving access to helpful documents from their private collection.

References

1. Nakamura R (1998) Serial experiments lain. Manga cartoon, Tokyo
2. Fischer Ø, Mapple B (eds) (1982) Superconductivity in ternary compounds I. Topics in current physics. Springer, Berlin
3. Penã O (2015). Physica C 514:95

4. Sergent M (1969) Sur des Thiomolybdites, des Thiotungstites et des Thiochromites Alcalins. Thesis dissertation, University of Rennes, in French
5. Sergent M, Prigent J (1965). CR Acad Sci Paris 261:5135
6. Espelund AW (1967). Acta Chem Scand 21:839
7. Brosset C (1945). Arkiv Kemi Mineral Geol A 20:16
8. Schäfer H, von Schnering HG, Tillack J, Kuhnen F, Wöhrle H, Baumann H (1967). Z Anorg Allg Chem 353:281
9. Chevrel R (1974) Nouveaux composes sulfurés ternaires du molybdène de basse valence, présentant des liaisons molybdène-molybdène sous forme de chaînes ou de clusters octaédriques. Thesis dissertation, University of Rennes, in French
10. Chevrel R, Sergent M, Prigent J (1971). J Solid State Chem 3:515
11. Cotton FA (1964). Inorg Chem 3:1217
12. Bars O, Sergent M, Grandjean D (1970). C R Acad Sci Paris Ser C 270:1233
13. Sergent M, Chevrel R (1973). J Solid State Chem 6:433
14. Fischer Ø, Treyvaud A, Chevrel R, Sergent M (1975). Solid State Commun 17:721
15. Sergent M, Chevrel R, Rossel C, Fischer Ø (1978). J Less-Common Met 58:179
16. Noël H, Chevrel R, Sergent M (1981) Actinides 1981, Los-Angeles, CA, 10–15 Sept 1981
17. Fischer Ø (1978). Appl Phys 16:1
18. Bars O, Guillevic J, Grandjean D (1973). J Solid State Chem 6:48
19. Opalovskii AA, Fedorov VE (1966). Izv Acad Nauk SSSR Neorg Mater 2:443
20. Swanson HE, Tatge E (1953). Natl Bur Standards Circ (U S) 539:1–95
21. Schäfer H, von Schnering HG (1964). Angew Chem 20:833
22. Bars O, Guillevic J, Grandjean D (1973). J Solid State Chem 6:335
23. Guillevic J, Bars O, Grandjean D (1973). J Solid State Chem 7:158
24. Marezio M, Dernier PD, Remeika JP, Corenzwit E, Matthias BT (1973). Mater Res Bull 8:657
25. Guillevic J, Lestrat H, Grandjean D (1976). Acta Cryst B32:1342
26. Yvon K, Paoli A, Flükiger R, Chevrel R (1977). Acta Cryst B33:3066
27. Crossman LD, Olsen DP, Duffey GH (1963). J Chem Phys 38:73
28. Cotton FA, Hass TE (1964). Inorg Chem 3:10
29. Kettle SFA (1965). Theor Chim Acta 3:211
30. Guggenberger LJ, Sleight AW (1969). Inorg Chem 8:2041
31. Yvon K, Paoli A (1977). Solid State Commun 24:41
32. Corbett JD (1981). J Solid State Chem 39:56
33. Andersen OK, Klose W, Nohl H (1978). Phys Rev B17:1209
34. Mattheis LF, Fong CY (1977). Phys Rev B15:1760
35. Bullett DW (1977). Phys Rev Lett 39:664
36. Jarlborg T, Freemann AJ (1980). Phys Rev Lett 44:178
37. Hughbanks T, Hoffmann R (1983). J Am Chem Soc 105:1150
38. Certain D, Le Beuze A, Lissillour R (1983). Solid State Commun 46:7
39. Certain D, Lissillour R (1986). Z Phys D 3:411
40. Matthias BT, Marezio M, Corenzwit E, Cooper AS, Barz HE (1972). Science 175:1465
41. Lawson AC (1972). Mater Res Bull 7:773
42. Fischer Ø, Odermatt R, Bongi G, Jones H, Chevrel R, Sergent M (1973). Phys Lett 45A:87
43. Chevrel R, Sergent M, Fischer Ø (1975). Mater Res Bull 10:1169
44. Odermat R, Fischer Ø, Jones H, Bongi G (1974). J Phys C 7:L13
45. Fischer Ø, Jones H, Bongi G, Sergent M, Chevrel R (1974). J Phys C 7:L450
46. Fischer Ø, Descroux M, Roth S, Chevrel R, Sergent M (1975). J Phys C 8:L474
47. Descroux M, Fischer Ø, Flükiger R, Seeber B, Delesclefs R, Sergent M (1978). Solid State Commun 25:393
48. Fischer Ø (1974) Proceedings in the conference of physics in high magnetic fields, Grenoble
49. Ishikawa M, Fischer Ø (1977). Solid State Commun 23:37
50. Chevrel R, Hirrien M, Sergent M (1986). Polyhedron 5:87

51. Meul HW, Rossel C, Descroux M, Fischer Ø, Remenyi G, Briggs A (1984). Phys Rev Lett 53:497
52. Decroux M, Fischer Ø, Chevrel R (1977). Cryogenics 17:291
53. Hirrien M, Chevrel R, Sergent M, Dubots P, Genevey P (1987). Mater Lett 5:173
54. Chevrel R, Hirrien M, Sergent M, Couach M, Dubots P, Genevey P (1989). Mater Lett 7:425
55. Decroux M, Selvam P, Cors J, Seeber B, Fischer Ø, Chevrel R, Rabiller P, Sergent M (1993). IEEE Trans Appl Supercond 3:1502
56. Cheggour N, Decroux M, Gupta A, Fischer Ø, Perenboom JAAJ, Bouquet V, Sergent M, Chevrel R (1998). J Appl Phys 81:6277
57. Chevrel R, Sergent M, Le Lay L, Padiou J, Peña O, Dubots P, Genevey P, Couach M, Vallier J-C (1988). Rev Phys Appl 23:1777
58. Banks CK, Kammerdiner L, Luo HL (1975). J Solid State Chem 15:271
59. Alterovitz SA, Woollam JA, Kammerdiner L, Luo HL (1977). Appl Phys Lett 31:233
60. Ohtaki R, Zao BR, Luo HL (1984). J Low Temp Phys 54:119
61. Webb RJ, Goldman AM, Kang JH, Maps J, Schmidt MF (1985). IEEE Trans Magn 21:835
62. Przyslupski P, Horyn R, Szymaszek J, Gren B (1978). Solid State Commun 28:869
63. Hertel GB, Orlando TP, Tarascon JM (1985). Physica B 135:168
64. Quéré Y, Perrin A, Padiou J, Perrin C, Seignac A, Horyn R, Sergent M (1984). Ann Chim 7-8:1065
65. Quéré Y, Perrin A, Horyn R, Sergent M (1985). Mater Lett 3:340
66. Lemée N, Guilloux-Viry M, Padiou J, Sergent M, Lesueur J, Lalu F (1997). Solid State Commun 101:909
67. Boursicot S, Bouquet V, Péron I, Guizouarn T, Potel M, Guilloux-Viry M (2012). Solid State Sci 14:719
68. Hinode H, Yamamoto S, Wakihara M, Taniguchi M (1985). Mater Res Bull 20:611
69. Perrin A, Perrin C, Chevrel R, Sergent M, Brochu R, Padiou J (1973) In: Groupe Français de Croissance Cristalline (ed) Cristallogénèse Expérimentale, pp 141–148
70. Krabbes G, Oppermann H (1981). Z Anorg Allg Chem 481:13
71. Horyn R, Peña O, Sergent M (1985). J Less-Common Met 105:55
72. Hauck J (1977). Mater Res Bull 12:1015
73. Flükiger R, Devantay M, Jorda JL, Muller J (1977). IEEE Trans Magn MAG-13:818
74. Takei H, Takahashi T, Miura T (1984). Jpn J Appl Phys 23:420
75. Govinda Rajan K, Chandra Shekar NV, Viswanath RN, Ramasamy S (1989). J Phys D 22:1205
76. Holtzberg F, LaPlaca SJ, McGuire TR, Webb RA (1984). J Appl Phys 55:2013
77. Horyn R, Peña O, Geantet C, Sergent M (1989). Supercond Sci Technol 2:71
78. Peña O, Sergent M (1989). Prog Solid State Chem 19:165
79. Le Berre F, Hamard C, Peña O, Wojakowski A (2000). Inorg Chem 39:1100
80. Chevrel R, Sergent M, Prigent J (1974). Mater Res Bull 9:1487
81. Schöllhorn R, Kümpers M, Besenhard JO (1977). Mater Res Bull 12:781
82. Takeda Y, Kanno R, Noda M, Yamamoto O (1985). Mater Res Bull 20:71
83. Boulanger C, Lecuire J-M (1987). Electrochim Acta 32:345
84. Wakihara M, Uchida T, Suzuki K, Taniguchi M (1989). Electrochim Acta 34:867
85. Wakihara M, Uchida T, Morishita T, Wakamatsu H, Taniguchi M (1987). J Power Sources 20:199
86. Tarascon JM, Disalvo FJ, Murphy DW, Hull GW, Rietman EA, Waszczak J (1984). J Solid State Chem 54:204
87. McKinnon WR, Dahn JR (1984). Solid State Commun 52:245
88. Lemée N, Guilloux-Viry M, Ferré V, Perrin A, Sergent M, Lesueur J, Lalu F (1997). J Alloys Compd 262–263:54
89. Kaidi Z, Boulanger C, Lecuire JM, Lemée N, Guilloux-Viry M, Perrin A (1999). Solid State Sci 1:623

90. Aurbach D, Lu Z, Schechter A, Gofer Y, Gizbar H, Turgeman R, Cohen Y, Moshkovich M, Levi E (2000). Nature 407:724
91. Saha P, Datta MK, Velikokhatnyi OI, Manivannan A, Alman D, Kumta PN (2014). Prog Mater Sci 66:1
92. McCarty KF, Schräder GL (1984). Ind Eng Chem Prod Res Dev 29:519
93. Rabiller-Baudry M, Sergent M, Chevrel R (1991). Mater Res Bull 26:519
94. Rabiller-Baudry M, Chevrel R, Sergent M (1992). J Alloys Compd 178:441
95. Even-Boudjada S, Burel L, Chevrel R, Sergent M (1998). Mater Res Bull 33:419
96. Harel-Michaud V, Pesnel-Leroux G, Burel L, Chevrel R, Geantet C, Cattenot M, Vrinat M (2001). J Alloys Compd 317–318:195
97. Kamiguchi S, Takeda K, Kajio R, Okumura K, Nagashima S, Chihara T (2013). J Clust Sci 24:559
98. Kamiguchi S, Arai K, Okumura K, Iida H, Nagashima S, Chihara T (2015). Appl Catal A 505:417
99. Slack GA (1995) In: Rowe DM (ed) CRC handbook of thermoelectrics. Chemical Rubber, Boca Raton. Chap. 34
100. Umarji AM, Subba Rao GV, Janawadkar MP, Radhakrishnan TS (1980). J Phys Chem Solids 41:421
101. Vasudeva Rao V, Rangarajan G, Srinivasan R (1984). J Phys F 14:973
102. Nunes RW, Mazin II, Singh DJ (1999). Phys Rev B 59:7969
103. Roche C, Chevrel R, Jenny A, Pecheur P, Scherrer H, Scherrer S (1999). Phys Rev B 60:16442
104. Caillat T, Fleurial J-P (1998). J Phys Chem Solids 59:1139
105. Caillat T, Fleurial J-P, Snyder GJ (1999). Solid State Sci 1:535
106. Zhou T, Lenoir B, Candolfi C, Dauscher A, Gall P, Gougeon P, Potel M, Guilmeau E (2011). J Electron Mater 40:508
107. Masschelein P, Candolfi C, Dauscher A, Gendarme C, Rabih ARAO, Gougeon P, Potel M, Gall P, Gauthier R, Lenoir B (2018). J Alloys Compd 739:360
108. Chevrel R, Sergent M, Seeber B, Fischer Ø, Grüttner A, Yvon K (1979). Mater Res Bull 14:567
109. Potel M, Chevrel R, Sergent M, Decroux M, Fischer Ø (1979). CR Acad Sci Ser C 288:429
110. Gougeon P, Potel M, Sergent M, Monceau P (1985). Physica B 135:386
111. Chevrel R, Gougeon P, Potel M, Sergent M (1985). J Solid State Chem 57:25
112. Gougeon P, Potel M, Padiou J, Sergent M (1983). CR Acad Sci Ser II 296:351
113. Picard S, Gougeon P, Potel M (1999). Angew Chem Int Ed 13–14:2034
114. Gougeon P, Potel M, Sergent M (1989). Acta Cryst C 45:182
115. Gougeon P, Potel M, Sergent M (1990). Acta Cryst C 46:2284
116. Gautier R, Gougeon P, Halet J-F, Potel M, Saillard J-Y (1997). J Alloys Compd 262–263:311
117. Al Rahal Al Orabi R, Boucher B, Fontaine B, Gall P, Candolfi C, Lenoir B, Gougeon P, Halet JF, Gautier R (2017). J Mater Chem C 5:12097
118. Kareem SA, Miranda R (1989). J Mol Catal 53:275
119. Armici JC, Decroux M, Fischer Ø, Potel M, Chevrel R, Sergent M (1980). Solid State Commun 33:607
120. Tarascon JM, Disalvo FJ, Chen CH, Carroll PJ, Walsh M, Rupp L (1985). J Solid State Chem 58:290
121. Gougeon P, Potel M, Sergent M (1990). Acta Cryst C 46:1188
122. Gall P, Gougeon P (2016). Acta Cryst E 72:995
123. Perrin A, Perrin C (2011). Eur J Inorg Chem 26:3848
124. Perrin A, Perrin C (2012). C R Chim 15:815
125. Sergent M, Fischer Ø, Decroux M, Perrin C, Chevrel R (1977). J Solid State Chem 22:87
126. Perrin C, Chevrel R, Sergent M, Fischer Ø (1979). Mater Res Bull 14:1505
127. Kimball CW, Weber L, Van Landuyt G, Fradin FY, Dunlap BD, Shenoy GK (1976). Phys Rev Lett 36:412
128. Rannou J-P, Sergent M (1967). C R Acad Sci Ser C 265:734

129. Opalovski AA, Fedorov VE, Khaldoyanidi KA (1968). Dokl Akad Nauk SSSR 182:1095
130. Marcoll J, Rabenau A, Mootz D, Wunderlich H (1974). Rev Chim Mineral 11:607
131. Perrin C, Sergent M, Le Traon F, Le Traon A (1978). J Solid State Chem 25:197
132. Pilet JC, Le Traon F, Le Traon A, Perrin C, Perrin A, Leduc L, Sergent M (1985). Surf Sci 156:359
133. Perrin C, Sergent M (1983). J Chem Res 2:38
134. Perrin C, Sergent M (1983). J Chem Res 38:449
135. Perrin C, Potel M, Sergent M (1983). Acta Cryst 39C:415
136. Perrin A, Sergent M, Fischer Ø (1978). Mater Res Bull 13:259
137. Perrin A, Chevrel R, Sergent M, Fischer Ø (1980). J Solid State Chem 33:43
138. Perrin A, Sergent M (1980). Bull Soc Chim Fr 11–12:66
139. Leduc L, Perrin A, Sergent M (1983). C R Acad Sci Paris Ser II 296:961
140. Leduc L, Padiou J, Perrin A, Sergent M (1983). J Less-Common Met 95:73
141. Le Nagard N, Perrin A, Sergent M, Levy-Clement C (1985). Mater Res Bull 20:835
142. Slougui A, Perrin A, Sergent M (1992). Acta Cryst C 48:1917
143. Slougui A, Ferron S, Perrin A, Sergent M (1996). Eur J Solid State Inorg Chem 33:1001
144. Pilet G, Perrin A (2005). C R Chim 8:1728
145. Gabriel J-CP, Boubekeur K, Uriel S, Batail P (2001). Chem Rev 101:2037
146. Kirakci K, Cordier S, Hernandez O, Roisnel T, Paul F, Perrin C (2005). J Solid State Chem 178:3117
147. Kirakci K, Cordier S, Perrin C (2005). Z Anorg Allg Chem 631:411
148. Perrin A (1990). New J Chem 14:561
149. Ouahab L, Batail P, Perrin C, Garrigou-Lagrange C (1986). Mater Res Bull 21:1223
150. Batail P, Ouahab L, Penicaud A, Lenoir C, Perrin A (1987). C R Acad Sci Ser II 304:1111
151. Hilsenbeck SJ, Young Jr VG, McCarley RE (1994). Inorg Chem 33:1822
152. Zheng Z, Long JR, Holm RH (1997). J Am Chem Soc 119:2163
153. Mironov YV, Virovets AV, Fedorov VE, Podberezkaya NY, Shishkin OV, Struchkov YT (1995). Polyhedron 14:3171
154. Slougui A, Mironov Y, Perrin A, Fedorov V (1995). Croat Chem Acta 68:885
155. Cordier S, Naumov NG, Salloum D, Paul F, Perrin C (2004). Inorg Chem 43:219
156. Yarovoi SS, Mironov YV, Naumov DY, Gatilov YV, Kozlova SG, Kim SJ, Fedorov VE (2005). Eur J Inorg Chem 2005:3945
157. Kim Y, Fedorov VE, Kim SJ (2009). J Mater Chem 19:7178
158. Fedin VP, Virovets AA, Sykes AG (1998). Inorg Chim Acta 271:228
159. Cordier S, Kirakci K, Pilet G, Méry D, Astruc D, Perrin A, Perrin C (2005). Prog Solid State Chem 33:81
160. Chevrel R, Sergent M, Prigent J (1968). C R Acad Sci 267:1135
161. Perrin C, Chevrel R, Sergent M (1975). C R Acad Sci Ser C 281:23
162. Perrin C, Chevrel R, Sergent M (1975). C R Acad Sci Ser C 280:949
163. Ben Yaich H, Jegaden JC, Potel M, Sergent M, Rastogi AK, Tournier R (1984). J Less-Common Met 102:9
164. Guérin R, Sergent M, Prigent J (1972). CR Acad Sci 274:1278
165. Geng L, Scheifers JP, Zhang J, Bozhilov KN, Fokwa BPT, Guo J (2018). Chem Mater 30:8420
166. Agiorgousis ML, Sun Y-Y, West D, Zhang S (2018). ACS Appl Energy Mater 1:440
167. Mao M, Gao T, Hou S, Wang C (2018). Chem Soc Rev 47:8804
168. Ojha K, Banerjee S, Sharma M, Dagar P, Ganguli AK (2018). Bull Mater Sci 41:119
169. Richard J, Benayad A, Colin J-F, Martinet S (2017). J Phys Chem C 121:17096
170. Yue J, Zhu X, Han F, Fan X, Wang L, Yang J, Wang C (2018). ACS Mater Interfaces 10:39645
171. Zhong X, Lee K, Choi B, Meggiolaro D, Liu F, Nuckolls C, Pasupathy A, De Angelis F, Batail P, Roy X, Zhu X (2018). Nano Lett 18:1483

172. Boursicot S, Bouquet V, Bombard A, Langer M, Boulanger C, Guilloux-Viry M (2017). Electrochem Acta 257:436
173. Gannon L, Boeri L, Howard CA, Gougeon P, Gall P, Potel M, Salloum D, Petrovic AP, Hoesch M (2018). Phys Rev B 98:014104
174. Camerel F, Kinloch F, Jeannin O, Robin M, Nayak SK, Jacques E, Brylev KA, Naumov NG, Molard Y (2018). Dalton Trans 47:10884
175. Guy K, Ehni P, Paofai S, Forschner R, Roiland C, Amela-Cortes M, Cordier S, Laschat S, Molard Y (2018). Angew Chem Int Ed 57:11692
176. Pellen-Mussi P, Tricot-Doleux S, Neaime C, Nerambourg N, Cabello-Hurtado F, Cordier S, Grasset F, Jeanne S (2018). J Nanosci Nanotechnol 18:3148
177. Gandubert A, Amela-Cortes M, Nayak SK, Vicent C, Meriadec C, Artzner F, Cordier S, Molard Y (2018). J Mater Chem 6:2556
178. Barbosa J, Prestipino C, Hernandez OJ, Paofai S, Dejoie C, Guilloux-Viry M, Boulanger C (2019). Inorg Chem 58:2158

Struct Bond (2019) 180: 31–74
DOI: 10.1007/430_2019_33

Published online: 28 April 2019

Octahedral Chalcogenide Rhenium Clusters: From Solids to Isolated Cluster Complexes

Vladimir E. Fedorov and Nikolay G. Naumov

Contents

V. E. Fedorov (✉) and N. G. Naumov
Nikolaev Institute of Inorganic Chemistry, Siberian Branch of the Russian Academy of Sciences, Novosibirsk, Russian Federation

Novosibirsk State University, Novosibirsk, Russian Federation
e-mail: fed@niic.nsc.ru

Abstract This review summarizes the numerous studies on the chemistry of molybdenum and rhenium octahedral chalcogenide cluster compounds carried out over the years at the Nikolaev Institute of Inorganic Chemistry in collaboration with international research groups. A pathway from classical solid-state cluster compounds Mo_6Se_8, Re_6Te_{15}, and $K_4Re_6S_{12}$, influenced by the French school of solid-state cluster chemistry, to soluble molecular complexes with Re_6Q_8 and Mo_6Q_8 cluster cores is provided. Both inorganic and organic ligands can be grafted onto cluster cages, resulting in a drastic change in the charge and properties of such complexes.

Keywords Cluster · Complex · Crystal structure · Luminescence · Molybdenum · Rhenium · Solid state

1 Introduction

For a long time, the classical Werner's theory served as the fundamental base of coordination chemistry. However, in the mid-1960s of the last century, this one-center theory underwent a certain "crisis." In 1964, Cotton [1, 2] introduced the term "metal atom cluster compounds," which defined groups of polynuclear metal complexes with direct metal–metal bonds. In subsequent decades, the chemistry of cluster compounds has been developing very intensively; the studies were carried out in two, largely independent directions, namely, in solid-state chemistry and in solution chemistry. In these years, M. Sergent and colleagues have studied the solid-state chemistry of transition metal compounds (niobium, molybdenum, etc.) [3, 4]. The systematic study of ternary systems M–Mo–S (where M = Sn, Pb, and other metals) led to the discovery of new ternary molybdenum chalcogenides containing octahedral metal cluster units Mo_6S_8 (Fig. 1). The crystal structures and precise compositions of these compounds were determined later.

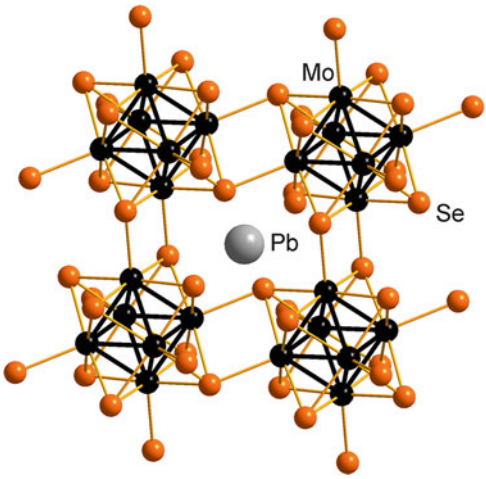

Fig. 1 Structural motif of $PbMo_6S_8$

This structural type can be considered as a prototype of the wide group of related ternary compounds MMo_6Q_8 (M = Pb, Sn, and other metals; Q = S or Se), which are now named in literature as "Chevrel phases," in honor of Marcel Sergent's then-PhD student Roger Chevrel [3]. These ternary chalcogenides were investigated very intensively in connection with their superconducting properties: for that period of time, some compounds of this type showed critical temperatures of about 15 K and record-breaking critical fields (about 60 Teslas) [5]. Today, the term "Chevrel phases" is included in educational and encyclopedic editions, along with Zintl phases, Laves phases, etc. Further development of the work of this group led to the synthesis of other new cluster solids with different nuclearities, including heterometallic clusters [6–13].

At the same time, the research on transition metal chalcogenides was initiated at Nikolaev Institute of Inorganic Chemistry (NIIC), Novosibirsk, Russia. The study of Mo/Se and Mo/Te systems has revealed that the lowest molybdenum selenide and telluride had analytical compositions of Mo_3Q_4 (Q = Se, Te) [14–17]. Later, single crystal X-ray diffraction showed that crystal structures of these binary chalcogenides contain octahedral metal clusters Mo_6Q_8 with the structural motif as in MMo_6Q_8 phases and, hence, they should be described as Mo_6Q_8.

A systematic investigation of binary rhenium chalcogenides has led to the discovery of a new rhenium telluride Re_2Te_5 [18]. Later, structural study proved its cluster nature: the compound comprises octahedral metallocluster core Re_6Te_8, similar to those in Chevrel phases. These cores Re_6Te_8 are linked in a three-dimensional array by unusual polytelluride Te_7 ligands (Fig. 2) [19].

In 1978, W. Bronger has described successively the synthesis and crystal structures of three new ternary rhenium cluster solids. Alkali metal carbonates reacted with elemental rhenium in an H_2S atmosphere at 800°C, producing $Cs_4Re_6S_{13}$, $K_4Re_6S_{12}$, and $Na_2Re_6S_{15}$. Structure investigations on single crystals showed that six rhenium atoms formed an almost regular octahedron with Re–Re distances of 2.61 Å. The eight sulfur atoms are arranged over the octahedron surface. Further S atoms or S_2 groups couple the $[Re_6S_8]$ units via the Re atoms (Fig. 3). The alkali

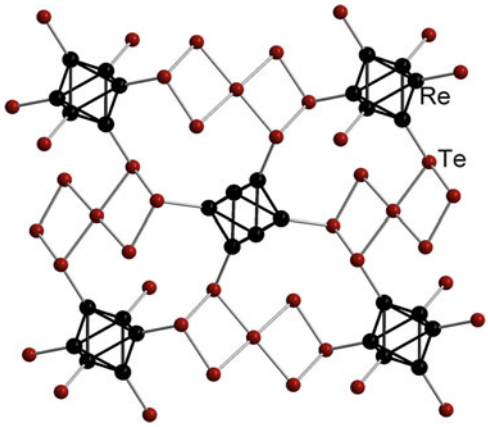

Fig. 2 Linking of cluster cores $\{Re_6Te_8\}$ through polytelluride Te_7 ligands in the structure of Re_6Te_{15}. Inner μ_3-Te atoms are omitted

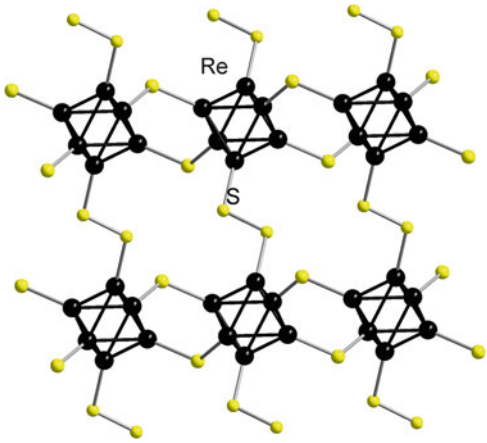

Fig. 3 Structure of the $\{[Re_6S_8]S_{4/2}(S_2)_{2/2}\}^{4-}$ network in $K_4Re_6S_{12}$. Inner μ_3-S atoms are omitted

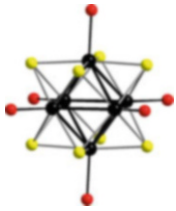

Fig. 4 Representation of the octahedral face-capped $[(M_6Q^i_8)L^a_6]$ unit

metal cations are intercalated in interstices of these skeletal structures [20, 21]. These findings opened the way toward a wide family of molybdenum and rhenium octahedral chalcogenide clusters.

Octahedral chalcogenide molybdenum and rhenium cluster compounds possess a typical structure with face-capped units $[M_6Q_8L_6]$. As sketched in Fig. 4, M_6 clusters are face-capped by eight inner ligands μ_3-Q and six inorganic and/or organic apical ligands L giving $[M_6Q_8L_6]$ complexes (M = Mo, Re, Q = S, Se, Te). The intrinsic properties of M_6 cluster complexes depend on the nature of the metal, the number of cluster valence electrons (CVE), and the nature of Q and L ligands. As we can see from Fig. 4, M_6 clusters in molecular complexes $[M_6Q_8L_6]$ have 14 ligands.

The 1995–2000 period of time has seen the development of various chemical modification methods suggested by different research groups, including both traditional exchange reactions of the outer ligands and atom substitutions in the positions of the cluster core resulting in heterometallic clusters (selected references: [22–29]).

In the present short contribution, we do not aim at giving a comprehensive survey of all research executed in the field of chemistry of molybdenum and rhenium chalcogenide octahedral clusters over the last years. This field of chemistry is well covered in numerous excellent reviews [30–38]. Here, we only focus on some fundamental results, obtained mainly at our Institute (NIIC) and in cooperation with colleagues from different scientific centers. Below, we present the most relevant examples of the excision reactions from cluster solids, assembly of new

molybdenum and rhenium clusters, as well as examples of "assembling" new cluster polymers from molecular complexes.

2 High-Temperature Reactions

2.1 *General Approach for the Synthesis of Octahedral Molybdenum and Rhenium Octahedral Chalcogenide Clusters*

To date, key octahedral molybdenum and rhenium cluster chalcogenides are synthesized by high-temperature reactions. Exceptions are scarce. The general approach is based on the thermodynamic stability of cluster solids at certain experimental conditions. Thus, they can be obtained from various initial compounds taken in the required stoichiometry. These may be either simple substances or their compounds, for example, chalcogenides and metal chalcohalides. For instance, Fig. 5 illustrates some possible strategies for the synthesis of $Re_6Se_4Br_{10}$.

A typical experimental technique for the synthesis of metal cluster chalcogenides may be outlined as follows: the initial reagents are loaded into a quartz ampoule; the ampoule is evacuated and then sealed. The sealed ampoule is placed in an oven and heated according to a selected regime. To complete the reaction, the mixture is kept at a chosen temperature for a required time, normally, tens of hours or several days.

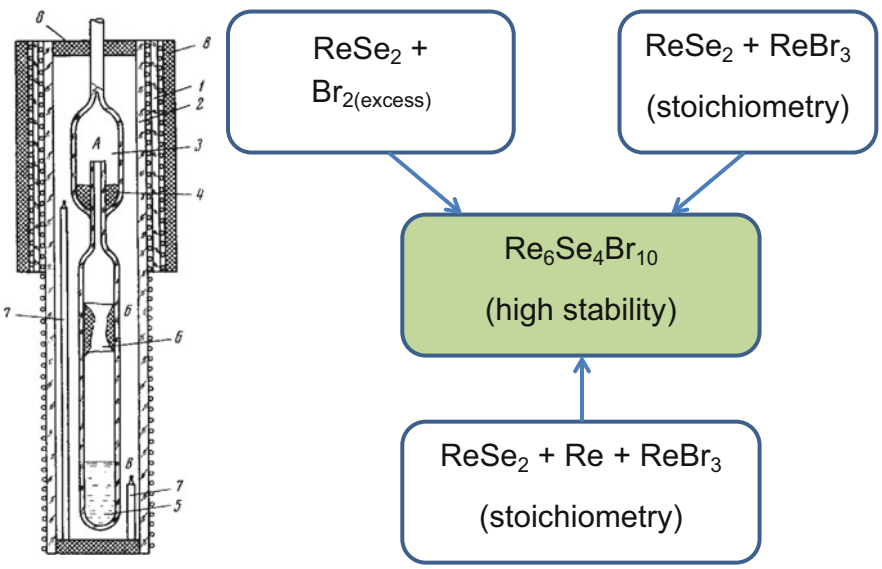

Fig. 5 Synthetic strategies to octahedral rhenium cluster complex $Re_6Se_4Br_{10}$

These cluster compounds usually possess polymeric structures with intercluster covalent bonding, translating into insolubility in water and organic solvents and low reactivity. Thus, their chemical properties remained poorly understood for a long time. A breakthrough in this area came after the discovery of the ways to transfer polymeric cluster arrays into soluble forms [23, 26]. In NIIC, some original approaches have been developed to convert insoluble polymeric cluster compounds into molecular soluble cluster complexes. Further progress in the study of the octahedral molybdenum and rhenium cluster chalcogenides is associated with solution chemistry.

2.2 Excision Reactions

As noted above, progress in the chemistry of molybdenum and rhenium chalcogenide octahedral clusters to a large degree is associated with solution chemistry. In particular, we have developed several simple and effective methods for converting the extended cluster compounds into soluble forms using reactions with molten KCN and KOH.

Historically, the first studied process was the reaction of Re_6Te_{15} with a melt of potassium thiocyanate KSCN at 600°C that gave the complex $[Re_6Te_2S_6(CN)_6]^{4-}$ [26, 39]. Such result can be explained based on thermal properties of KSCN, namely, potassium thiocyanate melts incongruently with the formation of KCN, potassium polysulfide, and sulfur. So, more nucleophilic sulfur atoms substitute tellurium in the cluster core $[Re_6Te_8]$, and CN ligands coordinate to rhenium atoms forming the cyanide complex $[Re_6Te_2S_6(CN)_6]^{4-}$. In subsequent experiments, we used melts of pure KCN or NaCN for synthesis of cyanide cluster complexes. Molten alkali metal cyanides constitute a fruitful media for excision reactions or assembling new clusters from binary compounds, owing to the combination of their high thermal stability, nucleophilicity of CN^- ions, as well as unique kinetic and hydrolytic stability of formed cluster cyanides (characteristic to all cyanides). For example, the reaction of Re_6Te_{15} with molten sodium or potassium cyanide at 550–650°C leads to the formation of sodium or potassium salt, respectively, of the anionic complex $[Re_6Te_8(CN)_6]^{4-}$ [26, 39, 40]:

$$Re_6Te_{15} + 6\ MCN = M_4\left[Re_6Te_8(CN)_6\right] + M_2Te_x + 7 - x\ Te\ (M = Na\ or\ K)$$

The reaction proceeds with a high yield by breaking of the polytelluride bridges, while retaining the cluster core. In literature, related processes are often referred to as cluster core excision reactions. Polymeric $Re_6Q_8Br_2$ (Q = S or Se) serves as a source of $Re_6Q_8^{2+}$ core for preparation of $[Re_6Q_8(CN)_6]^{4-}$ (Q = S, Se) [26, 41] in similar reactions with molten KCN or NaCN. All obtained anionic complexes $[Re_6Q_8(CN)_6]^{4-}$ are stable in aqueous and organic media and undergo reversible one-electron oxidation to $[Re_6Q_8(CN)_6]^{3-}$. To date, the cyano complexes

$[Re_6Te_8(CN)_6]^{4-/3-}$ are the only soluble complexes with $\{Re_6Te_8\}^{2+/3+}$ cluster core [40, 42]. Molybdenum cluster polymers – Chevrel phases Mo_6Se_8 and $ZnMo_6S_8$ – may also react with molten alkali cyanides giving molecular soluble complexes $[Mo_6Q_8(CN)_6]^{7-}$ (Q = S, Se) [43, 44].

It was found that the cluster cyanide complexes possess high hydrolytic stability. Their another promising and widely utilized property is the ability of ambidentate CN ligands to further coordination that makes such complexes good building blocks in the synthesis of complex structures, as a rule, of a polymeric nature. In particular, chalcocyanide cluster complexes were extensively utilized as building blocks for new generation of expanded Prussian blue-type framework solids and other extended networks and cluster-supported compounds. This research area will be discussed further.

Another simple and efficient approach to soluble $[Re_6Q_8]$ clusters is the excision reaction with molten KOH or CsOH to produce molecular octahedral cluster hexahydroxocomplexes $[Re_6Q_8(OH)_6]^{4-}$ [45, 46]. For example, the reaction of polymeric $Re_6Q_8Br_2$ (Q = S or Se) with molten KOH results in potassium salt of $[Re_6Q_8(OH)_6]^{4-}$ with a high yield. In this reaction, the highly nucleophilic OH ligands break both Re–Br–Re and rhombic Re_2-$(\mu_4$-Q$)_2$ bonds.

One more interesting and important reaction is the treatment of polymeric $Cs_4Re_6S_8(S)_{2/2}(CN)_4$ with aqueous KOH that leads to cleavage of intercluster S bridges in the structure and formation of ionic *trans*-$[Re_6S_8(CN)_4(OH)_2]^{4-}$ cluster complexes [47, 48].

2.3 *Formation of New Cluster Solids via High-Temperature Reactions with Molten Cyanides*

Along with excision reaction, it was found that the reaction of binary chalcogenides ReQ_2 (Q = S or Se) with molten KCN or NaCN is a very efficient way to prepare new cluster compounds. The reactions of ReS_2 or $ReSe_2$ with molten cyanides yield octahedral clusters of M_6Q_8-type. In this process, reduction of transition metal cations M^{4+} by CN^- anions takes place. Cyanide ions, as suggested, have been oxidized and transformed to a gaseous cyanogen $(CN)_2$ or amorphous solid paracyanogen $(CN)_n$. It is especially valuable that the practically simple method for obtaining cluster compounds in the melt of cyanides was found to be applicable for the synthesis of several complexes with different cluster cores, namely, $K_6[Mo_6Se_8(CN)_5]$ [49], $Cs_4[Re_6S_9(CN)_4]$ [50], $K_4[Re_6S_{10}(CN)_2]$ [51], $K_4[Re_6Se_{10}(CN)_4]$ [51], and $K_8[Re_{12}CS_{17}(CN)_6]$ [52]. For example, reaction of ReS_2 with KCN at elevated temperature leads to the formation of the layered compound $K_4Re_6S_{10}(CN)_2$ [51]. In this polymer, the Re_6S_8 units are linked into two-dimensional grids by sharing four apical sulfide ligands. Additionally, two "trans" rhenium atoms in the cluster core are coordinated by terminal cyano groups. Thus, according to Schäfer notation, the crystallographic formula of this compound

may be written as $K_4[Re_6S_8(CN)_2(S)_{4/2}]_\infty$. From a formal point of view, this compound could be imagined as the product of cleavage of two Re–μ-S–Re bridges in $[\{Re_6S_8\}(S)_{6/2}]$ and their substitution by terminal cyano ligands. The next member of a series of $M_4[\{Re_6S_8\}(CN)_{2x}(S)_{(6-2x)/2}]$, where M is an alkali metal, is the new chain polymer $Cs_4[\{Re_6S_8\}(CN)_4(S)_{2/2}]_\infty$, which was obtained with high yield by high-temperature reaction of ReS_2 with KCN in the presence of CsCl excess [50]. The compound completes a homologous series of octahedral cluster anions $[Re_6S_8S_{6/2}]^{4-}$, $[Re_6S_8(CN)_2S_{4/2}]^{4-}$, $[Re_6S_8(CN)_4S_{2/2}]^{4-}$, and $[Re_6S_8(CN)_6]^{4-}$ which could be described as consequent cleavage of Re–μ-S–Re bridges and substitution of the bridged sulfide ligands by terminal cyano ones (Fig. 6).

The reaction of the mixture of ReS_2 and MoS_2 in a molar ratio of 1:1 with an excess of KCN at 750°C leads to the formation of black crystals of $K_6[Re_3Mo_3S_8(CN)_5]$ that contains $\{M_6Q_8\}$-type Re–Mo heterometallic clusters. This compound is isostructural with $K_6[Mo_6Se_8(CN)_5]$, which was previously reported [49]. The metal atoms in the basal plane of each $\{Re_3Mo_3S_8\}$ cluster core are bound to four terminal CN ligands, and the clusters are covalently linked by the two remaining cyanide ligands into linear chains $[Re_3Mo_3S_8(CN)_4(CN)_{2/2}]^{6-}{}_\infty$ that lie along the c-axis (Fig. 7).

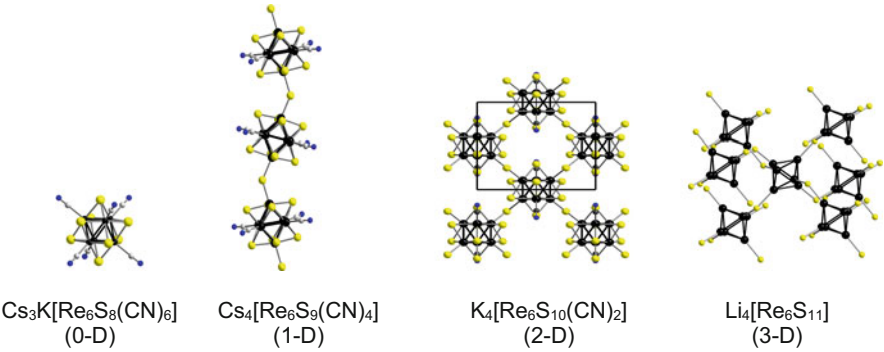

Fig. 6 Members of the $[\{Re_6S^i_8\}(CN)^a_{2x}(S)^{a-a}_{(6-2x)/2}]$ family

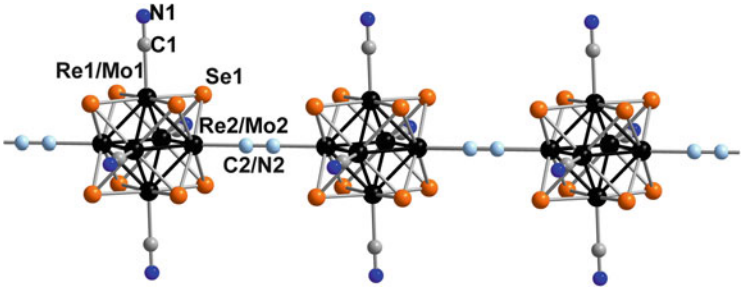

Fig. 7 Fragment of the polymeric chain $\{[Re_3Mo_3S_8(CN)_4(CN)_{2/2}]^{6-}\}_\infty$

The cluster core $\{Re_3Mo_3S_8\}$ has 24 CVE, as confirmed by the diamagnetism of the compound. From a formal point of view, as the reaction proceeds, the reduction of Mo^{4+} and Re^{4+} occurs [53–55]. We assume that KCN acted as a reducing agent according to the following reaction equation:

$$Re^{4+}S_2 + 3\,Mo^{4+}S_2 + 14\,KCN = K_6\left[Re_3{}^{2.5+}Mo_3{}^{2.5+}S_8(CN)_5\right] + 9/n\,(CN)_n + 4\,K_2S$$

Additional experiments supported by mass spectroscopy revealed that the reaction between $ReSe_2$, $MoSe_2$, and KCN leads to the formation of a complex product containing molecular and polymeric cluster species with a mixture of $\{Re_{6-x}Mo_xSe_8\}$ ($x = 0$–4) cluster cores.

Surprisingly, the reaction of ReS_2 with KCN at 750°C resulted in the formation of the diamagnetic compound $K_8[Re_{12}CS_{17}(CN)_6]$ [52] comprising the 48-electron cluster anion $[Re_{12}(\mu_3\text{-}S)_{14}(\mu_6\text{-}C)(\mu\text{-}S)_3(CN)_6]^{8-}$ (Fig. 8). This cluster can be considered as a dimer composed of two $\{Re_6\}$ octahedra face-capped by seven inner sulfide μ_3-S ligands and three terminal cyanide ligands. The rhenium atoms of two triangular faces of the $\{Re_6\}$ octahedra are connected through a μ_6-C interstitial atom and three μ_2-S ligands, thus, forming a $\{Re_6CS_3\}$ prism. Dissolution of this compound in H_2O in the presence of air oxygen led to the two-electron oxidation and formation of compounds based on 46-electron $[Re_{12}CS_{14}(\mu\text{-}S)_3(CN)_6]^{6-}$ anions. From the chemical point of view, the presence of μ_2-S ligands causes a significant difference between octahedral Re_6 and Re_{12} cluster compounds, first of all, due to the potential lability of μ_2-S ligands in comparison with μ_3-S ones. This is the main reason why the central fragment of $\{Re_{12}\}$ cluster complexes – the $\{Re_6CS_3\}$ prism – was considered to be the most interesting for investigation. The structural motif $[Re_{12}CS_{17}(CN)_6]^{8-}$ reminds that of $Mo_{12}S_{18}$, found in the ternary molybdenum sulfide $Ba_4Mo_{12}S_{18}$ [56].

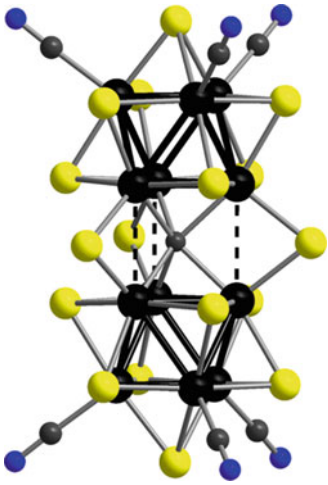

Fig. 8 Structure of anionic cluster complex $[Re_{12}CS_{17}(CN)_6]^{8-}$

The mean Re–Re distance between metalloclusters in $[Re_{12}CS_{17}(CN)_6]^{8-}$ is 3.17 Å. This distance is sensitive to charge of anion and drops to 2.90 Å after two-electron oxidation [52]. Later extensive substitution chemistry of both apical CN and bridging μ-S ligands was developed [57–59].

Thus, high-temperature chemistry of rhenium chalcogenides still demonstrates fascinating variety of thermodynamically stable compounds upon variation of reaction conditions (temperature, stoichiometry, presence of additional ions, etc.).

2.4 Condensation Reactions

M. Sergent's group synthesized ternary molybdenum chalcogenides, comprising condensed $Mo_{6+3x}Q_{8+3x}$ (Q = S, Se; x = 1–3) clusters. The formation of such clusters can be virtually described as the result of the successive condensation of Mo_3 triangles. The first member of this series, Mo_9Se_{11}, contains a bi-octahedral metal cluster Mo_9 [60, 61]. In this compound the metal cluster is ligated by eight μ_3 selenium atoms and three μ_4 selenium atoms located in the plane of the middle Mo_3 triangle. In the crystal structure of the compound, the metal atoms localized in the outer Mo_3 triangles are additionally coordinated by six Se atoms, which are bridging between adjacent cluster Mo_9Se_{11} fragments.

Similar cluster units have not been known to exist in the chemistry of rhenium. In 1999, we discovered the condensation reaction of triangular Re_3 fragments using rhenium tribromide Re_3Br_9 [62]. Reactions of the rhenium tribromide with cadmium chalcogenides led to formation of octahedral complexes of different compositions ($Re_6Q_4Br_{10}$ and $Re_6Q_8Br_2$) depending on the stoichiometric ratio of starting reagents:

$$2\ Re_3Br_9 + 4\ CdQ = [Re_6Q_4Br_4]Br_6 + 4\ CdBr_2\ (Q = S, Se, Te)$$

$$2\ Re_3Br_9 + 8\ CdQ = [Re_6Q_8]Br_2 + 8\ CdBr_2\ (Q = S, Se)$$

The idea of such an approach was that the formation of very stable cadmium bromide would take place in this reaction, as a result of the ligand exchange reaction with Re_3Br_9. In accordance with an ionic model, in such a reaction one divalent chalcogenide ion Q^{2-}, replacing two bromide ions Br^-, liberates one coordination site of the rhenium atom in the structure of Re_3Br_9. Two such coordination unsaturated fragments can be condensed by forming a rhenium–rhenium bond. As a result of such a condensation, octahedral clusters were obtained. But it is very interesting that similar cluster condensation can give bi-octahedral cluster motives of composition $Re_9Se_{11}Br_6$, which is the unique example in a family of condensed octahedral clusters [62]. This complex contains a cluster core similar to Mo_9Se_{11}, with only terminal bromine atoms acting as apical ligands (Fig. 9).

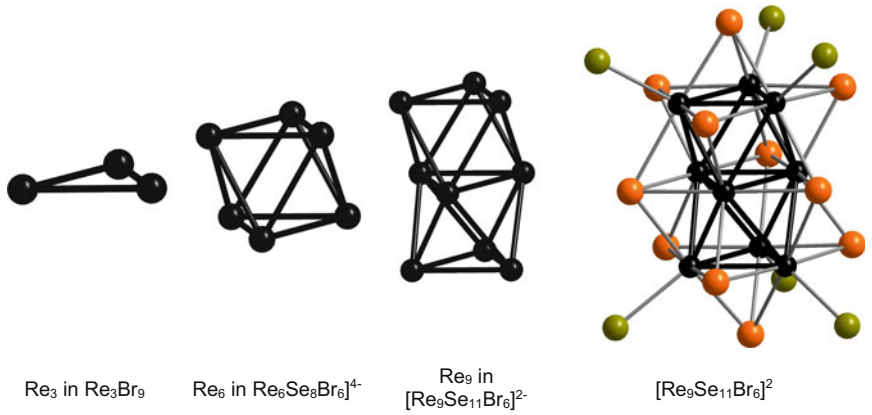

Fig. 9 Demonstration of formation of octahedral and bi-octahedral rhenium clusters by condensation of triangles

2.5 Reactions with Molten Organic Ligands

We proposed a simple and efficient approach to the ligand exchange reactions in molten organic compounds, which can serve as ligands. These reactions can be considered as a separate group of reactions. Starting compounds are cluster halides $[Re_6Q_8X_6]^{4-/3-}$ (Q = S or Se; X = Cl, Br, or I) [63–66]. Organic compounds are various N-donor heterocycles, triphenyl pnictogens, etc. melting congruently at temperatures of the order of 100–200°C, convenient for synthetic works. Upon completion of the reaction, the excess of organic compound can be easily washed off. Here are some examples of compounds produced by ligand exchange reactions, when apical halide ions were replaced by organic ligands. For example, the cluster complexes $[Re_6S_8(3,5\text{-}Me_2PzH)_6]Br_2{\cdot}2(3,5\text{-}Me_2PzH)$ where Q = S or Se, 3,5-Me_2PzH is 3,5-dimethylpyrazole, have been synthesized using reaction of rhenium chalcobromide complexes $Cs_4[Re_6S_8Br_6]{\cdot}2H_2O$ and $Cs_3[Re_6Se_8Br_6]{\cdot}H_2O$, respectively, with molten 3,5-dimethylpyrazole (Fig. 10).

This new synthetic approach for grafting various organic ligands to octahedral rhenium cluster compounds has been applied.

3 Properties of Cluster Complexes

As it was noted earlier, cluster solids prepared at high temperature with low ligand/metal ratio ($L/M_6 < 14$) are typically extended arrays where a strong intercluster bridging and even M–M interactions (as is the case of Chevrel phases) are realized. These compounds demonstrate cooperative properties typical for condensed matter, namely, band structure (in contrast to molecular orbitals for molecular complexes),

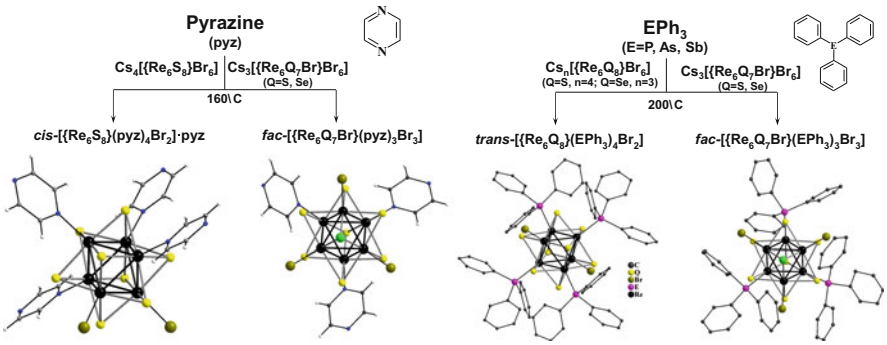

Fig. 10 Reactions in molten ligands: 3,5-dimethylpyrazole and EPh_3 [63, 66]

conductivity, superconducting properties coupled with very high critical fields [3, 5, 67], thermoelectricity [68–74], or catalytic properties [75, 76]. The features of the electronic structure of such compounds allow, in some cases, intercalation/deintercalation reactions of Mo_6Se_8 and $Li_4Re_6S_{12}$ [77].

The transition from extended arrays to isolated molecular cluster complexes causes the loss of some properties characteristic of extended arrays but allows us to get new information about the structure and new properties of cluster complexes. Molecular complexes are soluble and in some cases can be easily modified by the ligand exchange. Molecular complexes are better suitable for the research on such properties of the clusters as magnetism, redox reactions, and electron and optical spectra. On the other hand, molecular complexes, as building blocks, can be widely used for the synthesis of new compounds with a pre-planned composition and structure. The mutual transition of a condensed solid into molecular complexes and back is a fruitful strategy for study of properties and for the design of various materials.

3.1 Properties of Molecular Clusters

3.1.1 Electrochemical Behavior

Cyclovoltammetric studies of solutions of cluster salt anions $[Re_6Q_8(CN)_6]^{4-}$ (Q = S, Se, or Te) showed that these anions undergo quasi-reversible one-electron oxidation [78]:

$$\left[\mathrm{Re_6}Q_8(\mathrm{CN})_6\right]^{4-} - 1e \rightleftarrows \left[\mathrm{Re_6Q_8(CN)_6}\right]^{3-}$$

At higher potentials, the irreversible multi-electron oxidation was observed. Values of electrochemical potentials of some complexes $[Re_6Q_8(CN)_6]^{4-}$ (Q = S, Se, Te) vs. normal hydrogen electrode (NHE) are given in Table 1.

Table 1 Redox potentials of $[Re_6Q_8(CN)_6]^{4-}$, (Q = S, Se, Te) in acetonitrile and aqueous solution

Anion	$E_{1/2}$, V (CH_3CN)	$E_{1/2}$, V (H_2O)
$[Re_6S_8(CN)_6]^{4-}$	0.66	1.07
$[Re_6Se_8(CN)_6]^{4-}$	0.36	0.82
$[Re_6Te_8(CN)_6]^{4-}$	0.08	0.53

The decrease of $E_{1/2}$ in the S–Se–Te series indicates a significant contribution of chalcogen orbitals to HOMO levels of the cluster that was confirmed by density functional theory (DFT) calculations. As can be seen from Table 1, the solvent has a strong effect on the cluster redox potentials. The cluster anions can be chemically oxidized, for example, by saturated aqueous bromine solution, which appears to be a convenient oxidizing agent (E^0 = 1.07 V vs. NHE), as its oxidation potential is not too high for further irreversible oxidation of the cluster anion and its excess can be easily removed. Oxidation results in a change of the color of the solution (Se derivative changes color from orange to green). Oxidation by oxygen is also possible for $[Re_6Q_8(CN)_6]^{4-}$ (Q = Se, Te) in acidic aqueous solutions. The anions $[Re_6Q_8(CN)_6]^{3-}$ (Q = S, Se, Te) were successfully isolated and characterized.

In the IR spectra of oxidized anions, intense absorption bands appeared in the region of 500–600 nm, which is associated with a change in the color of the solution (in particular, solution of $[Re_6Se_8(CN)_6]^{4-}$ within oxidation changes color from orange to green). The position of these bands depends on the nature of the chalcogen, and, in the S, Se, Te series, they show a characteristic red shift. In addition, in the long-wavelength part of the spectra (800–1,000 nm), low-energy low-intensity wide absorption bands appeared [79]. Similar behavior was found in other rhenium clusters [12, 13, 31, 38, 80].

Electrochemical behavior of heterometallic clusters $[Re_3Mo_3Q_8(CN)_6]^{n-}$ (Q = S, Se) is more complicated and demonstrates several redox waves, for example: $[Re_3Mo_3Se_8(CN)_6]^{7-/6-}$ (24 → 23 CVE, $E_{1/2}$ = −1.410 V), $[Re_3Mo_3Se_8(CN)_6]^{6-/5-}$ (23 → 22 CVE, $E_{1/2}$ = −0.818 V) and $[Re_3Mo_3Se_8(CN)_6]^{5-/4-}$ (22 → 21 CVE, $E_{1/2} = -0.325$ V). The observed potentials agree well with inaccessibility of $[Re_3Mo_3Se_8(CN)_6]^{7-}$ and $[Re_3Mo_3Se_8(CN)_6]^{6-}$ anions in aqueous solutions, as well as with oxidation of $[Re_3Mo_3Se_8(CN)_6]^{5-}$ anion by air oxygen in CH_3CN or DMF solution. These properties show that mixed-metal clusters display dramatic decrease of 24/23 CVE redox potential in comparison with values for $[Re_6Se_8(CN)_6]^{3-/4-}$ cluster (Table 1). This complex behavior is associated with destabilization of two frontier molecular orbitals in heterometallic Re–Mo clusters [53, 54]. On the other hand, the $[Mo_6Se_8(CN)_6]^{n-}$ clusters display lower potentials of 22/21/20 CVE transitions in comparison with $[Re_3Mo_3Se_8(CN)_6]^{n-}$ [44, 81].

3.1.2 Protonation

Coordinated hydroxo-groups in $[Re_6Q_8(OH)_6]^{4-}$ (Q = S or Se) can be easily protonated by adjusting acidity of the aqueous solution. The protonation produces

a homologue series of $[Re_6Q_8(H_2O)_x(OH)_{6-x}]^{x-4}$ ($x = 0, 2, 4, 6$) that was isolated and structurally characterized [82]. Structures of these compounds comprise many short hydrogen bonds between coordinated H_2O and OH groups with O...O distances varying from 2.49 to 2.69 Å, which seems to be responsible for the low solubility of aqua-hydroxo complexes $K_2[Re_6S_8(H_2O)_2(OH)_4]\cdot 2H_2O$ and $[Re_6Q_8(H_2O)_4(OH)_2]\cdot 12H_2O$ (Fig. 11). Similar short bonds are also observed in salts based on $[Re_6S_8(CN)_4(OH)(H_2O)]^{3-}$ anion [47].

In contrast to $[Re_6Q_8(OH)_6]^{4-}$ precipitating at pH 5–9, the complex *trans*-$[Re_6S_8(CN)_4(OH)_2]^{4-}$ remains water soluble over a wide range of pH values that allowed to estimate the acidity constants of coordinated water molecules for the protonated form *trans*-$[Re_6S_8(CN)_4(OH)_2]^{4-}$. According to [47], there are two distinct steps that gave acidity constants to be $pK_{a1} = 3.3$, and $pK_{a2} = 6.6$ (Fig. 12).

$$\left[Re_6S_8(CN)_4(H_2O)_2\right]^{2-} + H_2O = \left[Re_6S_8(CN)_4(OH)(H_2O)\right]^{3-} + H_3O^+ \ (pK_{a1} = 3.3),$$

$$\left[Re_6S_8(CN)_4(OH)(H_2O)\right]^{3-} + H_2O = \left[Re_6S_8(CN)_4(OH)_2\right]^{4-} + H_3O^+ \ (pK_{a2} = 6.6)$$

Coordination to metal cations gives extended polymeric frameworks based on Re–OH–M–OH–Re interactions [83].

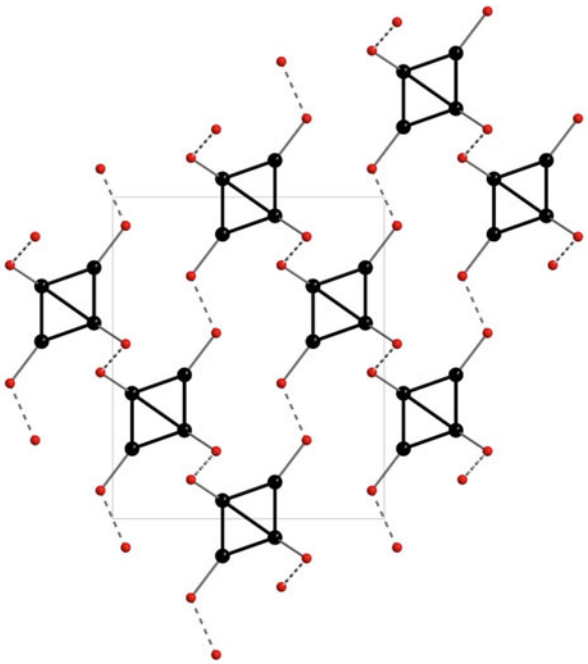

Fig. 11 Fragment of structure of $[Re_6Q_8(H_2O)_4(OH)_2]\cdot 12H_2O$ (Q = S or Se). Chalcogen and hydrogen atoms are not shown

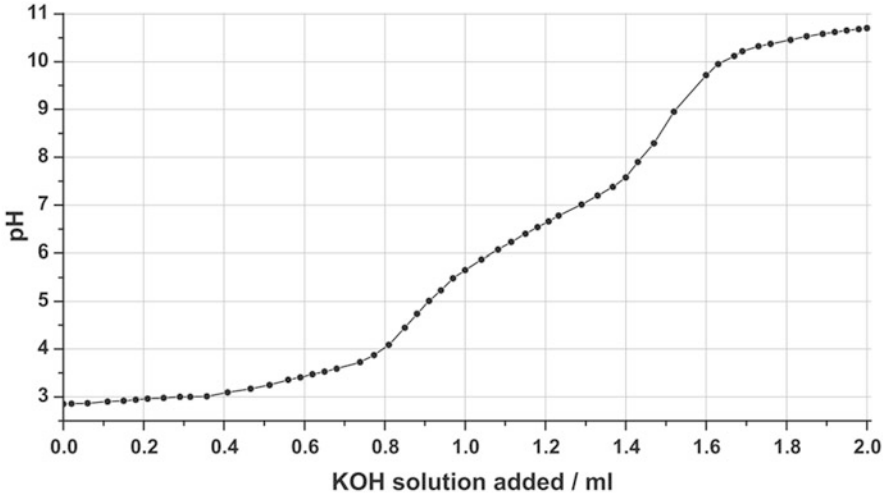

Fig. 12 Titration curve of the *trans*-$[Re_6S_8(CN)_4(H_2O)_2]^{2-}$ complex with 0.05 M solution of KOH

3.1.3 Apical Ligand Exchange

The chemistry of ligand exchange is well developed for coordination complexes, and the known approaches are successfully used in cluster chemistry. Kinetic measurements for this class of compounds are not typical. One rare example is the estimation of k_1 rate constants for $[Re_6Se_8(PEt_3)_5(CH_3CN)]^{2+}$ and $[Re_6Se_8(PEt_3)_5(DMSO)]^{2+}$, which are 3.9×10^{-7} s^{-1} and 7.5×10^{-8} s^{-1}, respectively. These values allowed classifying the rhenium octahedral complexes as kinetically inert like Ru^{3+} or Cr^{3+} complexes [84]. Usually, apical ligand exchange reactions take place in aqueous solutions or organic media. We proposed simple and efficient ligand exchange reactions in the melt of organic compounds, serving as ligands. These reactions can be considered as a separate group (see Sect. 2.5).

The suitable starting compounds for the ligand exchange reactions were cluster halides $Re_6Q_8X_6^{4-}$ (Q = S, Se; X = Cl, Br, I) and hydroxo complexes $[Re_6Q_8(OH)_6]^{4-}$. For example, ligand exchange reactions of $[Re_6Q_8(OH)_6]^{4-}$ produced acido complexes $[Re_6Q_8(RCOO)_6]^{4-}$ (R = H, CH_3) [85, 86], as well as N and P donor ligands [26, 40–42, 87] (Fig. 13).

We found that the promising complexes for ligand exchange are also mixed-ligand cyano-hydroxo complexes *trans*-$[Re_6Q_8(CN)_x(OH)_{6-x}]^{4-}$ (Q = S, Se) possessing both inert (cyano-) and labile (hydroxo-) ligands. The use of these complexes open the way to wide range of substituted derivatives with the general formulas *trans*-$[Re_6Q_8(CN)_4L_2]$ and *trans*-$[Re_6Q_8(CN)_2L_4]$ [47, 48, 88].

The apical ligand exchange chemistry of the $[Re_{12}CS_{14}(\mu\text{-}S)_3(CN)_6]^{6-}$ complex was also extensively studied. In recent years, its derivatives with apical OH^-, SO_3^{2-}, and Br^- ligands have been reported [89–91] (Fig. 14).

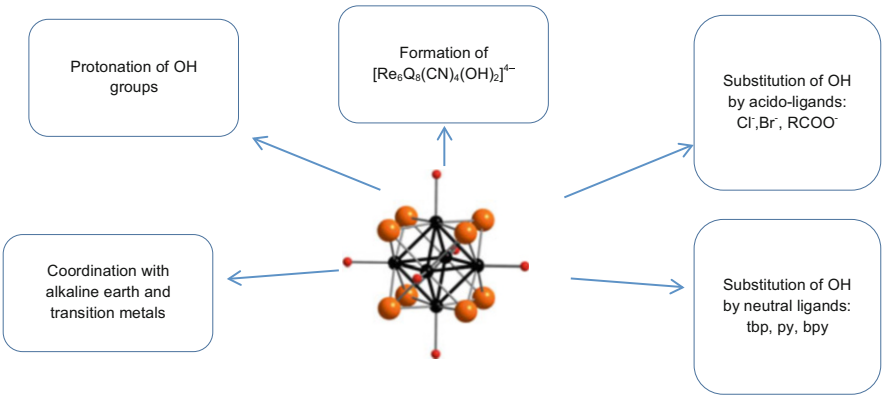

Fig. 13 Reactions of rhenium octahedral hexahydroxocomplexes $[Re_6Q_8(OH)_6]^{4-}$

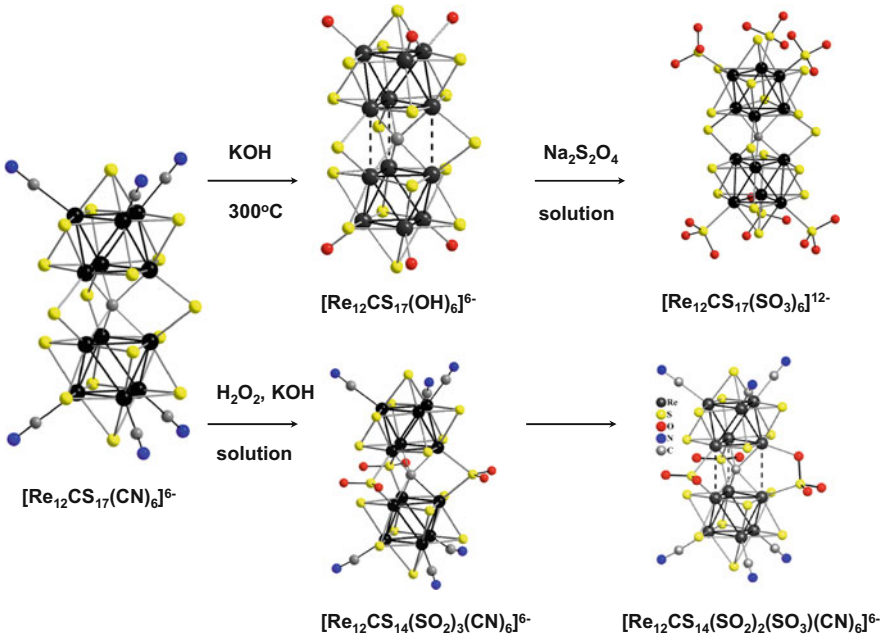

Fig. 14 Reactivity of $[Re_{12}CS_{17}(CN)_6]^{6-}$ cluster

3.1.4 Inner Ligand Exchange Reactions

As shown above, even apical ligands L in octahedral cluster complexes $[Re_6Q_8]L_6$ are quite inert. The inner chalcogenide ligands Q (S, Se, Te) are associated with the metal octahedral cluster of the μ_3-type, and their replacement is possible only under rather severe experimental conditions. For example, at high temperatures (>600°C),

it is possible to replace tellurium atoms by sulfur or selenium ones in a cluster core $[Re_6Te_8]$ within very wide limits: $[Re_6Te_{8-x}Q_x]$ $(0 < x < 8)$.

Generally speaking, complexes with mixed internal ligands can be formed in the synthetic process without a directed task to replace ligands. Principally, complexes with different chalcogenide ligands in the cluster core M_6Q_8 form as a set of isomers, the separation of which is usually a complicated task. For example, in the case of $M_6Q_6Q'_2$, there are three possible geometric isomers, and in the case of $M_6Q_4Q'_4$, they are six. In most cases, the structure of solids with mixed ligands tethered to the cluster core is characterized by the disordering of heteroatoms in all positions. However, there are examples of compounds with ordered structures; as a rule, they are formed in the case of a significant difference in the atomic radii of the internal ligands: Te and Cl in $Re_6Te_8Cl_{10} = Re_6Te_6Cl_2(TeCl_2)_2Cl_4$ [92] or Se and O in $[Re_6Se_4O_4Cl_6]^{4-}$ [93]. In $[Re_6Se_4O_4Cl_6]^{4-}$, the Re_6 cluster is surrounded by four oxygen atoms and four selenium atoms located on the opposite faces of the Se_4O_4 cube (Fig. 15). This ligand environment leads to a noticeable distortion of the metal cluster: Re–Re distances vary in the range from 2.46 Å for faces coordinated by μ_3 oxygen atoms up to 2.62 Å for the faces coordinated by μ_3 selenium atoms.

There was a fundamental question about the nature of the resulting solid solutions in the cluster core $[Re_6Te_{8-x}Q_x]$ (Q = S, Se; $x = 0$–8). In order to elucidate it, we carried out an NMR study of the potassium salt $K_4[Re_6Te_{8-x}Se_x(CN)_6]$ formed during the reaction of tellurium cluster with selenium [42, 87].

^{125}Te and ^{77}Se NMR spectra were recorded for aqueous solutions of $K_4[Re_6Te_{8-x}Se_x(CN)_6]$ with different Te/Se ratio (Fig. 16). Data evaluation was made using the additivity of mutual influence of inner ^{125}Te and ^{77}Se ligands on their chemical shifts of corresponding $[Re_6Te_{8-x}Se_x(CN)_6]$ isomers. Analysis of the data obtained showed that solid solutions $K_4[Re_6Te_{8-x}Se_x(CN)_6]$ are a set of isomers of different chemical composition, as is observed in mononuclear forms in the reactions of stepwise replacement of ligands. Thus, the ligand substitution in a cluster core

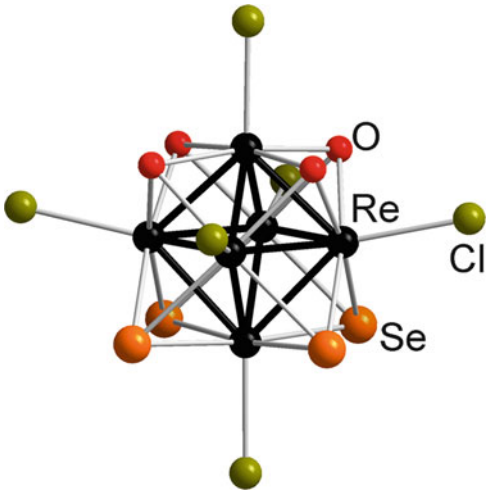

Fig. 15 Structure of $[Re_6Se_4O_4Cl_6]^{4-}$ in $Cs_{11}(H_3O)[Re_6Se_4O_4Cl_6]_3{\cdot}4H_2O$

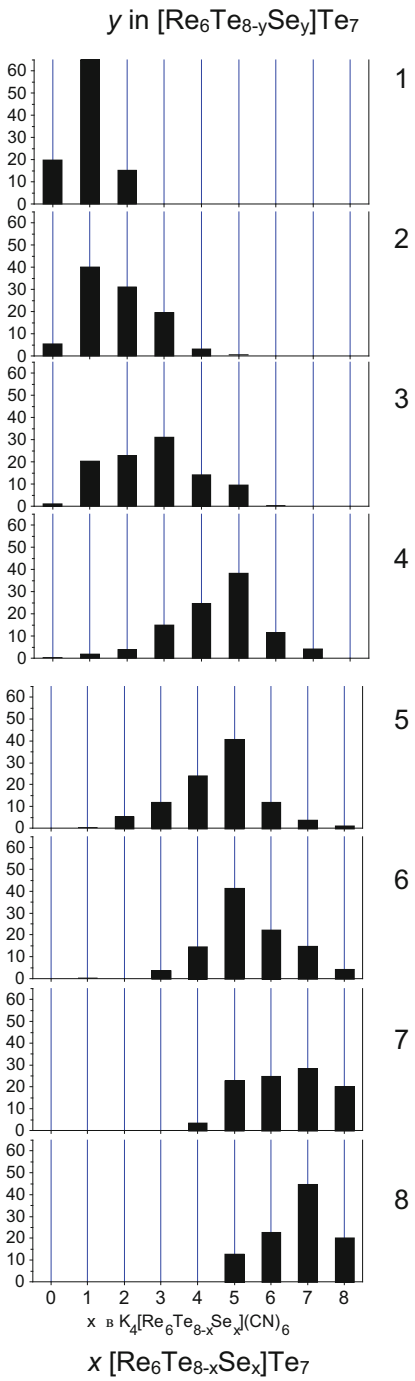

Fig. 16 Dependence of the amount of $[Re_6Te_{8-x}Se_x(CN)_6]^{4-}$ on composition in the parent $[Re_6Te_{8-y}Se_y]Te_7$ polymer

results in a complete series of mixed-ligand complexes that are in chemical equilibrium:

$$\begin{aligned}\left[Re_6Te_8(CN)_6\right]^{4-} + Se \rightarrow \left[Re_6Te_7Se(CN)_6\right]^{4-} + Se \rightarrow \left[Re_6Te_6Se_2(CN)_6\right]^{4-}\\ +Se \rightarrow \left[Re_6Te_5Se_3(CN)_6\right]^{4-} + Se \rightarrow \left[Re_6Te_4Se_4(CN)_6\right]^{4-}\\ +Se \rightarrow \left[Re_6Te_3Se_5(CN)_6\right]^{4-} + Se \rightarrow \left[Re_6Te_2Se_6(CN)_6\right]^{4-}\\ +Se \rightarrow \left[Re_6TeSe_7(CN)_6\right]^{4-} + Se \rightarrow \left[Re_6Se_8(CN)_6\right]^{4-}\end{aligned}$$

These results showed the fundamental similarity of mixed-ligand mononuclear and cluster metal complexes.

Inner μ_3 coordinated halide ligands in mixed-ligand complexes seem to be more labile and can be substituted under mild conditions. For example, one of the μ_3-Cl ligands in $[Re_6Q_5Cl_3Cl_6]^-$ (Q = S, Se) was successfully substituted using $(Me_3Si)E$ (E = S, Se, Te) in solution [27]. Substitution of the inner bromide in $Re_6Q_7Br_7$ (Q = S, Se) in molten organic ligands was also observed. Two rhenium octahedral cluster complexes, namely, $[Re_6S_7O(3,5Me_2PzH)_6]Br_2{\cdot}3,5Me_2PzH$ and $[Re_6Se_7O(3,5Me_2PzH)_6]Br_2{\cdot}3,5\text{-}Me_2PzH$, were synthesized by the reaction of rhenium chalcobromides $Cs_3[Re_6(\mu_3\text{-}Q_7Br)Br_6]$ (Q = S, Se) with molten 3,5-dimethylpyrazole (3,5-Me_2PzH) [65].

The $\mu\text{-}S^{2-}$ ligands in $[Re_{12}CS_{14}(\mu\text{-}S)_3(CN)_6]^{6-}$ anion can also be considered as inner ligands. In contrast to μ_3-S, they are easily oxidized in aqueous solution by H_2O_2 forming the $[Re_{12}CS_{14}(\mu\text{-}SO_2)_3(CN)_6]^{6-}$ anion [57]. $\mu\text{-}SO_2$ groups are chemically active and can be either oxidized to $\mu\text{-}SO_3$, forming $[Re_{12}CS_{14}(\mu\text{-}SO_2)_{3-x}(\mu\text{-}SO_3)_x(CN)_6]^{6-}$ [58], or reduced to μ-S. A series of Re_{12} complexes with mixed μ-S, μ-SO, and $\mu\text{-}SO_2$ groups were prepared and isolated [58, 94]. Recently, it was shown that $\mu\text{-}SO_2$ ligands can be also substituted by μ-O and μ-Se under mild conditions [59]. The following derivatives were isolated and characterized: $[Re_{12}CS_{14}(\mu\text{-}O)_3(CN)_6]^{6-}$, $[Re_{12}CS_{14}(\mu\text{-}O)_3(OH)_6]^{6-}$, and $[Re_{12}CS_{14}(\mu\text{-}Se)_3(CN)_6]^{6-}$. It is noteworthy that, during these transformations, the μ-bridging groups retain their formal oxidation state (2−), which causes the resulting anions to be of the same total charge (6−) and the same CVE number (46). The nature of the bridging ligands affects the properties of the Re_{12} clusters, such as absorption spectra, redox potentials, etc.

3.1.5 Magnetic Properties

Anionic complexes $[Re_6Q_8(CN)_6]^{4-}$ (24 CVE per Re_6) are diamagnetic, while oxidized species $[Re_6Q_8(CN)_6]^{3-}$ (23 CVE per Re_6) are paramagnetic [79, 95]. Magnetic behavior of $(Ph_4P)_3[Re_6S_8(CN)_6]$, $(Ph_4P)_2(H)[Re_6Se_8(CN)_6]{\cdot}4H_2O$, and $(Bu_4N)_2(H)[Re_6Te_8(CN)_6]$ salts was measured in the temperature range of 77–300 K. The temperature dependences followed a Curie–Weiss law with μ_{eff} changing from 1.75 to 1.81 μ_B in $(Ph_4P)_3[Re_6S_8(CN)_6]$, from 1.89 to 2.19 μ_B in

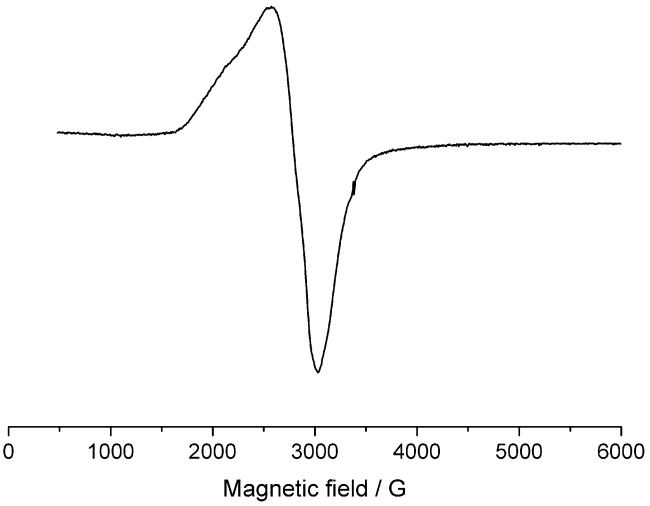

Fig. 17 EPR spectrum of polycrystalline $[Re_3Mo_3Q_8(CN)_6]$ sample at 77 K ($g = 2.430$)

$(Ph_4P)_2(H)[Re_6Se_8(CN)_6]\cdot 4H_2O$ and from 1.89 to 2.02 μ_B in $(Bu_4N)_2(H)[Re_6Te_8(CN)_6]$. Similar behavior was found in other rhenium clusters with 23 CVE [96–98].

Heterometallic clusters $[Re_3Mo_3Q_8(CN)_6]$ with an odd number of CVE (21 or 23) are also paramagnetic. EPR spectra of these complexes demonstrate broad signals with g-values lying in the range of 2.43–2.56 that is substantially higher than the conventional electron spin g-factor (Fig. 17).

3.1.6 Luminescence

Complexes with the general formula $[Re_6Q_8L_6]$ (Q = S, Se, or Te; L = halide, CN^-, NCS^-, N_3^-, OH^-/H_2O, anions of carboxylic acids, pyridine and phosphine derivatives, etc.) with the $Re_6Q_8^{2+}$ core having 24 CVE in the solid state and in solutions emit luminescence in visible and near-infrared (NIR) regions upon ultraviolet or blue light excitation (Fig. 18) with emission lifetimes in the microsecond range [47, 63, 64, 66, 78, 85, 86, 99–103]. They demonstrate long emission lifetimes indicating that the emitting excited state of the hexarhenium (III) complex is a spin-triplet type and involves orbitals that are primarily localized on the $(Re_6Q_8)^{2+}$ core. In addition to these experimental observations, theoretical studies of the excited state have demonstrated that the lowest-energy unoccupied molecular orbitals (LUMOs) are primarily localized on the $(Re_6Q_8)^{2+}$ core. The long lifetimes, large Stokes shifts, and excited-state quenching by O_2 indicate the spin-triplet nature of the luminescent excited state of the cluster complexes, i.e., the change in spin multiplicity is involved in the electronic transitions. The luminescence properties of Re_6 cluster complexes provided an incentive to establish their potential applications [104–106].

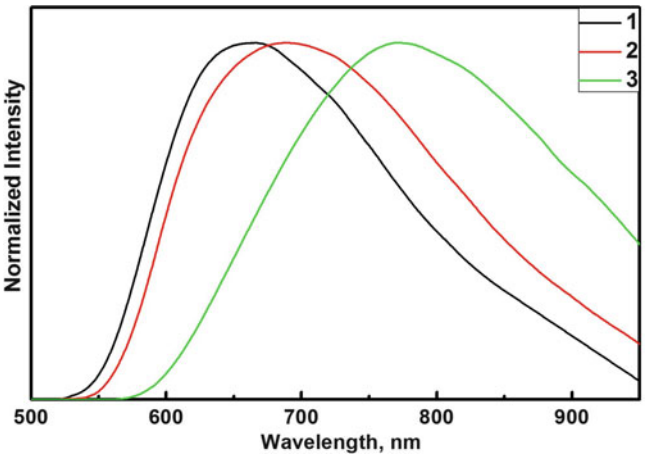

Fig. 18 Influence of the nature of apical ligands on emission maximum wavelength in the photoluminescence spectra of solutions of the complexes $[Re_6S_8(OH)_6]^{4-}$ (**1**), $[Re_6S_8(CH_3COO)_6]^4$ (**2**), and $[Re_6S_8Br_6]^{4-}$ (**3**)

Well-developed synthetic procedures for the preparation of $[Re_6Q_8L_6]$ complexes with various apical ligand environments afford a range of clusters for developing new luminescent materials. The quenching of the phosphorescence by O_2 suggests applications in optical sensor technology and singlet oxygen generation that can be used, for example, in the photodynamic therapy of cancer [107, 108].

3.2 Electronic Structure Calculations

According to extended Hückel calculations, electronic structure of octahedral cluster complexes $M_6Q_8L_6$ in which the upper molecular orbitals are represented by a d-block consisting of 12 MO is responsible for the metal–metal interaction. Twenty-four valence electrons are required for the formation of twelve covalent two-electron two-center metal–metal bonds in the metal cluster M_6. This is achieved in compounds where the metal ion has a d^4 electronic configuration. This rule is fulfilled in most Re (III) octahedral complexes containing the cluster core $Re_6Q_8^{2+}$. For chalcogenide complexes of chromium, molybdenum, and tungsten, compounds with electron-deficient cluster nuclei are stable (CVE = 20–22). The most prominent examples of such compounds are molybdenum chalcogenides Mo_6Se_8 (CVE = 20) and $PbMo_6S_8$ (CVE = 22).

DFT calculations of the electronic structures and UV–vis absorption spectra of the dia- and paramagnetic complexes $[Re_6Se_8(CN)_6]^{4-/3-}$ confirmed general motif of electronic structure [109]. According to the spin-restricted calculations, under the O_h symmetry, the ground HOMO states for both diamagnetic $[Re_6Se_8(CN)_6]^{4-}$ and paramagnetic $[Re_6Se_8(CN)_6]^{3-}$ complexes are characterized by the same orbital e_g

symmetry (Fig. 18). However, the occupation of e_g state is different: in the diamagnetic complex, it is completely occupied with electronic configuration e^4_g, but it is only partially occupied for the paramagnetic one, which is characterized by the electronic configuration e^3_g (Fig. 19). Similar electronic structure was found in other rhenium clusters [103, 110, 111].

The case of mixed-metal cluster compounds with $\{Re_3Mo_3Q_8\}$ core is more complicated due to the existence of two cluster core isomers, namely, *fac*- with C_{3v} symmetry and *mer*- with C_{2v} symmetry [53, 54]. DFT calculations of $[Re_3Mo_3Se_8(CN)_6]^{n-}$ (n = 4–7, CVE count from 21 to 24) were performed for both *fac*- and *mer*-isomers of the $\{Re_3Mo_3\}$ metallocluster. Molecular orbital (MO) diagrams for different isomers are shown in Fig. 20. Below the Fermi energy level, one can see the block of orbitals with mixed bonding–antibonding character, and above the Fermi energy level, there is an antibonding orbital block. The MO disposition for both heterometallic isomers $[Re_3Mo_3Se_8(CN)_6]^{n-}$ differs from that in homometallic $[Re_6Se_8(CN)_6]^{n-}$ ones by the presence of a gap between HOMO-1 and HOMO-2 orbitals for 24-electron cluster anions. The value of this energy gap is about 0.4 eV. Both orbitals are bonding in character.

The HOMO and HOMO-1 orbitals for the 24e cluster anion $[Re_3Mo_3Se_8(CN)_6]^{7-}$ are composed mostly of molybdenum atomic orbitals with minor contribution of rhenium and selenium. As one can see, consequent electron removal leads to energy decreasing of the HOMO-1.

The special feature of heterometallic clusters is the destabilization of two bonding levels (353A and 354A in Fig. 20) and the appearance of two additional gaps.

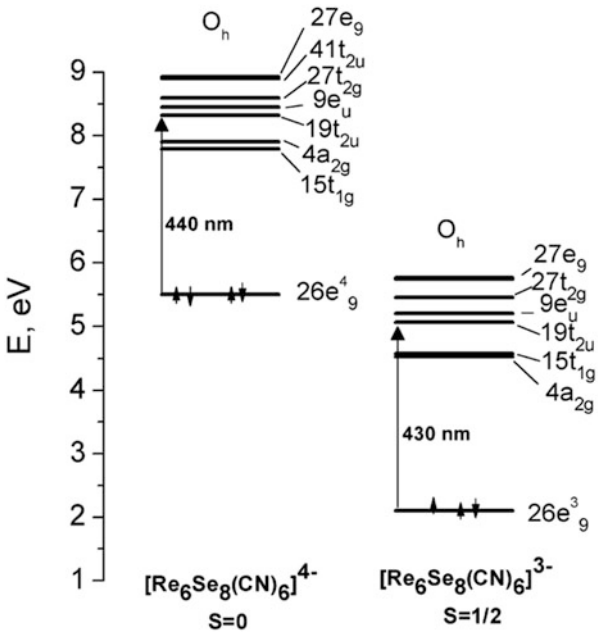

Fig. 19 Electronic level scheme for complexes $[Re_6Se_8(CN)_6]^{4-/3-}$

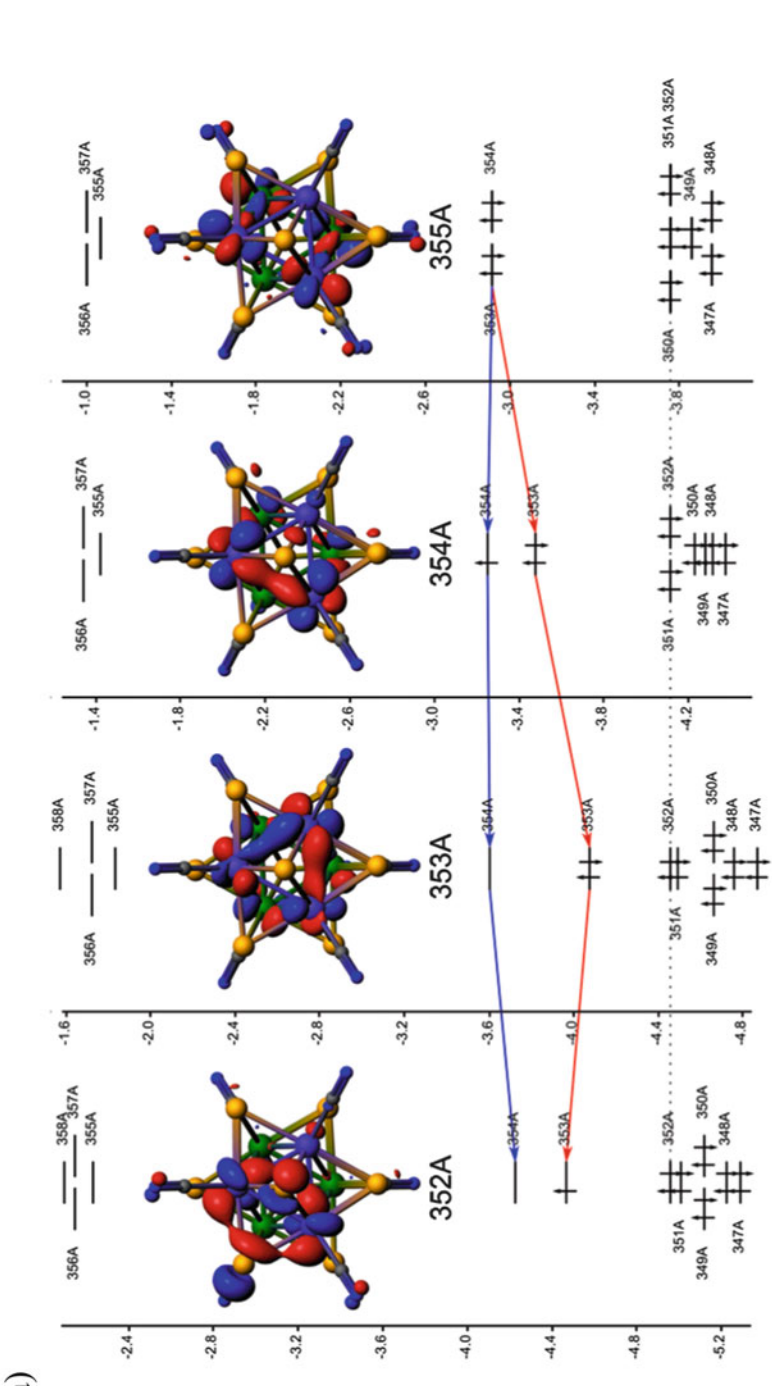

Fig. 20 Molecular orbital diagrams of *fac-* (**a**) and *mer-* (**b**) isomers of $[Re_3Mo_3Se_8(CN)_6]^{n-}$ ($n = 4$–7 from left to right). In the insets: typical view of the orbitals 355A, 354A, 353A, and 352A for the $[Re_3Mo_3Se_8(CN)_6]^{5-}$ anion. MO diagrams are aligned with respect to the energy of orbital 352A

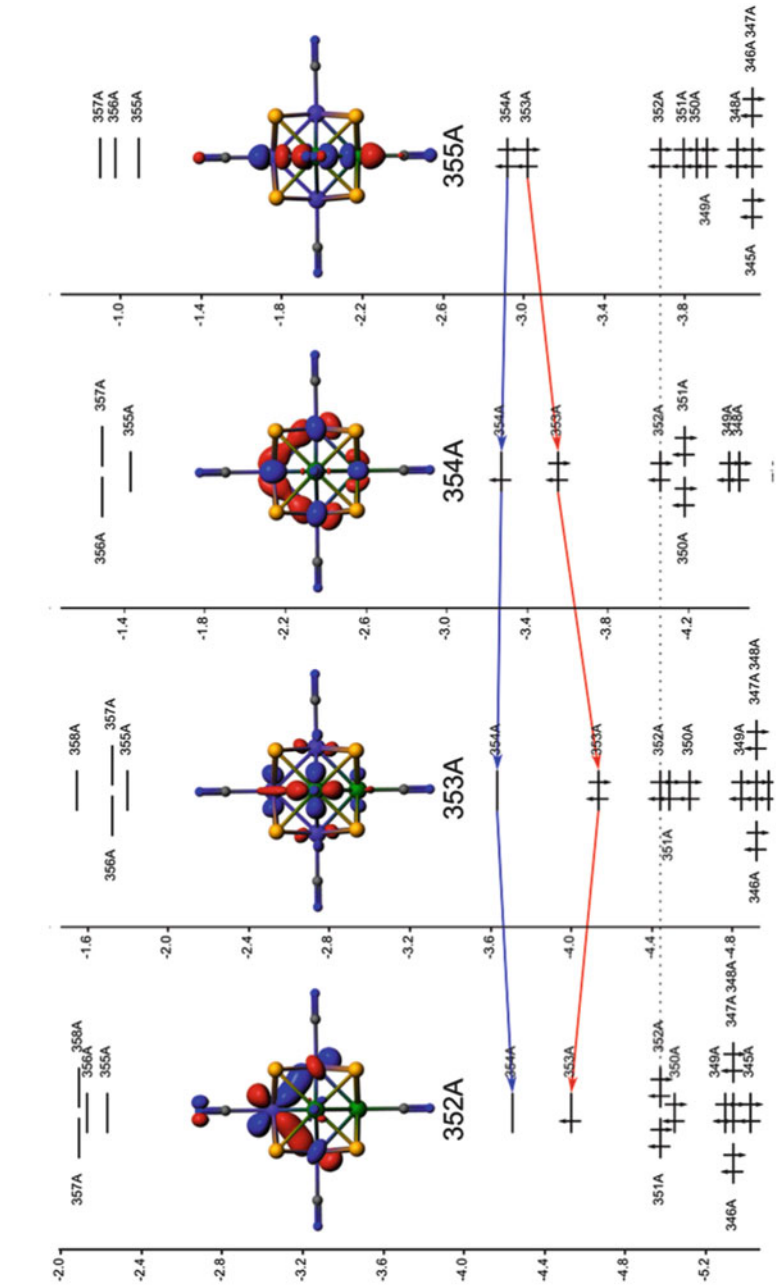

Fig. 20 (continued)

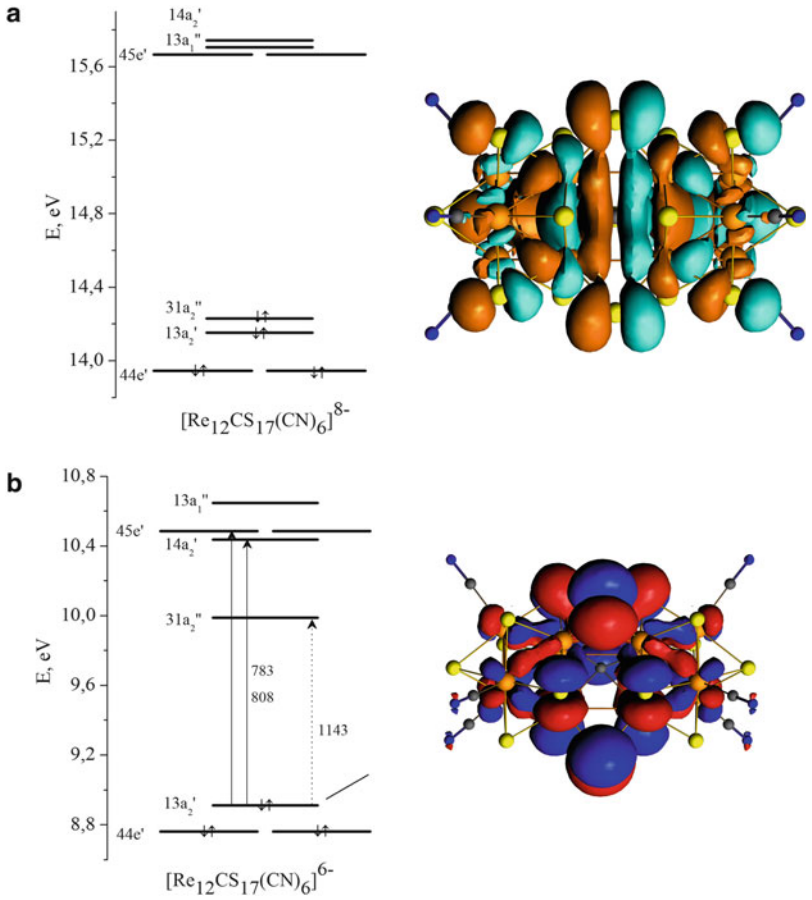

Fig. 21 Calculated energy level diagrams and HOMO orbitals: (**a**) $[Re_{12}CS_{17}(CN)_6]^{8-}$: The 31a2″ MO is shown perpendicular to the C_3 axis. Calculated charges: Re_{inner} (+0.083), Re_{outer} (+0.054), μ_6-C (−0.209). (**b**) $[Re_{12}CS_{17}(CN)_6]^{6-}$: The 13a2' MO is shown perpendicular to the C_3 axis. Arrows represent the forbidden (dotted) and allowed (solid) electronic transitions (in nm)

DFT calculations were also performed on the complexes $[Re_{12}CS_{17}(CN)_6]^{6-}$ and $[Re_{12}CS_{17}(CN)_6]^{8-}$ [52]. For the $[Re_{12}CS_{17}(CN)_6]^{6-}$ complex, the highest occupied molecular orbital (HOMO) consists predominantly of S 3p orbitals (80%) with a small contribution from the Re 5d orbitals. There is no contribution from the μ_6-C orbitals (Fig. 21). The HOMO shows antibonding properties between the Re atoms. The HOMO–LUMO gap is calculated to be 1.08 eV for the $[Re_{12}CS_{17}(CN)_6]^{6-}$ ion and 1.44 eV for the $[Re_{12}CS_{17}(CN)_6]^{8-}$ ion. One interesting feature of the cluster is the position of the 31a2″ orbital, which strongly depends on the anion charge (Fig. 21) and correlates with the length of the Re···Re distances. The absorption bands in the visible region of the electronic spectrum of $[Re_{12}CS_{17}(CN)_6]^{6-}$ are in good agreement with the calculated electronic structure. A simple valence electron

count shows that in the $[Re_{12}CS_{17}(CN)_6]^{8-}$ ion the rhenium atoms have a charge of +3 [52]. Accordingly, the $[Re_{12}CS_{17}(CN)_6]^{6-}$ ion contains slightly oxidized rhenium atoms ($Re^{3.17+}$), which correlates with charges of rhenium atoms calculated by DFT.

4 Coordination Polymers Based on $M_6Q_8(CN)_6$ Cluster Building Blocks

4.1 General Organization Principles

As it was mentioned above, the complexes $[M_6Q_8(CN)_6]$ are robust and inert toward ligand exchange. They are accessible to reversible oxidation/reduction. The number of reversible redox transitions depends strongly on the nature of the M_6Q_8 cluster core and ranges from one ($[Re_6Q_8(CN)_6]$, Q = S, Se, Te) to three ($[Re_3Mo_3Q_8(CN)_6]$, Q = S, Se). Structural study showed that geometry and size are independent on the number of CVE. Preliminary studies have shown that, like mononuclear cyanometallates, such cluster anions are capable of coordinating to transition metal cations, forming extremely poorly soluble precipitates, indicating the formation of strong cyanide bridges. Owing to their stability and rigid geometry, they are suitable to serve as the secondary building units (SBU) for obtaining coordination polymers via coordination of *d*- or *f*-metal cations through the nitrogen atoms of apical CN ligands, as it was shown for mononuclear cyano complexes. We should note that the topology of linking nodes resembles the one for hexacyanometallates (Fig. 22).

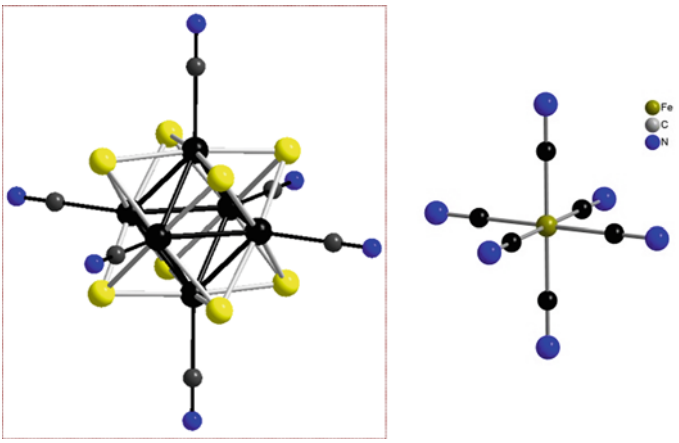

Fig. 22 Comparison of size of a chalcocyanide octahedral cluster complex $[M_6Q_8(CN)_6]^{n-}$ and hexacyanoferrate anion $[Fe(CN)_6]^{4-/3-}$

Van der Waals volumes of these clusters depend mainly on the nature of inner ligands and vary from 387 Å^3 for $[Re_6S_8(CN)_6]$ to 475 Å^3 for $[Re_6Te_8(CN)_6]$, and only slightly on the nature of metal atoms comprising metal core: 428 Å^3 for $[W_6S_8(CN)_6]$. In general, cyanides demonstrate geometric rigidity and stability in a wide range of experimental conditions and, meanwhile, have larger size and ability to one- or multi-electron redox transformations. Despite their differences (atomic compositions, electronic structures, CVE numbers), these cluster units have rather similar dimensions and topologies that favor the formation of common structural types. In recent years, it was shown that octahedral cluster cyano complexes of the general formula $[M_6L_{12}(CN)_6]^{n-}$ or $[M_6Q_8(CN)_6]^{m-}$ can be used in design of the coordination polymers with different dimensionality [55, 112–127]. Notably, they can serve as promising "building blocks" for the creation of new materials. The ambidentate nature of cyanide ligands is exploited to perform bridging coupling of moieties forming network structures via coordination of *d*- or *f*-metal cations. The high energy of M–CN–M' interactions usually lead to the formation of robust frameworks with a large number of covalent contacts. For several $[M_6Q_8(CN)_6]^{n-}$ anions, atom charges were calculated by DFT, which revealed predominant charge localization on nitrogen atoms (Table 2). The increase of the total anion charge, evidently, increases the charge of terminal nitrogen atoms, leading to high nucleophilicity of $[M_6Q_8(CN)_6]^{n-}$ as ligands and to the formation of strong M–CN...M'...NC bonds.

The first example of an interaction between $[Re_6Se_8(CN)_6]^{4-}$ and transition metal cations gave the unique structure type $(H_3O)_2[\{M(H_2O)_2\}_3\{Re_6Se_8(CN)_6\}_2]\cdot 9H_2O$ (Mn^{2+}, Co^{2+}) (Fig. 23) [128].

The structure of $Cs_2[\{Mn(H_2O)_2\}_3\{Re_6Se_8(CN)_6\}_2]\cdot 9H_2O$ includes a coordination framework constructed from cluster complexes linked together by cyanide bridges through manganese (II) cations. All six cyano groups of each cluster complex are involved in the formation of a coordination framework. In the structural motif of the framework $[\{Mn(H_2O)_2\}_3\{Re_6Se_8(CN)_6\}_2]_3^{2-}$, it is possible to distinguish a fragment formed by eight cluster complexes located at the vertices of the cube. Six manganese (II) cations, to which nitrogen atoms of these cluster complexes are coordinated in the equatorial plane, are located above the faces of the cube. In Fig. 23, such a selected fragment is shown schematically. In the coordination

Table 2 Calculated atoms charges (q) in complexes $[M_6Q_8(CN)_6]^{n-}$

	q, e$^-$			
Cluster anion	M	Q	C	N
$[Re_6S_8(CN)_6]^{4-}$	0.0656	−0.1524	−0.1232	−0.4058
$[Re_6Se_8(CN)_6]^{4-}$	0.0339	−0.1156	−0.1275	−0.4188
$[Re_6Te_8(CN)_6]^{4-}$	−0.0110	−0.0730	−0.1343	−0.4241
$[Mo_6S_8(CN)_6]^{6-}$	0.1408	−0.3342	−0.1803	−0.5149
$[Mo_6S_8(CN)_6]^{7-}$	0.1116	−0.3936	−0.1899	−0.5636
$[Mo_6Se_8(CN)_6]^{6-}$	0.1038	−0.3060	−0.1858	−0.5101
$[Mo_6Se_8(CN)_6]^{7-}$	0.0761	−0.3715	−0.1951	−0.5523

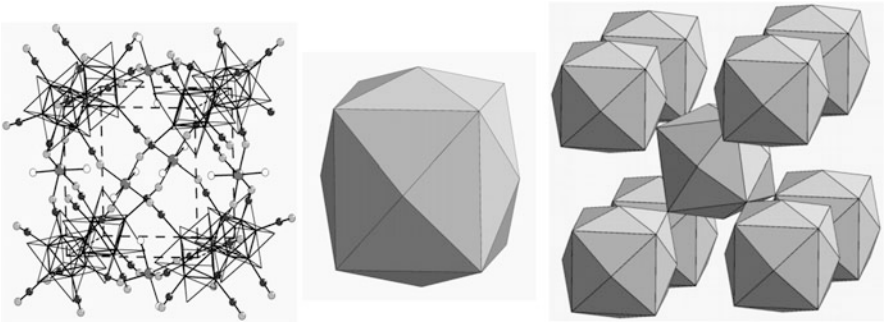

Fig. 23 Structure of $[\{M(H_2O)_2\}_3\{Re_6Se_8(CN)_6\}_2]^{2-}$ polymeric framework in $(H_3O)_2[\{Co(H_2O)_2\}_3\{Re_6Se_8(CN)_6\}_2]\cdot 8.5H_2O$ and $Cs_2[\{Mn(H_2O)_2\}_3\{Re_6Se_8(CN)_6\}_2]\cdot 9H_2O$

framework, these fragments are articulated at the vertices, i.e., two adjacent fragments have a common cluster complex. Figure 23 shows schematically the structural motif of the frame in the form of a package of "cubic" fragments. There are cavities in the frame that are filled with a large number of water molecules disordered over several positions.

Later, a large number of compounds with different cluster anions and transition metal cations were obtained. In general, the transition from one cluster to another gives new types of structures, and the general classification, which would have predictive functions, is, apparently, still impossible. It can be stated that in the interaction of metal aqua complexes, the charge of the cluster anion plays a significant role in the stoichiometry and topology of the resultant framework. However, for some types of structures, it has become possible to identify some trends.

4.2 Stable Structural Types of 3D Frameworks

The structures presented here have some similarities:

- The presence of a three-dimensional framework with large number of M–CN–M bridges.
- The presence of cavities and low packing coefficients making the frameworks topologically stable to compression and expansion. Such structures can easily adjust to small differences in volumes of the octahedral cluster anions, and more importantly, they allow inclusion of cations compensating their negative charge.

4.2.1 The Structural Type of $(H_3O)_2[\{Co(H_2O)_2\}_3\{Re_6Se_8(CN)_6\}_2]\cdot 9H_2O$

This structure was considered shortly in previous section (Fig. 23). This framework crystallizes in two space groups: $R\bar{3}c$ and $Im\bar{3}m$. Compounds

$(H_3O)_2[\{Co(H_2O)_2\}_3\{Re_6Se_8(CN)_6\}_2]\cdot 9H_2O$ and $Cs_2[\{Mn(H_2O)_2\}_3\{Re_6Se_8(CN)_6\}_2]\cdot 9H_2O$ crystallize in $R\bar{3}c$ space group [128]. This framework easily adopts a lot of solvate water molecules as in $(H_3O)_2[\{Mn(H_2O)_{1,5}\}_3\{Re_6Se_8(CN)_6\}_2]\cdot 19H_2O$, as well as Me_4N^+, Et_4N^+, compensating negative framework charge. A series of compounds $(R_4N)_2[\{M(H_2O)_n\}_3\{Re_6Q_8(CN)_6\}_2]\cdot xH_2O$ (Q = S, Se; n = 1,5, 2, M = Mn, Co, Ni) crystallize in space group $Im\bar{3}m$ [114]. Highly charged $[Mo_6Se_8(CN)_6]^{7-}$ anion also adopts this structure, forming $(Me_4N)_4[\{Mn(H_2O)_2\}_{1.5}Mo_6Se_8(CN)_6]\cdot 4H_2O$ [129].

4.2.2 The Structural Type of Prussian Blue

A series of compounds crystallize in highly symmetrical 3D framework with Prussian blue structural type with NaCl packing. The anions are bound through all six CN groups by M^{2+} cations, which occupy a special position 4*b* with the same high point symmetry located at the middle of the unit cell edge. In turn, the metal cations are surrounded by the nitrogen atoms of six cluster anions (Fig. 24). In a whole, the framework is topologically identical to observed in the Prussian blue

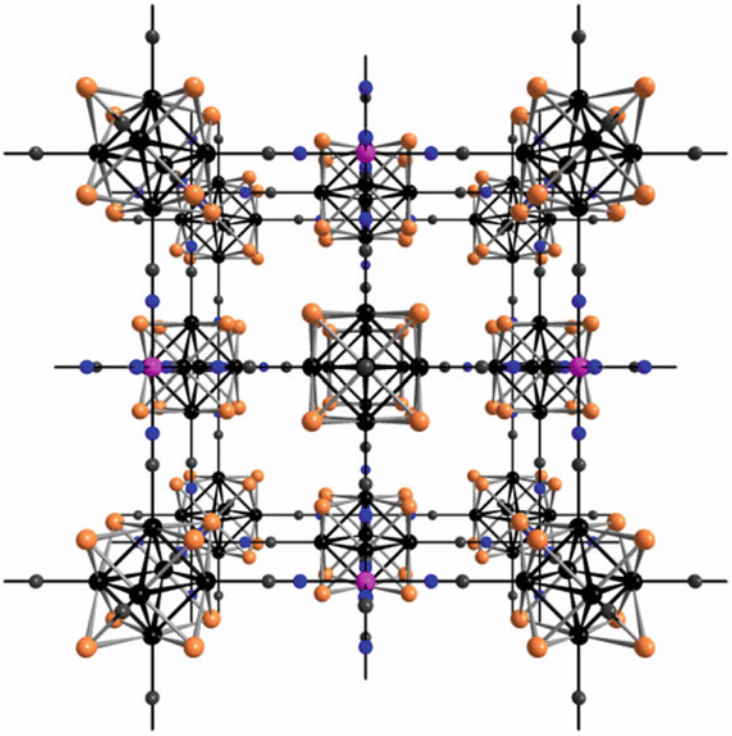

Fig. 24 Fragment of the coordination three-dimensional polymer $\{MnMo_6Se_8(CN)_6\}^{5-}$ in $K_5Mn[Mo_6Se_8(CN)_6]\cdot xH_2O$. View down [100] of the crystal packing

(M_2[Fe(CN)$_6$]) and the rock salt (NaCl) and has *pcu* symbol, according to O'Keeffe classification [130]. This framework occurs for $[Re_6Se_8(CN)_6]^{3-}$, with the charge 3- [118], and for highly charged $[Mo_6Se_2Br_6(CN)_6]^{4-}$, $[Re_3Mo_3S_8(CN)_6]^{6-}$ [131], and $[Mo_6Se_8(CN)_6]^{7-}$ [129] with various cations compensating the negative framework charge. Since the cluster anion size is considerably larger than the hexacyanoferrate size, there is an additional space in the framework available for various cations compensating its high charge and for solvate water molecules. Such framework type is as yet the most typical of the known coordination polymers based on different anionic cluster cyano complexes, namely, $[Nb_6Cl_{12}(CN)_6]^{4-}$, $[Nb_6Cl_9O_3(CN)_6]^{5-}$, $[Re_6Se_8(CN)_6]^{4-/3-}$, and $[Re_6Te_8(CN)_6]^{4-}$. All these compounds crystallize in the $Fm\bar{3}m$ space group, resulting in a high symmetry of the cluster anions in the structures, even in the case of asymmetric $[Nb_6Cl_9O_3(CN)_6]^{5-}$. In structures $Ga_4[Re_6Se_8(CN)_6]_3{\cdot}38H_2O$, $Fe_4[Re_6Te_8(CN)_6]_3{\cdot}xH_2O$ ($x \approx 27$) [132], $Fe_4[Re_6Se_8(CN)_6]_3{\cdot}36H_2O$, $Co_3[Re_6Se_8(CN)_6]_2{\cdot}25H_2O$, $Ni_3[Re_6Se_8(CN)_6]_2{\cdot}33H_2O$, $Ga[Re_6Se_8(CN)_6]{\cdot}6H_2O$ [118], $(Me_4N)_2Mn[Nb_6Cl_{12}(CN)_6]$ [133], and $Cs_3Mn[Nb_6Cl_9O_3(CN)_6]{\cdot}3H_2O$ [134], the frameworks carry a total charge from 0 (neutral framework) to −5, due to different charges of the counterions. Negative charges of the frameworks are compensated by additional cations located within the cavities.

4.2.3 Structures with Cationic Dimers

The polymeric framework with cationic dimers was found in the structures of $K_3\{\{Mn_2(H_2O)_4\}Mo_6Se_8(CN)_6\}$, $Cd_2(H_2O)_4[Re_6Se_8(CN)_6]{\cdot}14H_2O$ [135], $Co_2(H_2O)_4[Re_6S_8(CN)_6]{\cdot}10H_2O$ [115], and $Co_2(H_2O)_4[Re_6Se_8(CN)_6]{\cdot}8H_2O$ [136]. Their structure consists of cluster anions and $\{M_2(\mu\text{-}H_2O)_2(H_2O)_2\}^{4+}$ cationic dimers (Fig. 25). $\{M_2(\mu\text{-}H_2O)_2(H_2O)_2\}^{4+}/[M_6Q_8(CN)_6]^{n-}$ ratio is 1/1; therefore, in the case of rhenium cluster complexes, the framework is neutral, while in the

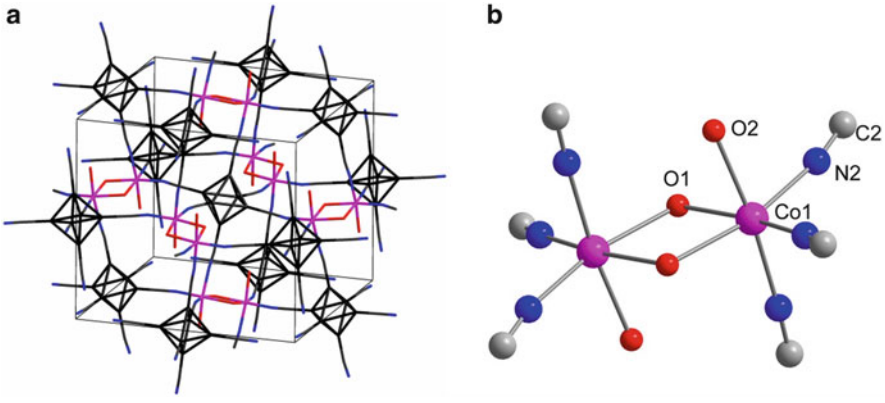

Fig. 25 Schematic representation of the framework (**a**) and structure of the cationic dimer $\{Co_2(\mu\text{-}H_2O)_2(H_2O)_2\}^{4+}$ (**b**) in $Co_2(H_2O)_4[Re_6Se_8(CN)_6]{\cdot}8H_2O$

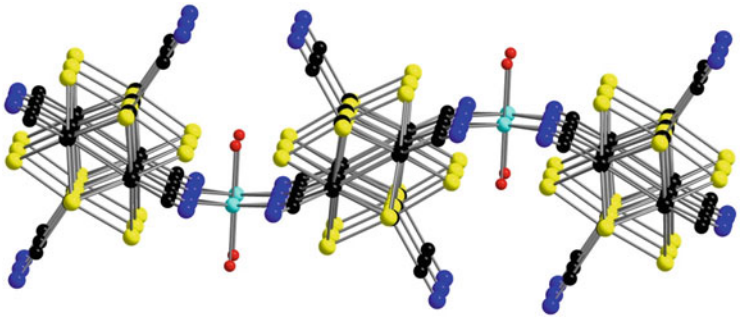

Fig. 26 Fragment of the coordination two-dimensional network $\{[Co(H_2O)_2Re_6S_8(CN)_6]^{2-}\}_\infty$ in $Cs_2[Co(H_2O)_2Re_6S_8(CN)_6]$

structure $K_3\{\{Mn_2((H_2O)_4\}Mo_6Se_8(CN)_6\}$, the framework is negatively charged adopting extra potassium cations. If the whole $\{M_2(\mu\text{-}H_2O)_2(H_2O)_2\}^{4+}$ dimer is considered as a cationic site, the framework topology corresponds to the one found in the Prussian blue and NaCl (*pcu*).

4.3 Layered Compounds

The compounds $Cs_2[trans\text{-}M(H_2O)_2][Re_6S_8(CN)_6]$ (M = Mn, Fe, Co, Zn, and Cd) [118, 137] have a layered structure, where the layers are formed by $[Re_6S_8(CN)_6]^{4-}$ cluster anions and M^{2+} cations. Four of six CN ligands of anion coordinate to M atoms, giving covalent Re–C ≡ N–M–N ≡ C–Re interactions, while the other two terminal CN groups are not coordinated. Metal cations M^{2+} have an octahedral environment, being coordinated by four nitrogen atoms of CN ligands of cluster anions and two water molecules in *trans*-position. The layer with a connectivity 4:4 presents a square lattice of clusters bonded through the metal atoms (Fig. 26). The connectivity of $\{M(H_2O)_2[Re_6S_8(CN)_6]\}^{2-}$ layers resembles that in $(NMe_4)_2[Mn(H_2O)_4][Fe(CN)_6]\cdot 4H_2O$ and Hofmann clathrates, having $Ni(CN)_4^{2-}$ anions linked by other transition metals in "planar" 4 + 2 coordination [138]. The same structural motif is observed in a series of isotypical compounds with the anions $[Mo_6Br_6S_2(CN)_6]^{4-/3-}$ and $[Mo_6Br_8(CN)_6]^{2-}$ [139].

4.4 Examples of One-Dimensional Polymers

As can be seen from previous sections, the interaction of aqueous solutions of transition metal cations and $[M_6Q_8(CN)_6]^{n-}$ cluster anions leads to formation of extended frameworks with numerous M–CN...M'–NC–M bridges. The use of polydentate ligands to restrict the coordination abilities of transition metals favors

the formation of low-dimensional frameworks (2D, 1D, and molecular). The list of chelate ligands includes bpy, en, dien, trien, threo-tab, salen, gly, erthitrhol, etc. Below some examples of low-dimensional structures are presented.

Reaction of $[Re_6Q_8(CN)_6]^{n-}$ with M^{2+} (M = Mn, Co, Ni) in the presence of ethylenediamine (en) resulted in the formation of numerous compounds with low-dimensional structures, depending on the nature of transition metal and reaction conditions [55, 121, 140]. Figure 27 shows two examples of these polymeric compounds, namely, $[M(NH_3)_2(en)_2]_2[\{M(en)_2\}Re_6Te_8(CN)_6]Cl_2{\cdot}xH_2O$ and $[\{Mn(H_2O)(en)_2\}\{Mn(en)_2\}Re_6Te_8(CN)_6]{\cdot}3H_2O$. Coordination of bridging $[Ni(en)2]^{2+}$ to *trans*-cyano ligands of octahedral clusters gives linear chain, while coordination of $[Mn(en)_2]$ to *cis*-cyano ligands results in zigzag chains.

A set of low-dimensional compounds was prepared with the use of $(SnMe_3)^+$ cation. This building block was successfully used earlier for linking cyanometallate complexes $[M(CN)_6]^{n-}$ to get highly porous compounds, namely, super Prussian blue [141–143]. In the case of the reaction of $[Re_6Q_8(CN)_6]^{n-}$ with $SnMe_3Cl$, low-dimensional compounds are usually formed where cluster anions are linked by tin atoms [122, 144]. The type of structure depends on the acidity of the solution. Compounds $[\{SnMe_3(H_2O)\}_2\{SnMe_3\}\{Re_6Se_8(CN)_6\}]{\cdot}H_2O$, $Cs[\{SnMe_3\}_3\{Re_6Se_8(CN)_6\}]$, and $[(SnMe_3)_3(OH)_2][\{SnMe_3\}_3\{Re_6Se_8(CN)_6\}]$ were obtained in acidic, neutral, and basic solutions, respectively. $Cs[\{SnMe_3\}_3\{Re_6Se_8(CN)_6\}]$ is a quite unique example, featuring anions linked into infinite chains by three bridges between two adjacent anions (Fig. 28).

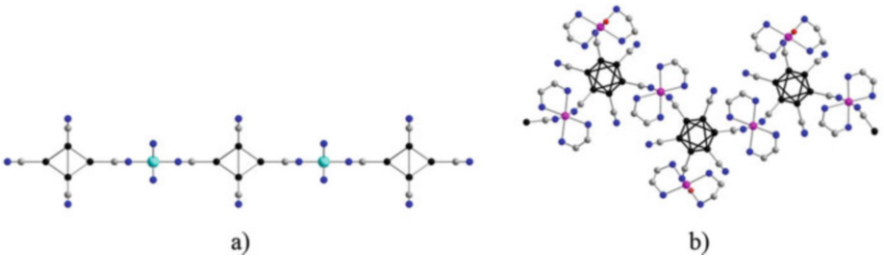

Fig. 27 Linear and zigzag chains in $[Ni(NH_3)_2(en)_2]_2[\{Ni(en)_2\}Re_6Te_8(CN)_6]Cl_2{\cdot}xH_2O$ (**a**) and $[\{Mn(H_2O)(en)_2\}\{Mn(en)_2\}Re_6Te_8(CN)_6]{\cdot}3H_2O$ (**b**). Hydrogen and tellurium atoms are omitted

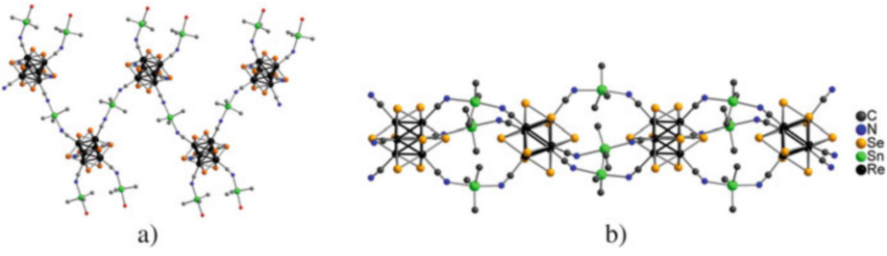

Fig. 28 One-dimensional chains in the $[\{SnMe_3(H_2O)\}_2\{SnMe_3\}\{Re_6Se_8(CN)_6\}]{\cdot}H_2O$ (**a**) and $Cs[\{SnMe_3\}_3\{Re_6Se_8(CN)_6\}]$ (**b**)

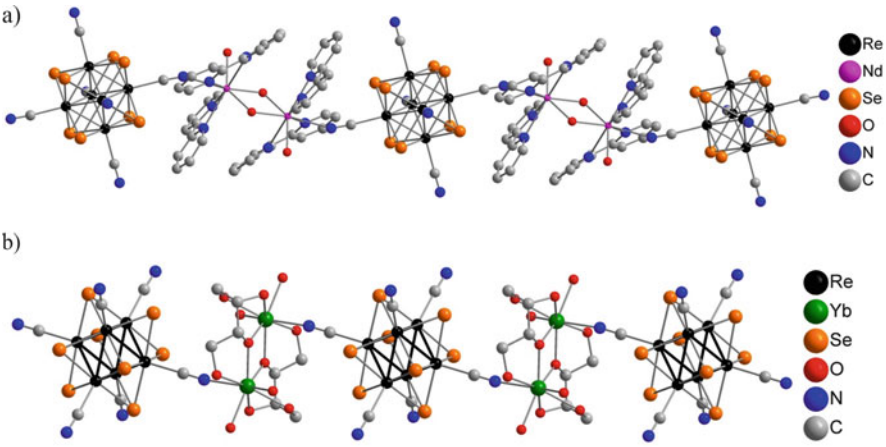

Fig. 29 Structural motif in (**a**) $[\{Nd_2(bpy)_4(H_2O)_2(\mu_2\text{-}OH)_2\}\{Re_6Se_8(CN)_6\}]$ and (**b**) $[\{Yb_2(C_4O_4H_9)_2(H_2O)_2\}\{Re_6Se_8(CN)_6\}]\cdot 5H_2O$. Hydrogen atoms are omitted

4.5 Formation of Polycationic Complexes

Large linear and voluminous dimensions of $[M_6Q_8(CN)_6]^{n-}$ cluster anions often favor stabilization of polycationic species in the crystal structures. In most cases with 3d transition metals and lanthanides, these polycationic species have a charge +4, balancing the charge of the $[Re_6Q_8(CN)_6]^{4-}$ anions, as it was found in $Co_2(H_2O)_4[Re_6Se_8(CN)_6]\cdot 8H_2O$ [136]. The compounds with rare earth elements coordinated by chelate ligands provide a large variety of binuclear cationic complexes. In the case of Ln^{3+}, 4+ charge can be achieved by deprotonation of bridging ligands (H_2O or polyalcohols). The structure of $[\{Ln_2(bpy)_4(H_2O)_2(\mu_2\text{-}OH)_2\}\{Re_6Se_8(CN)_6\}]\cdot 6H_2O$ (Ln = Nd, Eu) comprises $\{Ln_2(bpy)_4(H_2O)_2(\mu_2\text{-}OH)_2\}^{4+}$ dimers, where Ln atoms are bridged by two hydroxo-groups. Each Ln atom in the complex has one accessible site for coordination of CN ligands, giving the chain structure.

Compounds containing polyatomic alcohols, namely, glycerol and erythritol, comprise centrosymmetric binuclear cations, where Ln atoms are effectively coordinated by polyalcohols in a variety of ways. Partial deprotonation of the secondary OH group allows adjusting charge balance of the complexes. Structural motif in $[\{Yb_2(C_4O_4H_9)_2(H_2O)_2\}\{Re_6Se_8(CN)_6\}]\cdot 5H_2O$, for example, is given in Fig. 29.

4.6 Non-covalent Interactions Between Clusters

The high energy of M–CN–M' interactions usually leads to the formation of robust frameworks with a large number of covalent contacts. In general, strong M–CN–M'

covalent interactions dominate over weak dispersive forces. Nevertheless, the relatively weak interactions between specific groups often play a key role in the formation of polymeric structures from solutions. Along with strong and rigid coordination bonds, the structures of cluster compounds often comprise multiple non-covalent interactions determining the overall structure motif: hydrogen bonds and π–π stacking between aromatic rings [48, 145, 146].

Hydrogen bonds between solvate water molecules and cyano groups of cluster complexes are characteristic of most crystalline hydrates. The crystallization of the cluster anions $[Re_6Q_8(CN)_6]^{4-/3-}$ from acidic solutions (pH < 7) leads to the formation of acid salts containing hydrogen ions. Acidic protons can be localized either in the water sub-lattice $(H(H_2O)_n)^+$ [147, 148] or between cyano groups forming short and strong hydrogen bonds, as it was found in $[(H)\{Ln(H_2O)_4\}\{Re_6S_8(CN)_6\}]\cdot 2H_2O$, Ln = Yb, Lu [149] or in $H[cis\text{-}Fe(H_2O)_2][Re_6Se_8(CN)_6]\cdot 2H_2O$ [118]. CN...NC distances in these compounds range from 2.50 to 2.69 Å. The anions having both water molecules and hydroxo-groups form strong hydrogen bonding between OH and H_2O ligands, producing $H_3O_2^-$ groups with distances between donor oxygen atoms ranging from 2.33 to 2.50 Å. Such bonds determine the structures of aqua-hydroxo $Re_6Q_8(H_2O)_4(OH)_2\cdot 12H_2O$ and cyano-hydroxo complexes $(Bu_4N)_3[Re_6S_8(CN)_4(OH)(H_2O)]\cdot 2H_2O$ and $(Ph_4P)_3[Re_6S_8(CN)_4(OH)(H_2O)]\cdot 3.5H_2O$ (Fig. 30).

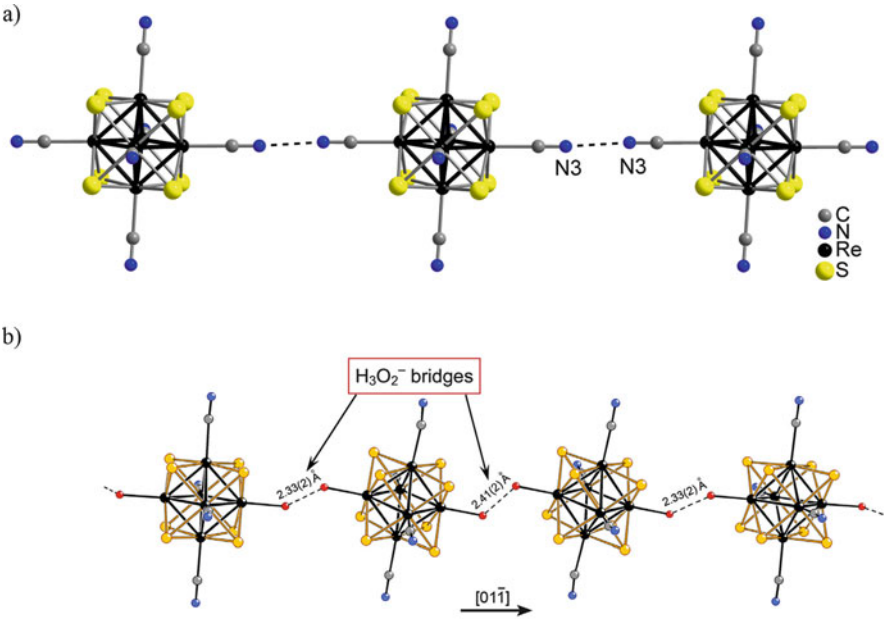

Fig. 30 (**a**) H-bonded chain with N...N separation of 2.673 Å in $[(H)\{Ln(H_2O)_4\}\{Re_6S_8(CN)_6\}]\cdot 2H_2O$, Ln = Yb, Lu. (**b**) The fragment of the anionic chain formed by hydrogen bonds (indicated by dashed lines) between the anions *trans*-$[Re_6S_8(CN)_4(OH)(H_2O)]^{3-}$·in $(Ph_4P)_3[Re_6S_8(CN)_4(OH)(H_2O)]\cdot 3.5H_2O$

5 Applications of Cluster Complexes

We should note the difference in the properties of condensed metal cluster materials and molecular cluster complexes. Strong intercluster interactions in the structures of condensed materials influence the band structure of solids and their wide range of transport and other physical properties, suggesting their potential use as superconductors [3], semiconductors, thermoelectrics (see, e.g., selected references: [63–66, 153]), catalysts, etc. Molecular complexes are able to go into solution and may be easily modified by ligand substitution. Molecular complexes, as building blocks, can be widely used in numerous reactions for the synthesis of new compounds with a predesigned composition and structure. Molecular complexes constitute convenient models to study such cluster properties as magnetism, redox reactions, electronic and optical spectra, and properties of metal-containing liquid crystals. Besides, they exhibit X-ray contrast properties, photocatalytic activity, and photoluminescence properties [102, 105, 107, 108, 150–152]. The mutual transition of a condensed solid into molecular complexes and back is a fruitful strategy in the design of various types of materials. Many interesting applied properties of chalcogenide cluster compounds are discussed in a recent review [153].

6 Conclusion

In this short review, we attempted to overview studies on the chemistry of molybdenum and rhenium octahedral chalcogenide cluster compounds carried out by NIIC researchers in collaboration with international research groups. We tried to show a pathway from classical solid-state cluster compounds Mo_6Se_8, Re_6Te_{15}, and $K_4Re_6S_{12}$ to soluble molecular complexes with Re_6Q_8 and Mo_6Q_8 cluster cores. Both inorganic and organic ligands can be grafted onto cluster cages, resulting in drastic change in the charge and properties of such complexes. Without diminishing the merits of other authors, we would like to emphasize here the role and importance of the research of the French school of chemistry, and first of all the University of Rennes 1, namely, the Laboratoire de Chimie du Solide et Inorganique Moléculaire (now known as the Institut des Sciences Chimiques de Rennes), where cluster chemistry of niobium, tantalum, molybdenum, and rhenium was developed. Professor Sergent and his closest colleagues made a great contribution to the cluster chemistry of transition metals including many rhenium chalcohalides, and this article dedicated to him is not only a tribute to his memory but also to his outstanding scientific achievements.

References

1. Cotton FA, Haas TE (1964) A molecular orbital treatment of the bonding in certain metal atom clusters. Inorg Chem 3:10–17. https://doi.org/10.1021/ic50011a003
2. Cotton FA (1964) Metal atom clusters in oxide systems. Inorg Chem 3:1217–1220. https://doi.org/10.1021/ic50019a003
3. Chevrel R, Sergent M, Prigent J (1971) Sur de nouvelles phases sulfurées ternaires du molybdène. J Solid State Chem 3:515–519. https://doi.org/10.1016/0022-4596(71)90095-8
4. Chevrel R, Sergent M, Fischer O (1975) Study of solid-solutions $Pb_yMo_6X_{8-x}X'_x$ and $Mo_6X_{8-x}X'_x$ (X,X′=S,Se,Te) and their superconducting properties. Mater Res Bull 10:1169–1174. https://doi.org/10.1016/0025-5408(75)90022-7
5. Fischer O, Maple MB (1982) Superconductivity in ternary compounds. Springer, Berlin
6. Perrin C, Chevrel R, Sergent M (1975) New tetrahedral cluster of molybdenum in chalcogenides MMo_4S_8(M=Al,Ga), $GaMo_4Se_8$ and thiohalides MoSX(X=Cl, Br, I). Cr Acad Sci C Chim 280:949–951
7. Perrin C, Chevrel R, Sergent M (1975) Structure of new molybdenum thiohalides MoSX (X=Cl,Br,I). Cr Acad Sci C Chim 281:23–25
8. Perrin A, Chevrel R, Sergent M (1976) New molybdenum ruthenium thio compounds with mixed tetrahedral cluster. J Solid State Chem 19:305–308. https://doi.org/10.1016/0022-4596(76)90181-X
9. Sergent M, Fischer O, Decroux M, Perrin C, Chevrel R (1977) Stabilization of Mo_6S_8 by halogens - new superconducting compounds - $Mo_6S_6Br_2$, $Mo_6S_6I_2$. J Solid State Chem 22:87–92. https://doi.org/10.1016/0022-4596(77)90192-X
10. Perrin A, Sergent M, Fischer O (1978) New compounds of type $Mo_2Re_4X_8$(X=S,Se) containing octahedral Mo_2Re_4 clusters. Mater Res Bull 13:259–264. https://doi.org/10.1016/0025-5408(78)90001-6
11. Gruttner A, Seeber B, Sergent M, Chevrel R, Fischer O, Yvon K (1978) $In_2Mo_{15}Se_{19}$, a new ternary compound containing Mo_6 and Mo_9 clusters. Acta Crystallogr A 34:S163–S163
12. Leduc L, Perrin A, Sergent M (1983) The structure of hexarhenium dichloride and octaselenide, Re6se8cl2 - a bidimensional compound of Re6 octahedral clusters. Acta Crystallogr C 39:1503–1506. https://doi.org/10.1107/S010827018300904x
13. Leduc L, Perrin A, Sergent M (1983) Chalcohalides and chalcogenides with octahedral clusters in low valency rhenium chemistry. Comptes Rendus 296:961–966
14. Opalovskii AA, Fedorov VE (1966) Vacuum-thermic dissociation of molybdenum diselenide and ditelluride. Neorg Mater 2:443–446
15. Opalovskii AA, Fedorov VE (1966) Synthesis of lowest molybdenum selenide and telluride. Neorg Mater 2:447–452
16. Opalovskii AA, Fedorov VE (1968). Neorg Mater 4:293
17. Bakakin VV, Mironov YI, Opalovskii AA, Fedorov VE (1966) X-ray study of lowest molybdenum chalcogenides. Izvestia SOAN, ser khim 11:98–100
18. Opalovskii AA, Fedorov VE, Erenburg BG, Lobkov EU, Vasiliev YV, Senchenko LN, Tsikanovskii BI (1971). Russ Phys Chem 45:2110–2115
19. Klaiber F, Petter W, Hulliger F (1983) The structure type of Re_2Te_5, a new $[M_6X_{14}]$ cluster compound. J Solid State Chem 46:112–120
20. Spangenberg M, Bronger W (1978) Ternary rhenium sulfides with $[Re_6S_8]$ clusters. Angew Chem 90:382–383
21. Bronger W, Spangenberg M (1980) Sodium thiorhenate ($Na_2Re_3S_6$) and potassium thiorhenate ($K_2Re_3S_6$), two thiorhenates with $[Re_6S_8]$ clusters. J Less-Common Met 76:73–79
22. Yaghi OM, Scott MJ, Holm RH (1992) Rhenium selenium chlorine solid-phases - cluster excision and core substitution-reactions of molecular-species. Inorg Chem 31:4778–4784
23. Long JR, Williamson AS, Holm RH (1995) Dimensional reduction of $Re_6Se_8Cl_2$ - sheets, chains, and discrete clusters composed of chloride-terminated $[Re_6Q_8]^{2+}$ (Q=S, Se) cores. Angew Chem Int Ed 34:226–229

24. Long JR, McCarty LS, Holm RH (1996) A solid-state route to molecular clusters: access to the solution chemistry of $[Re_6Q_8]^{2+}$ (Q=S, Se) core-containing clusters via dimensional reduction. J Am Chem Soc 118:4603–4616
25. Mironov YV, Cody JA, Ibers JA (1996) Hexachlorotetra-mu 3-chloro-tetra-mu 3-telluro-octohexarhenium(III). Acta Crystallogr C 52:281–283
26. Mironov YV, Virovets AV, Fedorov VE, Podberezskaya NV, Shishkin OV, Struchkov YT (1995) Synthesis and crystal structure of a hexanuclear rhenium cluster complex $Cs_3K[Re_6(\mu_3\text{-}S)_6(\mu_3\text{-}Te_{0.66}S_{0.34})_2(CN)_6]$ - cationic control over orientation of the cluster anion. Polyhedron 14:3171–3173
27. Uriel S, Boubekeur K, Batail P, Orduna J, Canadell E (1995) Solution chemistry of chalcohalide hexanuclear rhenium cluster monoanions - substitution reactions and structural and lsims characterization of the heterosubstituted cluster dianions, $(N\text{-}Bu_4N)_2[Re_6Q_5ECl_8]$ (Q=S,E=S,Se Q=Se,E=S,Se,Te). Inorg Chem 34:5307–5313
28. Hilsenbeck SJ, Young VG, McCarley RE (1994) Synthesis, structure, and characterization of N-ligated $Mo_6S_8I_6$ cluster complexes - molecular precursors to chevrel phases. Inorg Chem 33:1822–1832
29. Zhang X, McCarley RE (1995) High-yield synthesis of the W_6S_8 cluster unit as the pyridine complex $(W_6S_8)(Py)_6$ and attempts to prepare tungsten analogs of the chevrel phases. Inorg Chem 34:2678–2683
30. Saito T (1999) Rhenium sulfide cluster chemistry. J Chem Soc Dalton Trans:97–105. https://doi.org/10.1039/A806651E
31. Gabriel JCP, Boubekeur K, Uriel S, Batail P (2001) Chemistry of hexanuclear rhenium chalcohalide clusters. Chem Rev 101:2037–2066. https://doi.org/10.1021/cr980058k
32. Perrin A, Perrin C (2011) Low-dimensional frameworks in solid state chemistry of Mo_6 and Re_6 cluster chalcohalides. Eur J Inorg Chem:3848–3856. https://doi.org/10.1002/ejic.201100400
33. Fedorov VY, Mironov YV, Naumov NG, Sokolov MN, Fedin VP (2007) Group 5-7 metal chalcogenide clusters. Usp Khim 76:571–595
34. Sokolov MN, Naumov NG, Samoylov PP, Fedin VP (2013) Clusters and cluster assemblies. In: Jan Reedijk KR (ed) Comprehensive inorganic chemistry II, vol 2. Elsevier, Oxford, pp 271–310
35. Kim Y, Fedorov VE, Kim SJ (2009) Novel compounds based on $[Re_6Q_8(L)_6]^{4-}$ (Q = S, Se, Te; L = CN, OH) and their applications. J Mater Chem 19:7178–7190. https://doi.org/10.1039/b903929p
36. Gray TG (2003) Hexanuclear and higher nuclearity clusters of the groups 4-7 metals with stabilizing pi-donor ligands. Coord Chem Rev 243:213–235. https://doi.org/10.1016/s0010-8545(03)00083-3
37. Pilet G, Perrin A (2005) Octahedral rhenium cluster chemistry: from high-temperature syntheses to the elaboration of new inorganic/molecular hybrid compounds via solution route. C R Chim 8:1728–1742. https://doi.org/10.1016/j.crci.2005.03.017
38. Perrin A, Perrin C (2012) The molybdenum and rhenium octahedral cluster chalcohalides in solid state chemistry: from condensed to discrete cluster units. C R Chim 15:815–836. https://doi.org/10.1016/j.crci.2012.07.004
39. Slougui A, Mironov YV, Perrin A, Fedorov VE (1995) An octahedral rhenium cluster with (CN) ligands: the crystal structure of $KCs_3Re_6S_8(CN)_6$. Croat Chem Acta 68:885–890
40. Imoto H, Naumov NG, Virovets AV, Saito T, Fedorov VE (1998) Primitive cubic packing of anions in $Cs_4[Re_6Te_8(CN)_6]\cdot 2H_2O$ and $Ba_2[Re_6Te_8(CN)_6]\cdot 12H_2O$ crystals. J Struct Chem 39:720–727
41. Naumov NG, Virovets AV, Podberezskaya NV, Fedorov VE (1997) Synthesis and crystal structure of $K_4[Re_6Se_8(CN)_6]\cdot 3.5H_2O$. J Struct Chem 38:857–862
42. Mironov YV, Cody JA, AlbrechtSchmitt TE, Ibers JA (1997) Cocrystallized mixtures and multiple geometries: syntheses, structures, and NMR spectroscopy of the Re_6 clusters $[NMe_4]_4[Re_6(Te_{8-n}Se_n)(CN)_6]$ (n=0-8). J Am Chem Soc 119:493–498

43. Brylev KA, Virovets AV, Naumov NG, Mironov YV, Fenske D, Fedorov VE (2001) Synthesis and structure of a new octahedral molybdenum thiocyanide cluster complex $K_7[Mo_6(\mu_3\text{-}S)_8(CN)_6]\cdot 8H_2O$. Russ Chem Bull 50:1140–1143
44. Mironov YV, Virovets AV, Naumov NG, Ikorskii VN, Fedorov VE (2000) Excision of the $\{Mo_6Se_8\}$ cluster core from a chevrel phase: synthesis and properties of the first molybdenum octahedral cluster selenocyanide anions $[Mo_6Se_8(CN)_6]^{7-}$ and $[Mo_6Se_8(CN)_6]^{6-}$. Chem Eur J 6:1361–1365
45. Yarovoi SS, Mironov YV, Naumov DY, Gatilov YV, Kozlova SG, Kim SJ, Fedorov VE (2005) Octahedral hexahydroxo rhenium cluster complexes $[Re_6Q_8(OH)_6]^{4-}$ (Q = S, Se): synthesis, structure, and properties. Eur J Inorg Chem:3945–3949
46. Brylev KA, Mironov YV, Kim SJ, Fedorov VE (2007) Crystal structures of the octahedral rhenium cluster complexes Cs4[Re6S8(OH)6]·6H2O and Cs4[Re6Se8(OH)6]·8H2O. J Struct Chem 48:1118–1123
47. Ledneva AY et al (2014) Controlled synthesis and luminescence properties of trans-$Re_6S_8(CN)_4(OH)_{2\text{-}n}(H_2O)^{n\text{-}4}$ octahedral rhenium(III) cluster units (n=0, 1 or 2). Polyhedron 67:351–359. https://doi.org/10.1016/j.poly.2013.09.015
48. Naumov NG, Ledneva AY, Kim SJ, Fedorov VE (2009) New trans-$[Re_6S_8(CN)_4L_2]^{n\text{-}}$ rhenium cluster complexes: syntheses, crystal structures and properties. J Clust Sci 20:225–239
49. Magliocchi C, Xie XB, Hughbanks T (2000) A cyanide-bridged chain of Mo_6Se_8 clusters: a product of cyanide-melt cluster synthesis. Inorg Chem 39:5000–5001
50. Naumov NG, Kim SJ, Virovets AV, Mironov YV, Fedorov VE (2006) New rhenium octahedral cluster sulfido-cyanide chain polymer: the synthesis and crystal structure of $Cs_4[\{Re_6S_8\}(CN)_4S_{2/2}]$. Bull Kor Chem Soc 27:635–636
51. Mironov YV, Fedorov VE, McLauchlan CC, Ibers JA (2000) Layered $K_4[Re_6S_{10}(CN)_2]$ and chainlike $K_4[Re_6Se_{10}(CN)_4]$: new types of chalocyanide cluster compounds with bridging chalcogenide ligands. Inorg Chem 39:1809–1811
52. Mironov YV, Naumov NG, Kozlova SG, Kim SJ, Fedorov VE (2005) $[Re_{12}CS_{17}(CN)_6]^{n\text{-}}$ (n=6, 8): a sulfido-cyanide rhenium cluster with an interstitial carbon atom. Angew Chem Int Ed 44:6867–6871
53. Muravieva VK et al (2018) Mixed-metal clusters with a $\{Re_3Mo_3Se_8\}$ core: from a polymeric solid to soluble species with multiple redox transitions. Dalton Trans 47:3366–3377. https://doi.org/10.1039/c7dt03571c
54. Gayfulin YM, Naumov NG, Rizhikov MR, Smolentsev AI, Nadolinny VA, Mironov YV (2013) Heterometallic clusters with a new $\{Re_3Mo_3S_8\}$ core: direct synthesis, properties and DFT calculations. Chem Commun 49:10019–10021. https://doi.org/10.1039/C3cc44643c
55. Naumov NG, Brylev KA, Mironov YV, Virovets AV, Fenske D, Fedorov VE (2004) Synthesis and structures of new octahedral water-soluble heterometal rhenium-molybdenum clusters. Polyhedron 23:599–603
56. Salloum D, Gautier R, Potel M, Gougeon P (2005) $Ba_4Mo_{12}S_{18}$: a superconductor containing the dimeric unit $(Mo_6)_2S_{24}$, the missing link between the Mo_6S_{14} and Mo_9S_{17} units. Angew Chem Int Ed 44:1363–1365. https://doi.org/10.1002/anie.200461255
57. Mironov YV, Gayfulin YM, Kozlova SG, Smolentsev AI, Tarasenko MS, Nizovtsev AS, Fedorov VE (2012) Selective two-step oxidation of μ_2-S ligands in trigonal prismatic unit $\{Re_3(\mu_6\text{-}C)(\mu_2\text{-}S)_3Re_3\}$ of the bioctahedral cluster anion $[Re_{12}CS_{17}(CN)_6]^{6-}$. Inorg Chem 51:4359–4367. https://doi.org/10.1021/ic300051w
58. Gayfulin YM, Smolentsev AI, Yanshole LV, Kozlova SG, Mironov YV (2016) Reversible redox transformations of bridging sulfide ligands within bioctahedral rhenium cluster anions. Eur J Inorg Chem:4066–4075. https://doi.org/10.1002/ejic.201600588
59. Gayfulin YM, Smolentsev AI, Kozlova SG, Novozhilov IN, Plyusnin PE, Kompankov NB, Mironov YV (2017) Facile substitution of bridging SO_2^{2-} ligands in Re_{12} bioctahedral cluster complexes. Inorg Chem 56:12389–12400. https://doi.org/10.1021/acs.inorgchem.7b01889

60. Boulanger C, Lecuire JM, Gougeon P, Potel M, Sergent M (1986) Synthesis of a 1st metastable binary compound containing isolated Mo_9 clusters - Mo_9Se_{11}. Compt Rend 303:37–40
61. Gougeon P, Padiou J, Lemarouille JY, Potel M, Sergent M (1984) $Ag_{3.6}Mo_9Se_{11}$ - 1st compound with Mo_9 clusters in the Mo_9Se_{11} units. J Solid State Chem 51:218–226
62. Fedorov VE, Elsegood MRJ, Yarovoi SS, Mironov YV (1998) [Re9Se11Br6]2-: the first example of an Re9 condensed cluster. Chem Commun:1861–1862
63. Shestopalov MA et al (2007) Cluster core controlled reactions of substitution of terminal bromide ligands by triphenylphosphine in octahedral rhenium chalcobromide complexes. J Am Chem Soc 129:3714–3721. https://doi.org/10.1021/ja0668062
64. Mironov YV et al (2006) Octahedral rhenium cluster complexes with organic ligands: synthesis, structure and properties of $[Re_6Q_8(3,5\text{-}Me_2PzH)_6]Br_2 \cdot 2(3,5\text{-}Me_2PzH)$ (Q=S, Se). Inorg Chim Acta 359:1129–1134. https://doi.org/10.1016/j.ica.2005.08.012
65. Mironov YV et al (2005) $[Re_6Q_7O(3,5\text{-}Me_2PzH)_6]Br_2 \cdot 3,5\text{-}Me_2PzH$ (Q = S, Se) - new octahedral rhenium cluster complexes with organic ligands: original synthetic approach and unexpected ligand exchange in the cluster core. Eur J Inorg Chem:657–661. https://doi.org/10.1002/ejic.200400465
66. Shestopalov MA et al (2009) Self-assembly of ambivalent organic/inorganic building blocks containing Re-6 metal atom cluster: formation of a luminescent honeycomb, hollow, tubular metal-organic framework. Inorg Chem 48:1482–1489. https://doi.org/10.1021/ic8018277
67. Sokolov M (2007) Metal chalcogenides: clusters, layers, nanotubes. In: Devillanova FA (ed) Handbook of chalcogen chemistry: new perspectives in sulfur, selenium and tellurium. RSC Publishing, Cambridge, pp 511–550
68. Fischer C, Alonsovante N, Fiechter S, Tributsch H, Reck G, Schulz W (1992) Structure and photoelectrochemical properties of semiconducting rhenium cluster chalcogenides - $Re_6X_8Br_2$ (X = S, Se). J Alloys Compd 178:305–314. https://doi.org/10.1016/0925-8388(92)90272-b
69. Fischer C, Fiechter S, Tributsch H, Reck G, Schultz B (1992) Crystal-structure and thermodynamic analysis of the new semiconducting chevrel phase $Re_6S_8Cl_2$. Ber Der Bunsenges Phys Chem 96:1652–1658. https://doi.org/10.1002/bbpc.19920961124
70. Caillat T, Fleurial JP, IEEE (1997) New low thermal conductivity materials for thermoelectric applications. In: Proceedings ICT'97 - XVI international conference on thermoelectrics. https://doi.org/10.1109/ict.1997.667183
71. Dalafave SK (1998) Thermoelectric properties of Re_6Te_{15} and $Re_6Se_8Te_7$ cluster compounds. Mater Lett 37:177–181
72. Gougeon P et al (2012) Synthesis, crystal and electronic structures, and thermoelectric properties of the novel cluster compound $Ag_3In_2Mo_{15}Se_{19}$. Chem Mater 24:2899–2908. https://doi.org/10.1021/cm3009557
73. Al Orabi RA et al (2014) X-ray characterization, electronic band structure, and thermoelectric properties of the cluster compound $Ag_2Tl_2Mo_9Se_{11}$. Inorg Chem 53:11699–11709. https://doi.org/10.1021/ic501939k
74. Gougeon P, Gall P, Merdrignac-Conanec O, Aranda L, Dauscher A, Candolfi C, Lenoir B (2017) Synthesis, crystal structure, and transport properties of the hexagonal Mo_9 cluster compound $Ag_3RbMo_9Se_{11}$. Inorg Chem 56:9684–9692. https://doi.org/10.1021/acs.inorgchem.7b01200
75. Kamiguchi S, Ikeda N, Nagashima S, Kurokawa H, Miura H, Chihara T (2009) Catalytic condensation of primary amines, dehydrogenation of secondary amines, and dealkylation of tertiary amines over solid-state rhenium sulfide clusters with an octahedral metal framework. J Clust Sci 20:683–693. https://doi.org/10.1007/s10876-009-0271-4
76. McCarty KF, Anderegg JW, Schrader GL (1985) Hydrodesulfurization catalysis by Chevrel phase-compounds. J Catal 93:375–387. https://doi.org/10.1016/0021-9517(85)90185-x
77. Nemudry A, Schollhorn R (1994) Re_6S_{12}, a new binary rhenium cluster chalcogenide. J Chem Soc Chem Commun:2617–2618. https://doi.org/10.1039/C39940002617

78. Yoshimura T et al (1999) Unusual capping chalcogenide dependence of the luminescence quantum yield of the hexarhenium(III) cyano complexes $[Re_6(\mu_3\text{-}E)_8(CN)_6]^{4-}$, $E^{2-} = Se^{2-} > S^{2-} > Te^{2-}$. Chem Lett:1121–1122
79. Larina TV, Ikorskii VN, Vasenin NT, Anufrienko VF, Naumov NG, Ostanina EV, Fedorov VE (2002) Electronic state of rhenium complexes with octahedral chalcocyanide cluster anions $Re_6Q_8(CN)_6^{3-}$ (Q=S, Se, Te). EPR and magnetic susceptibility studies. Russ J Coord Chem 28:554–556
80. Zheng ZP, Gray TG, Holm RH (1999) Synthesis and structures of solvated monoclusters and bridged di- and triclusters based on the cubic building block [Re-6(mu(3)-Se)(8)](2+). Inorg Chem 38:4888–4895. https://doi.org/10.1021/Ic9906050
81. Magliocchi C, Xie XB, Hughbanks T (2004) Cyanide-melt synthesis of reduced molybdenum selenide clusters. Inorg Chem 43:1902–1911
82. Brylev KA et al (2007) A family of octahedral rhenium cluster complexes $[Re_6Q_8(H2O)_n(OH)_{6\text{-}n}]_{n\text{-}4}$ (Q = S, Se; n=0-6): structural and pH-dependent spectroscopic studies. Inorg Chem 46:7414–7422. https://doi.org/10.1021/Ic7005265
83. Mironov YV, Fedorov VE, Bang HJ, Kim SJ (2006) The first coordination polymers based on octahedral hexahydroxo rhenium cluster complexes $[Re_6Q_8(OH)_6]^{4-}$ (Q = S, Se) and alkaline earth metal cations. Eur J Inorg Chem 2006:553–557
84. Gray TG, Holm RH (2002) Site-differentiated hexanuclear rhenium(III) cyanide clusters $[Re_6Se_8(PEt_3)_n(CN)_{6\text{-}n}]_{n\text{-}4}$ (n = 4, 5) and kinetics of solvate ligand exchange on the cubic $[Re_6Se_8]^{2+}$ core. Inorg Chem 41:4211–4216. https://doi.org/10.1021/Ic020214c
85. Brylev KA et al (2010) A new hexanuclear rhenium cluster complex with six terminal acetate ligands: synthesis, structure, and properties of $K_4[Re_6S_8(CH3COO)_6]\bullet\ 8H_2O$. Inorg Chim Acta 363:2686–2691. https://doi.org/10.1016/j.ica.2010.04.042
86. Brylev KA et al (2009) The first octahedral cluster complexes with terminal formate ligands: synthesis, structure, and properties of $K_4[Re_6S_8(HCOO)_6]$ and $Cs_4[Re_6S_8(HCOO)_6]$. Inorg Chem 48:2309–2315. https://doi.org/10.1021/Ic802178q
87. Fedorov VE, Tkachev SV, Naumov NG, Mironov YV, Mironov YI (1998) Stepwise substitution for μ_3-Te ligands in the $[Re_6Te_8]^{2+}$ octahedral cluster core: NMR evidence for equilibrium between chemical forms. Russ J Inorg Chem 43:1562–1571
88. Mironov YV, Brylev KA, Smolentsev AI, Ermolaev AV, Kitamura N, Fedorov VE (2014) New mixed-ligand cyanohydroxo octahedral cluster complex trans-$[Re_6S_8(CN)_2(OH)_4]^{4-}$, its luminescence properties and chemical reactivity. RSC Adv 4:60808–60815. https://doi.org/10.1039/c4ra10697k
89. Mironov YV, Kozlova SG, Kim SJ, Sheldrick WS, Fedorov VE (2010) Dodecanuclear rhenium cluster complexes with an interstitial carbon atom: synthesis, structures and properties of two new compounds $K_6[Re_{12}Cs_{17}(OH)_6]\bullet\ 4H_2O$ and $Na_{12}Re_{12}Cs_{17}(SO_3)_6\bullet\ 48.5H_2O$. Polyhedron 29:3283–3286. https://doi.org/10.1016/j.poly.2010.09.010
90. Gayfulin YM, Ryzhikov MR, Samsonenko DG, Mironov YV (2018) Electron-rich bioctahedral rhenium chalcohalide clusters $[Re_{12}CS_{14}(\mu\text{-}S)_3Cl_6]^{8-}$ and $[Re_{12}CS_{14}(\mu\text{-}S)_3Br_6]^{8-}$: synthesis, structure and properties. Polyhedron 151:426–432. https://doi.org/10.1016/j.poly.2018.05.061
91. Gayfulin YM, Smolentsev AI, Kozlova SG, Yanshole VV, Mironov YV (2014) Synthesis, structure and DFT calculations of the first bioctahedral chalcohalide rhenium cluster complex $(Et_4N)_4(Me_2NH_2)_2$ $[Re_{12}Cs_{17}Br_6]$. Polyhedron 68:334–339. https://doi.org/10.1016/j.poly.2013.11.014
92. Mironov YV, Pell MA, Ibers JA (1996) The new inorganic ligands $TeCl_2$ and $TeBr_2$: syntheses and crystal structures of $Re_6Te_6Cl_6(TeCl_2)_2$ and $[Re_6Te_8(TeBr_2)_6]Br_2$. Inorg Chem 35:2709–2710
93. Yarovoi SS et al (2005) Unexpected ligand substitutions in the cluster core $\{Re_6Se_8\}$: synthesis and structure of the novel cluster compound $Cs_{11}(H_3O)[Re_6Se_4O_4Cl_6]_3\ 4H_2O$. Chem Commun:719–721. https://doi.org/10.1039/B412850H

94. Lappi TI, Gayfulin YM, Smolentsev AI, Mironov YV (2017) Structural characterization of a bioctahedral cluster $[Re_{12}CS_{14}(\mu\text{-}SO_2)(\mu\text{-}S)_2(CN)_6]^{6-}$ anion. J Struct Chem 58:835–837. https://doi.org/10.1134/S002247661704031x
95. Naumov NG, Ostanina EV, Virovets AV, Schmidtman M, Muller A, Fedorov VE (2002) 23-electron Re_6 metal clusters: syntheses and crystal structures of $(Ph_4P)_3Re_6S_8(CN)_6$, $(Ph_4P)_2(H)Re_6Se_8(CN)_6.8H_2O$, and $(Et_4N)_2(H)Re_6Te_8(CN)_6.2H_2O$. Russ Chem Bull 51:866–871
96. Guilbaud C, Deluzet A, Domercq B, Molinie P, Coulon C, Boubekeur K, Batail P (1999) $(NBu_4^{n+})_3[Re_6S_8Cl_6]^{3-}$: synthesis and luminescence of the paramagnetic, open shell member of a hexanuclear chalcohalide cluster redox system. Chem Commun:1867–1868. https://doi.org/10.1039/A904669k
97. Alvarez-Thon L, Hernandez-Acevedo L, Arratia-Perez R (2001) Calculated paramagnetic resonance parameters of the luminescent Re6S8Cl63-cluster ion. J Chem Phys 115:726–730. https://doi.org/10.1063/1.1379970
98. Arratia-Perez R, Hernandez-Acevedo L (2003) Calculated paramagnetic resonance parameters (g,A(hfi)) of the Re6S8Br63-, Re6S8I63-, and Re6Se8I63-cluster ions. J Chem Phys 118:7425–7430. https://doi.org/10.1063/1.1561851
99. Gray TG, Rudzinski CM, Nocera DG, Holm RH (1999) Highly emissive hexanuclear rhenium (III) clusters containing the cubic cores $[Re_6S_8]^{2+}$ and $[Re_6Se_8]^{2+}$. Inorg Chem 38:5932
100. Yoshimura T, Ishizaka S, Umakoshi K, Sasaki Y, Kim H-B, Kitamura N (1999) Hexarhenium (III) clusters $[Re_6(\mu_3\text{-}S)_8X_6]^{4-}$ (X- = Cl-, Br-, I-) are luminescent at room temperature. Chem Lett:697–698
101. Dorson F et al (2009) Selective functionalisation of Re_6 cluster anionic units: from hexahydroxo $[Re_6Q_8(OH)_6]^{4-}$ (Q = S, Se) to neutral *trans*-$[Re_6Q_8L_4L'_2]$ hybrid building blocks. Dalton Trans:1297–1299. https://doi.org/10.1039/B822105g
102. Molard Y et al (2010) Red-NIR luminescent hybrid poly(methyl methacrylate) containing covalently linked octahedral rhenium metallic clusters. Chem Eur J 16:5613–5619. https://doi.org/10.1002/chem.200902131
103. Gray TG, Rudzinski CM, Meyer EE, Nocera DG (2004) Excited-state distortion of rhenium (III) sulfide and selenide clusters. J Phys Chem A 108:3238–3243. https://doi.org/10.1021/Jp0358937
104. Choi SJ et al (2008) Cellular uptake and cytotoxicity of octahedral rhenium cluster complexes. J Inorg Biochem 102:1991–1996. https://doi.org/10.1016/j.jinorgbio.2008.07.013
105. Aubert T et al (2010) Synthesis and characterization of $A_4[Re_6Q_8L_6]@SiO_2$ red-emitting silica nanoparticles based on Re_6 metal atom clusters (A = Cs or K, Q = S or Se, and L = OH or CN). Langmuir 26:18512–18518. https://doi.org/10.1021/La103784v
106. Molard Y et al (2011) Ionically self-assembled clustomesogen with switchable magnetic/luminescence properties containing $[Re_6Se_8(CN)_6]^{n-}$ (n = 3, 4) anionic clusters. Chem Mater 23:5122–5130. https://doi.org/10.1021/Cm201589d
107. Solovieva AO et al (2017) Singlet oxygen production and biological activity of hexanuclear chalcocyanide rhenium cluster complexes $[\{Re_6Q_8\}(CN)_6]^{4-}$ (Q = S, Se, Te). Inorg Chem 56:13491–13499. https://doi.org/10.1021/acs.inorgchem.7b02212
108. Svezhentseva EV et al (2017) Materials based on X-ray contrast octahedral metal cluster complexes and hydrophilic polymers. Mater Today Proc 4:11430–11436
109. Kozlova SG, Gabuda SP, Brylev KA, Mironov YV, Fedorov VE (2004) Electronic spectra and DFT calculations of hexanuclear chalcocyanide rhenium clusters. J Phys Chem A 108:10565–10567. https://doi.org/10.1021/jp046753f
110. Rabanal-Leon WA, Murillo-Lopez JA, Paez-Hernandez D, Arratia-Perez R (2015) Exploring the nature of the excitation energies in [Re-6(mu(3)-Q(8))X-6](4-) clusters: a relativistic approach. Phys Chem Chem Phys 17:17611–17617. https://doi.org/10.1039/c5cp02003d
111. Rojas-Poblete M, Carreno A, Gacitua M, Paez-Hernandez D, Rabanal-Leon WA, Arratia-Perez R (2018) Electrochemical behaviors and relativistic DFT calculations to understand the terminal ligand influence on the [Re-6(mu(3)-Q)(8)X-6](4-) clusters. New J Chem 42:5471–5478. https://doi.org/10.1039/c7nj05114j

112. Beauvais LG, Shores MP, Long JR (1998) Cyano-bridged Re_6Q_8 (Q = S, Se) cluster-metal framework solids: a new class of porous materials. Chem Mater 10:3783
113. Naumov NG, Artemkina SB, Virovets AV, Fedorov VE (1999) Adjustment of dimensionality in covalent frameworks formed by Co^{2+} and rhenium cluster chalcocyanide $[Re_6S_8(CN)_6]^{4-}$. Solid State Sci 1:473–482
114. Naumov NG, Artemkina SB, Virovets AV, Fedorov VE (2000) Facile transformation of isolated fragments to infinite chains in rhenium chalcocyanide clusters: synthesis and structure of $(Pr_4N)_2M(H_2O)_5$ $[Re_6X_8(CN)_6]\cdot H_2O$ and $(Pr_4N)_2M(H_2O)_4[Re_6S_8(CN)_6]$ (X= S, Se; M= Mn, Ni). J Solid State Chem 153:195–204
115. Beauvais LG, Shores MP, Long JR (2000) Cyano-bridged Re_6Q_8 (Q = S, Se) Cluster-Cobalt (II) framework materials: versatile solid chemical sensors. J Am Chem Soc 122:2763–2772
116. Bennett MV, Shores MP, Beauvais LG, Long JR (2000) Expansion of the porous solid $Na_2Zn_3[Fe(CN)_6]_2.9H_2O$: enhanced ion-exchange capacity in $Na_2Zn_3[Re_6Se_8(CN)_6]_2.24H_2O$. J Am Chem Soc 122:6664–6668
117. Naumov NG, Soldatov DV, Ripmeester JA, Artemkina SB, Fedorov VE (2001) Extended framework materials incorporating cyanide cluster complexes: structure of the first 3D architecture accommodating organic molecules. Chem Commun:571–572. https://doi.org/10.1039/B008040N
118. Bennett MV, Beauvais LG, Shores MP, Long JR (2001) Expanded Prussian blue analogues incorporating $[Re_6Se_8(CN)_6]^{3-/4-}$ clusters: adjusting porosity via charge balance. J Am Chem Soc 123:8022–8032. https://doi.org/10.1021/ja0110473
119. Fedorov VE et al (2002) Inorganic coordination polymers based on chalcocyanide cluster complexes. J Struct Chem 43:669–684
120. Mironov YV, Naumov NG, Brylev KA, Efremova OA, Fedorov VE, Hegetschweiler K (2004) Rhenium-chalcogenide-cyano clusters, Cu^{2+} ions, and 1,2,3,4-tetraaminobutane as molecular building blocks for chiral coordination polymers. Angew Chem Int Ed 43:1297–1300. https://doi.org/10.1002/anie.200351595
121. Brylev KA, Pilet G, Naumov NG, Perrin A, Fedorov VE (2005) Structural diversity of low-dimensional compounds in $[M(en)_2]^{2+}/[Re_6Q_8(CN)_6]^{4-}$ systems (M = Mn, Ni, Cu). Eur J Inorg Chem:461–466. https://doi.org/10.1002/ejic.200400391
122. Tarasenko MS, Ledneva AY, Naumov NG, Naumov DY, Fedorov VE (2005) Novel low dimensional cluster compounds: syntheses and crystal structures of $Cs[\{Me_3Sn\}_3\{Re_6Se_8(CN)_6\}]$, $[\{Me_3Sn(H_2O)\}_2\{Me_3Sn\}\{Re_6Se_8(CN)_6\}]\cdot H_2O$, and $[(Me_3Sn)_3(OH)_2][\{Me_3Sn\}_3\{Re_6Se_8(CN)_6\}]$. pH control of the structural dimensionality. J Clust Sci 16:353–365
123. Kim S, Kim Y, Kal Y, Kim SJ (2007) A new organic-inorganic hybrid framework containing octahedral hexarhenium cluster and its transformation by ligand exchange. Inorg Chim Acta 360:1870–1874
124. Jin S, DiSalvo FJ (2002) 3-D coordination network structures constructed from $[W_6S_8(CN)_6]^{6-}$ anions. Chem Mater 14:3448–3457
125. Cordier S, Naumov NG, Salloum D, Paul F, Perrin C (2004) Synthesis and characterization of Mo_6 chalcobromides and cyano-substituted compounds built from a novel $[(((Mo_6Br_6Y_2^i)\text{-}Y^i)L_6^a)]^{n-}$ discrete cluster unit (Y^i = S or Se and L^a = Br or CN). Inorg Chem 43:219–226. https://doi.org/10.1021/Ic034443q
126. Zhang JJ, Zhou HJ, Lachgar A (2007) Directed assembly of cluster-based supramolecules into one-dimensional coordination polymers. Angew Chem Int Ed 46:4995–4998
127. Zhou HJ, Lachgar A (2007) Octahedral metal clusters $[Nb_6Cl_{12}(CN)_6]^{4-}$ as molecular building blocks: from supramolecular assemblies to coordination polymers. Eur J Inorg Chem 2007:1053–1066
128. Naumov NG, Virovets AV, Sokolov MN, Artemkina SB, Fedorov VE (1998) A novel framework type for inorganic clusters with cyanide ligands: crystal structures of $Cs_2Mn_3[Re_6Se_8(CN)_6]_2\cdot 15H_2O$ and $(H_3O)_2Co_3[Re_6Se_8(CN)_6]_2\cdot 14.5H_2O$. Angew Chem Int Ed 37:1943–1945

129. Brylev KA, Naumov NG, Virovets AV, Kim SJ, Fedorov VE (2009) Novel three-dimensional coordination polymers based on $[Mo_6Se_8(CN)_6]^{7-}$ anions and Mn^{2+} cations. J Clust Sci 20:165–176
130. Friedrichs OD, O'Keeffe MO, Yaghi OM (2003) Three-periodic nets and tilings: semiregular nets. Acta Crystallogr A 59:515–525. https://doi.org/10.1107/S0108767303017100
131. Virovets AV, Gayfulin YM, Peresypkina EV, Mironov YV, Naumov NG (2015) Novel 'anti-Prussian blue' structure based on Zn^{2+} nodes and $[Re_3Mo_3S_8(CN)_6]^{6-}$ heterometallic cluster spacers and its rearrangement to Prussian blue. CrystEngComm 17:1477–1482. https://doi.org/10.1039/C4ce02240h
132. Shores MP, Beauvais LG, Long JR (1999) Cluster-expanded Prussian blue analogues. J Am Chem Soc 121:775–779
133. Yan B, Zhou H, Lachgar A (2003) Octahedral niobium chloride clusters as building blocks of templated Prussian blue framework analogues. Inorg Chem 42:8818–8822
134. Naumov NG, Cordier S, Perrin C (2005) An extended open framework based on disordered $[Nb_6Cl_9O_3(CN)_6]^{5-}$ cluster units: synthesis and crystal structure of $Cs_3Mn[Nb_6Cl_9O_3(CN)_6]\cdot 0.6H_2O$. Solid State Sci 7:1517–1521
135. Shores MP, Beauvais LG, Long JR (1999) $[Cd_2(H_2O)_4][Re_6S_8(CN)_6]\cdot 14H_2O$: a cyano-bridged cluster-cluster framework solid with accessible cubelike cavities. Inorg Chem 38:1648–1649
136. Naumov NG, Sokolov MN, Imoto H, Saito T, Fedorov VE (2001) Synthesis and structure of $Co_2[Re_6Se_8(CN)_6]\cdot 12H_2O$. J Struct Chem 42:326–330
137. Naumov NG, Virovets AV, Mironov YI, Artemkina SB, Fedorov VE (1999) Synthesis and crystal structure of new layered cluster cyanides $Cs_2M[Re_6S_8(CN)_6]\cdot 2H_2O$ (M=Mn^{2+}, Fe^{2+}, Co^{2+}, Cd^{2+}): size control over framework dimension. Ukr Khim 65:21–27
138. Iwamoto T (1996) Past, present and future of the clathrate inclusion compounds built of cyanometallate hosts. J Incl Phenom Mol 24:61–132. https://doi.org/10.1007/Bf01053426
139. Daigre G et al (2018) Low dimensional solids based on Mo_6 cluster cyanides and Mn^{2+}, Mn^{3+} or Cd^{2+} metal ions: crystal chemistry, magnetic and optical properties. CrystEngComm 20:3396–3408. https://doi.org/10.1039/c8ce00113h
140. Naumov NG, Mironov YV, Brylev KA, Fedorov VE (2006) A new cyanobridged one-dimensional coordination polymer based on the octahedral rhenium cluster $[Re_6Se_8(CN)_6]^{4-}$: synthesis and crystal structure of $[\{Cu(H_2O)_{0.5}(en)_2\}\{Cu(en)_2\}Re_6Se_8(CN)_6].3H_2O$. J Struct Chem 47:771–776
141. Yunlu K, Hock N, Fischer D (1985) Polymeric tris[trimethyltin(IV)]hexacyanocobaltate(III), a compound non-analogous to super Prussian blue, and its tris[tricyclopentadienyluranium(IV)] homologue. Angew Chem Int Ed 24:879–881
142. Siebel E, Fischer RD (1997) Polymeric $[(Me_3Sn)_3Rh(SCN)_6]$: a novel "super-Prussian-blue" derivative containing the nonlinear-SCN-Sn-NCS-spacer. Chem Eur J 3:1987–1991
143. Schwarz P, Siebel E, Fischer RD, Apperley DC, Davies NA, Harris RK (1995) $[(CoCp_2)$ subset-of $Fe(\mu\text{-}CNSnMe_3NC)_3]$ - a purely organometallic channel inclusion compound. Angew Chem Int Ed 34:1197–1199
144. Tarasenko MS, Ledneva AY, Kurat'eva NV, Naumov DY, Kim SJ, Fedorov VE, Naumov NG (2007) Synthesis and structure of novel coordination compounds based on $[Re_6Q_8(CN)_6]^{4-}$ (Q = S, Se) and $(SnMe_3)^+$. Russ J Coord Chem 33:876–885
145. El Osta R et al (2015) Supramolecular frameworks built up from red-phosphorescent trans-Re_6 cluster building blocks: one pot synthesis, crystal structures, and DFT investigations. Z Anorg Allg Chem 641:1156–1163. https://doi.org/10.1002/zaac.201500074
146. Ledneva AY, Naumov NG, Virovets AV, Cordier S, Molard Y (2012) Crystal structures of trans-$[Re_6S_8(CN)_2L_4]$ complexes, L = pyridine or 4-methylpyridine. J Struct Chem 53:132–137. https://doi.org/10.1134/S0022476612010179
147. Naumov NG, Virovets AV, Fedorov VE (2000) Unusually high porosity in polymeric cluster cyanides: the synthesis and crystal structure of$(H_3O)_2Zn_3[Re_6Se_8(CN)_6]_2\cdot 20H_2O$. Inorg Chem Commun 3:71–72

148. Artemkina SB, Naumov NG, Virovets AV, Gromilov SA, Fenske D, Fedorov VE (2001) New polymeric structure of rhenium octahedral chalcocyanide complex: Ln^{3+}-derived network with one-dimensional channels. Inorg Chem Commun 4:423–426
149. Tarasenko MS, Golenkov EO, Naumov NG, Moroz NK, Fedorov VE (2009) Unusual H-bonding in novel cyano-cluster polymeric hydrates $[(H)\{Ln(H_2O)_4\}\{Re_6S_8(CN)_6\}]\cdot 2H_2O$ (Ln = Yb, Lu). Chem Commun:2655–2657
150. Kumar P, Naumov NLG, Boukherroub R, Jain SL (2015) Octahedral rhenium $K_4[Re_6S_8(CN)_6]$ and $Cu(OH)_2$ cluster modified TiO_2 for the photoreduction of CO_2 under visible light irradiation. Appl Catal A 499:32–38. https://doi.org/10.1016/j.apcata.2015.04.001
151. Elistratova J et al (2018) Structure optimization for enhanced luminescent and paramagnetic properties of hydrophilic nanomaterial based on heterometallic Gd-Re complexes. Mater Des 146:49–56. https://doi.org/10.1016/j.matdes.2018.03.006
152. Amela-Cortes M, Molard Y, Paofai S, Desert A, Duvail JL, Naumov NG, Cordier S (2016) Versatility of the ionic assembling method to design highly luminescent PMMA nanocomposites containing $[M_6Q_8^{i}\ L_6^{a}]^{n-}$ octahedral nano-building blocks. Dalton Trans 45:237–245. https://doi.org/10.1039/c5dt03734d
153. Cordier S, Molard Y, Brylev KA, Mironov YV, Grasset F, Fabre B, Naumov NG (2015) Advances in the engineering of near infrared emitting liquid crystals and copolymers, extended porous frameworks, theranostic tools and molecular junctions using tailored Re_6 cluster building blocks. J Clust Sci 26:53–81. https://doi.org/10.1007/s10876-014-0734-0

Struct Bond (2019) 180: 75–108
DOI: 10.1007/430_2019_32

Published online: 11 May 2019

Exploring the Breadth of Terminal Ligands Coordinated in $[Mo_6X_8]^{4+}$- and $[Re_6Q_8]^{2+}$-Based Cluster Complexes

Lisa F. Szczepura and Ernesto Soto

Contents

Abstract This survey provides an overview of the different types of terminal ligands incorporated into molybdenum halide and rhenium chalcogenide cluster complexes. While the incorporation of halide and pseudohalide ligands is prevalent with these systems, this article focuses on the coordination of other nitrogen-, oxygen-, sulfur-, and carbon-donor ligands. Emphasis has been placed on synthetic methodologies and the significance behind coordination of these ligands to discrete cluster complexes.

Keywords Cluster · Ligands · Molybdenum · Rhenium · Synthetic methodology

Honoring the legacy of Marcel Sergent.

L. F. Szczepura (✉) and E. Soto
Department of Chemistry, Illinois State University, Normal, IL, USA
e-mail: lfszcze@ilstu.edu

1 Introduction

The cluster chemistry of molybdenum and rhenium is dominated by polynuclear species having the $[Mo_6(\mu_3\text{-}X)_8]^{4+}$ or $[Re_6(\mu_3\text{-}Q)_8]^{2+}$ core, where X = halogen and Q = chalcogen. These cluster cores contain an octahedron of metal atoms inscribed in a cube of facially bridging heteroatoms. Discrete hexanuclear octahedral clusters are stabilized by six additional terminal or apical ligands (L) leading to molecular systems with the general abbreviated formula of $[Mo_6X_8L_6]^{n+}$ or $[Re_6Q_8L_6]^{n+}$. Although molybdenum(II) halides have been known for many years [1], the field was revolutionized in the 1970s when reports of octahedral metal sulfide clusters appeared in the literature. The discovery of Chevrel phases ($M'Mo_6S_8$) had the most significant impact [2]. The superconducting properties of these ternary molybdenum chalcogenides were discovered early on; further investigations have proven these materials to have numerous other interesting properties, with some of the recent studies examining their potential as cathode materials in rechargeable batteries [3–6]. Not long after the discovery of Chevrel phase materials, reports detailing the preparation of analogous hexanuclear rhenium chalcogenide clusters appeared in the literature [7–9]. However, it was Sergent who pioneered the preparation of rhenium chalcohalide cluster phases and recognized the potential associated with condensing discrete clusters to form higher dimensional materials and how this would enable one to control the physical properties of those materials [10–13]. Cluster excision, the reverse of cluster condensation, is what brought us discrete cluster complexes [14–16]. This process, which is also referred to as dimensional reduction, involves reacting cluster-based materials with simple salts which are able to decrease the bridging interactions, thereby reducing the dimensionality of a material; the dimensional reduction of $Re_6Se_8Cl_2$ is shown in Fig. 1 [17].

Owing to the electronic nature of these 24 electron cluster cores, the regular octahedral geometry and the stereochemical rigidity of these systems (i.e., they are non-fluxional), $[Mo_6X_8]^{4+}$- and $[Re_6Q_8]^{2+}$-containing clusters, are often considered to be larger versions of single metal octahedral complexes. Therefore, research involving these systems has partially been driven by the desire to use these clusters as building blocks in the preparation of novel supramolecular frameworks [18–21]. Efforts to expand on earlier reports detailing the unique photophysical and electrochemical properties displayed by these cluster systems have also been a major driving force [22–26]. In order to take advantage of the unique structural and functional properties associated with these octahedral clusters and design clusters for specific applications, it is necessary to have control over terminal ligand substitution and to have the ability to incorporate a wide variety of ligand types. We present this review in an effort to highlight the progress that has been made toward broadening the scope of terminal ligands coordinated to $[Mo_6X_8]^{4+}$ (X = Cl, Br, I) and $[Re_6Q_8]^{2+}$ (Q = S, Se) cluster cores. The focus of this account is on the preparation of discrete molybdenum halide and rhenium chalcogenide clusters containing novel terminal ligands, i.e., ligands other than halides or pseudohalides. At times, we refer to applications, reactivity, and physical studies which motivated

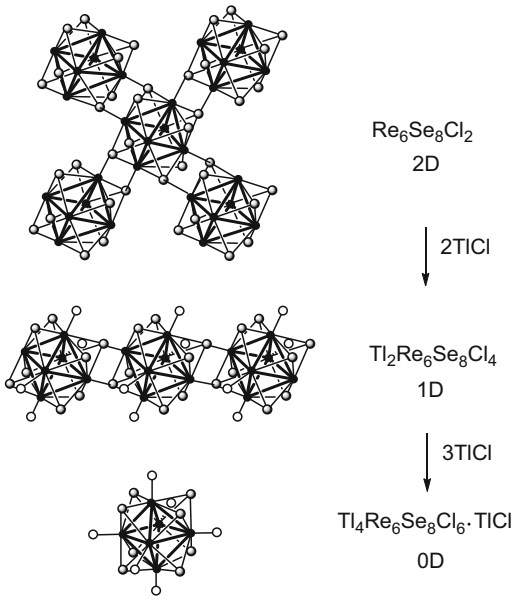

Fig. 1 Dimensional reduction of $Re_6Se_8Cl_2$ with TlCl to generate the discrete cluster $Tl_4[Re_6Se_8Cl_6]\cdot TlCl$. Adapted with permission from [17] Copyright 2001 American Chemical Society

researchers to pursue these synthetic endeavors. However, the aim of this article is to focus on the synthetic methodologies and significance behind the coordination of these ligands. In addition, it is important to note that this article does not delve into the materials chemistry of these systems (i.e., coordination polymers, nanoparticles, incorporation into organic polymers, etc.), but focuses on discrete systems that can be solubilized. An extensive review of rhenium chalcogenide clusters was published by Batail and coworkers in 2001 [27], and Prokopuk and Shriver published a review on the chemistry of Group 5 and 6 octahedral clusters in 1998 [28]. Our objective is to build on these and other more recent reviews [29–31] and to provide an up-to-date overview without duplicating material summarized in previous accounts.

2 $[Re_6Q_8]^{2+}$-Based Clusters

2.1 Nitrogen-Donor Ligands

2.1.1 Direct Coordination

Over the years, a number of cluster complexes containing neutral N-donor ligands have been prepared, common among these are nitriles and heterocyclic ligands such as pyridine and pyrazine [27]. Acetonitrile was one of the first nitriles to be coordinated by Holm and coworkers [32], by reacting a cluster complex containing one or more terminal halide ligands with silver(I) salts of non-coordinating anions (such as BF_4^- or SbF_6^-) in the presence of excess nitrile. Our group followed a

similar procedure in the preparation of $[Re_6Se_8(PEt_3)_5(NCC(CH_3)_3)](SbF_6)_2$, which contains the sterically bulky trimethylacetonitrile ligand [33]. Nitriles and pyridine are both readily coordinated to the cluster core; however, pyridine is more versatile in that there are numerous commercially available pyridine derivatives which can be used to enhance the functionality of the cluster. For example, Zheng and coworkers utilized 4,4′-dipyridyl and 1,2-bis(4-pyridyl)ethane to bridge $[Re_6Q_8]^{2+}$ cluster cores together [34]. Coordination of pyridine-based ligands has been achieved either by following a procedure similar to that used for the coordination of nitriles or by substitution of acetonitrile ligands by different pyridine donor ligands. It is worth mentioning the structural and functional advantages that these octahedral rhenium chalcogenide clusters have in comparison to other high-nuclearity transition metal clusters for the preparation of supramolecular arrays. The rigid (non-fluxional) nature of the cluster core, as well as the ability to site-differentiate the terminal ligands, allows for control over the positioning of ligands and the eventual connectivity between units. That is, these cluster cores can be viewed as building blocks in the design of supramolecular arrays. Key strategies for assembling these clusters into supramolecular arrays include (1) insertion of a cluster cation in place of a single metal center in a metal organic framework, (2) use of ligated clusters with appropriate functionalities to connect to other metal ions in solution ("cluster-as-ligand" approach), and (3) incorporating ligands that can self-assemble through secondary interactions such as hydrogen bonding and π-stacking. Zheng and coworkers have published some micro-reviews summarizing their (and others) contributions to this area [21, 35–37]. More recently, other pyridine-based ligands such as isonicotinic acid and 4-aminopyridine have been utilized to prepare discrete cluster complexes (e.g., *trans*-$[Re_6S_8(4\text{-aminopyridine})_4(OH)_2]$ [38] and *cis*- and *trans*-$[Re_6Se_8(PEt_3)_4(\text{isonicotinic acid})_2](SbF_6)_2$ [39]). The difference between the hydrogen-bonded networks formed when *cis*- and *trans*-$[Re_6Se_8(PEt_3)_4(\text{isonicotinic acid})_2](SbF_6)_2$ crystallize is shown in Fig. 2; two of the structures shown contain isonicotinate, indicating deprotonation of one of the isonicotinic acid units during crystallization. The successful coordination of six porphyrin rings to the rhenium sulfide and selenide cores emphasizes the increased size of the rhenium chalcogenide cores compared to their single metal counterparts, i.e., $[Re_6Q_8(H_2PyT_3P)_6]^{2+}$ (Fig. 3, left) and $[Re_6Q_8(ZnPyT_3P)_6]^{2+}$ (Q = S, Se; H_2PyT_3P = 5-(4-pyridyl)-10,15,20-tritolylporphyrin, and $ZnPyT_3P$ = 5-(4-pyridyl)-10,15,20-tritolylporphyrinatozinc (II)) [40]. Electrochemical studies of these and of disubstituted clusters bridged to ruthenium porphyrin complexes (*cis*- and *trans*-$[Re_6S_8Cl_4\{(\mu\text{-bpy})Ru(CO)(ttp)\}_2]^{2-}$ and *trans*-$[Re_6S_8Cl_4\{(\mu\text{-pyrazine})Ru(CO)(ttp)\}_2]^{2-}$ (Fig. 3, right) (ttp = tetratolylporphyrin) were undertaken to explore the redox communication between the cluster core and the porphyrin moieties.

The unique electrochemical and luminescent properties of the $[Re_6Q_8]^{2+}$ and $[Mo_6X_8]^{4+}$ systems are often cited as reasons behind the sustained interest in these octahedral clusters. The following are examples where functionalized pyridines were used to control the physical properties of the cluster complexes. Guldi and coworkers modified the pyridine ligand with a fullerene in the preparation of a covalently linked donor-acceptor dyad, wherein a rhenium chalcogenide cluster core was the donor

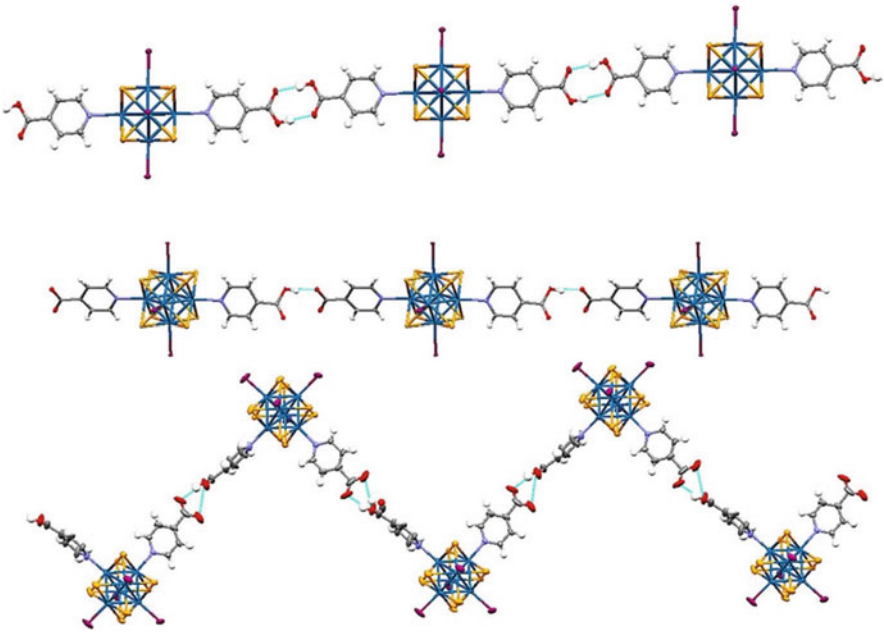

Fig. 2 The structures of *trans*-$[Re_6Se_8(PEt_3)_4(\text{isonicotinic acid})_2]^{2+}$, *trans*-$[Re_6Se_8(PEt_3)_4(\text{isonicotinic acid})(\text{isonicotinate})]^{+}$, and *cis*-$[Re_6Se_8(PEt_3)_4(\text{isonicotinic acid})(\text{isonicotinate})]^{+}$ (top to bottom), where intermolecular hydrogen bonding (blue lines) is observed. Reprinted by permission from Springer Nature Customer Service Centre GmbH [39] Copyright 2015

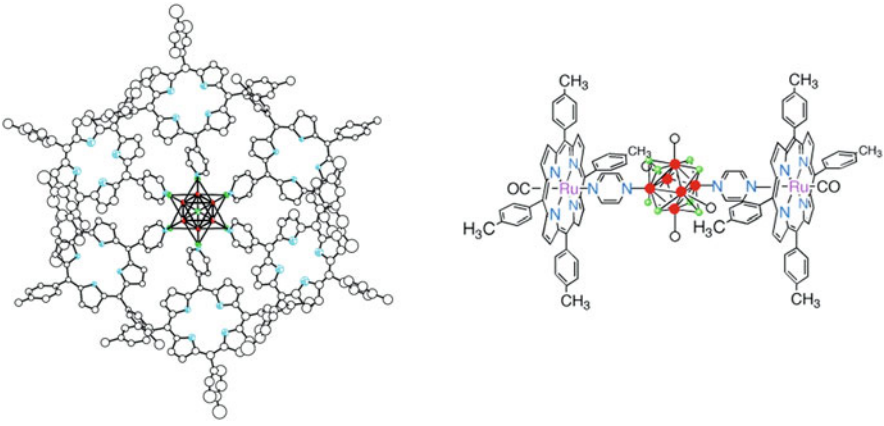

Fig. 3 Structure of $[Re_6Se_8(H_2PyT_3P)_6]^{2+}$ (left) and a schematic structure of $[Re_6S_8Cl_4\{(\mu\text{-pyrazine})Ru(CO)(ttp)\}_2]^{2-}$ (right). Reprinted with the permission from [40] Copyright 2002 Wiley-VCH Verlag GmbH & Co

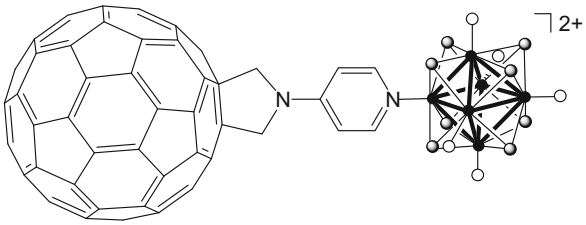

Fig. 4 Visual representation of $[Re_6Se_8(PEt_3)_5(N\text{-pyridyl-3,4-fulleropyrrolidine})]^{2+}$. Reprinted with the permission from [41] Copyright 2010 Wiley-VCH Verlag GmbH & Co

and C_{60}-fullerene the acceptor (Fig. 4) [41]. Such a design was inspired by the multicomponent systems found in natural photosynthetic processes. It is proposed that a light-induced energy transfer from the cluster to the C_{60}-fullerene in the $[Re_6Se_8(PEt_3)_5(N\text{-pyridyl-3,4-fulleropyrrolidine})]^{2+}$ complex occurs. Another example, published by Kitamura and coworkers, involves fine-tuning the photophysical properties of the rhenium sulfide cluster core by controlling the energy between the $[Re_6S_8]^{2+}$ core centered HOMO and the π^* orbital of the ligand. In this example, the phenylpyridine ligand in $(Bu_4N)_3[Re_6S_8Cl_5(4\text{-phenylpyridine})]$ (obtained by photoirradiation of a MeCN solution of $(Bu_4N)_4[Re_6S_8Cl_6]$ in the presence of 4-phenylpyridine) was found to enhance metal-to-ligand charge-transfer emission leading to a longer excited state lifetime [42]. This provides an example of how the synthetic chemistry of these systems has improved in such a way that subtle control over the physical properties of the rhenium chalcogenide clusters is becoming a reality.

In an effort to expand the type of potential organic linkers to rhenium chalcogenide cluster cores, Mironov et al. developed a synthetic route toward the coordination of neutral pyrazole ligands. Heating a mixture of $Cs_4[Re_6Q_8Br_6]$ (Q = S or Se) with 3,5-dimethylpyrazole at 200°C led to the isolation of $[Re_6Q_8(3,5\text{-}Me_2PzH)_6]Br_2{\cdot}2(3,5\text{-}Me_2PzH)$ (Q = S, Se) [43]. Substitution of the starting material with $Cs_3[Re_6Q_7Br_7]$ (Q = S, Se) resulted in the formation of $[Re_6Q_7O(3,5\text{-}Me_2PzH)_6]Br_2{\cdot}3,5\text{-}Me_2PzH$ [44]. This is a rare example of a facially bridging ligand undergoing exchange where the oxygen is believed to have come from trace water present in the starting material. These are also the first examples where hot molten ligands were utilized as the reaction medium for a ligand substitution reaction involving octahedral rhenium clusters (i.e., the cluster and ligand are mixed and sealed in a glass ampoule which is then heated past the melting point of the organic ligands). The advantage of this type of synthetic route is discussed by the authors.

Most of the nitrogen-donor ligands mentioned so far have been neutral in charge. However, Brylev et al. reported the direct coordination of anionic benzotriazolate (BTA) ligands. When the hexahydroxo species, $[Re_6Q_8(OH)_6]^{4-}$ (Q = S or Se), is heated with 1*H*-benzotriazole at 150°C, the products $K_4[Re_6S_8(BTA)_6]{\cdot}3.5EtOH{\cdot}4H_2O$ and $K_{2.75}H_{1.25}[Re_6Se_8(BTA)_6]{\cdot}3EtOH{\cdot}7H_2O$ are isolated [45] (Fig. 5). The latter complex is considered to be a 3:1 mix of $[Re_6Se_8(1H\text{-BTA})(BTA)_5]^{3-}$ and $[Re_6Se_8(1H\text{-BTA})_2(BTA)_4]^{2-}$ along with the potassium ions and solvate molecules; the weaker electron-accepting ability of the selenide core compared to the sulfide core is believed to be the reason behind the isolation of slightly

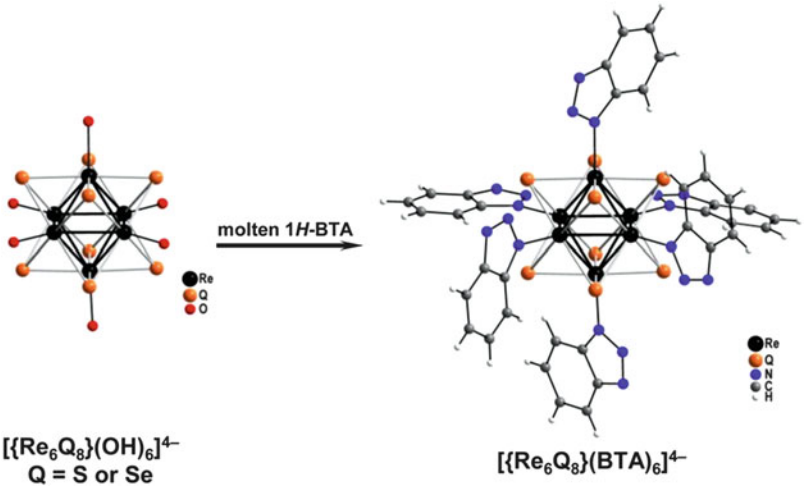

Fig. 5 The formation of $[Re_6Q_8(BTA)_6]^{4-}$ from $[Re_6Q_8(OH)_6]^{4-}$ and molten 1*H*-benzotriazole (1*H*-BTA). Reprinted with permission from [45] Copyright 2014 American Chemical Society

different formulations. Acidifying aqueous solutions of these complexes leads to the precipitation of $[Re_6Q_8(1H\text{-}BTA)_4(BTA)_2]$ (Q = S or Se). These clusters represent the first water-soluble rhenium sulfide clusters containing a heterocyclic ligand and were specifically designed to test their potential for biological applications. The authors report that both $K_4[Re_6S_8(BTA)_6]\cdot 3.5EtOH\cdot 4H_2O$ and $K_{2.75}H_{1.25}[Re_6Se_8(BTA)_6]\cdot 3EtOH\cdot 7H_2O$ were taken up by human cells and at the same time did not show any acute cytotoxic effects [45]. In addition, photophysical properties suggest that these complexes could have applications in bioimaging or photodynamic therapy. Also, the incorporation of BTA ligands shows a marked stability over the carboxylate-containing clusters (vide infra) in that the BTA ligands do not exchange with water over an extended period of time.

2.1.2 Formation of Novel Ligands via Small Molecule Activation

Small molecule activation is frequently associated with catalytic processes whereby substrates undergo transformation during their association with a metal center. It is well known that metals can alter the chemistry of coordinated ligands, yet metal reactivity is often selective making it challenging to predict which of these transformations will be achieved by a given complex. Of interest to this review is that rhenium chalcogenide cluster cores have been proven to be strong Lewis acids. In fact, they are strong enough to activate small molecules to undergo transformations either faster or under milder conditions (or both) than what would be required if the molecule was not coordinated to the cluster. Unlike so many other Lewis acidic centers, the rhenium chalcogenide clusters are relatively stable upon exposure to air and water, making them potentially attractive alternatives to other, less robust,

systems. It is important to note that, as of yet, there are no reported examples of catalysis by a rhenium chalcogenide cluster core (i.e., examples where more than one equivalent of substrate is transformed at a given time). The ability of rhenium chalcogenide clusters to activate small molecules has enabled species such as nitriles, coordinated to the $[Re_6Se_8]^{2+}$ core, to be converted into unique ligands, thereby expanding the number and type of ligands incorporated into these supraoctahedral cluster complexes. Here we discuss the application of this synthetic methodology toward the coordination of unique terminal N-donor ligands. Rhenium chalcogenide clusters are known to be substitutionally inert, normally requiring heat and extended reaction times for reaction to occur. One attractive feature of small molecule activation is that novel ligands can often be incorporated under milder conditions. Here we discuss reactions in which different anionic and neutral nucleophiles attack nitriles coordinated to the $[Re_6Se_8]^{2+}$ core.

In 2007, we discovered that inorganic azides, such as NaN_3, react with the acetonitrile ligand in $[Re_6Se_8(PEt_3)_5(NCCH_3)](BF_4)_2$ to form tetrazolate complexes [46]. Coordination of acetonitrile to the Lewis acidic rhenium selenide cluster core activates the ligand to undergo a [2 + 3] cycloaddition with N_3^- within minutes at room temperature to form $[Re_6Se_8(PEt_3)_5(1,5\text{-methyltetrazolate})]^+$. This cycloaddition was classified as "click chemistry" due to the mild conditions, rapid reaction time, high yield, and purity of the product generated. This is the first click reaction reported for this family of clusters. Electrochemical studies enabled the determination of an electronic parameter (E_L) for a tetrazolate ligand and demonstrated that Lever's method can be applied to higher-nuclearity clusters. Cyclic voltammetric studies also revealed an unusual oxidative decomposition process indicating formation of the starting nitrile complex after accessing the $[Re_6Se_8(PEt_3)_5(1,5\text{-methyltetrazolate})]^{2+/+}$ couple. That same year, Orto et al. published the formation of imino ester complexes generated when simple alcohols react with analogous acetonitrile complexes [47]. Zheng recently summarized this chemistry, where hydrogen bonding of the alcohol with the bridging selenide ligands on the cluster core is proposed to explain the predominant formation of the Z-isomer [48].

This click chemistry was extended to a series of benzonitrile clusters, $[Re_6Se_8(PEt_3)_5(N{\equiv}CC_6H_4Y)](BF_4)_2$ (Y = –H, $–NH_2$, $–NO_2$, –OMe, and $–COCH_3$), and the electrochemical, substitution chemistry and reactivity with inorganic azides were investigated [49]. Figure 6 shows click reactions involving $[Re_6Se_8(PEt_3)_5(N{\equiv}CR)]^{2+}$and various nucleophilic groups. These coordinated benzonitriles also undergo cyclization; however, only the N2 isomers are isolated, e.g., $[Re_6Se_8(PEt_3)_5(2,5\text{-phenyltetrazolate})](BF_4)$ was the sole product isolated when $[Re_6Se_8(PEt_3)_5(N{\equiv}CC_6H_5)](BF_4)_2$ was reacted with NaN_3 [46, 49]. This is in contrast to the reaction with coordinated acetonitrile, which forms the N1 isomer at room temperature and a 50/50 mixture of isomers upon heating, demonstrating how the steric size of the nitrile substituent influences the coordination mode of the tetrazolate ring (Fig. 7). Although changing the *para* substituent on the phenyl ring had negligible impact on the redox potentials of these clusters, it did impact the rates of substitution of the coordinated nitriles. Heating $[Re_6Se_8(PEt_3)_5(1,5\text{-methyltetrazolate})]^+$ (or $[Re_6Se_8(PEt_3)_5(2,5\text{-phenyltetrazolate})]^+$)

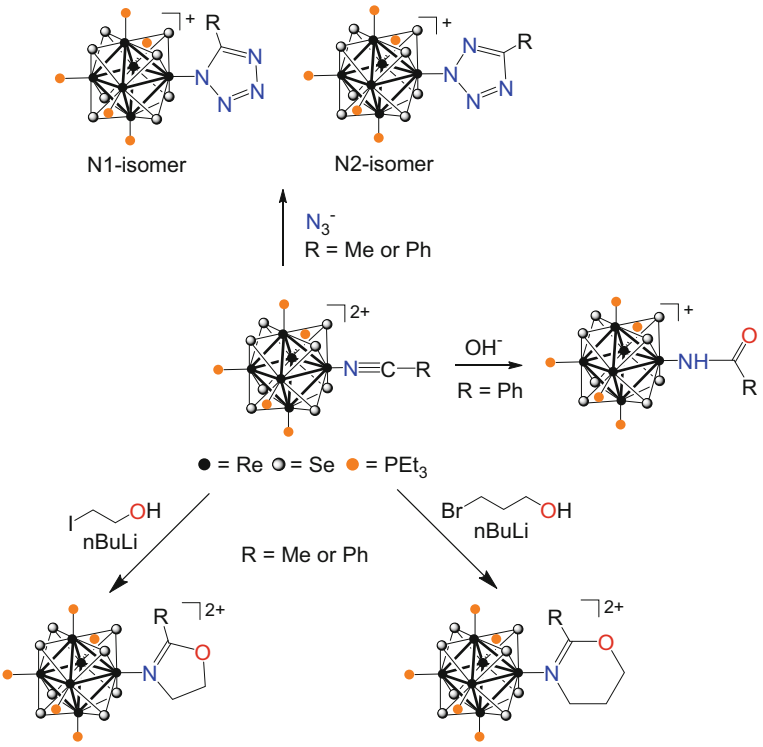

Fig. 6 Schematic diagram showing some of the click chemistry facilitated by the $[Re_6Se_8]^{2+}$ cluster core, formation of tetrazolate, oxazoline, and oxazine rings in addition to formation of a carboxamide ligand

with a strong acid in CH_3CN leads to the release of 5-methyltetrazole (or 5-phenyltetrazole) and formation of the nitrile complex, $[Re_6Se_8(PEt_3)_5(NCCH_3)]^{2+}$, indicating potential for catalysis. Disubstituted tetrazoles could also be generated using alkylating agents such as MeI and BnBr. Even when starting with a single tetrazolate isomer (N1 or N2), mixtures of 1,5- and 2,5-disubstituted tetrazoles were formed, and potential mechanisms for this isomerization process were discussed. It is interesting to note that nitriles coordinated to the rhenium selenide cluster core do not click with organic azides, instead, substitution and subsequent photodecomposition leads to the formation of cluster imino complexes. Zheng discusses this reaction in greater detail in a recent account [48].

Our group also reported the formation of heterocyclic triazolate ligands. Like the formation of tetrazolate ligands, the triazolates were also prepared via a click reaction. However, the triazolates were formed when coordinated azides react with free alkynes [50]. Three different triazolate cluster complexes were synthesized, $[Re_6Se_8(PEt_3)_5$(4,5-bis(methoxycarbonyl)-1,2,3-triazolate)$](BF_4)$ (Fig. 8), $[Re_6Se_8(PEt_3)_5$(4-methoxycarbonyl-5-(1-propanol)-1,2,3-triazolate)$](BF_4)$, and

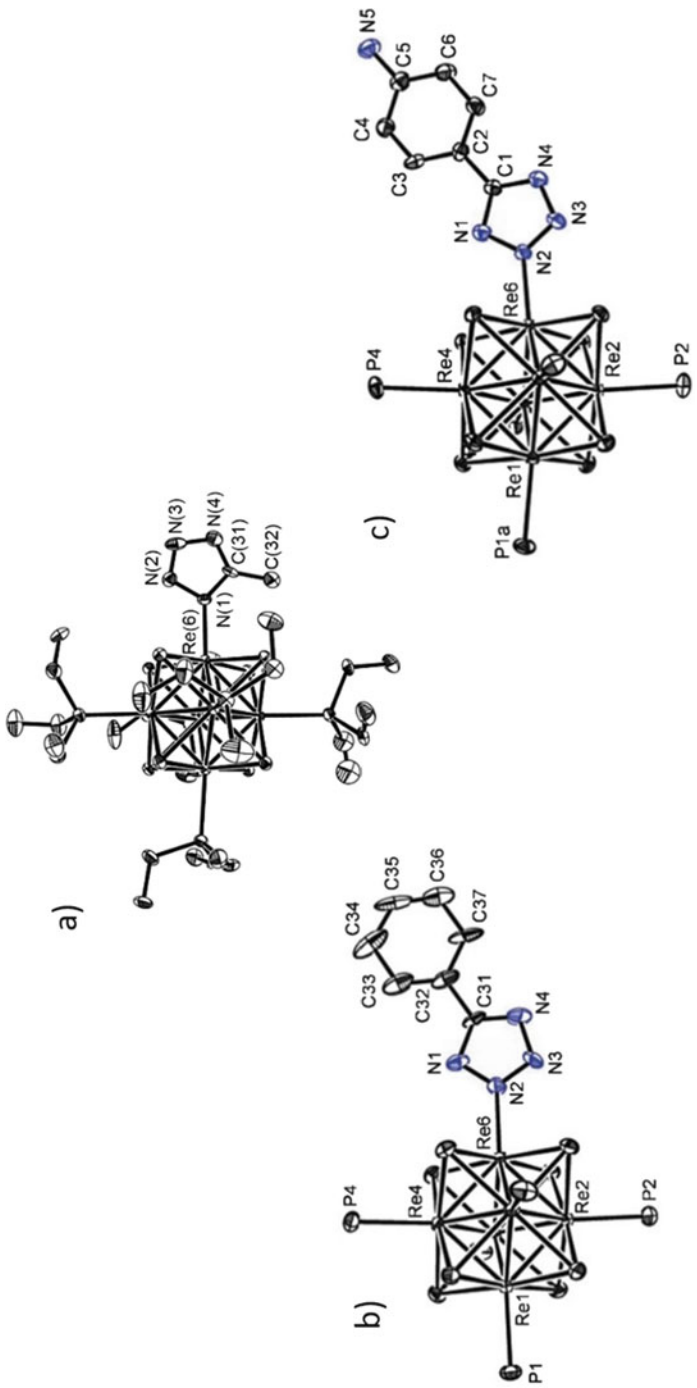

Fig. 7 Structures of (**a**) $[Re_6Se_8(PEt_3)_5(1,5\text{-methyltetrazolate})]^+$, (**b**) $[Re_6Se_8(PEt_3)_5(2,5\text{-phenyltetrazolate})]^+$, and (**c**) $[Re_6Se_8(PEt_3)_5(2,5\text{-}p\text{-aminophenyltetrazolate})]^+$. (**a**) [46]–Reproduced by permission of The Royal Society of Chemistry. (**b**, **c**) Reprinted with permission from [49] Copyright 2012 American Chemical Society

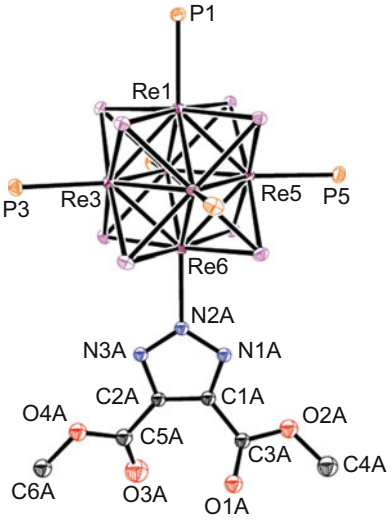

Fig. 8 Structure of $[Re_6Se_8(PEt_3)_5(4,5\text{-bis}(methoxycarbonyl)\text{-}1,2,3\text{-}triazolate)]^+$. [50]–Reproduced by permission of The Royal Society of Chemistry

cis-$[Re_6Se_8(PEt_3)_4(4,5\text{-bis}(methoxycarbonyl)\text{-}1,2,3\text{-}triazolate)_2]$. The latter complex demonstrates that these clusters can promote multiple azide moieties to undergo heterocyclic ring formation. Reaction of the triazolate complexes with electrophilic reagents such as methyl iodide and benzyl bromide leads to the formation of free triazoles as well as the halide containing cluster complexes, e.g., $[Re_6Se_8(PEt_3)_5X]^+$ (X = I, Br).

In addition to reacting with simple alcohols, nitriles coordinated to the rhenium selenide cluster core also react with ammonia (Fig. 9). Specifically, addition of ammonia to coordinated nitriles in $[Re_6Se_8(PEt_3)_5(MeCN)](BF_4)_2$ and *cis*- and *trans*-$[Re_6Se_8(PEt_3)_4(MeCN)_2](BF_4)_2$ leads to quantitative conversion to the corresponding acetamidine complexes, $[Re_6Se_8(PEt_3)_5(HN{=}C(NH_2)CH_3)](BF_4)_2$, and *cis*- and *trans*-$[Re_6Se_8(PEt_3)_4(HN{=}C(NH_2)CH_3)_2](BF_4)_2$, respectively [51]. As observed with the addition of alcohols to coordinated nitriles, the Z-isomer of the acetamidine cluster is favored. Amidine ligand removal is achieved through reaction with trifluoroacetate, which generates acetamidinium trifluoroacetate along with the starting nitrile complex.

Most recently, we published a report detailing the reaction of coordinated nitriles with hydroxide and haloalcohols in the presence of *n*BuLi [52]. Reaction of $[Re_6Se_8(PEt_3)_5(benzonitrile)](BF_4)_2$ with an aqueous solution of KOH at room temperature led to the formation of $[Re_6Se_8(PEt_3)_5(phenylcarboxamide)]^+$ (Fig. 10). In addition, heterocyclic oxazine and oxazoline formation occurs when $[Re_6Se_8(PEt_3)_5(NCPh)](BF_4)_2$ and $[Re_6Se_8(PEt_3)_5(NCCH_3)](BF_4)_2$ undergo reaction with $BrCH_2CH_2CH_2O^-$ and $ICH_2CH_2O^-$ (generated in situ). The incorporation of four new heterocyclic ligands was achieved by these reactions; these include 2-methyloxazoline, 2-phenyloxazoline, 2-methyloxazine, and 2-phenyloxazine. Of

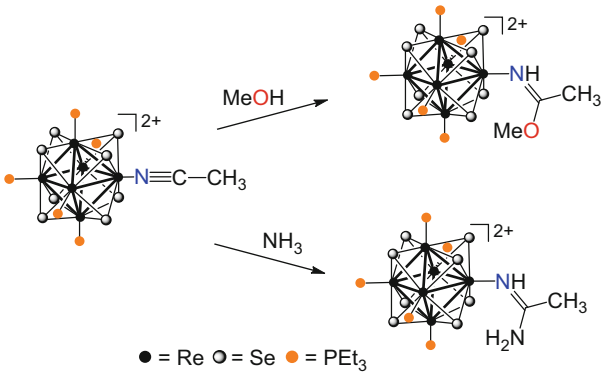

Fig. 9 Schematic diagram showing the reaction of $[Re_6Se_8(PEt_3)_5(NCMe)]^{2+}$ with methanol to form an imino ester ligand and with ammonia to form a acetamidine ligand

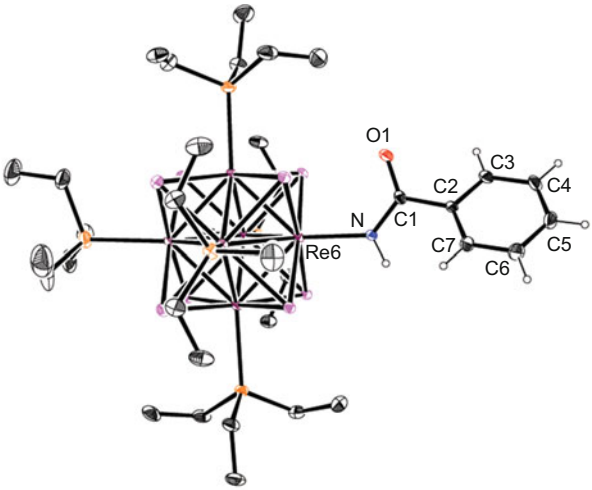

Fig. 10 Structure of $[Re_6Se_8(PEt_3)_5(phenylcarboxamide)]^+$. [52]–Reproduced by permission of The Royal Society of Chemistry

interest is that isolation of $[Re_6Se_8(PEt_3)_5(2\text{-phenyloxazine})](SbF_6)_2$ could only be achieved in the absence of light. Exposure of $[Re_6Se_8(PEt_3)_5(2\text{-phenyloxazine})]^{2+}$ to ambient light at room temperature led to the expulsion of 2-phenyloxazine; this represents the first time ligand removal has occurred without the addition of other reagents and under such mild conditions. Heat and UV light were shown to facilitate ligand removal of the other oxazine and oxazoline rings, and the relative strength of all four heterocyclic ligands was reported as phenyloxazine < phenyloxazoline < methyloxazine < methyloxazoline. This ranking indicates that ligand strength is dependent on both steric and electronic factors. As with some of the ligand removal studies already mentioned, the formation of the starting nitrile cluster complexes is

observed upon ligand removal indicating the potential for catalytic activity. These examples demonstrate the versatility of small molecule activation in the generation of cluster complexes containing novel ligands.

2.2 Oxygen- and Sulfur-Donor Ligands

Preparation of the first hexaaqua rhenium chalcogenide cluster, $[Re_6S_8(H_2O)_6]^{2+}$, was reported in 1998 [53], and a couple of years later, reports of mixed aqua/hydroxo cluster complexes appeared. The first of these, $[Re_6Se_8(H_2O)_4(OH)_2]\cdot 12H_2O$, was generated via the reaction of $(Bu_4N)_4[Re_6Se_8I_6]$ and aqueous NaOH [54]. Reports of the hexahydroxo complexes, $K_4[Re_6Se_8(OH)_6]\cdot 8H_2O$ and $K_4[Re_6S_8(OH)_6]\cdot 8H_2O$, followed; these were prepared from the chalcohalides, $Re_6Q_8Br_2$ [55]. As with so many of the single metal aqua/hydroxo complexes, the nature of the ligands is dependent on pH. A study involving the dependence of formulation and spectroscopic properties of $K_4[Re_6Se_8(OH)_6]\cdot 8H_2O$ and $K_4[Re_6S_8(OH)_6]\cdot 8H_2O$ as a function of pH led to the formation of $K_2[Re_6Se_8(H_2O)_2(OH)_4]\cdot 2H_2O$, $[Re_6S_8(H_2O)_4(OH)_2]\cdot 12H_2O$, $[Re_6S_8(H_2O)_6][Re_6S_8Br_6]\cdot 10H_2O$, and $[Re_6Se_8(H_2O)_4(OH)_2]$ [56]. A number of these aqua/hydroxo cluster complexes have been characterized via X-ray crystallography, and the data show extensive hydrogen-bonding interactions in the solid state. In fact, a comparison of the structures of $[Re_6Se_8(H_2O)_4(OH)_2]$ [56] and $[Re_6Se_8(H_2O)_4(OH)_2]\cdot 12H_2O$ [54] emphasizes how much the hydration of these complexes can influence the solid-state structure. Brylev et al. also studied the chemical and spectroscopic properties of these compounds in solution and were able to describe the equilibrium that takes place as pH is varied [56]. There are also examples of complexes containing mixed terminal ligands, hydroxide/water with ligands such as cyanide (or cyanide bridging to another metal complex), or pyridine-based ligands (e.g., $[Re_6Se_8(CN)_4(OH)_2]^{4-}$ and $[Re_6S_8(OH)_2(4,4'\text{-bipyridine})_4]$) [38, 57]. A unique feature of these complexes is that they often display an extensive array of hydrogen bonding to the coordinated aqua or hydroxo ligands as well as to waters of solvation.

The hydroxo ligands are reported to be relatively labile in that they can be readily substituted by halides; they can also act as bridging ligands in the formation of coordination polymers with Group 2 metal ions [55, 58]. Carboxylate coordination to the rhenium chalcogenide cluster cores is not as common as with $[Mo_6X_8]^{4+}$ clusters but has been achieved via the reaction of the aforementioned hydroxide-containing clusters with free carboxylic acids. The first reported example of carboxylate coordination involved an amphiphilic diblock copolymer, $CH_3O(CH_2CH_2O)_{12}CH_2CONH\text{-}GlyPheLeuGlyPheLeu\text{-}COO^-$, with a carboxylate terminus. This was coordinated to the rhenium sulfide cluster core forming $K_4[Re_6S_8(OH)_5(CH_3O(CH_2CH_2O)_{12}CH_2CONH\text{-}GlyPheLeuGlyPheLeu\text{-}COO)]$.
This long-chain carboxylate was designed to improve cellular uptake, and studies comparing $K_4[Re_6Q_8(OH)_6]\cdot 8H_2O$ (Q = S or Se) and $K_4[Re_6S_8(OH)_5(CH_3O(CH_2CH_2O)_{12}CH_2CONH\text{-}GlyPheLeuGlyPheLeu\text{-}COO)]$ were tested for cellular

uptake and toxicity with HeLa cells (human cervical epithelial adenocarcinoma cells) [59]. Notably, both $K_4[Re_6S_8(OH)_6]\cdot 8H_2O$ and $K_4[Re_6S_8(OH)_5(CH_3O(CH_2CH_2O)_{12}CH_2CONH\text{-}GlyPheLeuGlyPheLeu\text{-}COO)]$ were found to permeate cell walls and populate the cytoplasm and nucleus. The absence of acute cytotoxic properties at low concentrations indicates that there is potential for using rhenium sulfide clusters for diagnostic or therapeutic agents; however, as noted below, the stability of rhenium chalcogenide carboxylates in aqueous solution limits the applicability of carboxylate-containing clusters.

Hexacarboxylate clusters were obtained when hexahydroxo clusters were utilized as starting materials. For example, reaction of $M_4[Re_6S_8(OH)_6]\cdot 8H_2O$ ($M = K^+$ or Cs^+) with formic acid leads to the generation of $M_4[Re_6S_8(HCOO)_6]$ ($M = K^+$ or Cs^+). Figure 11 shows the structure of $Cs_4[Re_6S_8(HCOO)_6]$. ^1H NMR studies of $K_4[Re_6S_8(HCOO)_6]$ in D_2O indicate a small amount of free formate is present upon immediate dissolution, the resonance for which increases in intensity over time (weeks) [60]. Studies in H_2O indicate that additional further substitutions occur, leading to the eventual precipitation of $[Re_6S_8(H_2O)_4(OH)(HCOO)]$. In order to better understand the ligand substitution chemistry of the hexahydroxo species, reactions involving $[Re_6Q_8(OH)_6]^{4-}$ with different pyridine ligands were undertaken [61]. Reaction with 4-*t*-butylpyridine (TBP) led to the formation of *trans*-$[Re_6Q_8(TBP)_4(OH)_2]$. It is believed that the bulky *t*-butyl groups prevent

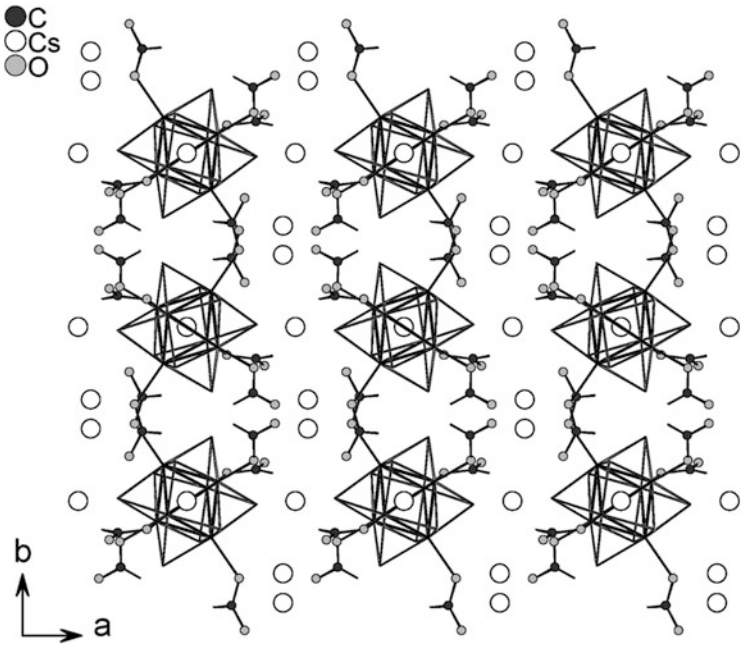

Fig. 11 The crystal structure of $Cs_4[Re_6S_8(HCOO)_6]$ is shown to have an alternation of cationic and anionic layers parallel to the *bc* plane. Reprinted with permission from [60] Copyright 2009 American Chemical Society

aggregation and allow for a clean substitution to take place. Unlike substitution of the halide ligands in $[Re_6Q_8X_6]^{4-}$ with triethylphosphine, site-differentiation appears to favor formation of the neutral species, which precipitate from the aqueous reaction mixture. The authors comment on how this can be used as a general procedure for the formation of *trans*-$[Re_6Q_8L_4(OH)_2]$ (L = a neutral ligand) clusters. Of interest here is that reaction of *trans*-$[Re_6Q_8(TBP)_4(OH)_2]$ with derivatives of 3,4,5-trihydroxybenzoic acid (or gallic acid) leads to the formation of *trans*-$[Re_6Q_8(TBP)_4$(3,4,5-trismethoxybenzoate)$_2]$ and *trans*-$[Re_6Q_8(TBP)_4$(3,4,5-tris (octyloxy)benzoate)$_2]$; these gallic acid derivatives were utilized in attempts to generate mesomorphic materials [61]. All of the reported carboxylate ligands act as monodentate ligands.

The only example of sulfonate ligand coordination is that of $[Re_6Se_8(PEt_3)_5(OTs)](OTs)$; this was prepared from the reaction of $[Re_6Se_8(PEt_3)_5I]I$ with silver(I) *p*-toluenesulfonate (OTs^-) [62]. Sulfonate ligands are traditionally weakly coordinating; therefore, this complex was prepared to be utilized as a starting material for the preparation of other cluster complexes. A few rhenium chalcogenide clusters containing alkoxide ligands have been reported, but they are not well studied. The synthesis and X-ray structures of the mono-alkoxide complexes, $[Re_6Se_8(PEt_3)_5(OMe)](PF_6)$ and $[Re_6Se_8(PEt_3)_5(OPh)](PF_6)$, were reported [63, 64]. The methoxy complex was prepared from $[Re_6Se_8(PEt_3)_5(py)](PF_6)_2$ and NaOMe, while the phenoxy complex was prepared via reaction of $[Re_6Se_8(PEt_3)_5(OMe)](PF_6)$ with phenol. The only other known alkoxide complex is $(Bu_4N)_4[Re_6S_8(OC_6H_4NO_2)_6]$ which was reported as a private communication (S. Nagashima, private communication, Cambridge structural database, 2018).

2.3 Carbon-Donor Ligands

Cyanide is by far the most common terminal C-donor ligand that has been incorporated into hexanuclear $[Re_6Q_8]^{2+}$-based cluster compounds [27]. However, since CN^- is typically considered a pseudohalide, we will not delve into this area any further. Here, we will focus on studies involving more traditional organometallic ligands such as carbonyls and carbenes. Numerous examples of transition metal cluster carbonyls have been reported in the literature, so many in fact that there are books dedicated to the topic [65]. Thus, it is somewhat surprising that there are so few examples of organometallic octahedral clusters.

Zheng et al. prepared the first examples of organometallic rhenium chalcogenide clusters by coordinating CO to the $[Re_6Se_8]^{2+}$ core. The synthesis involved reacting $[Re_6Se_8(PEt_3)_xI_{6-x}]^{x-4}$ ($x = 4$ and 5) with $AgSbF_6$ in a methylene chloride solution saturated with CO to generate $[Re_6Se_8(PEt_3)_5(CO)](SbF_6)_2$ and *cis*- and *trans*-$[Re_6Se_8(PEt_3)_4(CO)_2](SbF_6)_2$, respectively [66, 67]. Of interest is that the CO stretching frequency, ν(CO), shifts to lower wavenumbers upon coordination. This was surprising at first since it was originally believed that the highest occupied molecular orbitals (HOMOs) of $[Re_6Se_8]^{2+}$ did not have the appropriate orientation for back donation to CO. Computational studies revealed that backbonding from the

cluster core is possible; however, the majority of the electron density (approximately 50%) comes from the nearby selenide ligands. In terms of reactivity of the coordinated carbonyl, it was mentioned that methyl lithium does react with $[Re_6Se_8(PEt_3)_5(CO)](SbF_6)_2$ to form the corresponding acyl complex; as of yet, there are no reports discussing conversion of this acyl complex into a carbene. A more detailed summary of these studies has been published [48].

Incorporation of carbene ligands, another important organometallic ligand, into transition metal clusters is quite limited in comparison with the chemistry of single metal complexes. Our group has begun to investigate the viability of carbene containing rhenium chalcogenide clusters. In 2015, we reported the preparation and study of $[Re_6Se_8(PEt_3)_5(SIMes)](OTs)_2$, *trans*-$[Re_6Se_8(PEt_3)_4(SIMes)_2](OTs)_2$, and $[Re_6S_8(PEt_3)_2(IMes)_2Cl_2]$ (SIMes = 1,3-bis(dimesityl)imidazol-4,5-dihydro-2-ylidene and IMes = 1,3-bis(dimesityl)-imidazol-2-ylidene) (Fig. 12) [68]. These represent the first examples of hexanuclear cluster complexes containing a carbene ligand of any type (*N*-heterocyclic carbene, Fischer or Schrock). $[Re_6Se_8(PEt_3)_5(OTs)](OTs)$ was initially used as the starting material for the preparation of $[Re_6Se_8(PEt_3)_5(SIMes)]^{2+}$. However, we later found that SIMes was strong enough to replace the iodo ligand in $[Re_6Se_8(PEt_3)_5I]^+$. This is the only example of substitution of a $[Re_6Q_8]^{2+}$ coordinated halide where substitution did not require the use of heat, silver(I) salts, or photoirradiation. NHCs are considered spectator ligands, and as such the chemistry of $[Re_6Se_8(PEt_3)_5(SIMes)](OTs)_2$ was limited. The advantage of $[Re_6S_8(PEt_3)_2(IMes)_2Cl_2]$ is that there is potential for further reactivity of the halide ligands. The Re-C bond lengths averaged about 2.22 Å, slightly longer than the Re-CO bond lengths reported by Zheng and coworkers (average of 2.04 Å) in the carbonyl-containing clusters discussed above. We are currently in the process of investigating the possibility of incorporating other types of carbene ligands into these cluster complexes. Our group has also prepared the isonitrile cluster complex, $[Re_8Se_8(PEt_3)_5(C{\equiv}NPh)](SbF_6)_2$ [69]. We are in the process of conducting X-ray crystal structure analyses as well as investigating the physical properties of this newly prepared species.

3 $[Mo_6X_8]^{4+}$-Based Clusters

3.1 Nitrogen-Donor Ligands

Shriver and coworkers reported the reaction of $(Bu_4N)_2[Mo_6Cl_8(OTf)_6]$ ($^-OTf = CF_3SO_3^-$) with 4,4′-bipyridine in the preparation of microporous xerogels and with 4-vinylpyridine in the preparation of polymeric materials [70, 71]. However, the first discrete molybdenum halide cluster complex containing a non-pseudohalide N-donor ligand to be isolated was reported about 10 years later by Perrin and Astruc and coworkers; $[Mo_6Br_8L_6](OTf)_4$ (L = pyridine, 4-*t*-butylpyridine, 4-vinylpyridine, and a new dendronic pyridine derivative 3,3′-$\{CH_2Op\text{-}C_6H_4C(CH_2CH{=}CH_2)_3\}_2$py) were synthesized via the reaction of the corresponding

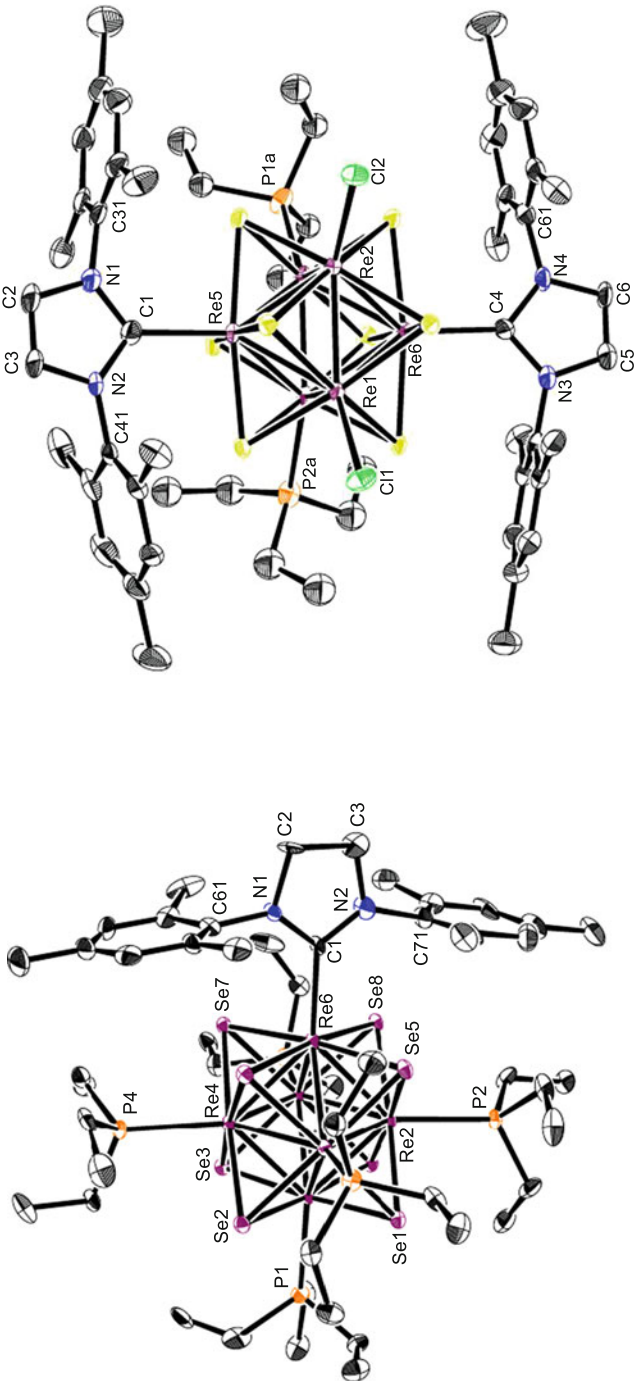

Fig. 12 Structures of $[Re_6Se_8(PEt_3)_5(SIMes)]^{2+}$ (left) and $[Re_6S_8(PEt_3)_2(IMes)_2Cl_2]$ (right) [68]. Reproduced by permission of The Royal Society of Chemistry

hexatriflate cluster with an excess of the given pyridine ligand [72]. Another report details the synthesis of the iodo-based clusters $[Mo_6I_8L_6](OTf)_4$ (L = pyridine, 4-*t*-butylpyridine, 4-vinylpyridine) and $(Bu_4N)[Mo_6Br_{13}L]$ (L = 4-*t*-butylpyridine, 4-vinylpyridine, and pyridine-based dendrons) [73]. $[Mo_6Br_8(py)_6](OTf)_4$ is only sparingly soluble in organic solvents making it somewhat challenging to work with. In addition, stability studies indicate that while $[Mo_6Br_8(py)_6](OTf)_4$ is stable in air and acetone, even in the presence of light, the complex decomposes in methanol and in water [72]. As was seen with the rhenium chalcogenide clusters, the advantage of incorporating pyridine-based ligands is that cluster functionalization can be achieved simply by utilizing substituted pyridines. For example, the organometallic pyridine ligands [Ru(Cp(PPh$_3$)$_2$(η^1-C≡C-4-pyridinyl)] and 1-ferrocenyl-2-(4-pyridinyl)acetylene were incorporated through reaction with $(Bu_4N)_2[Mo_6Br_8(OTf)_6]$ leading to the formation of light-sensitive clusters surrounded by organometallic fragments (Fig. 13) [73, 74]. Cluster-cored dendrimers were also prepared through the reaction of $(Bu_4N)_2[Mo_6X_8(OTf)_6]$ (X = Br or I) or $(Bu_4N)_2[Mo_6Br_{13}(OTf)]$ with a variety of monopyridine dendrons. Based on the extensive chemistry of rhenium chalcogenide clusters containing pyridine-based ligands, it is somewhat surprising that there are not more examples of pyridine containing molybdenum halide clusters; this could be due to issues of solubility as well as stability issues of these cluster complexes.

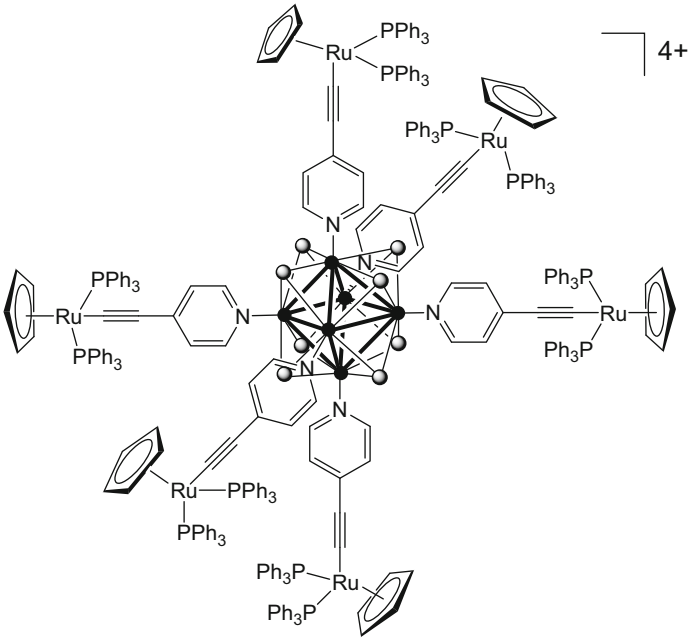

Fig. 13 Visual representation of $[Mo_6Br_8(\mu\text{-py-C}\equiv\text{C-RuCp(PPh}_3)_2)_6]^{4+}$. Adapted with permission from [73] Copyright 2006 American Chemical Society

3.2 Oxygen- and Sulfur-Donor Ligands

Carboxylate ligands have become the most widely incorporated apical ligand in molybdenum halide cluster complexes. The most common synthetic route used to prepare carboxylate-containing cluster complexes involves the reaction of $(Bu_4N)_2[Mo_6X_{14}]$ (X = Cl, Br, I) with silver(I) carboxylates, where the removal of the terminal halogens and precipitation of silver halide salts drives the reaction to completion. One disadvantage of this synthesis is that commercially available functionalized carboxylates are limited; therefore, these often need to be synthesized as well. Another popular route for the molybdenum iodide clusters uses $Na_2[Mo_6I_8(OMe)_6]$ and free carboxylic acids. The key advantage to this method is that the methanol by-product that is generated upon reaction is easily removed, simplifying the purification process. In the studies discussed here, both synthetic methods have been utilized. The first example of a carboxylate-containing $[Mo_6X_8]^{4+}$ cluster complex was that of $(Bu_4N)_2[Mo_6Cl_8(CF_3COO)_6]$, which was prepared from the starting hexahalide cluster and silver(I) trifluoroacetate [75]. Attempts at substituting the trifluoroacetate ligands of $[Mo_6Cl_8(CF_3COO)_6]^{2-}$ with sodium acrylate resulted in an incomplete substitution and the isolation of a mixture of complexes, i.e., $(Bu_4N)_2[Mo_6Cl_8(CF_3COO)_{6-n}(CH_2{=}CHCOO)_n]$. A study of a series of molybdenum halide complexes containing the heptafluorobutyrate ($C_3F_7COO^-$) ligands was significant in that it led to the discovery that (1) the cluster containing bridging iodide ligands, i.e., $(Bu_4N)_2[Mo_6I_8(C_3F_7COO)_6]$ (Fig. 14, left), possessed enhanced photophysical properties compared to the corresponding molybdenum chloride and bromide clusters and (2) modifying the terminal ligands can improve the photophysical performance of these luminescent cluster complexes [76]. These findings motivated Kirakci and coworkers to prepare the trifluoroacetate iodo cluster, $(Bu_4N)_2[Mo_6I_8(CF_3COO)_6]$ (Fig. 14, right), and to conduct a comparative study

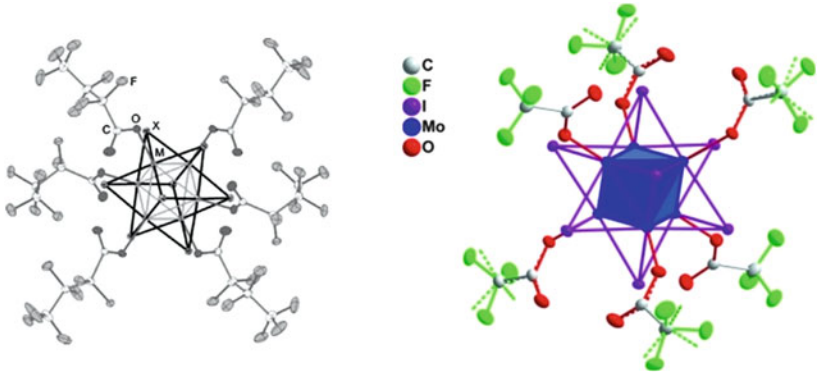

Fig. 14 Structures of $[Mo_6Cl_8(C_3F_7COO)_6]^{2-}$ (left). Reproduced from [76] with permission from The Royal Society of Chemistry and $[Mo_6I_8(CF_3COO)_6]^{2-}$ (right). Reprinted with permission from [77] Copyright 2012 Wiley-VCH Verlag GmbH & Co

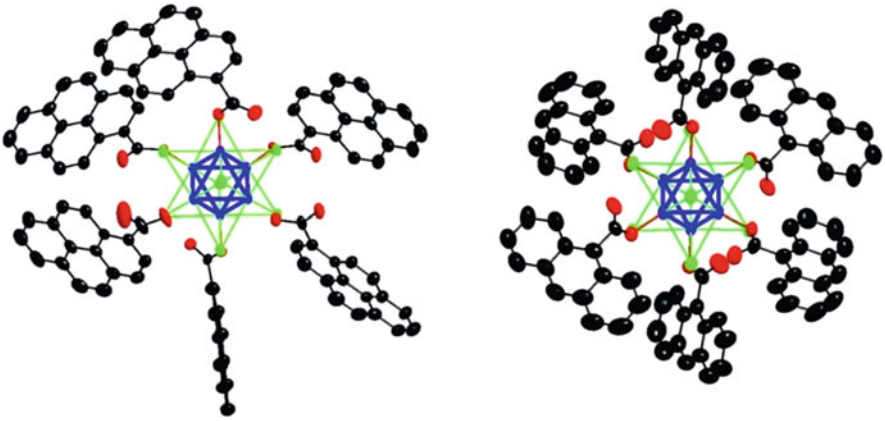

Fig. 15 Structures of $[Mo_6I_8(pyrene–COO)_6]^{2-}$ (left) and $[Mo_6I_8(anthracene–COO)_6]^{2-}$ (right). Reprinted with permission from [79] Copyright 2014 Wiley-VCH Verlag GmbH & Co

of the redox and excited state properties of the following six complexes, $(Bu_4N)_2[Mo_6X_8(CF_3COO)_6]$ and $(Bu_4N)_2[Mo_6X_{14}]$ (X = Cl, Br, I) [77, 78]. The data show that both $(Bu_4N)_2[Mo_6Br_8(CF_3COO)_6]$ and $(Bu_4N)_2[Mo_6I_8(CF_3COO)_6]$ display long excited state lifetimes and high yields of singlet oxygen formation. However, $(Bu_4N)_2[Mo_6I_8(CF_3COO)_6]$ is unique in that it has an extremely high quantum yield ($\phi_{em} = 1$, or 100% efficient) and a narrower emission band than the other complexes. This comparative study led to the conclusion that pairing terminal carboxylate ligands with the $[Mo_6I_8]^{4+}$ core optimizes the luminescent properties of these clusters. However, hexanuclear molybdenum clusters typically display relatively low molar absorption coefficients, which is a disadvantage in that higher concentrations would be needed for a reasonable response in an application setting. In order to address this issue, aromatic carboxylates, which could potentially act as an antenna and transfer their absorbed energy to the cluster core for a brighter luminescence, were incorporated. Reaction of $Na_2[Mo_6I_8(MeO)_6]$ with carboxylic acids of anthracene and pyrene led to the formation of $(Bu_4N)_2[Mo_6I_8(pyrene–COO)_6]$ and $(Ph_4P)_2[Mo_6I_8(anthracene–COO)_6]$ (Fig. 15) [79]. Grafting strongly absorbing chromophores such as anthracene and pyrene to the carboxylate ligand did increase molar absorption coefficients; however, there was a marked decrease in the quantum efficiency of the $(Ph_4P)_2[Mo_6I_8(anthracene–COO)_6]$ complex indicating the fine balance required in tuning the luminescent properties of these systems.

In an effort to develop the applications of these clusters, adamantane carboxylate was coordinated to the molybdenum iodide cluster core. The synthesis of $(Bu_4N)_2[Mo_6I_8(adamantane–COO)_6]$ (from $Na_2[Mo_6I_8(MeO)_6]$ and adamantane-1-COOH) was published along with its incorporation into films and nanoparticles [80]. This complex is reported to be the first radioluminescent octahedral complex capable of X-ray-induced singlet oxygen, making it the first in a new class of nanoscintillators with potential applications in X-ray-induced photodynamic therapy. The ability of these clusters to generate singlet oxygen upon excitation means

that they could have practical applications for oxygen probing or singlet oxygen sensitization in biological systems. However, their low stability in water at physiological pH leads to the formation of aqua-hydroxo complexes, which have been known to be toxic once aggregated. Kirakci and coworkers explored the idea of utilizing ligands that form inclusion complexes with macrocycles which would provide a hydrophobic environment for the cluster. This led to the formation of molybdenum clusters containing *closo*-dicarbaborane C-carboxylates: $Na_2[Mo_6I_8(1\text{-}OOC\text{-}1,2\text{-}closo\text{-}C_2B_{10}H_{11})_6]$, $Na_2[Mo_6I_8(1\text{-}OOC\text{-}1,7\text{-}closo\text{-}C_2B_{10}H_{11})_6]$, and $Na_2[Mo_6I_8(1\text{-}OOC\text{-}1,12\text{-}closo\text{-}C_2B_{10}H_{11})_6]$ all of which have an affinity for a β-cyclodextrin polymer [81]. The physical properties of the β-cyclodextrin polymer containing $Na_2[Mo_6I_8(1\text{-}OOC\text{-}1,7\text{-}closo\text{-}C_2B_{10}H_{11})_6]$ were investigated, and potential applications discussed. Another example involves the coordination of a benzoate ligand containing a diphenylphosphino moiety at the *para* position, i.e., $Na_2[Mo_6I_8(OOCC_6H_4PPh_2)_6]$ (Fig. 16). Although sterically crowded, the phosphorus atom is still able to donate to another metal center enabling the formation of coordination polymers. Kirakci and coworkers took advantage of this property in designing coordination polymers with palladium that were capable of catalyzing cross-coupling reactions [82].

Multiple cluster complexes containing a wide variety of carboxylate ligands have been prepared and studied in order to learn how to gain better control over these various factors. Two series of molybdenum clusters, $(Bu_4N)_2[Mo_6I_8(RCOO)_6]$ ($RCOO^-$ = acetate, pivalate, α-furancarboxylate, benzoate, 3,5-dimethylbenzoate, perfluorobenzoate, 3,5-dinitrobenzoate, 1-naphthoate, and perfluoropropionate) and $(Bu_4N)_2[Mo_6Br_8(RCOO)_6]$ ($RCOO^-$ = acetate, pivalate, α-furancarboxylate, 3,5-dimethylbenzoate, perfluorobenzoate, 3,5-dinitrobenzoate, 1-naphthoate, 4-nitrobenzoate, 4-cyanobenzoate, 3,5-dimethylbenzoate, and 4-methoxybenzoate), were synthesized and fully characterized and their structural, electrochemical, and

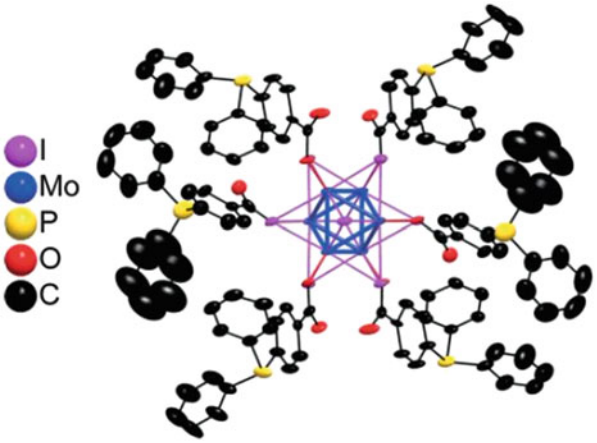

Fig. 16 Structure of $[Mo_6I_8(OOCC_6H_4PPh_2)_6]^{2-}$. Reprinted with permission from [82] Copyright 2016 Wiley-VCH Verlag GmbH & Co

photophysical properties investigated [83–86]. The dependence of some of these properties on the p*K*as of the carboxylic acids and how this dependence can be used to tune the redox, spectroscopic, and luminescent properties is discussed. It is worth noting that with increasing knowledge of how terminal ligands can be used to tune the physical properties of the octahedral molybdenum clusters and with a variety of carboxylate ligands available, researchers have started to design materials which incorporate these carboxylate-containing clusters for specific applications. We provide a few references as an example of some research in this area [87–90], but since this review is focused on discrete/soluble cluster systems, we will not describe these studies in further detail.

There are examples of molybdenum halide clusters containing alkoxide ligands, although this area of research is not as well developed as that of the carboxylate ligands. In an effort to utilize $[Mo_6X_8]^{4+}$ clusters as building blocks in the generation of supramolecular arrays, Shriver and coworkers utilized the 4-hydroxybenzamide to prepare $Na_2[Mo_6Cl_8(OC_6H_4CONH_2)_6]$ [91]. The addition of 2.2.2-cryptand to the reaction mixture leads to the crystallization of $(cryptNa)_2[Mo_6Cl_8(OC_6H_4CONH_2)_6]$, which is described as a hydrogen-bonded organic-inorganic network. In trying to prepare hybrid dendrimers that could potentially take advantage of the interesting electrochemical and photophysical properties of the molybdenum halide cluster core, Gorman and coworkers also incorporated phenolate-based ligands in the preparation of dendrimers. Different focally substituted phenol dendrons, containing 0–2 hyperbranches, were prepared and then coordinated to the $[Mo_6Cl_8]^{4+}$ cluster core [92]. This synthesis involved reacting $(Bu_4N)_2[Mo_6Cl_8(OMe)_6]$ with different dendrons, where the methoxide ligand is believed to deprotonate the incoming substituted phenols. The structure of the $[Mo_6Cl_8(p\text{-methoxyphenolate})_6]^{2-}$ anion is shown in Fig. 17; this is the cluster containing the zero-hyperbranched ligand. These cluster dendrimers are reported as having the potential to be utilized for catalysis and for potentially controlling electron transfer. In a separate study, Méry et al. incorporated dendronic phenolate ligands $(OC_6H_4C\{CH_2CH_2CH_2Si(Me)_2Fc\}_3)$ to the $[Mo_6Br_8]^{4+}$ core generating an octadecylferrocenyl dendrimer which is able to recognize the biologically important adenosyl triphosphate di-anion (ATP^{2-}) [74]. Two nitrophenolate cluster complexes, $(Bu_4N)_2[Mo_6I_8(4\text{-nitrophenolate})_6]$ and $(Bu_4N)_2[Mo_6I_8(2,4\text{-dinitrophenolate})_6]$, were prepared by Sokolov and coworkers in an effort to test the luminescent properties of another $[Mo_6I_8]^{4+}$ cluster containing terminal ligands with different electronic properties [93]. These were prepared from $(Bu_4N)_2[Mo_6I_{14}]$ using silver salts of 4-nitrophenolate and 2,4-dinitrophenolate. The resulting cluster complexes were shown to have high molar absorption coefficients, indicative of a strong ligand-cluster electronic interaction; this is believed to impact the intensity of the emission band. Although these complexes are also strong emitters, their quantum yields and excited state lifetimes do not match those of some other molybdenum iodide clusters, such as $[Mo_6I_8(C_3F_7COO)_6]^{2-}$ [76] and as $[Mo_6I_8(CF_3COO)_6]^{2-}$ [77].

The preparation of sulfonate complexes has been driven by the desire to prepare cluster complexes with weakly coordinating ligands that can be used as starting materials in the preparation of other cluster complexes. Shriver prepared triflate

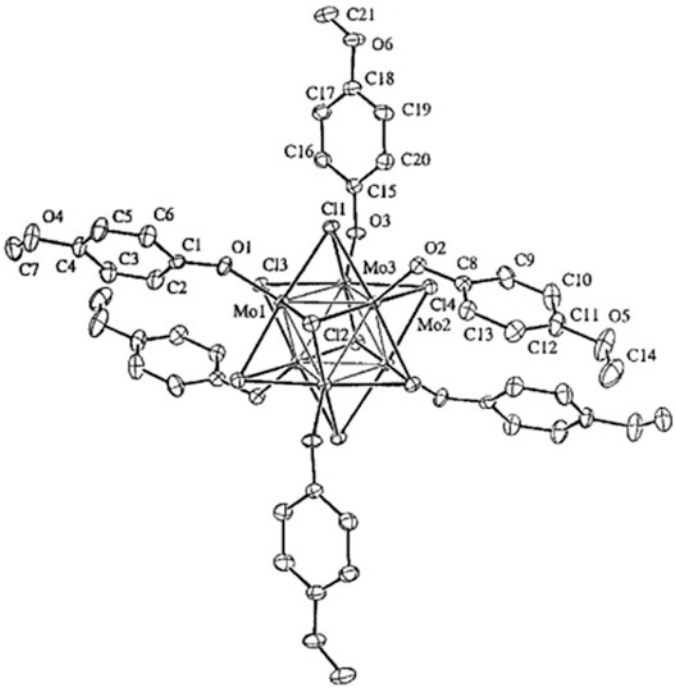

Fig. 17 Structure of $[Mo_6Cl_8(OC_6H_4OCH_3)_6]^{2-}$. Reproduced from [92] with permission from The Royal Society of Chemistry

($^{-}$OTf) and tosylate ($^{-}$OTs) cluster complexes, i.e., $(Bu_4N)_2[Mo_6Cl_8(OTf)_6]$ and $(Bu_4N)_2[Mo_6Cl_8(OTs)_6]$ and conducted ligand substitution studies [28, 94]. More recently the complete series of molybdenum halide hexatosylate ($^{-}$OTs) and hexabenzenesulfonate ($PhSO_3^{-}$) complexes were synthesized and structurally characterized, $(Bu_4N)_2[Mo_6X_8(OTs)_6]$ and $(Bu_4N)_2[Mo_6X_8(PhSO_3)_6]$ (X = Cl, Br, I) [95, 96]. These were prepared in acetone by reacting silver(I) tosylate, or silver(I) benzenesulfonate, with the hexahalide clusters, $(Bu_4N)_2[Mo_6X_{14}]$, and both the electrochemical and photophysical properties of these clusters were investigated. The latest study in this area reports the preparation and study of $(Bu_4N)_2[Mo_6I_8(OTf)_6]$ along with some tungsten halide cluster complexes containing triflate ligands [97]. Cyclic voltammetric studies show that substitution of the terminal halide ligands for sulfonate ligands increases the stability of the cluster complex toward oxidation. In addition, the iodo-bridged clusters, $[Mo_6I_8(sulfonate)_6]^{2-}$, show superior luminescent properties (longer excited state lifetimes and higher quantum yields) compared with $[Mo_6X_8(sulfonate)_6]^{2-}$ (X = Br, Cl) as was observed with the molybdenum clusters containing carboxylate ligands. However, there are issues with the long-term stability of the sulfonate containing

cluster complexes in solution, indicating clusters containing these ligands are better suited as precursors in the coordination of more strongly donating ligands.

Nitrate (NO_3^-) and nitrito (ONO^-) ligands have also been coordinated to molybdenum halide cluster cores. The hexasubstituted complexes that have been isolated include $(Bu_4N)_2[Mo_6X_8(NO_3)_6]$ (X = Cl, Br, I) [98, 99] and $(Bu_4N)_2[Mo_6X_8(NO_2)_6]$ (X = Cl and Br) [98]. These were all prepared from $(Bu_4N)_2[Mo_6X_{14}]$ and either $AgNO_3$ or $AgNO_2$, and X-ray structural data was reported for $A_2[Mo_6X_8(NO_3)_6]$ (A = Bu_4N or $AsPh_4$; X = Cl, Br, I) and $(PPh_4)_2[Mo_6Cl_8(NO_2)_6]$. Figure 18 shows the structure of the $[Mo_6I_8(NO_3)_6]^{2-}$ anion. The structural data indicates O-bound coordination for all species, and IR spectroscopy confirmed O-bound coordination of the nitrito ligands. Photophysical measurements of $(Bu_4N)_2[Mo_6I_8(NO_3)_6]$ show that it has the highest quantum yield and longest excited state lifetime of any previously reported metal cluster complex with an exclusively inorganic ligand environment. Not surprisingly, however, the nitrate ligands are similar to the sulfonate ligands in that they are reported to be labile making these complexes potentially useful precursors. The authors demonstrated this by using the hexanitrate cluster to incorporate the $[Mo_6I_8]^{4+}$ cluster core into thiol-functionalized polystyrene microspheres [99].

Two phosphine oxide ligands were coordinated in the synthesis of $[Mo_6Cl_8(OPEt_3)_2Cl_4]$ and $[Mo_6Cl_8(OP(n\text{Pr})_3)_2Cl_4]$ [100]. These complexes were prepared in a manner similar to how the analogous phosphine clusters, $[Mo_6Cl_8(PR_3)_2Cl_4]$, were prepared [101], by reaction of Mo_6Cl_{12} with the corresponding phosphine oxides. Reactivity studies show that the coordinated phosphine ligands in $[Mo_6Cl_8(PR_3)_2Cl_4]$ (R = Et or *n*Pr) were susceptible to oxidation by H_2O_2 as well as by Me_3NO. The reaction with Me_3NO was surprising since even free phosphines do not react with this oxidant; it is likely that the Lewis acidic cluster

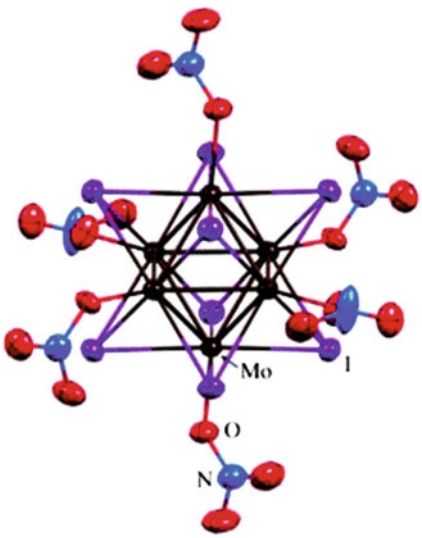

Fig. 18 Structure of $[Mo_6I_8(NO_3)_6]^{2-}$. Reproduced from [99] with permission from The Royal Society of Chemistry

core facilitates oxidation of the coordinated phosphine ligand by Me_3NO. To the best of our knowledge, this is the only example where coordination to a molybdenum halide cluster core significantly alters the reactivity of a ligand in this manner.

The instability of the $[Mo_6X_{14}]^{2-}$ (X = Cr, Br, I) anions to hydrolysis is well known and has been discussed previously [28]. However, there are two hydrolysis studies that are worth mentioning. The first involves the structural characterization of three new molybdenum iodide cluster, $[Mo_6I_8(OH)_4(H_2O)_2]\cdot nH_2O$ (n = 2, 12, 14) [102]. These were obtained by controlled hydrolysis of $[K(diglyme)(NCCH_3)_2][Mo_6I_{14}]$ in sodium borate buffer solutions. All three complexes show extensive hydrogen bonding in their solid-state structures as observed with many of the rhenium chalcogenide clusters containing hydroxo/aqua ligands. The second report describes the unexpected formation of the first oxo-bridged dimer of a molybdenum halide cluster. During the recrystallization of $(Bu_4N)_2[Mo_6I_8(N_3)_6]$ out of acetone/diethyl ether, crystals of a minor by-product, $(Bu_4N)_4[(Mo_6I_8(N_3)_5)_2O]$, also formed and were structurally characterized [103]. Although the authors have not been able to optimize the synthesis of $(Bu_4N)_4[(Mo_6I_8(N_3)_5)_2O]$, this study is significant in pointing out the viability of oxo-bridged molybdenum halide clusters.

The first example of sulfur-donor ligand coordination is that of thiophenol coordinated in $(Bu_4N)_2[Mo_6Cl_8(SPh)_6]$. Two synthetic procedures were reported, reaction of $Na_2[Mo_6Cl_8(OMe)_6]$ with thiophenol or reaction of Mo_6Cl_{12} with NaSPh [104]. The authors utilized this complex in analyzing Raman spectroscopic data of a series of $[M_6X_8Y_6]^{2-}$ clusters (M = Mo, W; X, Y = Cl, Br, I). Thiolate ligands are an important class of ligands in the chemistry of iron-sulfur clusters; therefore, in an effort to explore the chemistry of thiolate ligands coordinated to molybdenum chloride clusters, we prepared a series of thiolate-containing clusters $[Mo_6Cl_8(SR)_6]^{2-}$ (SR^- = ethanethiolate, *n*-butylthiolate, benzylthiolate, 3-indolylthiolate) [105]. The structures of $(PPN)_2[Mo_6Cl_8(SEt)_6]\cdot Et_2O$ and $(PPh_3Me)_2[Mo_6Cl_8(SBn)_6]\cdot 2NO_2CH_3$ were reported (Fig. 19). At a time when it was thought that only the donor ligand would affect the photophysical properties, we demonstrated that the thiolate substituent also impacted these properties [106]. The reaction of $(Bu_4N)_2[Mo_6Cl_8(SEt)_6]$ with other thiols leads to thiolate ligand substitution, i.e., reaction of $[Mo_6Cl_8(SEt)_6]^{2-}$ with benzythiol leads to the formation of $[Mo_6Cl_8(SBn)_6]^{2-}$. $(Bu_4N)_2[Mo_6Cl_8(SEt)_6]$ also undergoes reaction with electrophilic reagents such as MeI and HCl. This reactivity is reminiscent of the chemistry of thiolate ligands coordinated to iron-sulfur clusters, indicating that the molybdenum chloride core does not alter the reactivity of thiolate ligands as was observed with coordinated phosphine ligands [100]. The only example of thiolate ligand coordination to the molybdenum iodide core is that of $(Bu_4N)_2[Mo_6I_8(SC_6F_4H)_6]$, which was reported by Fedin and coworkers. As discussed above, the molybdenum bromide and iodide clusters with fluorinated carboxylates show long excited state luminescence in the red region; therefore, there was interest in examining fluorinated thiolate ligands. $(Bu_4N)_2[Mo_6I_8(SC_6F_4H)_6]$ was synthesized from the reaction of $(Bu_4N)_2[Mo_6I_{14}]$ and silver(I) 2,3,5,6-tetrafluorothiolate [107]; unlike the series of molybdenum chloride thiolate complexes, $(Bu_4N)_2[Mo_6I_8(SC_6F_4H)_6]$ shows improved luminescence compared to $(Bu_4N)_2[Mo_6I_{14}]$.

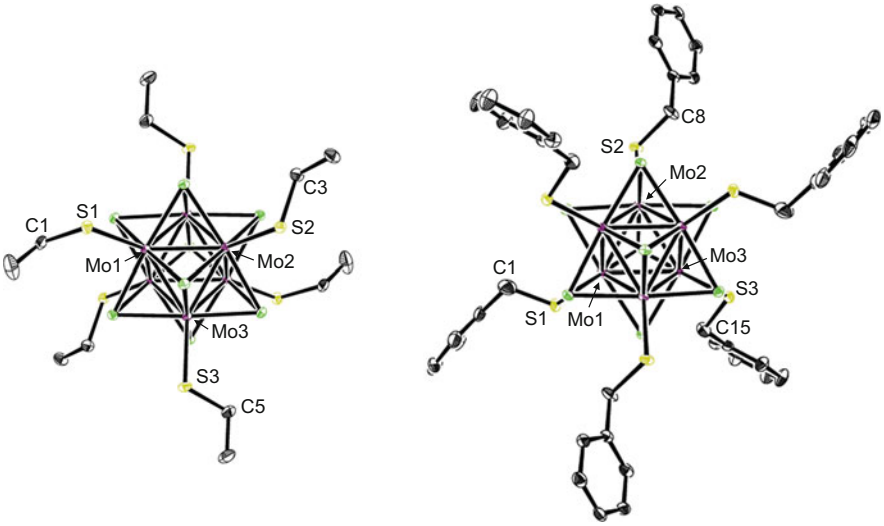

Fig. 19 Crystal structure of $[Mo_6Cl_8(SEt)_6]^{2-}$ (left) and $[Mo_6Cl_8(SBn)_6]^{2-}$ (right). Reprinted with permission from [105] Copyright 2008 American Chemical Society

3.3 Carbon-Donor Ligands

The first non-pseudohalide C-donor ligands coordinated to a $[Mo_6X_8]^{4+}$ cluster core were alkyl ligands; these were prepared using alkylaluminum reagents [28, 101]. In 1997, Saito reported the structures of two additional organometallic cluster complexes, *trans*-$[Mo_6Cl_8(P\textit{n}Bu_3)_2(CH_2Ph)_4]$ and *trans*-$[Mo_6Cl_8(P\textit{n}Bu_3)_2(\text{phenylethynyl})_4]$. Both of these were prepared from *trans*-$[Mo_6Cl_8(P\textit{n}Bu_3)_2Cl_4]$ undergoing reaction with solutions of tribenzylaluminum or tris(phenylethynyl)aluminum [108]. More recently, Sokolov and coworkers synthesized $[Mo_6I_8(C{\equiv}CC(O)OMe)_6]^{2-}$, the first fully organometallic molybdenum halide cluster complex [109]. This complex was prepared from $(Bu_4N)_2[Mo_6I_{14}]$, silver(I) triflate, and methyl propiolate (HC≡CC(O)OMe) in the presence of triethylamine. The authors note that they were unsuccessful in preparing the analogous molybdenum bromide and chloride clusters using the same synthetic route. Crystals of $(PPh_4)_2[Mo_6I_8(C{\equiv}CC(O)OMe)_6]$ were obtained (Fig. 20) and the structure reported. This cluster is highly luminescent, and although it has a shorter excited state lifetime and lower quantum yield in comparison to $[Mo_6I_8(C_3F_7COO)_6]^{2-}$, it is also a good candidate for singlet oxygen generation or luminescent O_2 sensors.

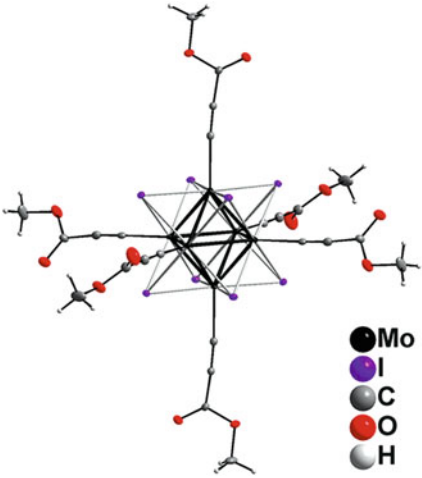

Fig. 20 Crystal structure of $[Mo_6I_8(C{\equiv}CC(O)OMe)_6]^{2-}$. Reprinted with permission from [109] Copyright 2013 American Chemical Society

4 Summary and Perspectives

As detailed in this chapter, the type and scope of terminal ligands coordinated to octahedral cluster cores have greatly increased over the past 20 years. Key advancements in the chemistry of rhenium chalcogenide clusters include the expansion of pyridine-based ligands toward the functionalization of these cluster complexes and the discovery of small molecule activation facilitated by the $[Re_6Se_8]^{2+}$ cluster core. Both of these have greatly expanded the variety of N-donor ligands coordinated to hexanuclear rhenium clusters, which are better stabilized by nitrogen-donor ligands. The most significant development involving molybdenum halide cluster complexes was the discovery that molybdenum iodide clusters containing fluorinated carboxylate ligands (e.g., trifluoroacetate and heptafluorobutyrate) possess exceptional photophysical properties. The fact that carboxylate ligands form stable clusters, and that incorporation of these clusters into materials does not diminish their luminescent properties, makes them ideal moieties for a wide variety of applications such as sensing, imaging, photocatalysis, and photodynamic therapy, to name a few.

Looking forward, although there has been substantial progress in expanding the breadth of terminal ligands coordinated to these cluster cores, there is substantial room for growth. The variety of nitrogen- and oxygen-donor ligands still does not match the type and scope of ligands incorporated into single metal coordination complexes, and carbon- and sulfur-donor ligands are underexplored. The potential applications of these systems keep growing as we learn more about the luminescent properties of these systems and how to develop octahedral cores as building blocks in the preparation of larger complexes and supramolecular arrays. Understanding how to incorporate different apical ligands, and how these ligands can be used to tune the spectral, photophysical, and electrochemical properties of these systems, is

what will make incorporating clusters into devices, and commercially available materials, a reality. We look forward to seeing both the fundamental and applied chemistry of molybdenum halide and rhenium chalcogenide clusters develop even further in future years.

Acknowledgments We thank the National Science Foundation (CHE RUI-1401686 and RUI-0957729) for financial support of this work.

References

1. Bloomstrand W (1859) Ueber unorganische Haloidverbindungen, die sich wie Radicale verhalten. J Prakt Chem 77:88–119
2. Chevrel R, Sergent M, Prigent J (1971) Sur de nouvelles phases sulfurées ternaires du molybdène. J Solid State Chem 3:515–519
3. Chevrel R, Hirrien M, Sergent M (1986) Superconducting Chevrel phases: prospects and perspectives. Polyhedron 5:87–94
4. Brorson M, King JD, Kiriakidou K, Prestopino F, Nordlander E (1999) Metal clusters as models for hydrodesulfurization catalysts. Metal Clust Chem 2:741–781
5. Peña O (2015) Chevrel phases: past, present and future. Phys C 514:95–112
6. Saha P, Jampani PH, Datta MK, Hong D, Okoli CU, Manivannan A, Kumta PN (2015) Electrochemical performance of chemically and solid state-derived Chevrel phase Mo_6T_8 (T= S, Se) positive electrodes for sodium-ion batteries. J Phys Chem C 119:5771–5782
7. Spangenberg M, Bronger W (1978) Ternary rhenium sulfides with $[Re_6S_8]$-clusters. Angew Chem Int Ed Engl 17:368–369
8. Chen S, Robinson WR (1978) An octahedral rhenium(III) cluster: X-ray crystal structure of $Na_4Re_6S_{10}(S_2)$. J Chem Soc Chem Commun 20:879–880
9. Opalovskii AA, Fedorov VE, Lobkov EU, Erenburg BG (1971) New rhenium halochalcogenides. Zh Neorg Khim 16:3175–3177
10. Leduc L, Perrin A, Sergent M (1983) Structure du dichlorure et octaséléniure d'hexarhénium, $Re_6Se_8Cl_2$: composé bidimensionnel à clusters octaédriques Re_6. Acta Cryst C39:1503–1506
11. Perrin A, Perrin C, Sergent M (1988) Octahedral clusters in molybdenum(II) and rhenium(III) chalcohalide chemistry. J Less Common Met 137:241–265
12. Leduc L, Padiou J, Perrin A, Sergent M (1983) Synthèse et caractérisation d'un nouveau chalcohalogénure à clusters octaédriques de rhénium à caractère bidimensionnel: $Re_6Se_8Cl_2$. J Less Common Met 95:73–80
13. Leduc L, Perrin A, Sergent M, Le Traon F, Pilet JC, Le Traon A (1985) Rhenium octahedral clusters: characterization of $Re_6Se_4Cl_{10}$ and the parent compound $Re_6S_4Br_{10}$. Mater Lett 3:209–215
14. Yaghi OM, Scott MJ, Holm RH (1992) Rhenium-selenium-chlorine solid phases: cluster excision and core substitution reactions of molecular species. Inorg Chem 31:4778–4784
15. Long JR, Williamson AS, Holm RH (1995) Dimensional reduction of $Re_6Se_8Cl_2$: sheets, chains, and discrete clusters composed of chloride-terminated $[Re_6Q_8]^{2+}$ (Q= S, Se) cores. Angew Chem Int Ed Engl 34:226–229
16. Long JR, McCarty LS, Holm RH (1996) A solid-state route to molecular clusters: access to the solution chemistry of $[Re_6Q_8]^{2+}$ (Q= S, Se) core-containing clusters via dimensional reduction. J Am Chem Soc 118:4603–4616
17. Tulsky EG, Long JR (2001) Dimensional reduction: a practical formalism for manipulating solid structures. Chem Mater 13:1149–1166

18. Shestopalov MA, Cordier S, Hernandez O, Molard Y, Perrin C, Perrin A, Fedorov VE, Mironov YV (2009) Self-assembly of ambivalent organic/inorganic building blocks containing Re_6 metal atom cluster: formation of a luminescent honeycomb, hollow, tubular metal-organic framework. Inorg Chem 48:1482–1489
19. Shores MP, Beauvais LG, Long JR (1999) Cluster-expanded Prussian blue analogues. J Am Chem Soc 121:775–779
20. Naumov NG, Soldatov DV, Ripmeester JA, Artemkina SB, Fedorov VE (2001) Extended framework materials incorporating cyanide cluster complexes: structure of the first 3D architecture accommodating organic molecules. Chem Commun 6:571–572
21. Selby HD, Roland BK, Zheng Z (2003) Ligand-bridged oligomeric and supramolecular arrays of the hexanuclear rhenium selenide clusters−exploratory synthesis, structural characterization, and property investigation. Acc Chem Res 36:933–944
22. Maverick AW, Gray HB (1981) Luminescence and redox photochemistry of the molybdenum (II) cluster $Mo_6Cl_{14}^{2-}$. J Am Chem Soc 103:1298–1300
23. Maverick AW, Najdzionek JS, MacKenzie D, Nocera DG, Gray HB (1983) Spectroscopic, electrochemical, and photochemical properties of molybdenum(II) and tungsten(II) halide clusters. J Am Chem Soc 105:1878–1882
24. Perruchas S, Avarvari N, Rondeau D, Levillain E, Batail P (2005) Multielectron donors based on TTF-phosphine and ferrocene-phosphine hybrid complexes of a hexarhenium(III) octahedral cluster core. Inorg Chem 44:3459–3465
25. Gray TG, Rudzinski CM, Meyer EE, Holm RH, Nocera DG (2003) Spectroscopic and photophysical properties of hexanuclear rhenium(III) chalcogenide clusters. J Am Chem Soc 125:4755–4770
26. Yoshimura T, Ishizaka S, Umakoshi K, Sasaki Y, Kim H-B, Kitamura N (1999) Hexarhenium (III) clusters $[Re_6(\mu_3\text{-}S)_8X_6]^{4-}$ ($X^- = Cl^-$, Br^-, I^-) are luminescent at room temperature. Chem Lett 28:697–698
27. Gabriel J-CP, Boubekeur K, Uriel S, Batail P (2001) Chemistry of hexanuclear rhenium chalcogenide clusters. Chem Rev 101:2037–2066
28. Prokopuk N, Shriver DF (1998) The octahedral M_6Y_8 and M_6Y_{12} clusters of group 5 and 6 transition metals. Adv Inorg Chem 46:1–49
29. Fedorov VE, Mironov YV, Naumov NG, Sokolov MN, Fedin VP (2007) Chalcogenide clusters of groups 5-7. Russ Chem Rev 76:529–552
30. Pilet G, Perrin A (2005) Octahedral rhenium cluster chemistry: from high-temperature syntheses to the elaboration of new inorganic/molecular hybrid compounds via solution route. C R Chim 8:1728–1742
31. Perrin A, Perrin C (2012) The molybdenum and rhenium octahedral cluster chalcohalides in solid state chemistry: from condensed to discrete cluster units. C R Chim 15:815–836
32. Zheng Z, Long JR, Holm RH (1997) A basis set of Re_6Se_8 cluster building blocks and demonstration of their linking capability: directed synthesis of an $Re_{12}Se_{16}$ dicluster. J Am Chem Soc 119:2163–2171
33. Ren YX, Bruck AM, Szczepura LF (2014) Octa-μ_3-selenido-pentakis(triethylphosphane-κP)(trimethylacetonitrile-κN)-octahedro-hexarhenium(III) bis(hexafluoridoantimonate) trimethylacetonitrile monosolvate. Acta Cryst E70:m242–m243
34. Selby HD, Zheng Z, Gray TG, Holm RH (2001) Bridged multiclusters derived from the face-capped octahedral $[Re_6{}^{III}(\mu_3\text{-}Se)_8]^{2+}$ cluster core. Inorg Chim Acta 312:205–209
35. Selby HD, Zheng Z (2005) New directions of cluster chemistry – the story of the $[Re_6(\mu_3\text{-}Se)_8]^{2+}$ clusters. Comment Inorg Chem 26:75–102
36. Selby HD, Roland BK, Cole JR, Zheng Z (2004) Supramolecular architectures featuring stereoisomeric cluster complexes of the $[Re_6(\mu_3\text{-}Se)_8]^{2+}$ core. Macromol Symp 209:23–39
37. Zheng Z, Tu X (2009) Crystal engineering supported by the $[Re_6(\mu_3\text{-}Se)_8]^{2+}$ core-containing clusters. CrystEngComm 11:707–719
38. El Osta R, Demont A, Audebrand N, Molard Y, Nguyen T, Gautier R, Brylev K, Mironov Y, Naumov NG, Kitamura N, Cordier S (2015) Supramolecular frameworks built up from

red-phosphorescent *trans*-Re_6 cluster building blocks: one pot synthesis, crystal structures, and DFT investigations. Z Anorg Allg Chem 641:1156–1163
39. Corbin WC, Nichol GS, Zheng Z (2015) $[Re_6(\mu_3\text{-}Se)_8]^{2+}$ core-containing cluster complexes with isonicotinic acid: synthesis, structural characterization, and hydrogen-bonded assemblies. J Clust Sci 26:279–290
40. Itasaka A, Abe M, Yoshimura T, Tsuge K, Suzuki M, Imamura T, Sasaki Y (2002) Octahedral arrangement of porphyrin moieties around hexarhenium(III) cluster cores: structure of (μ_3-selenido)hexa(5-(4-pyridyl)-10,15,20-tritolylporphyrin)hexarhenium(III) (2+). Angew Chem Int Ed 41:463–466
41. Kahnt A, Heiniger L-P, Liu S-X, Tu X, Zheng Z, Hauser A, Decurtins S, Guldi DM (2010) An electrochemical and photophysical study of a covalently linked inorganic–organic dyad. ChemPhysChem 11:651–658
42. Yoshimura T, Ishizaka S, Kashiwa T, Ito A, Sakuda E, Shinohara A, Kitamura N (2011) Direct observation of a $\{Re_6(\mu_3\text{-}S)_8\}$ core-to-ligand charge-transfer excited state in an octahedral hexarhenium complex. Inorg Chem 50:9918–9920
43. Mironov YV, Brylev KA, Shestopalov MA, Yarovoi SS, Fedorov VE, Spies H, Pietzsch H-J, Stephan H, Geipel G, Bernhard G, Kraus W (2006) Octahedral rhenium cluster complexes with organic ligands: synthesis, structure and properties of $[Re_6Q_8(3,5\text{-}Me_2PzH)_6]Br_2{\cdot}2(3,5\text{-}Me_2PzH)$ (Q = S, Se). Inorg Chim Acta 359:1129–1134
44. Mironov YV, Shestopalov MA, Brylev KA, Yarovoi SS, Romanenko GV, Fedorov VE, Spies H, Pietzsch H-J, Stephan H, Geipel G, Bernhard G, Kraus W (2005) $[Re_6Q_7O(3,5\text{-}Me_2PzH)_6]Br_2{\cdot}3,5\text{-}Me_2PzH$ (Q = S, Se) – new octahedral rhenium cluster complexes with organic ligands: original synthetic approach and unexpected ligand exchange in the cluster core. Eur J Inorg Chem 4:657–661
45. Shestopalov MA, Zubareva KE, Khripko OP, Khripko YI, Solovieva AO, Kuratieva NV, Mironov YV, Kitamura N, Fedorov VE, Brylev KA (2014) The first water-soluble hexarhenium cluster complexes with a heterocyclic ligand environment: synthesis, luminescence, and biological properties. Inorg Chem 53:9006–9013
46. Szczepura LF, Oh MK, Knott SA (2007) Synthesis and electrochemical study of the first tetrazolate hexanuclear rhenium cluster complex. Chem Commun 44:4617–4619
47. Orto P, Selby HD, Ferris D, Maeyer JR, Zheng Z (2007) Alcohol addition to acetonitrile activated by the $[Re_6(\mu_3\text{-}Se)_8]^{2+}$ cluster core. Inorg Chem 46:4377–4379
48. Zheng Z (2012) Chemical transformations supported by the $[Re_6(\mu_3\text{-}Se)_8]^{2+}$ cluster core. Dalton Trans 41:5121–5131
49. Durham JL, Tirado JT, Knott SA, Oh MK, McDonald R, Szczepura LF (2012) Preparation of a family of hexanuclear rhenium cluster complexes containing 5-(phenyl)tetrazol-2-yl ligands and alkylation of 5-substituted tetrazolate ligands. Inorg Chem 51:7825–7836
50. Knott SA, Templeton JN, Durham JL, Howard AM, McDonald R, Szczepura LF (2013) Azide alkyne cycloaddition facilitated by hexanuclear rhenium chalcogenide cluster complexes. Dalton Trans 42:8132–8139
51. Corbin WC, Nichol GS, Zheng Z (2016) Amidine production by the addition of NH_3 to nitrile(s) bound to and activated by the Lewis acidic $[Re_6(\mu_3\text{-}Se)_8]^{2+}$ cluster core. Inorg Chem 55:9505–9508
52. Chin CP, Ren Y, Berry J, Knott SA, McLauchlan CC, Szczepura LF (2018) Small molecule activation of nitriles coordinated to the $[Re_6Se_8]^{2+}$ core: formation of oxazine, oxazoline and carboxamide complexes. Dalton Trans 47:4653–4660
53. Fedin FP, Virovets AA, Sykes AG (1998) Synthesis of the first sulfido-bridged octahedral rhenium(III) aqua ion $[Re_6S_8(H_2O)_6]^{2+}$. Inorg Chim Acta 271:228–230
54. Zheng Z, Selby HD, Roland BK (2001) The first 'hexaaqua-' complex of the $[Re_6Se_8]^{2+}$ cluster core, $[Re_6Se_8(OH)_2(H_2O)_4]{\cdot}12H_2O$. Acta Cryst Sect E E57:i77–i79
55. Yarovoi SS, Mironov YV, Naumov DY, Gatilov YV, Kozlova SG, Kim S-J, Fedorov VE (2005) Octahedral hexahydroxo rhenium cluster complexes $[Re_6Q_8(OH)_6]^{4-}$ (Q = S, Se): synthesis, structure, and properties. Eur J Inorg Chem 2005:3945–3949

56. Brylev KA, Mironov YV, Yarovoi SS, Naumov NG, Fedorov VE, Kim S-J, Kitamura N, Kuwahara Y, Yamada K, Ishizaka S, Sasaki Y (2007) A family of octahedral rhenium cluster complexes $[Re_6Q_8(H_2O)_n(OH)_{6-n}]^{n-4}$ (Q = S, Se; $n = 0-6$): structural and pH−dependent spectroscopic studies. Inorg Chem 46:7414–7422
57. Mironov YV, Brylev KA, Kim S-J, Kozlova SG, Kitamura N, Fedorov VE (2011) Octahedral cyanohydroxo cluster complex *trans*-$[Re_6Se_8(CN)_4(OH)_2]^{4-}$: synthesis, crystal structure, and properties. Inorg Chim Acta 370:363–368
58. Selby HD, Orto P, Carducci MD, Zheng Z (2002) Novel concentration-driven structural interconversion in shape-specific solids supported by the octahedral $[Re_6(\mu_3\text{-}Se)_8]^{2+}$ cluster core. Inorg Chem 41:6175–6177
59. Choi S-J, Brylev KA, Xu J-Z, Mironov YV, Fedorov VE, Sohn YS, Kim S-J, Choy J-H (2008) Cellular uptake and cytotoxicity of octahedral rhenium cluster complexes. J Inorg Biochem 102:1991–1996
60. Brylev KA, Mironov YV, Kozlova SG, Fedorov VE, Kim S-J, Pietzsch H-J, Stephan H, Ito A, Ishizaka S, Kitamura N (2009) The first octahedral cluster complexes with terminal formate ligands: synthesis, structure, and properties of $K_4[Re_6S_8(HCOO)_6]$ and $Cs_4[Re_6S_8(HCOO)_6]$. Inorg Chem 48:2309–2315
61. Dorson F, Molard Y, Cordier S, Fabre B, Efremova O, Rondeau D, Mironov Y, Cîrcu V, Naumov N, Perrin C (2009) Selective functionalisation of Re_6 cluster anionic units: from hexahydroxo $[Re_6Q_8(OH)_6]^{4-}$ (Q = S, Se) to neutral *trans*-$[Re_6Q_8L_4L'_2]$ hybrid building blocks. Dalton Trans:1297–1299
62. Edwards JA, McDonald R, Szczepura LF (2015) Crystal structure of octa-μ_3-selenido-(p-toluenesulfonato-κO)pentakis(triethylphosphane-κP)-octahedro-hexarhenium(III) p-toluenesulfonate dichloromethane disolvate. Acta Cryst E71:m158–m159
63. Templeton JN (2006) Progress towards the synthesis of site-differentiated hexanuclear molybdenum and rhenium clusters containing sulfur donor ligands. Dissertation, Illinois State University, Normal
64. Edwards JA (2008) Synthesis, characterization, and reactivity studies of hexanuclear rhenium cluster complexes with oxygen and sulfur donor ligands. Dissertation, Illinois State University, Normal
65. McIndoe SJ, Dyson PJ (2000) Transition metal carbonyl cluster chemistry. CRC Press, Amsterdam
66. Orto PJ, Nichol GS, Wang R, Zheng Z (2007) Cluster carbonyls of the $[Re_6(\mu_3\text{-}Se)_8]^{2+}$ core. Inorg Chem 46:8436–8438
67. Orto PJ, Nichol GS, Okumura N, Evans DH, Arratia-Peréz R, Ramirez-Tagle R, Wang R, Zheng Z (2008) Cluster carbonyls of the $[Re_6(\mu_3\text{-}Se)_8]^{2+}$ core: synthesis, structural characterization, and computational analysis. Dalton Trans 6:4247–4253
68. Durham JL, Wilson WB, Huh DN, McDonald R, Szczepura LF (2015) Organometallic rhenium(III) chalcogenide clusters: coordination of N-heterocyclic carbenes. Chem Commun 51:10536–10538
69. Wilson WB (2015) Synthesis, characterization, and reactivity of hexarhenium selenide cluster complexes containing carbon-coordinating ligands. Dissertation, Illinois State University, Normal
70. Bain RL, Shriver DF, Ellis DE (2001) Extended materials based on the $[Mo_6Cl_8]^{4+}$ building block bridged by 4,4′-bipyridine. Inorg Chim Acta 325:171–174
71. Robinson LM, Shriver DF (1996) Synthesis and photophysical properties of polymer-bound hexanuclear molybdenum clusters. J Coord Chem 37:119–129
72. Méry D, Ruiz J, Nlate S, Astruc D, Cordier S, Kirakci K, Perrin C (2005) The simple hexapyridine cluster $[Mo_6Br_8Py_6][OSO_2CF_3]_4$ and substituted hexapyridine clusters including a cluster-cored polyolefin dendrimer. Z Anorg Allg Chem 631:2746–2750
73. Méry D, Plault L, Ornelas C, Ruiz J, Nlate S, Astruc D, Blais J-C, Rodrigues J, Cordier S, Kirakci K, Perrin C (2006) From simple monopyridine clusters $[Mo_6Br_{13}(Py\text{-}R)][n\text{-}Bu_4N]$ and

hexapyridine clusters $[Mo_6X_8(Py\text{-}R)_6][OSO_2CF_3]_4$ (X = Br or I) to cluster-cored organometallic stars, dendrons, and dendrimers. Inorg Chem 45:1156–1167
74. Méry D, Ornelas C, Daniel M-C, Ruiz J, Rodrigues J, Astruc D, Cordier S, Kirakci K, Perrin C (2005) Mo_6Br_8-cluster-cored organometallic stars and dendrimers. C R Chim 8:1789–1797
75. Adamenko OA, Lukova GV, Golubeva ND, Smirnov VA, Boiko GN, Pomogailo AD, Uflyand IE (2001) Synthesis, structure, and physicochemical properties of $[Mo_6Cl_8]^{4+}$-containing clusters. Dokl Phys Chem 381:275–278
76. Sokolov MN, Mihailov MA, Peresypkina EV, Brylev KA, Kitamura N, Fedin VP (2011) Highly luminescent complexes $[Mo_6X_8(n\text{-}C_3F_7COO)_6]^{2-}$ (X = Br, I). Dalton Trans 40:6375–6377
77. Kirakci K, Kubát P, Dušek M, Fejfarová K, Šícha V, Mosinger J, Lang K (2012) A highly luminescent hexanuclear molybdenum cluster – a promising candidate toward photoactive materials. Eur J Inorg Chem 2012:3107–3111
78. Kirakci K, Kubát P, Langmaier J, Polívka T, Fuciman M, Fejfarová K, Lang K (2013) A comparative study of the redox and excited state properties of $(nBu_4N)_2[Mo_6X_{14}]$ and $(nBu_4N)_2[Mo_6X_8(CF_3COO)_6]$ (X = Cl, Br, or I). Dalton Trans 42:7224–7232
79. Kirakci K, Fejfarová K, Kučeraková M, Lang K (2014) Hexamolybdenum cluster complexes with pyrene and anthracene carboxylates: ultrabright red emitters with the antenna effect. Eur J Inorg Chem 2014:2331–2336
80. Kirakci K, Kubát P, Fejfarová K, Martinčík J, Nikl M, Lang K (2016) X-ray inducible luminescence and singlet oxygen sensitization by an octahedral molybdenum cluster compound: a new class of nanoscintillators. Inorg Chem 55:803–809
81. Kirakci K, Šícha V, Holub J, Kubát P, Lang K (2014) Luminescent hydrogel particles prepared by self-assembly of β-cyclodextrin polymer and octahedral molybdenum cluster complexes. Inorg Chem 53:13012–13018
82. Bůžek D, Hynek J, Kučeráková M, Kirakci K, Demel J, Lang K (2016) Mo^{II} cluster complex-based coordination polymer as an efficient heterogeneous catalyst in the Suzuki-Miyaura coupling reaction. Eur J Inorg Chem 2016:4668–4673
83. Akagi S, Fujii S, Horiguchi T, Kitamura N (2017) p$K_a(L)$ dependences of structural, electrochemical, and photophysical properties of octahedral hexamolybdenum(II) clusters: $[Mo_6X_8L_6]^{2-}$ (X = Br or I; L = carboxylate). J Clust Sci 28:757–772
84. Fujii S, Horiguchi T, Akagi S, Kitamura N (2016) Quasi-one-step six-electron electrochemical reduction of an octahedral hexanuclear molybdenum(II) cluster. Inorg Chem 55:10259–10266
85. Mikhailov MA, Brylev KA, Abramov PA, Sakuda E, Akagi S, Ito A, Kitamura N, Sokolov MN (2016) Synthetic tuning of redox, spectroscopic, and photophysical properties of $\{Mo_6I_8\}^{4+}$ core cluster complexes by terminal carboxylate ligands. Inorg Chem 55:8437–8445
86. Akagi S, Horiguchi T, Fujii S, Kitamura N (2019) Terminal ligand (L) effects on zero-magnetic-field splitting in the excited triplet states of $[\{Mo_6Br_8\}L_6]^{2-}$ (L = aromatic carboxylates). Inorg Chem 58:703–714
87. Molard Y, Dorson F, Cîrcu V, Roisnel T, Artzner F, Cordier S (2010) Clustomesogens: liquid crystal materials containing transition-metal clusters. Angew Chem Int Ed 49:3351–3355
88. Amela-Cortes M, Molard Y, Paofai S, Desert A, Duvail J-L, Naumov NG, Cordier S (2016) Versatility of the ionic assembling method to design highly luminescent PMMA nanocomposites containing $[M_6Q^i{}_8L^a{}_6]^{n-}$ octahedral nano-building blocks. Dalton Trans 45:237–245
89. Beltran A, Mikhailov M, Sokolov MN, Pérez-Laguna V, Rezusta A, Revillo MJ, Galindo F (2016) A photobleaching resistant polymer supported hexanuclear molybdenum iodide cluster for photocatalytic oxygenations and photodynamic inactivation of *Staphylococcus aureus*. J Mater Chem B 4:5975–5979
90. Kirakci K, Zelenka J, Rumlová M, Martinčík J, Nikl M, Ruml T, Lang K (2018) Octahedral molybdenum clusters as radiosensitizers for X-ray induced photodynamic therapy. J Mater Chem B 6:4301–4307

91. Prokopuk N, Weinert CS, Siska DP, Stern CL, Shriver DF (2000) Hydrogen-bonding hexamolybdenum clusters: formation of inorganic-organic networks. Angew Chem Int Ed 112:3450–3453
92. Gorman CB, Su WY, Jiang H, Watson CM, Boyle P (1999) Hybrid organic–inorganic, hexa-arm dendrimers based on an Mo_6Cl_8 core. Chem Commun 10:877–878
93. Mikhailov MA, Brylev KA, Virovets AV, Gallyamov MR, Novozhilova I, Sokolov MN (2016) Complexes of $\{Mo_6I_8\}$ with nitrophenolates: synthesis and luminescence. New J Chem 40:1162–1168
94. Johnston DH, Gaswick DC, Lonergan MC, Stern CL, Shriver DF (1992) Preparation of bis (tetrabutylammonium) octa(μ_3-chloro)hexakis(trifluoromethanesulfonato)-octahedro-hexamolybdate(2-), $(Bu_4N)_2[Mo_6Cl^i_8(CF_3SO_3)^a_6]$: a versatile starting material for substituted Mo(II) clusters containing the $[Mo_6Cl_8]^{4+}$ core. Inorg Chem 31:1869–1873
95. Efremova OA, Vorotnikov YA, Brylev KA, Vorotnikova NA, Novozhilov IN, Kuratieva NV, Edeleva MV, Benoit DM, Kitamura N, Mironov YV, Shestopalov MA, Sutherland AJ (2016) Octahedral molybdenum cluster complexes with aromatic sulfonate ligands. Dalton Trans 45:15427–15435
96. Mikhailov MA, Gushchin AL, Gallyamov MR, Virovets AV, Sokolov MN, Sheven DG, Pervukhin VV (2017) Tosylate cluster complexes $(Bu_4N)_2[M_6I_8(O_3SC_6H_4CH_3)_6]$ (M = Mo, W). Russ J Coord Chem 43:172–180
97. Fuhrmann A-D, Seyboldt A, Schank A, Zitzer G, Speiser B, Enseling D, Jüstel T, Meyer H-J (2017) Luminescence quenching of ligand-substituted molybdenum and tungsten halide clusters by oxygen and their oxidation electrochemistry. Eur J Inorg Chem 2017:4259–4266
98. Braack P, Simsek MK, Preetz W (1998) Darstellung, kristallstrukturen und schwingungsspektren von $[(Mo_6X^i_8)Y^a_6]^{2-}$; X^i=Cl, Br; Y^a=NO_3, NO_2. Z Anorg Allg Chem 624:375–380
99. Efremova OA, Shestopalov MA, Chirtsova NA, Smolentsev AI, Mironov YV, Kitamura N, Brylev KA, Sutherland AJ (2014) A highly emissive inorganic hexamolybdenum cluster complex as a handy precursor for the preparation of new luminescent materials. Dalton Trans 43:6021–6025
100. Szczepura LF, Ooro BA, Wilson SR (2002) Synthesis of hexanuclear molybdenum clusters containing phosphine oxide ligands. J Chem Soc Dalton Trans 16:3112–3116
101. Saito T, Nishida M, Yamagata T, Yamagata Y, Yamaguchi Y (1986) Synthesis of hexanuclear molybdenum cluster alkyl complexes coordinated with trialkylphosphines: crystal structures of *trans*-$[(Mo_6Cl_8)Cl_4\{P(nC_4H_9)_3\}_2]$ and all-*trans*-$[(Mo_6Cl_8)Cl_2(C_2H_5)_2\{P(nC_4H_9)_3\}_2]$ $\bullet C_6H_5CH_3$. Inorg Chem 25:1111–1117
102. Mikhaylov MA, Abramov PA, Komarov VY, Sokolov MN (2017) Cluster aqua/hydroxocomplexes supporting extended hydrogen bonding networks. Preparation and structure of a unique series of cluster hydrates $[Mo_6I_8(OH)_4(H_2O)_2]\cdot nH_2O$ (n = 2, 12, 14). Polyhedron 122:241–246
103. Vorotnikov YA, Efremova OA, Novozhilov IN, Yanshole VV, Kuratieva NV, Brylev KA, Kitamura N, Mironov YV, Shestopalov MA (2017) Hexaazide octahedral molybdenum cluster complexes: synthesis, properties and the evidence of hydrolysis. J Mol Struct 1134:237–243
104. Schoonover JR, Zietlow TC, Clark DL, Heppert JA, Chisholm MH, Gray HB, Sattelberger AP, Woodruff WH (1996) Resonance raman spectra of $[M_6X_8Y_6]^{2-}$ cluster complexes (M = Mo, W; X, Y = Cl, Br, I). Inorg Chem 35:6606–6613
105. Szczepura LF, Ketcham KA, Ooro BA, Edwards JA, Templeton JN, Cedeño DL, Jircitano AJ (2008) Synthesis and study of hexanuclear molybdenum clusters containing thiolate ligands. Inorg Chem 47:7271–7278
106. Szczepura LF, Edwards JA, Cedeno DL (2009) Luminescent properties of hexanuclear molybdenum(II) chloride clusters containing thiolate ligands. J Clust Sci 20:105–112

107. Sokolov MN, Mikhailov MA, Virovets AV, Brylev KA, Bredikhin RA, Maksimov AM, Platonov VE, Fedin VP (2013) Synthesis, structure, and luminescence of the octahedral molybdenum cluster $[Mo_6I_8(SC_6F_4H)_6]^{2-}$. Russ Chem Bull 62:1764–1767
108. Yamagata T, Okiyama H, Imoto H, Saito T (1997) *trans*-$[(Mo_6Cl_8)(C_7H_7)_4\{P(n\text{-}C_4H_9)_3\}_2]$ and *trans*-$[(Mo_6Cl_8)(C_8H_5)_4\{P(n\text{-}C_5H_{11})_3\}_2]\cdot 2C_7H_8$. Acta Cryst C53:859–862
109. Sokolov MN, Mikhailov MA, Brylev KA, Virovets AV, Vicent C, Kompankov NB, Kitamura N, Fedin VP (2013) Alkynyl complexes of high-valence clusters. Synthesis and luminescence properties of $[Mo_6I_8(C{\equiv}CC(O)OMe)_6]^{2-}$, the first complex with exclusively organometallic outer ligands in the family of octahedral $\{M_6X_8\}$ clusters. Inorg Chem 52:12477–12481

Struct Bond (2019) 180: 109–124
DOI: 10.1007/430_2019_34

Published online: 28 April 2019

Rhenium Hexanuclear Clusters: Bonding, Spectroscopy, and Applications of Molecular Chevrel Phases

Alvaro Muñoz-Castro, Dayan Paez-Hernandez, and Ramiro Arratia-Perez

Contents

Abstract The discovery in 1971 of the high critical field superconducting properties of Chevrel phases with transition temperatures T_c between 10 and 18 K stimulated extensive research to improve their superconducting behavior. This fact was also the starting point for a new research area in solid-state and molecular chemistry involving the Mo_6 and Re_6 clusters where the intercluster bonding interactions seen in the solid phases are lacking, so a more localized cluster wave function at the Fermi level arises, as suggested by Fischer in 1978. Here, we describe the bonding, optical, magnetic, redox, and biological properties of related hexanuclear species given by $M_6(Q, X)_8L_6$ (M = Mo, W, Re; Q = S, Se, Te; X = Cl, Br, I; and L = σ or π ligand) molecular clusters. Noteworthy, cancer cells are more sensitive to $[Re_6Se_8I_6]^{3-}$ cluster-induced cell death than normal cells. The molecular view of such species offers a fresh perspective enabling further rational design of building blocks for interesting materials.

Keywords Chevrel phases · Molecular cluster · Relativistic effects

A. Muñoz-Castro
Centro de Química Inorgánica y Materiales Moleculares, Facultad de Ingeniería, Universidad Autónoma de Chile, Santiago, Chile

D. Paez-Hernandez and R. Arratia-Perez (✉)
Center for Applied Nanosciences (CANS), Universidad Andres Bello, Santiago, Chile

1 Introduction

The discovery of the $A_xMo_6Q_8$ (A = cation, Q = chalcogen) superconducting Chevrel phases by Chevrel, Sergent, and Prigent in Rennes University in 1971 [1, 2] (A being Sn, Pb, Cu, Ag, La, Ga) gave rise to a new class of solid superconductors with transition temperatures T_c between 10 K and 18 K. The high critical field superconducting properties of Chevrel phases stimulated extensive research to explain and improve their superconducting behavior [3–5]; this fact was also the starting point for a new research area in solid-state chemistry involving the Mo_6 and Re_6 chalcohalide clusters obtained at high temperatures via solid-state routes [3, 4].

Earlier electronic structure studies evidenced that the number of valence electrons per octahedral cluster unit (VEC) plays an essential role in their superconductivity suggesting that the Mo_6Q_8 building blocks exhibit some molecular character [6, 7], where the superconducting properties of the solid phases are related to their unique crystallographic structure, in which the distorted Mo_6S_8 discrete cluster units are well separated and weakly coupled by bonding interaction through the capping S atoms suggesting that a localized character of the cluster wave functions could be responsible for their superconductivities [3, 7–10].

About three decades ago, Saito et al. reported the first molecular analogue examples, namely, $M_6S_8(PEt_3)_6$ (M = Mo, W), of the superconducting AMo_6S_8 Chevrel's ternary solid phases [11–13]. These molecular clusters display a regular M_6 octahedron enclosed by a cubic S_8 cage in which intercluster bonding interactions seen in the solid phases are lacking, so a more localized cluster wave function at the Fermi level was expected [11–16].

We studied in 1993 [16] the $M_6S_8L_6$ (M = Mo, W) cluster electronic structure resembling Saito's molecular analogue [11–13] using a full approximate relativistic calculations (SCSF-DSW) that allowed us to compare against resolved X-ray and UV photoelectron data of Saito's molecular analogue and on the AMo_6S_8 (A = Sn or Pb) solid phases [17–19]. Two significant experimental values were obtained for Saito's cluster, the ultraviolet photoemission spectroscopy (UPS) spin-orbit splitting of the Mo ($3d_{3/2}$–$3d_{5/2}$) = 3.2 eV (*calculated*, 3.3 eV [16]) and the S ($2p_{1/2}$–$2p_{3/2}$) = 1.2 eV (*calculated*, 1.3 eV) [11–13, 16]. While the measured X-ray photoemission spectroscopy (XPS) outer spin-orbit splitting seen in the AMo_6S_8 (A = Pb, Ln, Ag, In) solid phases reported by Rao [19] for the Mo($3p_{1/2}$–$3p_{3/2}$) splitting fluctuates between 18.0 and 17.6 eV (*calculated*, 17.6 eV [16]), that for the Mo ($3d_{3/2}$–$3d_{5/2}$) splitting fluctuates between 3.1 and 3.5 eV (*calculated*, 3.3 eV [16]). The VEC value of Saito's molecular clusters is 24e, while, in the Chevrel phases, the VEC value may vary from 20e to 24e, depending on A. The intercluster interactions seen in the solid phases lead to a band structure for metallic conduction when the bands are partly filled, while the molecular clusters (VEC = 24e) could be semiconducting or even insulating [10].

The close agreement between the spectroscopic values seen in the molecular clusters and in the solid phases – corroborated by our calculations [16] – clearly demonstrates the valid suggestion about cluster-like behavior at the Fermi level

arising from the Mo_6(4d) electrons of the connected octahedral cluster in the solid phases by Fischer [7–9]. Since Chevrel's phases discovery, substantial parts of modern solid-state inorganic chemistry may be now identified with extended frameworks which contain the well-known polynuclear octahedral building blocks $M_6X_8L_6$ and $M_6Q_8L_6$, where M = Mo, W, and Re; X = Cl, Br, and I; L = any terminal α or π ligand; and Q = S, Se, and Te [20–26]. The appearance of the chemical protocol of dimensional reduction of extended cluster frameworks to obtain soluble isostructural molecular hexanuclear rhenium(III) chalcogenide clusters [27–29] initiated a rapid and fruitful development of their solution chemistry, where the isostructural cubic $Re_6Q_8(L,X)_6$ clusters, characterized by having capping chalcogenide ligands Q = S, Se, and Te, and terminal X (α or π) ligands were obtained (see Fig. 1) [30–51].

Interestingly, several studies have found that the isostructural 24e molybdenum, tungsten, and rhenium chalcogenide clusters are luminescent, displaying long emissive lifetimes (at the microsecond scale) and significant quantum yields (at room temperature) and undergo facile ground- and excited-state multielectron transfer, thus representing a new class of cluster photoreceptors for chemical reactions induced by light [25, 26]. They also undergo reversible oxidation process at very low potentials [36, 37, 53], and both terminal and capping (L and Q) ligands induce a modulated dependence on the luminescence quantum yield [27–35]. Moreover, the substitutional lability of the outer terminal L ligands makes the $M_6(X,Q)_8L_6$ molecular clusters a reasonable point of departure for constructing functional multicluster aggregates for technological applications [37–58]. The luminescence and magnetic properties seen in the hexanuclear rhenium clusters are well documented [34, 35, 37, 39–48, 51, 53–63].

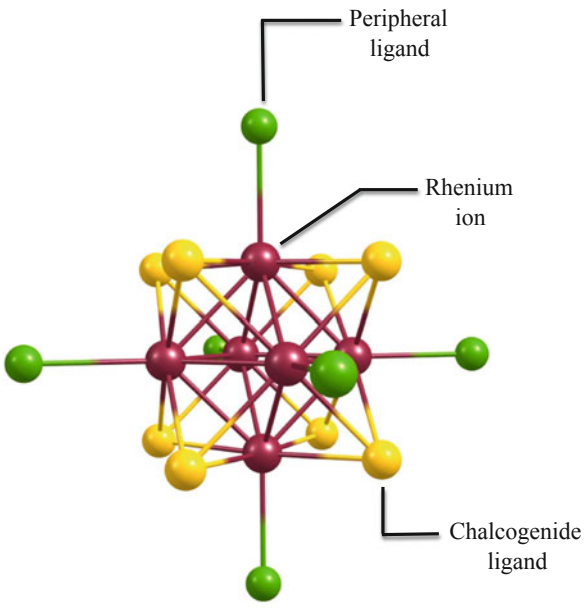

Fig. 1 Molecular model of the $[Re_6(\mu_3\text{-}Q_8)X_6]^{4-}$ cluster

Due to the interesting photophysical and redox properties of the Mo, W, and Re hexanuclear clusters, these can be viewed as potential candidates for their uses as X-ray contrast agents, or useful photoredox sensitizers toward electron acceptors, or as a novel class of metal cluster photoreceptors for chemical reactions induced by light [22, 37–39, 46, 52, 57].

Thus, it is now clear that Chevrel phases discovery originated very innovative molecular chemical research due to the functional hexanuclear clusters synthesized in many laboratories around the world, and the work continues with many new applications. Here, we focus on clusters with an $[Re_6(\mu_3\text{-}Q_8)]^{2+}$ core, depicted as Re_6Q_8 in short.

2 Bonding and Stability

The first successful synthesis of the hexarhenium chalcogenide-capped clusters was reported in 1971 by Opalovskii et al. [60, 61]. Twelve years later, in 1983, the 24-electron octahedral cluster core was identified in a group of chalcohalide hexarhenium compounds obtained by Leduc et al. [62]. These works paved the way for the further development and study of the solution chemistry of hexanuclear rhenium chalcogenide clusters and became the base for a profitable syncretism with solid-state chemistry.

From the perspective of creating novel materials, the attractive electrochemical and photophysical properties that are present in these kinds of clusters must be taken into account. First, a reversible one-electron oxidation event is typically observed. Moreover, these clusters are phosphorescent, which depends on the coordination environment of the cluster, particularly of the terminal (or peripheral) ligands that are coordinated with the $[Re_6(\mu_3\text{-}Q_8)]^{2+}$ core. These interesting peculiarities, though not yet fully understood largely because of the complicated electronic structures of the cluster system, suggest the possibility of creating cluster-based functional materials, as it is well-studied experimentally by Long et al. [27, 38, 51–70].

Computational methods are useful in the rationalization of bonding properties between different ligands and the hexanuclear cluster core. Particular attention has been paid to hexanuclear chalcocyanide rhenium clusters, their electronic structure of which is well discussed in literature [6, 51, 53]. Their geometrical distortion owing to Jahn-Teller effect upon oxidation toward 23e species was explained on the basis of theoretical calculations [63, 67] where the doubly degenerated HOMO of the parent 24e system (e_g symmetry) splits into a_{1g} and b_{1g} orbitals driven by the one-electron oxidation, resulting in a contracted configuration of D_{4h} symmetry.

The presence of different chalcogenide atoms within the hexanuclear core leads to a similar behavior between isoelectronic compounds as discussed, for example, for $[Re_6S_8(OH)_6]^{4-}$ and $[Re_6Se_8(OH)_6]^{4-}$ species [64], which exhibit related frontier orbital structure. This is also observed for $[Re_6Q_8(CN)_6]^{4-}$ (Q = S, Se), involving also Tc counterparts [69]. Moreover, the bonding characteristic of the Re_6Se_8 core toward classical ligands such as carbonyls [70] has been studied on the basis of the

monocarbonyl $[Re_6Se_8(PEt_3)_5(CO)]^{2+}$ and dicarbonyl $[Re_6Se_8(PEt_3)_4(CO)_2]^{2+}$ species. By using a pictorial analysis, the formation of a $2\pi^*$ backbonding is found where the most significant π overlap occurred by contribution from Se atoms, which provides charge for the Re→$2\pi^*$-CO backdonation, giving rise to the established synergistic bonding mode usually found in metal-carbonyl structures.

The possibility to attach different ligands to the Re_6Q_8 core allows evaluating the bonding strength in relation to the nature of the ligands, which is of particular interest since this enables the possibility to modify terminal ligands for new developments in their chemistry, owing to the promising biomedical applications by taking advantage of its luminescent behavior [71]. Moreover, a systematic study of the cluster ligand interaction along the $[Re_6(\mu_3\text{-}Q_8)X_6]^{4-}$ ($Q = S^{2-}, Se^{2-}, Te^{2-}$; $X = F^-, Cl^-, Br^-, I^-, CN^-, NC^-, SCN^-, NCS^-, OCN^-, NCO^-$) series leads to a detailed description of the electronic structure of these complexes and the character of the $[Re_6(\mu_3\text{-}Q_8)]^{2+}$ core-ligand interaction [72, 73]. Theoretical calculations allow concluding that all cores of rhenium chalcogenide clusters have a strong electrophilic behavior, which tends to interact preferentially with the most polarizable peripheral ligands. This interaction has a predominantly ionic character (~78% on average) and is independent of the chalcogenide bridge ligand; the remaining covalent contribution (~22%) is mainly related to the possibility of σ-donation from the peripheral ligands to the core, which appears for all the ligands. It is revealed that the most stable clusters are those that present stronger σ-donor terminal ligands, whereas cluster stability starts to decrease when the π-acceptor effect is stronger. This observation can be directly related to the terminal ligand lability and the strong electrophilic character of the $[Re_6(\mu_3\text{-}Q_8)]^{2+}$ core (see Fig. 2).

3 Redox and Magnetic Behavior

In addition to the electronic and bonding property calculations, recently the redox potentials have been achieved theoretically for a series of $[Re_6(\mu_3\text{-}Q_8)X_6]^{4-}$ clusters, where Q = S and Se and X = F^-, Cl^-, Br^-, I^-, CN^-, NC^-, SCN^-, NCS^-, OCN^-, and NCO^- [75], by using the Born-Haber thermodynamic cycle along DFT calculations involving relativistic and solvent effects (see Fig. 3). The obtained values agree well with the experimental data related to the free energy of the reversible $Re(III)_6/Re(III)_5Re(IV)$ process. In addition, the molecular orbital analysis revealed that the redox process is localized in the cluster core, $[Re_6(\mu_3\text{-}Q_8)]^{2+}$, where the peripheral ligands contribute into a lesser extent which can be employed to tune the redox properties.

As a counterpart of the experimental results, several theoretical works have been reported by Arratia-Pérez and coworkers, especially in the field of the magnetic properties for hexarhenium face-capped chalcohalide clusters [54, 55]. These studies were developed on the framework of approximated four-component relativistic density functional theory to introduce in a proper way the intrinsic relativistic effects related to heavy atoms. The ground state of each $23e^-$ $[Re_6Q_8X_6]^{3-}$ cluster ion is a

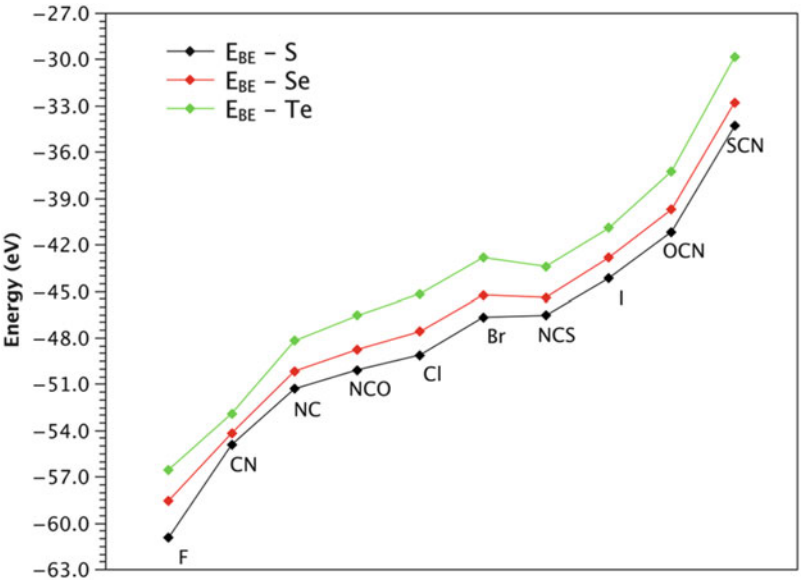

Fig. 2 Variation of the bonding energy (E_{BE}) for all peripheral ligands in the $[Re_6Q_8X_6]^{4-}$ cluster. Reprinted with permission from Ref. [72]. Copyright 2014 American Chemical Society

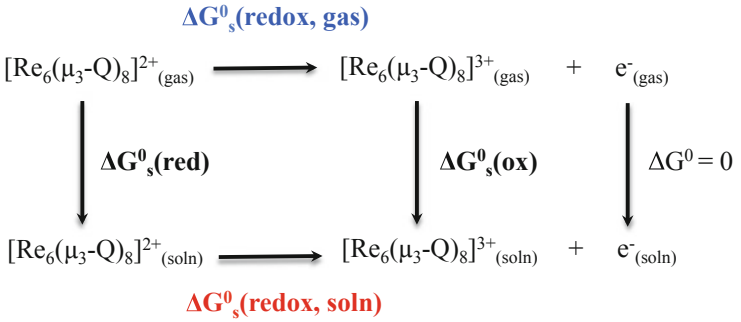

Fig. 3 Thermodynamic free energy cycle used to calculate the redox potential for $[Re_6(\mu_3\text{-}Q)_8]^{2+}$/$[Re_6(\mu_3\text{-}Q)_8]^{3+}$ pair. ΔG^0s(redox, gas) and ΔG^0s(redox, soln) are the free energy changes for the redox process in gas phase and in the presence of solvent, respectively. ΔG^0s(red) and ΔG^0s(ox) are the solvation free energy changes for the reduced and oxidized form, respectively. Reproduced from Ref. [74] with permission from the Centre National de la Recherche Scientifique (CNRS) and the Royal Society of Chemistry

Kramers doublet. The calculations predicted isotropic Zeeman tensors, which are in good agreement with single crystal solid-state cluster EPR experiments, and the metal and terminal ligand hyperfine tensors are anisotropic, while the hyperfine tensor arising from the capping S ligands is small and isotropic [54, 55].

All these studies have in common the conclusion that these reversible redox couples $[Re_6(\mu_3\text{-}Q_8)X_6]^{4-}/[Re_6(\mu_3\text{-}Q_8)X_6]^{3-}$ could constitute suitable nanoscale materials for applications in optical and magnetic data storage, ultrafast data communication, and solar energy conversion devices, among others.

4 Optical Properties

In reference to the optical properties, time-dependent density functional theory (TD-DFT) calculations were carried out with the aim of simulating UV-vis spectra and understanding the role of the terminal ligands on the absorption band shifting as well as the composition of the molecular orbitals (spinors) involved in these electronic transitions. Particularly, the luminescence exhibited by the hexanuclear rhenium chalcogenide clusters was firstly predicted theoretically by Arratia-Pérez et al. for the sulfide/selenide rhenium clusters, on the basis of the structural similarities with the well-known luminescent hexanuclear tungsten halide clusters $[W_6X_{14}]^{2-}$ and with the clusters contained in the superconducting Chevrel phases [34, 35]. After this theoretical prediction, many other experimental studies corroborated this hypothesis with some relevant results. For instance, one of the longest excited-state lifetimes for a transition metal complex was attributed to the hexanuclear molybdenum cluster of the form $[Mo_6\ (\mu_3\text{-}Cl_8)\ Cl_6]^{2-}$, and similar results were found by a family of Mo clusters of the form $[Mo_6\ (\mu_3\text{-}Cl_8)\ (SR)_6]^{2-}$ (-SR are different thiolates) [75]. This allowed to elaborate an early prediction of luminescent behavior of clusters derived from the hexarhenium cluster core, $[Re_6S_8X_6]^{4-}$ (X = Cl, Br, I), which was latter extended to the related $[Re_6Se_8X_6]^{4-}$ structure [34, 35]. The luminescence properties were experimentally corroborated by Yoshimura et al. [42], Gabriel et al. [51], and Zheng et al. [38]. They found that the luminescence of the $[Re_6(\mu_3\text{-}Q_8)]^{2+}$ clusters occurs at excitation wavelengths in the range of their most intense absorption bands at around 350–450 nm. Furthermore, it was found that the luminescence for these series of halide rhenium chalcogenide clusters shifts to a longer wavelength when we move down to the halogen group and also that their emission spectra are analogous to that of hexanuclear molybdenum(II) and tungsten(II) species, which establish these clusters as promising luminophores for a wide range of light-based applications. Yoshimura and coworkers found that for the same $\mu_3\text{-}Q^{2-}$ ligand, the plot of the nonradiative rate versus emission wavelength has a linear behavior not only in rhenium clusters but also in similar cases with other metals [69]. However, for the same peripheral ligands, the change in the capping ligand does not produce the same behavior, concluding that the electronic states of the hexanuclear complexes are influenced largely by the nature of the capping ligands. The latest efforts to design novel luminescent materials are focused on the construction of framework structures containing the $[M_6(\mu_3\text{-}Q_8)]^{2+}$ build linker to incorporate red/near-infrared luminescence in the construction of functional materials.

From a theoretical point of view to calculate the absorption spectra of these molecules, some technical aspect needs to be considered. Time-dependent density

functional theory (TD-DFT) combined with relativistic Hamiltonians has proven to be an indispensable tool. In the same way, a correct assignment of the spectra requires the use of the double-valued octahedral (O_h*) symmetry constraint that indicates that it is necessary to change the framework from molecular orbitals to molecular spinors. Thus, the molecular spinors are considered to transform according to the octahedral extra irreducible representations. In our notation, these double-valued irreducible representations are related to the usual Griffith's notation as follows: $E_{1/2g,u}$, $E_{5/2g,u}$, and $U_{3/2g,u}$. Here, E and U extra irreps correspond to two- and fourfold symmetries, respectively. The traditional irreducible representations of the single group commonly used in the O_h can be translated as follows:

$$A_{1g} = E_{1/2g}$$
$$A_{2g} = E_{5/2g}$$
$$E_g = U_{3/2g}$$
$$T_{1g} = E_{1/2g} + U_{3/2g}$$
$$T_{2g} = E_{5/2g} + U_{3/2g}$$
$$A_{1u} = E_{1/2u}$$
$$A_{2u} = E_{5/2u}$$
$$E_u = U_{3/2u}$$
$$T_{1u} = E_{1/2u} + U_{3/2u}$$
$$T_{2u} = E_{5/2u} + U_{3/2u}$$

These compatibility relationships were obtained as a consequence of the interaction of the single-valued irreducible representations with the spin-irreducible representation. It should be clear that the spin-orbit coupling (SOC) splits the orbital degeneracy and breaks the optical selection rules. Moreover, for the octahedral point group, it is easy to obtain the double-group symmetry-allowed electronic transitions, resulting as:

$$E_{1/2g} \leftrightarrow E_{1/2u}$$
$$E_{1/2g} \leftrightarrow U_{3/2u}$$
$$E_{1/2g} \leftrightarrow E_{5/2u}$$
$$U_{3/2g} \leftrightarrow E_{1/2u}$$
$$U_{3/2g} \leftrightarrow E_{5/2u}$$
$$E_{5/2g} \leftrightarrow U_{3/2u}$$

These symmetry (and spin)-allowed transitions should be taken into account while assigning the absorption and emission bands.

In the case of the halide terminal ligands (F, Cl, Br, and I) and independently of the chalcogenide in the $[Re_6(\mu_3\text{-}Q_8)]^{2+}$ core (Q = S^{2-}, Se^{2-}, and Te^{2-}), a redshift is observed when the halide terminal ligand becomes heavier (more labile) (Fig. 4). This redshift for the halide series is directly related to the nature of the spinors involved in the main electronic transitions of their spectra. In all cases, the electronic transitions occur from molecular spinors centered in the core to spinors also centered in the core, but with a progressive increment of the terminal ligand contribution. Then, these transitions are halide dependent with a progressive increment of the metal-to-ligand charge transfer (MLCT) character [72, 73].

By taking advantage of the $[Re_6Se_8I_6]^{3-}$ predicted luminescence [55], we reported in 2012 for the first time that cancer cells are more sensitive to $[Re_6Se_8I_6]^{3-}$ cluster-induced cell death than normal cells [71]. This effect is probably mediated by an apoptotic-like cell death. Thus, the $[Re_6Se_8I_6]^{3-}$ cluster may be useful for cancer diagnostics and localization of tumors and may enable the observation through fluorescence of tumor regression during treatment.

For the CN^- and NC^- π-acceptor ligands, in the case where the donation and backdonation phenomena are the same for both terminal ligands, the most important electronic transitions can be characterized as intra-core with some ligand contribution. In this case, the ligand contribution is similar to those showed by fluoride and chloride ligands, and the absorption bands appear in the same region. The same behavior is observed for the $–OCN^-$/$–NCO^-$ couple. In this case the absorption spectra, as in the case of the halides and the $–CN^-$/$–NC^-$ couple, are directly related to the ligand participation in the orbitals involved in the electronic transitions, but for this couple of ligands, both molecular orbitals involved in the transitions have a slight contribution from the terminal ligand atomic orbitals. Similar behavior has been reported by Yoshimura and coworkers in another group of clusters of the form $[Tc_6(\mu_3\text{-}Q_8)(CN)_6]^{4-}$ (Q = S^{2-}, Se^{2-}) [39, 69]. TD-DFT calculations for both sulfide- and selenide-capped hexatechnetium complexes indicate that the substantially allowed transitions in the range of 400–500 nm are ascribed to the core, concluding that the electronic structure and electronic transition properties of $[Tc_6(\mu_3\text{-}Q_8)(CN)_6]^{4-}$ are similar to those of the hexarhenium analogues [76].

On the other hand, when the chalcogenide ion is changed instead of the terminal ligand, a bathochromic effect in the absorption spectra possibly due to a heavy atom effect of the chalcogenide in the hexarhenium chalcogenide core is observed, which produces an energetic rearrangement of the orbitals and excitation energies shifting it to longer wavelengths regions, as can be observed in Fig. 5. Moreover, a decrease in the calculated oscillator strengths is exhibited in the following way: $S^{2-} > Se^{2-} > Te^{2-}$; this tendency is in agreement with the absorption intensities observed experimentally [37, 39, 69].

Finally, for the $–SCN^-$ and $–NCS^-$ terminal ligands, the nature of the orbitals involved in the electronic transition is significantly different with respect to all the other σ-donor and π-acceptor terminal ligands. In this case, the ligand contribution is bigger than the core contribution for the departure orbitals and around 20% for the arrival orbitals [73, 76].

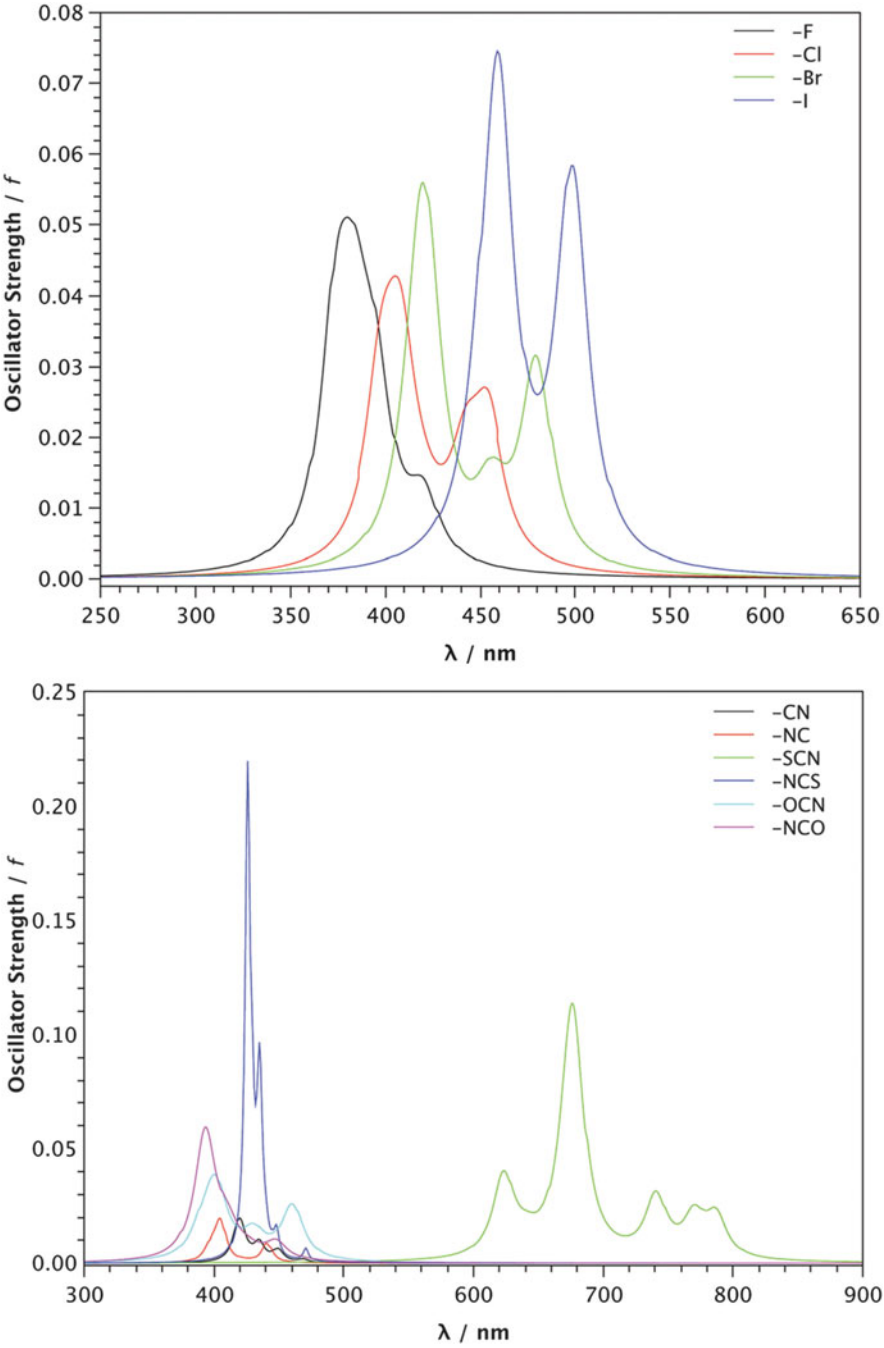

Fig. 4 Calculated excitation energies for the $[Re_6(\mu_3\text{-}Q_8)X_6]^{4-}$ cluster series at the spin-orbit relativistic level considering acetonitrile as solvent. Reproduce with permission from Ref. [73]. Copyright 2015 Royal Society of Chemistry

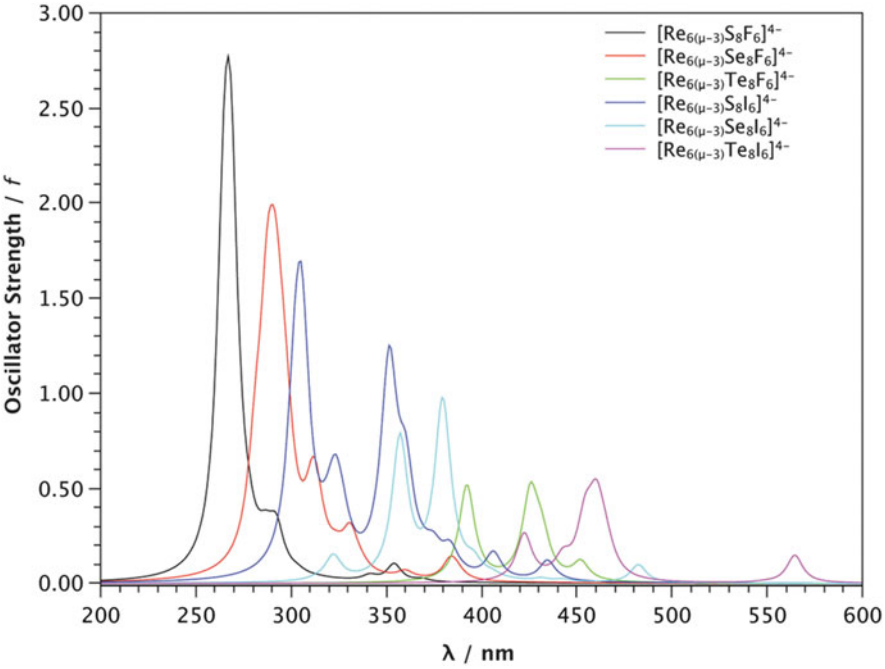

Fig. 5 Calculated excitation energies for the $[Re_6(\mu_3\text{-}Q_8)X_6]^{4-}$ (Q = S^{2-}, Se^{2-}, Te^{2-} and X = F^-, I^-) cluster series at the spin-orbit relativistic level considering acetonitrile as solvent. Reproduced with permission from Ref. [73]. Copyright 2015 Royal Society of Chemistry

5 Conclusions

The close agreement between the spectroscopic XPS and UPS values seen in the solid phases and in the molecular clusters clearly demonstrated the clever suggestion by Fischer about the cluster-like behavior at the Fermi level arising from the Mo_6(4d) electrons of the connected octahedral cluster in the solid phases. Due to this, extended frameworks and clusters in solution now contain the well-known polynuclear octahedral building blocks $M_6X_8L_6$ and Chevrel-like octahedral $M_6Q_8L_6$ clusters, where M = Mo, W, and Re; X = Cl, Br, and I; L = any terminal α or π ligand; and Q = S, Se, and Te. The hexanuclear tungsten(II), molybdenum(II), and Re(III) cluster emission spectra are analogous, thus establishing their role as potential luminophores for a wide range of light-based applications, like cancer cells that are more sensitive to $[Re_6Se_8I_6]^{3-}$ cluster-induced cell death than normal cells [71].

In the case of the halide terminal ligands (F, Cl, Br, and I) and independently of the chalcogenide in the $[Re_6(\mu_3\text{-}Q_8)]^{2+}$ core (Q = S^{2-}, Se^{2-}, and Te^{2-}), a redshift is observed when the halide terminal ligand becomes more labile**.** This redshift for the halide series is halide dependent with a progressive increment of the MLCT character. Also, reversible redox couples $[Re_6(\mu_3\text{-}Q_8)X_6]^{4-}/[Re_6(\mu_3\text{-}Q_8)X_6]^{3-}$ could

constitute suitable nanoscale materials for applications in optical and magnetic data storage and ultrafast data communication technologies.

Acknowledgments We thank Fondecyt 1180683, 1180017, and 1150629 for funding this work.

References

1. Chevrel R, Sergent M, Prigent J (1971) Sur de nouvelles phases sulfurées ternaires du molybdène. J Solid State Chem 3:515–519
2. Perrin C, Sergent M, Prigent J (1973) Chalcohalogénures de basse valence du molybdène. C R Acad Sci Paris Ser C 277:465–468
3. Chevrel R, Hirrien M, Sergent M (1986) Superconducting Chevrel phases: prospects and perspectives. Polyhedron 5:87–94
4. Chevrel R, Gougeon P, Potel M, Sergent M (1985) Ternary molybdenum chalcogenide: a route to new extended clusters. J Solid State Chem 15:25–33
5. Chevrel R, Sergent M (1982) In: Fischer O, Maple MB (eds) Topics in current physics: superconductivity in ternary compounds I, vol 32. Springer, Berlin, p 25
6. Hugbanks T, Hoffmann R (1983) Molybdenum chalcogenides: clusters, chains, and extended solids. The approach to bonding in three dimensions. J Am Chem Soc 105:1150–1162
7. Fischer O (1978) Chevrel phases: superconducting and normal state properties. Appl Phys 16:1–28
8. Fisher O, Treyvaud A, Chevrel R, Sergent M (1975) Superconductivity in the RexMo6S8. Solid State Commun 17:721–724
9. Fisher O, Jones H, Bondi G, Sergent M, Chevrel R (1974) Measurements of critical fields up to 500kG in the ternary molybdenum sulphides. J Phys C 7:LA50
10. Perrin A, Perrin C (2012) The molybdenum and rhenium octahedral cluster chalcohalides in solid state chemistry: from condensed to discrete cluster units. CR Chim 15:815–836
11. Saito T, Yamamoto N, Yamagata T, Imoto H (1988) Synthesis of $[Mo_6S_8(PEt_3)_6]$ by reductive dimerization of a trinuclear molybdenum chloro sulfido cluster complex coordinated with triethylphosphine and methanol: a molecular model for superconducting Chevrel phases. J Am Chem Soc 110:1646–1647
12. Saito T, Yoshikawa Y, Yamagata T, Imoto H, Unoura K (1989) Synthesis, structure and electronic properties of octakis ($\mu_3$sulfido) hexakis(triethylphosphine) hexatungsten as a tungsten analog of the molecular model for superconducting Chevrel phases. Inorg Chem 28:3588–3592
13. Saito T, Yamamoto N, Nagase T, Tsuboi T, Kobayashi T, Yamagata T, Imoto H, Unoura K (1990) Molecular models of the superconducting chevrel phases: syntheses and structures of $[Mo_6X_8(PEt_3)_6]$ and $[PPN][Mo_6X_8(PEt_3)_6]$ (X = S, Se; PPN = $(Ph_3P)_2N$). Inorg Chem 29:764–770
14. Le Beuze L, Makyoun MA, Lissilour R, Chermette H (1982) Electronic structure and chemical bonding in metallic clusters of binary and ternary transition metal chalcogenides. I. SCF MS Xα study including relativistic effect of $PbMo_6S_8$. J Chem Phys 76:6060–6066
15. Woolley RG (1985) Bonding in transition-metal cluster compounds. 1. The $M_6(\mu_3\text{-}X)_8$ cluster. Inorg Chem 24:3519–3525
16. Arratia-Perez R (1993) The $M_6S_8L_6$ clusters: an example in cluster and condensed phase chemistry. Chem Phys Lett 213:547–553
17. Ihara H, Kimura Y (1978) Photoelectron spectra of ternary molybdenum sulphides. Jpn J Appl Phys 17:281–283

18. Kurmaev EZ, Yarmoshenko YM, Nyholm R, Martenson N, Jarlborg T (1981) Investigation of electronic structure of ternary molybdenum sulphides by means of x-ray emission and photoelectron spectroscopy. Solid State Commun 37:647–651
19. Yabonath S, Hedge MS, Serode PR, Rao CN, Umarji KM, Subba Rao GV (1981) Charge transfer in Chevrel phases. Solid State Commun 37:325
20. Corbett JD (1992) Coordination chemistry in the solid state: cluster and condensed cluster halides of the early transition metals. Pure Appl Chem 64:1395–1408
21. Arratia-Perez R, Hernández Acevedo L (1997) A Dirac molecular orbital study for hexanuclear tungsten cluster structures. Chem Phys Lett 277:223–226
22. Zietlow TC, Hopskin MD, Gray HB (1985) Electronic spectroscopy and photophysics of d4 clusters. J Solid State Chem 57:112–119
23. Zietlow TC, Schaefer WP, Sadeghi B, Hua N, Gray HB (1986) Hexanuclear tungsten cluster structures: tetradecachlorohexatungstate(2-), tetradecabromohexatungstate(2-), and tetradecaiodohexatungstate(2-) relevance to unusual emissive behavior. Inorg Chem 25:2195–2198
24. Maverick AW, Nadzionek JS, Mackenzie D, Nocera D, Gray HB (1983) Spectroscopic, electrochemical, and photochemical properties of molybdenum(II) and tungsten(II) halide clusters. J Am Chem Soc 105:1878–1882
25. Gray HB, Maverick AW (1981) Solar chemistry of metal complexes. Science 214:1201–1205
26. Schoonover JR, Zietlow TC, Clark DL, Heppert JA, Chisholm MH, Gray HB, Sattelberger AP, Woodruff WH (1996) Resonance Raman spectra of $[M_6X_8Y_6]^{2-}$ cluster complexes (M = Mo, W; X, Y = Cl, Br, I). Inorg Chem 35:6606–6613
27. Long JR, McCarty LS, Holm RH (1996) A solid-state route to molecular clusters: access to the solution chemistry of $[Re_6Q_8]^{2+}$ (Q = S, Se) core-containing clusters via dimensional reduction. J Am Chem Soc 118:4603–4616
28. Zheng Z, Holm RH (1997) Cluster condensation by thermolysis: synthesis of a rhomb-linked $Re_{12}Se_{16}$ dicluster and factors relevant to the formation of the $Re_{24}Se_{32}$ tetracluster. Inorg Chem 36:5173–5178
29. Zheng Z, Long JR, Holm RH (1997) A basis set of Re_6Se_8 cluster building blocks and demonstration of their linking capability: directed synthesis of an $Re_{12}Se_{16}$ dicluster. J Am Chem Soc 119:2163–2171
30. Mironov YV, Cody JA, Albretch-Schmith T, Ibers JT (1997) Cocrystallized mixtures and multiple geometries: syntheses, structures, and NMR spectroscopy of the Re_6 clusters $[NMe_4]_4[Re_6(Te_8\text{-nSen})(CN)_6]$ (n = 0−8). J Am Chem Soc 119:493–498
31. Emirdag-Eanes M, Ibers JA (2002) Conversion of a Re(IV) tetrahedral cluster to a Re(III) octahedral cluster: synthesis of $[(CH_3)C(NH_2)_2]_4[Re_6Se_8(CN)_6]$ by a solvothermal route. Inorg Chem 41:6170–6171
32. Miller W, Long JR, McLauchlan C, Holm RH (1998) Ligand substitution reactions of $[Re_6S_8Br_6]^{4-}$: a basis set of Re_6S_8 clusters for building multicluster assemblies. Inorg Chem 37:328–333
33. Beauvais L, Schores MP, Long JR (1998) Cyano-bridged Re_6Q_8 (Q = S, Se) cluster-metal framework solids: a new class of porous materials. Chem Mater 10:3783–3786
34. Arratia-Perez R, Hernandez-Acevedo L (1999) The hexanuclear rhenium cluster ions $Re_6S_8X_6^{4-}$ (X=Cl, Br, I): are these clusters luminescent? J Chem Phys 110:2529–2532
35. Arratia-Perez R, Hernandez-Acevedo L (1999) The $Re_6Se_8Cl_6^{4-}$ and $Re_6Se_8I_6^{4-}$ cluster ions: another example of luminescent clusters? J Chem Phys 111:168–172
36. Guilbaud C, Deluzet A, Domercq B, Molinie P, Coulon C, Boubekeur K, Batail P (1999) $(NBun_4^+)_3[Re_6S_8Cl_6]^{3-}$·: synthesis and luminescence of the paramagnetic, open shell member of a hexanuclear chalcohalide cluster redox system. J Chem Soc Chem Commun 18:1867–1868
37. Gray TG, Rudzinski CM, Nocera DG, Holm RH (1999) Highly emissive hexanuclear rhenium (III) clusters containing the cubic cores $[Re_6S_8]^{2+}$ and $[Re_6Se_8]^{2+}$. Inorg Chem 38:5932–5933

38. Zheng Z, Gray TG, Holm RH (1999) Synthesis and structures of solvated monoclusters and bridged di- and triclusters based on the cubic building block $[Re_6(\mu_3\text{-}Se)_8]^{2+}$. Inorg Chem 38:4888–4895
39. Yoshimura T, Ishizaka S, Umakosh K, Sasaki Y, Kim HB, Kitamura N (1999) Hexarhenium (III) clusters $[Re_6(\mu_3\text{-}S)_8X_6]^{4-}$ (X− = Cl−, Br−, I−) are luminescent at room temperature. Chem Lett 28:697–698
40. Wang R, Zheng Z (1999) Dendrimers supported by the $[Re_6Se_8]^{2+}$ metal cluster core. J Am Chem Soc 121:3549–3550
41. Yoshimura T, Ishizaka S, Sasaki Y, Kim HB, Kitamura N, Naumov NG, Sokolov MN, Fedorov VE (1999) Unusual capping chalcogenide dependence of the luminescence quantum yield of the hexarhenium (III) cyano complexes $[Re_6E_8(CN)_6]^{4-}$, $E^{2-} = Se^{2-} > S^{2-} > Te^{2-}$. Chem Lett 28:1121–1122
42. Yoshimura T, Umakoshi K, Sasaki Y, Sykes AG (1999) Synthesis, structures, and redox properties of octa(μ_3-sulfido)hexarhenium(III) complexes having terminal pyridine ligands. Inorg Chem 38:5557–5564
43. Schores MP, Beauvais L, Long R (1999) $[Cd_2(H_2O)_4][Re_6S_8(CN)_6]\cdot 14H_2O$: a cyano-bridged cluster−cluster framework solid with accessible cubelike cavities. Inorg Chem 38:1648–1649
44. Schores MP, Beauvais L, Long JR (1999) Cluster-expanded Prussian blue analogues. J Am Chem Soc 121:775–779
45. Yoshimura YN, Umakoshi T, Sasaki K, Ishizaka Y, Kim S, Kitamura HB (2000) Emission and metal- and ligand-centered-redox characteristics of the hexarhenium(III) clusters trans- and cis-$[Re_6(\mu_3\text{-}S)_8Cl_4(L)_2]^{2-}$, where L is a pyridine derivative or pyrazine. Inorg Chem 39:1765–1772
46. Kobayashi N, Ishizaka S, Yoshimura T, Kim HB, Sasak Y, Kitamura N (2000) Photoredox ability of a Hexarhenium cluster $[Re_6S_8(Cl)_6]^{4-}$. Chem Lett 29:234–235
47. Beauvais L, Schores M, Long JR (2000) Cyano-bridged Re_6Q_8 (Q = S, Se) cluster-cobalt(II) framework materials: versatile solid chemical sensors. J Am Chem Soc 122:2763–2772
48. Chen ZN, Yoshimura T, Abe M, Sasaki Y, Ishizaka S, Kim HB, Kitamura N (2000) Chelate formation around a hexarhenium cluster core by the diphosphane ligand $Ph_2P(CH_2)_6PPh_2$. Angew Chem Int Ed Engl 40:239–242
49. Selby HD, Zheng Z, Gray TG, Holm RH (2001) Bridged multiclusters derived from the face-capped octahedral $[Re_6III(\mu_3\text{-}Se)_8]^{2+}$ cluster core. Inorg Chim Acta 312:205–209
50. Selby HD, Orto P, Carducci MD, Zheng Z (2002) Novel concentration-driven structural interconversion in shape-specific solids supported by the octahedral $[Re_6(\mu_3\text{-}Se)_8]^{2+}$ cluster core. Inorg Chem 41:6175–6177
51. Gabriel JP, Boubekeu K, Uriel S, Batail P (2001) Chemistry of hexanuclear rhenium chalcohalide clusters. Chem Rev 101:2037–2066
52. Tulsky E, Long JR (2001) Heterometal substitution in the dimensional reduction of cluster frameworks: synthesis of soluble $[Re_{6\text{-}n}Os_nSe_8Cl_6]^{(4\text{-}n)\text{-}}$ (n = 1−3) cluster-containing solids. Inorg Chem 40:6990–7002
53. Bennett MV, Beauvais LG, Shores MP, Long JR (2001) Expanded Prussian blue analogues incorporating $[Re_6Se_8(CN)_6]^{3-/4-}$ clusters: adjusting porosity via charge balance. J Am Chem Soc 123:8022–8032
54. Alvarez-Thon L, Hernandez-Acevedo L, Arratia-Perez R (2001) Calculated paramagnetic resonance parameters of the luminescent $Re_6S_8Cl_6^{3-}$ cluster ion. J Chem Phys 115:726
55. Arratia-Perez R, Hernandez-Acevedo L (2003) Calculated paramagnetic resonance parameters (g,Ahfi) of the $Re_6S_8Br_6^{3-}$, $Re_6S_8I_6^{3-}$, and $Re_6Se_8I_6^{3-}$ cluster ions. J Chem Phys 118:7425
56. Roland BK, Carter C, Zheng Z (2002) Routes to metallodendrimers of the $[Re_6(\mu_3\text{-}Se)_8]^{2+}$ core-containing clusters. J Am Chem Soc 124:6234–6235
57. Gray TG, Holm RH (2002) Site-differentiated hexanuclear rhenium(III) cyanide clusters $[Re_6Se_8(PEt_3)_n(CN)_{6\text{-}n}]^{n\text{-}4}$ (n = 4, 5) and kinetics of solvate ligand exchange on the cubic $[Re_6Se_8]^{2+}$ core. Inorg Chem 41:4211–4216
58. Yu SB, Watson AD (1999) Metal-based X-ray contrast media. Chem Rev 99:2353–2378

59. Kozlova SG, Gabuda SP, Brylev KA, Mironov YV, Fedorov VE (2004) Electronic spectra and DFT calculations of hexanuclear chalcocyanide rhenium clusters. J Phys Chem A 108:10565–10567
60. Opalovskii AA, Fedorov VE, Lobkov EU (1971). Russ J Inorg Chem 16:790
61. Opalovskii AA, Fedorov VE, Lobkov EU, Erenburg BG (1971). Russ J Inorg Chem 16:1685
62. Leduc L, Perrin A, Sergent M (1983) Chalcohalogénures et Chalcogénures à Clusters Octaédriques dans la Chimie de Basse Valence du Rhéium. C R Acad Sci Paris Ser II 296:961
63. Baudron SA, Deluzet A, Boubekeur K, Batail P (2002) Jahn–Teller distortion of the open-shell 23-electron chalcogenide rhenium cluster cores in crystals of the series, $\{[Re_6Q_8]^{3+}(X^-)_6\}^{3-}$ (Q = S, Se; X = Cl, CN). Chem Commun 18:2124–2125
64. Mironov YV, Brylev KA, Kim S-J, Kozlova SG, Kitamura N, Fedorov VE (2011) Octahedral cyanohydroxo cluster complex trans-$[Re_6Se_8(CN)_4(OH)_2]^{4-}$: synthesis, crystal structure, and properties. Inorg Chim Acta 370:363–368
65. Brylev KA, Mironov YV, Kozlova SG, Fedorov VE, Kim SJ, Pietzsch HJ, Stephan H, Ito A, Ishizaka S, Kitamura N (2009) The first octahedral cluster complexes with terminal formate ligands: synthesis, structure, and properties of $K_4[Re_6S_8(HCOO)_6]$ and $Cs_4[Re_6S_8(HCOO)_6]$. Inorg Chem 48:2309–2315
66. Gancheff JS, Denis PA (2011) Time-dependent density functional theory investigation of the electronic spectra of hexanuclear chalcohalide rhenium(III) clusters. J Phys Chem A 115:211–218
67. Deluzet A, Duclusaud H, Sautet P, Borshch SA (2002) Electronic structure of diamagnetic and paramagnetic hexanuclear chalcohalide clusters of rhenium. Inorg Chem 41:2537–2542
68. Yarovoi SS, Mironov YV, Naumov DY, Gatilov YV, Kozlova SG, Kim S-J, Fedorov VE (2005) Octahedral hexahydroxo rhenium cluster complexes $[Re_6Q_8(OH)_6]^{4-}$·(Q = S, Se): synthesis, structure, and properties. Eur J Inorg Chem 19:3945–3949
69. Yoshimura T, Ikai T, Takayama T, Sekine T, Kino Y, Shinohara A (2010) Synthesis, spectroscopic and electrochemical properties, and electronic structures of octahedral hexatechnetium (III) clusters $[Tc_6Q_8(CN)_6]^{4-}$ (Q = S, Se). Inorg Chem 49:5876–5882
70. Orto PJ, Nichol GS, Okumura N, Evans DH, Arratia-Pérez R, Ramirez-Tagle R, Wang R, Zheng Z (2008) Cluster carbonyls of the $[Re_6(\mu_3\text{-}Se)_8]^{2+}$ core: synthesis, structural characterization, and computational analysis. Dalton Trans 32:4247–4253
71. Echeverría C, Becerra A, Nuñez-Villena F, Muñoz-Castro A, Stehberg J, Zheng Z, Arratia-Perez R, Simon F, Ramírez-Tagle R (2012) The paramagnetic and luminescent $[Re_6Se_8I_6]^{3-}$ cluster. Its potential use as an antitumoral and biomarker agent. New J Chem 36:927–932
72. Rabanal-León WA, Murillo-López JA, Páez-Hernández D, Arratia-Pérez R (2014) Understanding the influence of terminal ligands on the electronic structure and bonding nature in $[Re_6(\mu_3\text{-}Q_8)]^{2+}$ clusters. J Phys Chem A 118:11083–11089
73. Rabanal-León WA, Murillo-López JA, Páez-Hernández D, Arratia-Pérez R (2015) Exploring the nature of the excitation energies in $[Re_6(\mu_3\text{-}Q_8)X_6]^{4-}$ clusters: a relativistic approach. Phys Chem Chem Phys 17:17611–17617
74. Rojas-Poblete M, Carreño A, Gacitúa M, Páez-Hernández D, Rabanal-León WA, Arratia-Pérez R (2018) Electrochemical behaviors and relativistic DFT calculations to understand the terminal ligand influence on the $[Re6(\mu_3\text{-}Q)_8X_6]^{4-}$ clusters. New J Chem 42:5471–5478
75. Szczepura LF, Edwards JA, Cedeño DL (2009) Luminescent properties of hexanuclear molybdenum(II) chloride clusters containing thiolate ligands. J Clust Sci 20:105–112
76. Yoshimura T, Chen Z-N, Itasaka A, Abe M, Sasaki Y, Ishizaka S, Kitamura N, Yarovoi SS, Solodovnikov SF, Fedorov VE (2003) Preparation, structures, and redox and emission characteristics of the isothiocyanate complexes of hexarhenium(III) clusters $[Re_6(\mu_3\text{-}E)_8(NCS)_6]^{4-}$ (E = S, Se). Inorg Chem 42:4857–4863

Struct Bond (2019) 180: 125–142
DOI: 10.1007/430_2019_36

Published online: 28 April 2019

Thermoelectric Properties of Ternary and Quaternary Mo_6 and Mo_9 Cluster Selenides

Christophe Candolfi, Patrick Gougeon, Philippe Gall, Michel Potel, Anne Dauscher, and Bertrand Lenoir

Contents

Abstract Mo-based cluster compounds containing Mo_6 and Mo_9 cluster units have long been known for their rich chemistry and the diversity and complexity of their crystal structures. While most studies have mainly focused on their crystallographic properties, recent investigations have pointed out their potential for thermoelectric applications in power generation. These compounds derive their good properties from the three-dimensional arrangement of the clusters between which cations reside. This inherent disorder strongly limits the ability of these materials to transport heat that often leads to a temperature dependence of the lattice thermal conductivity that mirrors that observed in glassy systems. In addition, most of these compounds can be driven from a metallic toward a semiconducting state through insertion of additional cations. Here, we review the recent progress made on determining the transport properties of these compounds, discussing in particular the key ingredients

C. Candolfi (✉), A. Dauscher, and B. Lenoir
Institut Jean Lamour, UMR 7198 CNRS – Université de Lorraine, Nancy, France
e-mail: christophe.candolfi@univ-lorraine.fr

P. Gougeon, P. Gall, and M. Potel
Institut des Sciences Chimiques de Rennes, UMR 6226 CNRS – Université de Rennes 1 - INSA de Rennes, Rennes, France

that lead to their peculiar thermal properties, and examine possible future directions to further enhance their thermoelectric properties.

Keywords Chalcogenide · Cluster · Semiconductor · Thermal conductivity · Thermoelectric

1 Introduction

Thermoelectric materials in which a temperature difference generates an electric field and vice versa enable direct solid-state energy conversion between heat and electricity [1–3]. While thermoelectric refrigerators would provide an elegant alternative to replace compression-based refrigerators, thermoelectric generators would allow for a systematic production of electricity from waste-heat sources. The design and optimization of efficient thermoelectric devices is intimately linked to the physical properties of the materials that constitute their active part [1–3]. The conversion efficiency of the device is governed by the so-called dimensionless thermoelectric figure of merit ZT defined at the absolute temperature T as $ZT = \alpha^2 T/\rho\kappa$ where ρ is the electrical resistivity, α is the thermopower (or Seebeck coefficient), and κ is the total thermal conductivity which is the sum of a lattice (κ_L) and an electronic (κ_e) contribution [1–3]. The interdependence of these three transport properties via the carrier concentration makes the optimization of thermoelectric materials a challenging task. Among the various strategies used to identify promising systems, the search for materials that inherently behave as good thermal insulators can be driven by simple guiding rules based on their crystallographic characteristics. A complex unit cell containing a large number of heavy atoms has been traditionally a fruitful guiding principle to discover compounds that exhibit low lattice thermal conductivity values [4–14].

The diversity, flexibility, and complexity of the crystal structures formed by cluster compounds based on molybdenum atoms naturally make these materials worthy of detailed experimental and theoretical investigations. The Chevrel phases $M_x Mo_6 X_8$ (M = alkali, alkaline-earth, rare-earth, transition metals; X = S, Se, and Te; $0 \leq x \leq 4$), the crystal structure of which is based on the octahedral Mo_6 cluster, are one of the most famous family of such compounds widely investigated for their magnetic, superconducting, and thermoelectric properties [15, 16]. A remarkable property of their crystal structure is the possibility to accommodate various types of cations in the voids existing between the Mo_6X_8 clusters. These cations provide additional electrons that drive the compound toward a semiconducting state and help to lower the lattice thermal conductivity. From these two combined effects, interesting thermoelectric properties emerge with a peak ZT value of 0.6 at 1,150 K achieved in the composition $(Cu/Fe)Mo_6Se_8$ [17].

Clusters with higher nuclearities (Mo_9, Mo_{12}, Mo_{15}, Mo_{18}, Mo_{21}, Mo_{24}, Mo_{30}, and Mo_{36} cluster units) have been obtained in more than 40 different structure types and extensively studied over the last decades [18–29]. As in Chevrel phases, various

cations can be inserted in the intercluster space to stabilize the structure. These voids are significantly larger than those present in the Chevrel phases, often leading to very large, anisotropic thermal displacement parameters for the cations [18–29]. The strong disorder induced by the presence of these intercluster atoms is an important ingredient that helps to limit the propagation of heat-carrying acoustic phonons [30–41].

In this chapter, we provide a brief overview of the results obtained experimentally on the thermoelectric properties of these materials over the last few years. Due to the diversity of structures that can be built with Mo-based clusters, we will focus on compounds that are formed by Mo_6 and Mo_9 cluster units with known transport properties. We will also present the main crystallographic features that give rise to very low, glass-like lattice thermal conductivity. Our main objective is to highlight the potential of this large class of materials for thermoelectric applications and present possible future directions to further enhance their thermoelectric properties.

2 Synthesis and Crystal Structure

2.1 Syntheses and Crystal Growths

Most of the synthetic routes used to prepare polycrystalline samples are based on direct reactions of powders (Mo, Ag) and precursors ($MoSe_2$, InSe, TlSe) in sealed silica tubes at high temperatures [30–41]. Prior to use, Mo powders are reduced under H_2 flowing gas at 1,000°C during 10 h in order to eliminate traces of oxygen. The precursors are also synthesized by direct reaction of elements of high purity in sealed silica tubes. Monophasic powders of $MoSe_2$, InSe, and TlSe are obtained by heating stoichiometric mixtures of elemental powders at 700, 800, and 500°C, respectively, during 48 h.

For the series $Ag_xMo_9Se_{11}$ with nominal compositions $x = 3.4$, 3.5, 3.75, 3.8, 3.9, and 4.0, stoichiometric amounts of $MoSe_2$, Mo, and Ag in powder form are cold pressed into cylindrical pellets which are subsequently placed in silica tubes sealed under vacuum [30, 31, 36, 37, 40]. The tubes are then heated at 950°C for 48 h.

In some cases, a quaternary phase can be obtained by direct reaction of a ternary cluster compound with an excess of another element during long-term annealing at high temperatures. This kind of synthesis has been successfully applied to $Tl_2Mo_9Se_{11}$ in the presence of Ag powders which led to the formation of the novel quaternary compound $Ag_2Tl_2Mo_9Se_{11}$ after annealing at 800°C during 2 weeks [32]. Subsequent syntheses of polycrystalline samples of nominal compositions $Ag_xTl_{4-x}Mo_9Se_{11}$ ($1.9 \leq x \leq 2.3$) by heating stoichiometric mixtures of Ag, TlSe, $MoSe_2$, and Mo at 1,180°C for 48 h in evacuated silica tubes evidenced the possibility to vary the Ag-to-Tl ratio while maintaining the monophasic nature of the sample.

The quaternary cluster compound $Ag_3RbMo_9Se_{11}$ has also been discovered following a similar annealing treatment [38]. Reactions of $MoSe_2$, Ag, and Mo

powders mixed with powders of the ternary compound $Rb_2Mo_6Se_6$ at 1,200°C for 48 h in sealed silica tubes led to the formation of a phase-pure polycrystalline sample of $Ag_3RbMo_9Se_{11}$. Further experiments revealed that the Ag content can be slightly decreased down to 2.6 atoms per formula unit.

For the $Ag_3In_2Mo_{15}Se_{19}$ and $Ag_3Tl_2Mo_{15}Se_{19}$ compounds [33, 41], direct reactions of the precursors InSe, TlSe, and $MoSe_2$ together with Mo and Ag powders have been realized at 1,300°C for 40 h. Due to the high temperature required for these reactions, the mixtures were sealed in molybdenum crucibles under a low argon pressure (c.a. 0.6 bar) using an arc welding system.

Some Mo-based cluster compounds cannot, however, be obtained via direct reactions of elements with precursors. This is, for instance, the case of the above-mentioned ternary compound $Rb_2Mo_6Se_6$ used as a precursor [38]. In such a case, a two-step synthesis needs to be considered that notably includes an ion-exchange reaction. As a first step, the ternary compound $In_2Mo_6Se_6$ has been synthesized by heating a stoichiometric mixture of InSe, $MoSe_2$, and Mo powders at 1,000°C during 36 h in a sealed silica tube. The second step then consists in an ion-exchange reaction of $In_2Mo_6Se_6$ with RbCl at 800°C. For this reaction, $In_2Mo_6Se_6$ and RbCl powders are mixed in the proportion 1:2.5 and cold pressed into a cylindrical pellet which is placed in a long silica tube sealed under vacuum. The end of the ampule where the pellet is located is introduced in a furnace, heated at 800°C during 2 days while maintaining the other end of the tube at room temperature.

The growth of single crystals of these various compounds could be realized by either a vapor-transport technique or by a recrystallization process by subjecting the polycrystalline pellets to an annealing treatment at very high temperature [31–33, 38, 41]. The former technique has been considered to grow single crystals of $Ag_xMo_9Se_{11}$ using AgCl as the transport agent in a sealed silica tube [31]. A temperature gradient of 30°C has been applied between both ends of the tube kept at 1,030 and 1,060°C during 10 days. The later route has been used to obtain single crystals of the cluster compounds $Ag_3RbMo_9Se_{11}$ [38], $Ag_3In_2Mo_{15}Se_{19}$ [33], and $Ag_3Tl_2Mo_{15}Se_{19}$ [41]. While single crystals of $Ag_3RbMo_9Se_{11}$ were obtained by prolonged annealing at 1,250°C for 96 h, single crystals of $Ag_3In_2Mo_{15}Se_{19}$ and $Ag_3Tl_2Mo_{15}Se_{19}$ could be grown by heating cold-pressed pellets in molybdenum crucibles at 1,650°C during 3 h with applied heating and cooling rates of 300°C/h and 100°C/h, respectively.

2.2 *Crystal Structures*

The $Ag_xMo_9Se_{11}$ ($3.4 \leq x \leq 3.9$) compounds crystallize in the orthorhombic space group *Cmcm* [30, 31, 36, 37, 40, 42]. The building block of the crystal structure of these compounds is the $Mo_9Se_{11}Se_6$ cluster unit (Fig. 1a), which can be seen as the fusion of two octahedral $Mo_6Se_8Se_6$ cluster units (Fig. 1b) similar to those found in the Chevrel phases [42].

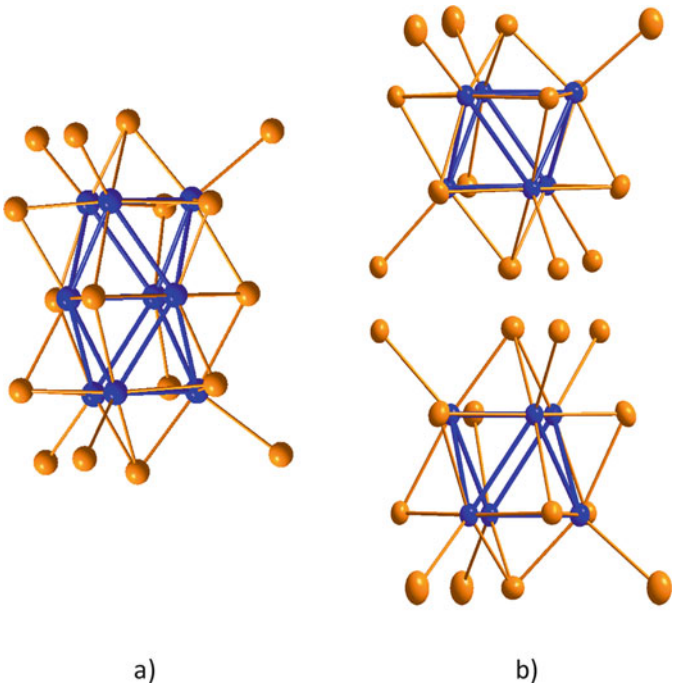

Fig. 1 Schematic representation of the formation of the $Mo_9Se_{11}Se_6$ cluster unit (**a**) resulting from the condensation of two octahedral $Mo_6Se_8Se_6$ cluster units (**b**). The Mo and Se atoms are represented in blue and orange, respectively. In both figures, the thermal ellipsoids are represented at the 97% probability level

The $Mo_9Se_{11}Se_6$ units of point group symmetry C_{2v} or *mm*2 share a part of the Se atoms to form the Mo_9Se_{11} network. In this arrangement, each of the $Mo_9Se_{11}Se_6$ unit is surrounded by eight other $Mo_9Se_{11}Se_6$ units. This structural arrangement differs from that of the Chevrel phases for which each of the $Mo_6X_8X_6$ unit is only surrounded by six other units. While in the *c* direction the interconnection between the $Mo_9Se_{11}Se_6$ units is similar to that observed in the Chevrel phases (i.e., each $Mo_9Se_{11}Se_6$ shares eight Mo-Se or Se-Mo interunit bonds; see Fig. 2), only four Mo-Se or Se-Mo interunit bonds occur along the *b* direction (Fig. 2). Consequently, the crystal structure of $Ag_xMo_9Se_{11}$ presents a pseudo-bidimensional character as reflected by the intercluster distance of 3.728 Å in the (*ac*) plane and 4.960 Å in the *b* direction. The Ag atoms are delocalized over four independent sites. The Ag non-stoichiometry in these compounds arises essentially from the filling of the Ag_4 site (shown in dark gray in Fig. 2) located in rhomboid cross-sectional channels running along the *a* direction. The occupation of this site varies from 10 (in $Ag_{3.4}Mo_9Se_{11}$) up to 25% (in $Ag_4Mo_9Se_{11}$).

While partial substitutions of Cu, Cs, or Cl for Ag and Te and S for Se have been successfully realized leaving unchanged the orthorhombic symmetry of the unit cell [18, 36, 37], other substitutions such as Tl and Rb for Ag result in a different

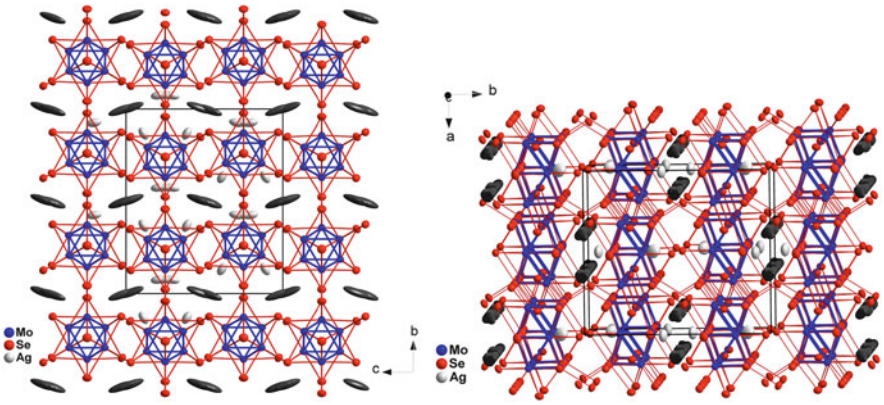

Fig. 2 Projection of the crystal structure of the $Ag_xMo_9Se_{11}$ compounds (space group *Cmcm*, No. 63) in ellipsoid representation (97% probability level) along the *a* axis (left) and *c* axis (right). The Ag, Mo, and Se atoms are in gray, blue, and red, respectively. The Ag_4 atoms are distinguished from the other Ag atoms by their dark gray color

arrangement of the $Mo_9Se_{11}Se_6$ cluster units [32, 38]. Hence, the crystal structures of the quaternary compounds $Ag_2Tl_2Mo_9Se_{11}$ and $Ag_3RbMo_9Se_{11}$ are described in the space groups *R*-3*c* and $P6_3/m$, respectively.

The crystal structure of $Ag_2Tl_2Mo_9Se_{11}$ consists in a three-dimensional framework formed by interconnected $Mo_9Se_{11}Se_6$ clusters as illustrated in Fig. 3 [32]. The $Mo_9Se_{11}Se_6$ unit has here the point symmetry *32* or D_3. The outer and inner atoms display different environments. The environment of the former is similar to that encountered in the $Mo_6X_8X_6$ units (X = S, Se) of the Chevrel phases. They are surrounded by four Mo atoms and four Se atoms, in an approximately coplanar coordination, with another Se atom belonging to an adjacent Mo_9Se_{11} cluster. This last atom constitutes the apex of a square-based pyramidal environment. The Mo atoms of the median Mo_3 triangles are surrounded by six Mo and only four Se atoms belonging to the same cluster unit. The Mo-Mo distances range from 2.62 up to 2.75 Å. The Mo-Se bond distances are typical, ranging between 2.56 Å and 2.67 Å. Each unit is connected to six adjacent units via 12 interunit Mo-Se bonds of 2.66 Å to form a three-dimensional Mo-Se framework with the connective formula $[Mo_9Se_5{}^{i}Se_{6/2}{}^{i\text{-}a}]Se_{6/2}{}^{a\text{-}i}$ according to Schäfer's notation and in which the shortest intercluster distance is 3.69 Å. While the Ag atoms occupy a distorted trigonal bipyramidal site formed by the Se atoms, the Tl atoms occupy sites of ten Se atoms forming a distorted tetrahedron. The three faces of these tetrahedra are capped with three edges bridged with Tl-Se distances in the range 3.02–4.38 Å or surrounded by 6 Se atoms at 3.40 Å forming a trigonal antiprism.

The Mo-Se network of the $Ag_3RbMo_9Se_{11}$ compound [38] also originates from interlinked $Mo_9Se_{11}Se_6$ clusters via Mo-Se bonds (Fig. 4). The Mo_9Se_{11} unit has the point symmetry C_{3h}. The connective formula of the molybdenum-selenium framework is $[Mo_9Se_5{}^{i}Se_{6/2}{}^{i\text{-}a}]Se_{6/2}{}^{a\text{-}i}$ according to the notation of Schäfer.[28]

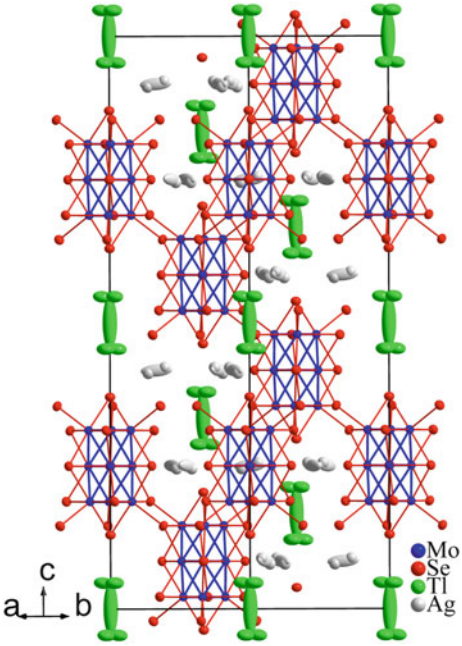

Fig. 3 Perspective view of the crystal structure of $Ag_2Tl_2Mo_9Se_{11}$ (space group *R-3c*, No. 167) in ellipsoid representation (97% probability level). The Ag, Tl, Mo, and Se atoms are in light gray, green, blue, and red, respectively

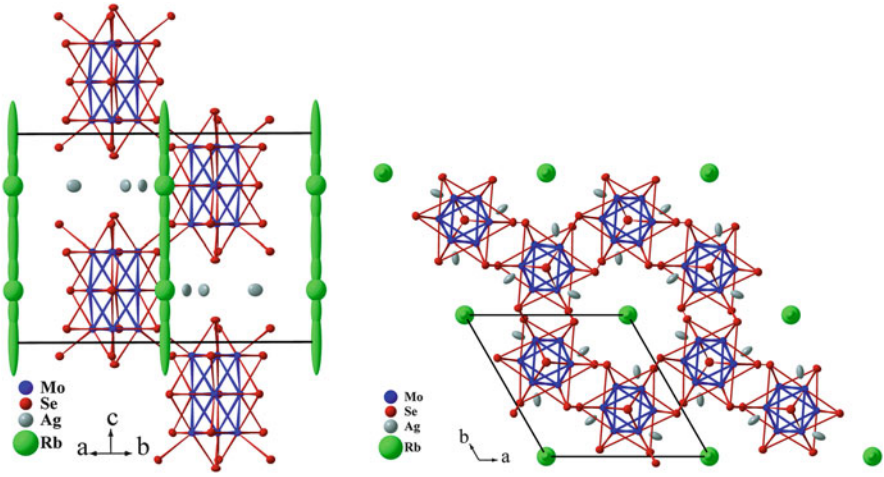

Fig. 4 (Left) Perspective view of the crystal structure of $Ag_2Tl_2Mo_9Se_{11}$ (space group $P6_3/m$, No. 176) in ellipsoid representation (97% probability level). (Right) Projection of the crystal structure onto the (*ab*) plane. The Ag, Rb, Mo, and Se atoms are in light gray, green, blue, and red, respectively

As shown in Fig. 4, which shows the crystal structure of $Ag_3RbMo_9Se_{11}$ projected onto the (*ab*) plane, large hexagonal tunnels that are randomly filled by the Rb^+ cations run along the *c* axis. The Ag^+ cations partially occupy positions in the mirror planes around the ternary axes between adjacent $Mo_9Se_{11}Se_6$ units located on the threefold axis. The Se environment of Ag atoms can be seen as a distorted square pyramid with Ag-Se bond lengths ranging from 2.64 to 2.93 Å. One of the Rb cations resides in distorted tri-capped trigonal prismatic Se environment, while the other ones are each surrounded by six Se atoms forming flattened octahedra along the ternary axis. The Rb-Se distances spread over a wide range of 3.41–3.99 Å.

The Mo-Se framework of the $Ag_3M_2Mo_{15}Se_{19}$ (M = In, Tl) compounds [33, 41] is similar to that of $In_2Mo_{15}Se_{19}$ which was the first compound in which the Mo_9 clusters were observed in 1980 [43] (Fig. 5).

Consequently, the crystal structure of these quaternary compounds is based on an equal mixture of $Mo_6Se_8{}^iSe_6{}^a$ and $Mo_9Se_{11}{}^iSe_6{}^a$ cluster units interconnected through Mo-Se bonds. The first unit can be described as a Mo_6 octahedron surrounded by eight face-capping inner Se^i and six apical Se^a ligands and is identical to that encountered in the Chevrel phases. The second unit is similar to those observed in the three abovementioned compounds. The $Mo_6Se_8{}^iSe_6{}^a$ and $Mo_9Se_{11}{}^iSe_6{}^a$ units are centered at the 6*b* and 6*a* positions with the point-group symmetry -3 and 32, respectively. The Mo-Mo distances within the Mo_6 clusters are about 2.67 Å for the intra-triangle distances (distances within the Mo_3 triangles formed by the Mo atoms related through the threefold axis) and 2.70 Å for the inter-triangle distances.

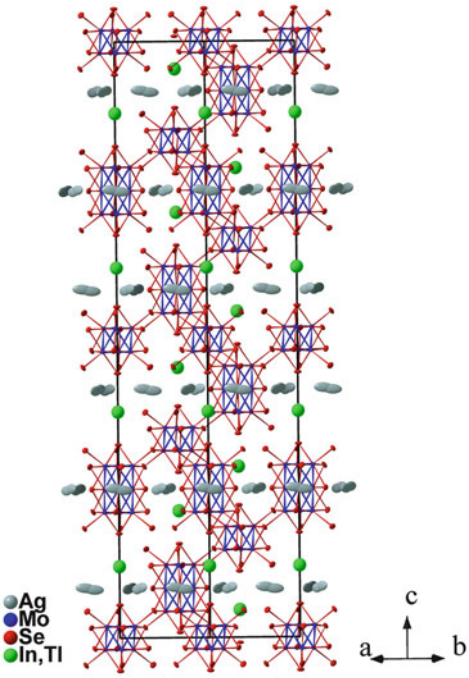

Fig. 5 Perspective view of the crystal structure of $Ag_3M_2Mo_{15}Se_{19}$ with M = In or Tl (space group *R-3c*, No. 167) in ellipsoid representation (97% probability level). The Ag, *M*, Mo, and Se atoms are in light gray, green, blue, and red, respectively

The Mo-Mo distances within the Mo_9 clusters are around 2.65 and 2.74 Å for the intra-triangle distances and 2.68 and 2.78 Å for the distances between the triangles. The Mo-Se distances range between 2.57 and 2.63 Å within the $Mo_6Se_8{}^iSe_6{}^a$ unit and between 2.54 and 2.70 Å within the $Mo_9Se_{11}{}^iSe_6{}^a$ unit, as usual. The three-dimensional packing arises from the interconnection of the $Mo_6Se_8{}^iSe_6{}^a$ and $Mo_9Se_{11}{}^iSe_6{}^a$ cluster units through Mo-Se bonds with each $Mo_6Se_8{}^iSe_6{}^a$ unit interconnected to 6 $Mo_9Se_{11}{}^iSe_6{}^a$ units (and vice versa) via Mo-Se interunit bonds. Because of this arrangement, the shortest distance between the Mo_6 and Mo_9 clusters is of the order of 3.60 Å, indicating only weak metal-metal interaction. In these structures, the Ag atoms occupy distorted triangular bipyramid sites located between two consecutive *M* sites with Ag-Se distances ranging from 2.58 to 2.88 Å. The In and Tl atoms are surrounded by seven Se atoms forming a monocapped octahedron compressed along the threefold axis (see Fig. 5).

One common feature of these various crystal structures relevant to understanding their thermal properties is the large, anisotropic thermal displacement parameters (ADPs) of the cations located in the intercluster spaces [30–41]. The largest thermal ellipsoids are observed for the Rb and Tl atoms in the $Ag_3RbMo_9Se_{11}$ and $Ag_2Tl_2Mo_9Se_{11}$ compounds [32, 38], respectively. Low-temperature single-crystal X-ray diffraction measurements performed on $Ag_2Tl_2Mo_9Se_{11}$ evidenced that the ADP values of the Tl atoms exhibit a nearly temperature-independent behavior down to 85 K [32]. We will see below that the thermal motions of the cations are likely a key ingredient in determining the lattice thermal conductivity.

3 Thermoelectric Properties

3.1 Electronic Properties

The electronic structure of most of the Mo-based cluster compounds can be deduced from the molecular orbital diagram of the isolated cluster units [18, 27, 28, 39, 44–47]. This approach proves to be efficient whenever the clusters in the crystal structure are isolated enough from the neighboring clusters. It has been indeed shown that the interactions between the chalcogen atoms that connect the clusters are not strong enough to perturb the electronic structure of the isolated cluster unit. In such a case, the number of electrons available for metal-metal bonds, called the metallic electron count (MEC), is the critical parameter that determines the metallic or semiconducting nature of the compound. Semiconducting behavior is predicted to develop when the MEC reaches the optimum value for the cluster unit. In the case of the Mo_9Se_{11} clusters, the optimum MEC has been determined to be equal to 36 [45]. Assuming ionic interactions between the cations and the clusters and a +1 valence state for the former, several atoms such as Ag, In, Tl, or Rb may thus help to achieve an optimum MEC for the Mo_9Se_{11} clusters. Varying the concentration of these cations may also allow for a fine control of the electronic properties by adjusting the carrier concentration.

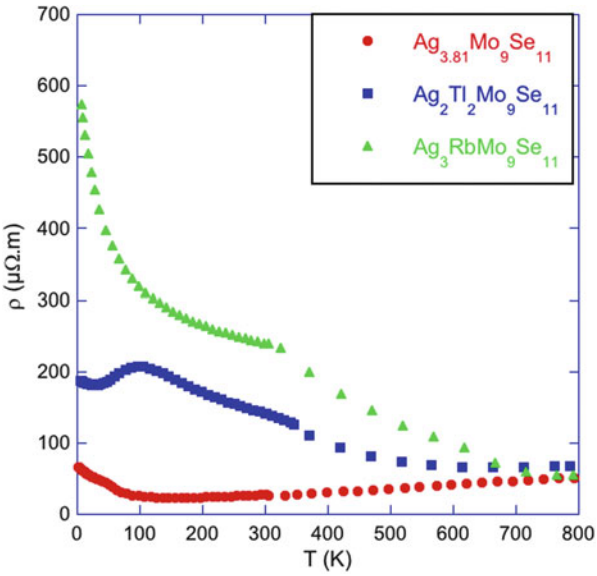

Fig. 6 Comparison of the temperature dependences of the electrical resistivity ρ of $Ag_{3.81}Mo_9Se_{11}$, $Ag_2Tl_2Mo_9Se_{11}$, and $Ag_3RbMo_9Se_{11}$

The thermoelectric potential of materials based on Mo_9Se_{11} clusters has been first assessed on the $Ag_xMo_9Se_{11}$ series [30, 31]. Based on the abovementioned considerations, a semiconducting state is predicted to be reached for $x = 4$. Experimentally, the Ag content can be continuously varied between $x = 3.41$ and $x = 3.81$ leading to a gradual shift from a *p*-type metallic-like behavior ($x = 3.41$) to a *p*-type heavily doped semiconducting state ($x = 3.81$) (Fig. 6) [30, 31]. Despite being close to the predicted threshold of $x = 4.0$, the highest Ag content achieved experimentally remains limited to $x = 3.81$. Recent high-resolution fluorescence detection X-ray absorption spectroscopy (HERFD-XAS) and resonant inelastic X-ray scattering (RIXS) experiments have provided experimental evidence of the presence of subvalent Ag atoms [40], which contribute to limit the electronic properties to a heavily doped regime. Hence, if the overall effect of Ag on the electronic properties can be fairly well understood by a rigid-band picture, these results nevertheless suggest that the evolution of the electronic structure with x is not entirely captured by this simple picture.

Although the maximum Ag content accessible is too low to reach a semiconducting behavior, the concomitant increase in the electrical resistivity and thermopower values result in a significant enhancement in the power factor leading to an optimum ZT value of 0.65 at 800 K for $x = 3.81$. This value is higher than the maximum value achieved in the Chevrel phases demonstrating that many of these cluster compounds may show interesting thermoelectric properties at high temperatures.

Attempt at reaching a semiconducting state by insertion of Cu atoms (up to $y = 0.4$ when considering the formula $Ag_{3.6}Cu_yMo_9Se_{11}$) in the $Ag_{3.6}Mo_9Se_{11}$ compound was unsuccessful [37], even though some enhancement in the power factor α^2/ρ has been observed. Further adjustment of the hole concentration in the $Ag_xMo_9Se_{11}$ series has been realized through isovalent substitutions on the Ag site

and of Te or S for Se [36]. The substitution ranges of these two elements were found to be rather limited with maximum contents of 0.5. These concentrations were too low to significantly influence the transport properties resulting in *ZT* values comparable to those achieved in unsubstituted samples [31].

Other elements such as Tl and Rb have been considered as possible alternatives to provide the missing charges to the Mo_9Se_{11} cluster unit. The addition of Tl and Rb atoms in the crystal structure has been successful, giving rise to two new cluster compounds of chemical compositions $Ag_2Tl_2Mo_9Se_{11}$ and $Ag_3RbMo_9Se_{11}$ [32, 38]. As mentioned above, these partial substitutions are accompanied by a change in the lattice symmetry from orthorhombic to hexagonal due to a different arrangement of the Mo_9Se_{11} cluster units. Based on their respective chemical compositions, both compounds are predicted to be semiconducting (i.e., 36 electrons per Mo_9) if Ag, Rb, and Tl are monovalent. Unlike the $Ag_xMo_9Se_{11}$ compounds, this prediction has been verified experimentally with an electrical resistivity following a semiconducting-like temperature dependence (see Fig. 6). These results suggest that the specific arrangement of the cluster units can play an important role in determining the electronic properties of these compounds.

The transport properties of compounds built up from an equal mixture of $Mo_6Se_8{}^{i}Se_6{}^{a}$ and $Mo_9Se_{11}{}^{i}Se_6{}^{a}$ cluster units have so far been investigated only on the ternary compound $Rb_2Mo_{15}Se_{19}$ [35] and on the quaternary compounds $Ag_3In_2Mo_{15}Se_{19}$ and $Ag_3Tl_2Mo_{15}Se_{19}$ [33, 41]. The optimal MEC for the Mo_6Se_8 and Mo_9Se_{11} clusters are equal to 24 and 36, respectively, yielding an optimum MEC of 60 for the $Mo_{15}Se_{19}$ clusters [33]. Due to the monovalent character of Rb, the total MEC is equal to 54 in $Rb_2Mo_{15}Se_{19}$ and should thus give rise to *p*-type metallic properties. Measurements of the thermoelectric properties at high temperatures have confirmed this prediction [35]. Further optimization of the thermoelectric properties of $A_2Mo_{15}Se_{19}$ compounds implies the introduction of additional charges to bring the MEC closer to 60. Experimentally, this approach can be realized through the insertion of other atoms such as Ag or Cu. The two compounds $Ag_3In_2Mo_{15}Se_{19}$ and $Ag_3Tl_2Mo_{15}Se_{19}$ provide two examples of such a strategy [33, 41]. The presence of Ag helps to achieve heavily doped semiconducting properties and, hence, higher *ZT* values compared to ternary compositions with a peak value of 0.45 at 1,100 K in $Ag_3In_2Mo_{15}Se_{19}$ [33]. The comparison of the electronic properties of both compounds nevertheless indicates that the above-mentioned charge counting scheme is somewhat too simple. The more metallic character of $Ag_3Tl_2Mo_{15}Se_{19}$ with respect to $Ag_3In_2Mo_{15}Se_{19}$ promotes the idea that the valence of the cations deviates from the expected +1 value [33, 41]. The sensitivity of the transport properties to the nature of the cations should be further investigated by considering other combinations of elements. This might help to determine the important factors behind this behavior, thereby guiding the choice of the most judicious combinations leading to high thermoelectric performances.

One important aspect of the transport in these compounds is the presence of weakly dispersive valence bands that give rise to electron-like and hole-like contributions to the transport [30–41]. The contributions to the thermopower of these two types of carriers are of opposite sign and thus usually tend to lower the measured

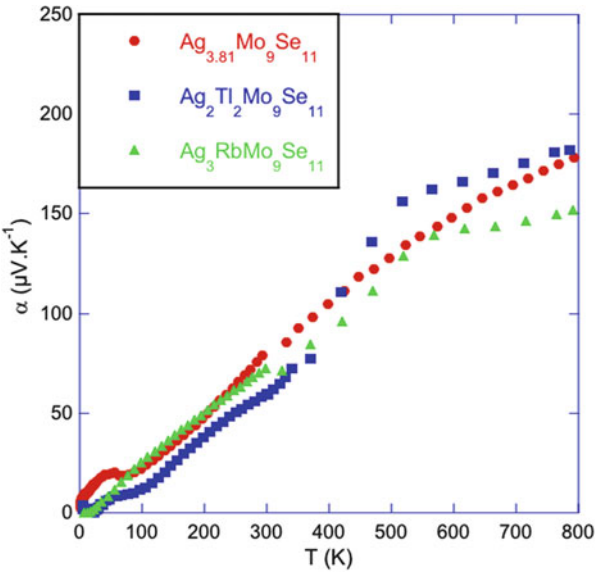

Fig. 7 Comparison of the temperature dependences of the thermopower α of $Ag_{3.81}Mo_9Se_{11}$, $Ag_2Tl_2Mo_9Se_{11}$, and $Ag_3RbMo_9Se_{11}$

values. In spite of this characteristic, high thermopower values have been nevertheless measured in the compounds containing Mo_9 cluster units (Fig. 7).

Direct experimental evidence for multiband transport has been provided by Hall effect measurements at low temperatures. In the $Ag_xMo_9Se_{11}$ series, the Hall data show a complex behavior as a function of x with a sign change of the Hall coefficient evidenced upon cooling below 200 K [31]. The $Ag_2Tl_2Mo_9Se_{11}$ compound shows an even more complex behavior with a double sign change of the Hall coefficient upon cooling down to 5 K [32]. These complex temperature dependences make it difficult to determine the actual hole concentration in these compounds. Another complex evolution of the Hall data has been evidenced in the $Ag_3In_2Mo_{15}Se_{19}$ compound [33], indicating that the presence of hole-like and electron-like contributions to the transport is neither tied to a particular cluster arrangement nor to a specific cluster unit. The fact that so far most of the compounds studied exhibit this characteristic suggests that this property may prove to be universal in these materials. It seems therefore natural to ask whether other compounds containing Mo clusters of higher nuclearity may follow this trend or provide a mean to circumvent this problem.

3.2 Thermal Properties

One of the distinguishing and common features of these materials is their extremely low lattice thermal conductivity κ_L that is typically well below 1 W m^{-1} K^{-1}, with a value of 0.5 W m^{-1} K^{-1} often achieved at high temperatures [30, 41]. The

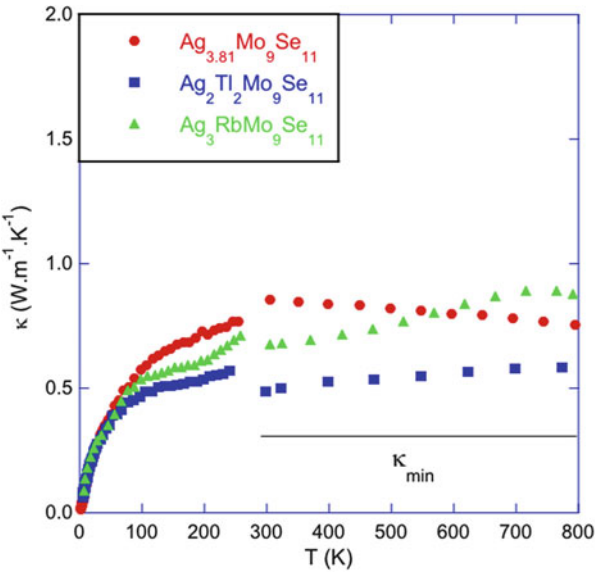

Fig. 8 Comparison of the temperature dependences of the thermal conductivity κ of $Ag_{3.81}Mo_9Se_{11}$, $Ag_2Tl_2Mo_9Se_{11}$, and $Ag_3RbMo_9Se_{11}$. The horizontal black solid line represents the minimum thermal conductivity (~0.3 W m^{-1} K^{-1}) determined by sound velocity measurements. The data between 250 and 300 K have been discarded due to the thermal radiations that accompany low-temperature thermal conductivity measurements

Table 1 Largest ADP values (in $Å^2$) for the different cluster compounds determined by single-crystal X-ray diffraction data at 300 K [19, 32, 33, 38, 41]

$Ag_{3.4}Mo_9Se_{11}$	$Ag_{2.25}Tl_{1.75}Mo_9Se_{11}$	$Ag_{2.6}RbMo_9Se_{11}$	$Ag_3In_2Mo_{15}Se_{19}$	$Ag_{2.57}Tl_2Mo_{15}Se_{19}$
Ag_2	Tl_2	Rb_3	Ag	Tl
0.080	0.314	0.280	0.046	0.035

The difference in the stoichiometry of these single crystals and of the polycrystalline compounds is due to the high temperature used during the growth process that leads to a slight loss of Ag

temperature dependence of κ_L resembles that observed in amorphous systems, a remarkable physical property for a well-crystallized compound (Fig. 8) [48].

Several key characteristics of the crystal structure of these compounds likely concur to yield the observed very low, glass-like lattice thermal conductivity. In addition to the large unit cells that result in low phonon cutoff wave vectors [49, 50], the large, anisotropic atomic displacement parameters (ADP) values of the cations (Table 1) likely lead to low-lying optical modes that cut the acoustic phonon dispersions. The phase space available for acoustic phonons is thus strongly reduced resulting in a significant reduction of the lattice thermal conductivity.

Low-energy optical modes also open an additional channel for Umklapp scattering events which persist down to low temperatures and suppress the dielectric maximum. This mechanism would be then similar to what has been observed in tetrahedrites, for instance, a class of sulfur-based compounds exhibiting similar thermal transport [51, 52]. In these minerals, the low-energy optical modes have been shown to be strongly anharmonic [51]. Because anharmonicity determines the scattering probability of phonons during phonon-phonon interactions, highly anharmonic bonds favor these scattering events and, hence, help to maintain low

lattice thermal conductivity upon increasing temperature. This anharmonicity can have several physical origins such as lone-pair electrons [51–53], resonant bonds [54], and flat or double-well potentials felt by atoms in cages or tunnels, for instance [55–57]. Among these possibilities, the presence of double-well potentials is suggested by the nearly temperature-independent ADP values observed for the Tl and Rb atoms in the $Ag_2Tl_2Mo_9Se_{11}$ and $Ag_3RbMo_9Se_{11}$ compounds, respectively [32, 38]. Similar values have been reported in the type-I clathrates $Sr_8Ga_{16}Ge_{30}$ and $Eu_8Ga_{16}Ge_{30}$ for which Sr and Eu atoms are off-centered in their cages and can tunnel between potential minima [58–62]. Possible experimental evidence of this behavior in the $Ag_xMo_9Se_{11}$ series has been obtained by measurements of the specific heat down to 0.35 K [31]. Centered near 1 K, a peak in the lattice contribution to the specific heat when plotted as C_p/T^3 versus T has been evidenced with a magnitude of the peak scaling with the Ag content. While such a peak can be usually well explained via simple models taking into account Einstein-like contributions, the temperature at which this peak is observed is too low to be reasonably accounted for by such models. Thus, this behavior might be due to some of the Ag cations experiencing double-well potentials. More systematic measurements of the low-temperature specific heat of other Mo-based cluster compounds would be worthwhile to determine whether such characteristic is universal in Mo-based cluster compounds.

Although phonon calculations may provide relevant information about the thermal properties of these compounds, the large number of atoms in the unit cell combined with the partial occupancies of the cations makes them highly challenging. It is thus clear that a deeper understanding of the relationships between the key characteristics of the crystal structure and the heat transport will benefit from detailed inelastic neutron and X-ray scattering experiments on both polycrystalline and single-crystalline compounds.

4 Conclusion

Mo-based cluster compounds are a large class of materials in which interesting electronic and thermal phenomena have been evidenced over the last years. The Chevrel phases (based on Mo_6 cluster units) are the most famous representatives of this class where superconductivity, magnetic orders, and thermoelectric properties have been studied in detail since their discovery. Despite compounds built by clusters of higher nuclearity (Mo_9 up to Mo_{36}) are known for several decades, it is not until recently, however, that their transport properties have been studied thoroughly. Their structural complexity is a key characteristic that can potentially result in extremely low lattice thermal conductivity which is one of the prerequisites to make them become potential candidates for thermoelectric applications. Over the last years, several theoretical and experimental studies have revealed that these phases have indeed interesting thermoelectric properties, some of them rivalling with more conventional thermoelectric materials.

While their electronic properties can be often well explained and predicted by simple valence electron counting rules, the microscopic origin of their thermal properties is less well understood. The large thermal displacement parameters of the cations inserted in the intercluster voids likely give rise to low-lying optical modes that strongly limit the available phase space for acoustic phonons. The anomalously large ADP values determined in some compounds point to the presence of double-well potentials, as observed in some clathrates, for instance. Further spectroscopic tools such as inelastic neutron scattering studies on both single-crystalline and polycrystalline specimens would be particularly illuminating and would provide a better understanding of the influence of these characteristics on the heat transport.

Given the large variety of crystal structures that can be synthesized with Mo-based cluster units as fundamental building blocks, the surface of this remarkably family of materials has been only barely scratched. Further combined experimental and theoretical studies on these compounds will likely lead to the discovery of efficient thermoelectric materials. Beyond the borders of thermoelectricity, the fact that cluster compounds are often prone to various lattice and electronic instabilities also makes studies of their low-temperature transport properties an important area of fundamental interest.

References

1. Goldsmid HJ (1964) Thermoelectric refrigeration. Temple Press Books, London. https://doi.org/10.1007/978-1-4899-5723-8
2. Rowe DM (2012) Thermoelectrics and its energy harvesting. CRC Press, Boca Raton
3. Tan G, Zhao L-D, Kanatzidis MG (2016). Chem Rev 116:12123
4. Brown SR, Kauzlarich SM, Gascoin F, Snyder GJ (2006). Chem Mater 18:1873
5. Aydemir U, Zevalkink A, Ormeci A, Gibbs ZM, Bux S, Snyder GJ (2015). Chem Mater 27:1622
6. Ortiz BR, Gorai P, Stevanovic V, Toberer ES (2017). Chem Mater 29:4523
7. Wu Z, Li J, Li X, Zhu M, Wu K, Tao X, Huang B-B, Xia S (2016). Chem Mater 28:6917
8. Zhang H, Borrmann H, Oeschler N, Candolfi C, Schnelle W, Schmidt M, Burkhardt U, Baitinger M, Zhao J-T, Grin Y (2011). Inorg Chem 50:1250
9. Guo Q, Assoud A, Kleinke H (2014). Adv Energy Mater 4:1400348
10. Suekuni K, Tsuruta K, Ariga T, Koyano M (2012). Appl Phys Express 5:051201
11. Lu X, Morelli DT, Xia Y, Zhou F, Ozolins V, Chi H, Zhou X, Uher C (2013). Adv Energy Mater 3:342
12. Bourgès C, Bouyrie Y, Supka AR, Al Orabi RAR, Lemoine P, Lebedev OI, Ohta M, Suekuni K, Nassif V, Hardy V, Daou R, Miyazaki Y, Fornari M, Guilmeau E (2018). J Am Chem Soc 140:2186
13. Bouyrie Y, Candolfi C, Dauscher A, Malaman B, Lenoir B (2015). Chem Mater 27:8354
14. Sassi S, Candolfi C, Delaizir G, Migot S, Ghanbaja J, Gendarme C, Dauscher A, Malaman B, Lenoir B (2018). Inorg Chem 57:422
15. Chevrel R, Sergent M, Prigent J (1971). J Solid State Chem 3:515
16. Yvon K (1979) In: Kaldis E (ed) Current topics in material science, vol 3. North-Holland Publishing, Amsterdam, p 53
17. Caillat T, Fleurial J-P, Snyder GJ (1999). Solid State Sci 1:535

18. Gougeon P, Potel M, Gautier R (2004). Inorg Chem 43:1257
19. Gougeon P, Padiou J, Lemarouille JY, Potel M, Sergent M (1984). J Solid State Chem 51:218
20. Gougeon P, Potel M, Padiou J, Sergent M (1987). Mater Res Bull 22:1087
21. Gautier R, Picard S, Gougeon P, Potel M (1999). Mater Res Bull 34:93
22. Gougeon P, Potel M, Sergent M (1989). Acta Crystallogr C45:182
23. Gougeon P, Potel M, Sergent M (1989). Acta Crystallogr C45:1413
24. Gougeon P, Potel M, Padiou J, Sergent M (1988). Mater Res Bull 23:453
25. Picard S, Gougeon P, Potel M (1997). Acta Crystallogr C53:1519
26. Picard S, Gougeon P, Potel M (1999). Angew Chem 38:2034
27. Picard S, Saillard J-Y, Gougeon P, Noël HP, Potel M (2000). J Solid State Chem 155:417
28. Picard S, Halet J-F, Gougeon P, Potel M (1999). Inorg Chem 38:4422
29. Gougeon P, Gall P, Gautier R, Potel M (2010). Acta Crystallogr C66:i67
30. Zhou T, Lenoir B, Colin M, Dauscher A, Al Orabi RAR, Gougeon P, Potel M, Guilmeau E (2011). Appl Phys Lett 98:162106
31. Zhou T, Colin M, Candolfi C, Boulanger C, Dauscher A, Santava E, Hejtmanek J, Baranek P, Al Orabi RAR, Potel M, Fontaine B, Gougeon P, Gautier R, Lenoir B (2014). Chem Mater 26:4765
32. Al Orabi RAR, Gougeon P, Gall P, Fontaine B, Gautier R, Colin M, Candolfi C, Dauscher A, Hejtmanek J, Malaman B, Lenoir B (2014). Inorg Chem 53:11699
33. Gougeon P, Gall P, Al Orabi RAR, Fontaine B, Gautier R, Potel M, Zhou T, Lenoir B, Colin M, Candolfi C, Dauscher A (2012). Chem Mater 24:2899
34. Al Orabi RAR, Fontaine B, Gautier R, Gougeon P, Gall P, Bouyrie Y, Dauscher A, Candolfi C, Lenoir B (2016). Inorg Chem 55:6616
35. Daigre G, Gougeon P, Gall P, Gautier R, Guillou-Viry O, Vaney J-B, Candolfi C, Dauscher A, Lenoir B (2016). J Solid State Chem 237:1–6
36. Masschelein P, Candolfi C, Dauscher A, Gendarme C, Al Orabi RAR, Gougeon P, Potel M, Gall P, Gautier R, Lenoir B (2018). J Alloys Compd 739:360
37. Colin M, Zhou T, Lenoir B, Dauscher A, Al Orabi RAR, Gougeon P, Potel M, Baranek P, Semprimoschnig C (2012). J Electron Mater 41:1360
38. Gougeon P, Gall P, Merdrignac-Conanec O, Aranda L, Dauscher A, Candolfi C, Lenoir B (2017). Inorg Chem 56:9684
39. Al Orabi RAR, Boucher B, Fontaine B, Gall P, Candolfi C, Lenoir B, Gougeon P, Halet J-F, Gautier R (2017). J Mater Chem C 5:12097
40. Butorin SM, Kvashnina KO, Klintenberg M, Kavcic M, Zitnik M, Bucar K, Gougeon P, Gall P, Candolfi C, Lenoir B (2018). ACS Appl Energy Mater 1:4032
41. Gougeon P, Al Orabi RAR, Boucher B, Gall P, Fontaine B, Gautier R, Dauscher A, Candolfi C, Lenoir B. Inorg Chem. https://doi.org/10.1021/acs.inorgchem.8b03452
42. Gougeon P, Padiou J, Le Marouille JY, Potel M, Sergent M (1984). J Solid State Chem 51:218
43. Lipka A, Yvon K (1980). Acta Cryst B36:2123
44. Hughbanks T, Hoffmann R (1983). J Am Chem Soc 105:1150
45. Gautier R, Gougeon P, Halet J-F, Potel M, Saillard J-Y (1997). J Alloys Compd 262–263:311
46. Salloum D, Gautier R, Gougeon P, Potel M (2004). J Solid State Chem 177:1672
47. Salloum D, Gougeon P, Potel M, Gautier R (2005). C R Chim 11–12:1743
48. Slack GA, Oliver DW, Horn FH (1971). Phys Rev B 4:1714
49. Slack GA (1979) In: Seitz F, Turnbull D, Ehrenreich H (eds) Semiconductors and semimetals, vol 34. Academic Press, New York, p 1
50. Mori T (2017). Small 13:1702013
51. Bouyrie Y, Candolfi C, Pailhès S, Koza MM, Malaman B, Dauscher A, Tobola J, Boisron O, Saviot L, Lenoir B (2015). Phys Chem Chem Phys 17:19751
52. Lai W, Wang Y, Morelli DT, Lu X (2015). Adv Funct Mater 25:3648
53. Nielsen MD, Ozolins V, Heremans JP (2013). Energy Environ Sci 6:570
54. Lee S, Esfarjani K, Luo T, Zhou J, Tian Z, Chen G (2014). Nat Commun 5:3525

55. Safarik DJ, Llobet A, Byler DD, Lashley JC, O'Brien JR, Dilley NR (2012). Phys Rev B 85:014103
56. Koza MM, Leithe-Jasper A, Sischka E, Schnelle W, Borrmann H, Mutka H, Grin Y (2014). Phys Chem Chem Phys 16:27119
57. Koza MM, Mutka H, Okamoto Y, Yamaura J-I, Hiroi Z (2015). Phys Chem Chem Phys 17:24837
58. Chakoumakos BC, Sales BC, Mandrus DG (2001). J Alloys Compd 322:127
59. Paschen S, Carrillo-Cabrera W, Bentien A, Tran VH, Baenitz M, Grin Y, Steglich F (2001). Phys Rev B 64:214404
60. Xu J, Tang J, Sato K, Tanabe Y, Miyasaka H, Yamashita M, Heguri S, Tanigaki K (2010). Phys Rev B 82:085206
61. Umeo K, Avila MA, Sakata T, Suekuni K, Takabatake TJ (2005). Phys Soc Jpn 74:2145
62. Sales BC, Chakoumakos BC, Jin R, Thompson JR, Mandrus D (2001). Phys Rev B 63:245113

Struct Bond (2019) 180: 143–190
DOI: 10.1007/430_2019_39

Published online: 1 June 2019

Inorganic Niobium and Tantalum Octahedral Cluster Halide Compounds with Three-Dimensional Frameworks: A Review on Their Crystallographic and Electronic Structures

Pierric Lemoine, Jean-François Halet, and Stéphane Cordier

Contents

P. Lemoine (✉), J.-F. Halet, and S. Cordier
Univ Rennes, CNRS, ISCR - UMR 6226, Rennes, France
e-mail: pierric.lemoine@univ-rennes1.fr

Abstract This review summarizes the development of the rich crystal and bonding chemistry of face-capped and edge-bridged inorganic niobium and tantalum octahedral cluster halide compounds, with a particular emphasis on those showing three-dimensional cluster frameworks. Discussion is made on varied structures and bonding which are intimately linked to the valence electron concentration, i.e., the number of electrons that held the octahedral metal cluster architecture. Exploration of the literature indicates that apart from Nb_6I_{11} and derivatives, which show electron-deficient face-capped $M_6X^i_8X^a_6$ units, compounds containing edge-bridged $M_6X^i_{12}X^a_6$ motifs are the most largely encountered. Closed-shell compounds with a valence electron concentration of 16 are predominant, although a few 15-electron open-shell magnetic compounds or even 14-electron closed-shell species have also been reported. Particularly interesting from a structural point of view is the fashion in which these face-capped and edge-bridged clusters "pack" in crystals. The astonishing diversity of structural types, which are observed, is mainly due to the flexibility of the halogen ligands to coordinate in various manners to metal atoms. However, a rigorous structural analysis of these compounds reveals no close relationship between the valence electron concentration and the variability of the intercluster connections and/or the nature of the counterions. Indeed, the main bonding features of these compounds can be understood from the delocalized bonding picture of isolated "molecular-like" $M_6X^i_8X^a_6$ or $M_6X^i_{12}X^a_6$ clusters.

Keywords Crystal structure · Electronic effect · Electronic structure · Halide · Inorganic compound · Interatomic distance · Intercluster distance · Ligand · Matrix effect · Metal-metal bond · Niobium · Octahedral cluster · Structure type · Tantalum · Three-dimensional framework · Valence electron concentration

1 Introduction

Between niobium metal and niobium oxides and halides in their highest oxidation state (i.e., Nb_2O_5 and NbX_5), metal atom cluster-based compounds form a particular class of compounds wherein metal atoms are associated and held together by metal-metal bonds. Such an association leads to well-defined aggregates of low nuclearities such as dimers, trimers, tetramers, and octahedra [1–5]. They are separated one from another by a matrix of ligands (i.e., oxygen, halogen, or chalcogen) that are bonded to the cluster in terminal (X^a), edge-bridging, or face-capping positions (X^i). Locally the metal is in a square pyramidal $NbX^i_4X^a$ arrangement of ligands wherein Nb-X^i bonds exhibit a stronger covalent character than the Nb-X^a one. Similar clusters are also formed with tantalum, and despite a same number of valence electrons, it turns out that less cluster compounds are reported for this element than for its niobium congener. In the present study, we will focus on octahedral cluster halide compounds prepared by solid-state synthesis at high temperature. Resulting compounds are made of niobium or tantalum and are associated with halogen ligands forming predominantly edge-bridged $M_6X^i_{12}X^a_6$ building blocks, with M = Nb and Ta and

X= F, Cl, Br, and I (Fig. 1, left), except in the case of niobium iodides and some derivative compounds based on face-capped $M_6X^i_8X^a_6$ building blocks (Fig. 1, right) which are largely encountered with transition elements from groups 6 and 7. Within the solid, the building blocks can be either discrete or they can share ligands to form different types of bridges, namely, apical-apical, apical-apical-apical, apical-inner, and inner-apical that are noted $X^{a\text{-}a}$, $X^{a\text{-}a\text{-}a}$, $X^{a\text{-}i}$, and $X^{i\text{-}a}$ (Fig. 2), respectively, according to the notation developed by Schäfer and Schnering [6]. The cluster building blocks can be viewed as monomers [7] forming polymeric frameworks through the association of ligands. Thanks to the orthogonal disposition of ligands around the clusters, the connectivity can be developed in one-dimensional (1D), bi-dimensional (2D), or three-dimensional (3D) directions. When alkali metals, alkaline earth metals, *p*-block metals, and rare earth metals are used during the synthesis of clusters, they act as counter-cations, and the cluster unit building block is negatively charged [8–23]. The size and the charge of the counterions as

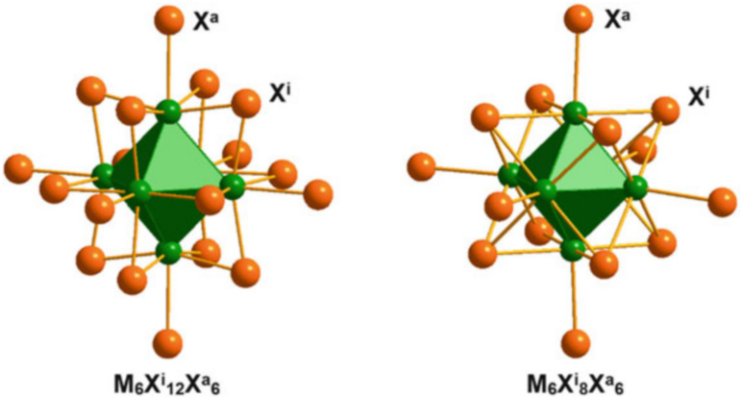

Fig. 1 Representation of the edge-bridged $M_6X^i_{12}X^a_6$ (left) and face-capped $M_6X^i_8X^a_6$ (right) building blocks

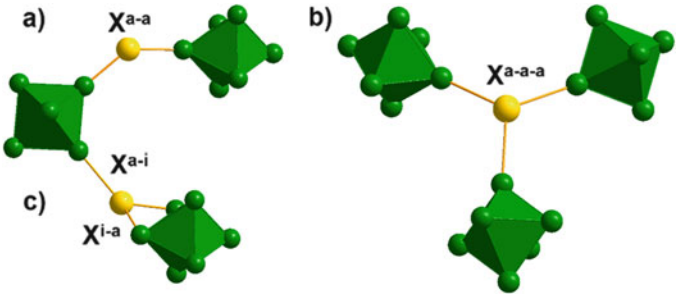

Fig. 2 Representation of the different types of building block bridges encountered in inorganic niobium and tantalum octahedral cluster halide compounds: (**a**) apical-apical $X^{a\text{-}a}$, (**b**) apical-apical-apical $X^{a\text{-}a\text{-}a}$, and (**c**) apical-inner $X^{a\text{-}i}$ and inner-apical $X^{i\text{-}a}$

well as the total charge, the nature of halogen, and the metal atoms of the units are the keystones that govern crystal packing. The average oxidation state of M in the M_6 clusters ranges from +2.67 in $Ta_6Br_{15}(TaBr_6)$ to +1.67 in $CsNb_6I_{11}$. However, the metal atoms cannot be considered independently since overlapping occurs between them leading to metal-metal bonds. Consequently, for a better description of the bonds within the cluster units, one must consider the number of valence electrons that are available to form metal-metal bonds, the so-called valence electron concentration (VEC). It can be simply calculated considering an ionic Zintl-Klemm model with a total transfer of electrons from the counterions to the cluster and from the cluster to the ligands. The VEC value ranges between 14 as in $Ta_6Br_{15}(TaBr_6)$ and 20 as in $CsNb_6I_{11}$. The VEC value drives the physical properties such as magnetism and absorption in the UV-visible region. Beyond fascinating structures and unusual specific physical properties, some of these cluster-based solid-state compounds are soluble. Solution chemistry not only revealed interesting redox properties enabling to stabilize species with lower VEC values, but it also enabled the use of metal clusters as redox active or UV-IR blocking building blocks for the design of composites and electrochromic cells [24, 25], nanoparticles [26], or modified electrodes [27], for instance.

Herein, we review the crystal chemistry and electronic structure of inorganic solid-state compounds based on Nb_6 and Ta_6 cluster halides actively studied earlier in the group of Marcel Sergent enlarged to more contemporary work reported in the literature. The structural richness encountered in this class of compounds is illustrated in Table 1 where a classification with respect to structural network dimensionality, as well as main information of the different structure types, is given. Due to the limited allotted space, solid-state oxyhalides, which constitute an important class of cluster species (see, e.g., [36] and references therein), are excluded, as well as the halide compounds for which the structure is discretely molecular (see, e.g., [37] and references therein). Thus, the following discussion will focus on inorganic solid-state halide compounds containing three-dimensional niobium and tantalum octahedral cluster frameworks through description and analysis of the electronic and steric factors that drive their crystal chemistry and bonding. Unit cell parameters and main interatomic distances of three-dimensional cluster frameworks compounds with complete crystal structure data available in literature are gathered in Tables 2 and 3, respectively.

2 Cluster Frameworks of Structural Formula $[M_6X^i_8X^{a\text{-}a}_{6/2}]$

2.1 Nb_6I_{11} Type (HT and LT Forms)

The existence of the binary compound Nb_6I_{11} (i.e., $NbI_{1.83}$) was first reported in 1965 [30, 44] and interpreted as a cluster compound with $[Nb_6I^i_8I^{a\text{-}a}_{6/2}]$ structural

Table 1 Main informations about structure types reported for inorganic niobium and tantalum octahedral cluster halide compounds

Structure type	Network	SG stand.[a]	SG publ.[b]	Symm.[c]	SG No.	Centro.[d]	VEC[e]	Oxi. state[f]	Published chemical formula	Reference
$[M_6X^i_8X^{a\text{-}a}_{6/2}]$										
Nb_6I_{11} (HT)	3D	*Pccn*		O	56	Yes	19	+1.83	Nb_6I_{11}	[28]
Nb_6I_{11} (LT)	3D	$Pna2_1$	$P2_1cn$	O	33	No	19	+1.83	Nb_6I_{11}	[29]
$CsNb_6I_{11}$	3D	$P6_322$		H	182	No	20	+1.67	$CsNb_6I_{11}$	[9]
$[M_6X^i_{10}X^{i\text{-}a}_{2/2}X^{a\text{-}i}_{2/2}X^{a\text{-}a}_{4/2}]$										
Nb_6Cl_{14}	3D	*Cmca*	*Bbcm*	O	64	Yes	16	+2.33	Nb_6Cl_{14}	[30]
$[M_6X^i_{12}X^{a\text{-}a\text{-}a}_{6/3}]$										
$Nb_6Cl_{12}I_2$	3D	$Pa\bar{3}$		C	205	Yes	16	+2.33	$Nb_6Cl_{12}I_2$	[31]
$[M_6X^i_{12}X^{a\text{-}a}_{6/2}]$										
Nb_6F_{15}	3D	$Im\bar{3}m$		C	229	Yes	15	+2.50	Nb_6F_{15}	[32]
$CsNb_6Cl_8F_7$	3D	$Pm\bar{3}m$		C	221	Yes	16	+2.33	$Cs_{1.3}Nb_6Cl_8F_7$	[20]
$Na_2Nb_6Cl_8F_7(NbF_6)$	3D	$Pm\bar{3}m$		C	221	Yes	16	+2.33	$Na_{1.9}Nb_6Cl_8F_7(NbF_6)$	[19]
Ta_6Cl_{15}	3D	$Ia\bar{3}d$		C	230	Yes	15	+2.50	Ta_6Cl_{15}	[33]
$NaNb_6Cl_{15}$	3D	$Ia\bar{3}d$		C	230	Yes	16	+2.33	$NaNb_6Cl_{15}$	[16]
$KNb_6Cl_{10}F_5$	3D	$Ia\bar{3}d$		C	230	Yes	16	+2.33	$K_{1.2}Nb_6Cl_{10}F_5$	[20]
$Nb_6Br_8F_7$	3D	$R\bar{3}c$		Tg	167	Yes	15	+2.50	$Nb_6Br_{8.32}F_{6.68}$	[34]
$Ta_6Br_{15}(TaBr_6)$	3D	$R\bar{3}c$		Tg	167	Yes	14	+2.67	$Ta_6Br_{15}(TaBr_6)_{0.86}$	[35]
$InNb_6Cl_{15}$	3D	*Pmma*		O	51	Yes	16	+2.33	$InNb_6Cl_{15}$	[18]
$[M_6X^i_{12}X^a_2X^{a\text{-}a}_{4/2}]$										
$Li_2Nb_6Cl_{16}$	2D	*Cmca*		O	64	Yes	16	+2.33	$Li_2Nb_6Cl_{16}$	[17]
$[M_6X^i_{12}X^a_4X^{a\text{-}a}_{2/2}]$										
$Cs_2Nb_6Br_5F_{12}$	1D	*Cccm*		O	66	Yes	15	+2.50	$Cs_{2.1}Nb_6Br_{4.73}F_{12.27}$	[21]
$[M_6X^i_{12}X^a_6]$										
$K_4Nb_6Cl_{18}$	0D	*C2/m*		M	12	Yes	16	+2.33	$K_4Nb_6Cl_{18}$	[8]
$Cs_4Nb_6I_{9.5}F_{8.5}$	0D	*C2/m*		M	12	Yes	16	+2.33	$Cs_{4.03}Nb_6I_{9.42}F_{8.58}$	[22]

(continued)

Table 1 (continued)

Structure type	Network	SG stand.[a]	SG publ.[b]	Symm.[c]	SG No.	Centro.[d]	VEC[e]	Oxi. state[f]	Published chemical formula	Reference
$LuNb_6Cl_{18}$	0D	$R\bar{3}$		Tg	148	Yes	15	+2.50	$LuNb_6Cl_{18}$	[12]
$Cs_2EuNb_6Br_{18}$	0D	$R\bar{3}$		Tg	148	Yes	16	+2.33	$Cs_2EuNb_6Br_{18}$	[14]
$KGdNb_6Cl_{18}$	0D	$R\bar{3}$		Tg	148	Yes	16	+2.33	$KGdNb_6Cl_{18}$	[11]
$CsLuNb_6Cl_{18}$	0D	$P\bar{3}1c$		Tg	163	Yes	16	+2.33	$CsLuNb_6Cl_{18}$	[13]
$Li_2In_2Nb_6Cl_{18}$	0D	$P\bar{1}$		Tc	2	Yes	16	+2.33	$Li_2In_2Nb_6Cl_{18}$	[15]

[a]Standard space group
[b]Published space group
[c]Symmetry: *C* cubic; *H* hexagonal; *Tg* trigonal; *O* orthorhombic; *M* monoclinic; *Tc* triclinic
[d]Centrosymmetric
[e]Valence electron concentration
[f]Average oxidation state of M in the M_6 clusters

Table 2 Compilation of the crystallographic data of inorganic niobium and tantalum octahedral cluster halide compounds with three-dimensional cluster frameworks

Compound	Structure type	SG stand.	VEC	T (K)	a (Å)	b (Å)	c (Å)	V (Å^3)	Z	V/Z (Å^3)	Ref.
Nb_6I_{11}	Nb_6I_{11} (HT)	*Pccn*	19	–	11.299(5)	15.309(5)	13.558(5)	2,345.21	4	586.3	[28]
Nb_6I_{11}	Nb_6I_{11} (HT)	*Pccn*	19	298	11.319(2)	15.310(4)	13.552(3)	2,348.48	4	587.1	[29]
$Nb_6I_{10.5}Br_{0.5}$	Nb_6I_{11} (HT)	*Pccn*	19	298	11.280(1)	15.302(1)	13.524(1)	2,334.33	4	583.6	[38]
$Nb_6I_{8.7}Br_{2.3}$	Nb_6I_{11} (HT)	*Pccn*	19	298	11.167(2)	15.091(3)	13.431(3)	2,263.41	4	565.9	[38]
$D_{0.45}Nb_6I_{11}$[a]	Nb_6I_{11} (HT)	*Pccn*	19/20	350	11.334	15.421	13.579	2,373.36	4	593.3	[39]
HNb_6I_{11}	Nb_6I_{11} (HT)	*Pccn*	20	–	11.299(5)	15.454(5)	13.470(5)	2,352.06	4	588.0	[40]
HNb_6I_{11}	Nb_6I_{11} (HT)	*Pccn*	20	347	11.344(2)	15.502(4)	13.530(2)	2,379.31	4	594.8	[29]
$Mo_{4.7}Nb_{1.3}I_{11}$	Nb_6I_{11} (HT)	*Pccn*	23/24	295	11.0950(2)	15.3216(4)	13.1567(3)	2,236.54	4	559.1	[41]
$Mo_5Nb_1I_{11}$	Nb_6I_{11} (HT)	*Pccn*	24	110	11.0364(9)	15.2588(10)	13.0874(10)	2,203.94	4	551.0	[41]
$Mo_5Nb_1I_{11}$	Nb_6I_{11} (HT)	*Pccn*	24	220	11.0571(10)	15.2873(14)	13.1289(9)	2,219.22	4	554.8	[41]
Nb_6I_{11}	Nb_6I_{11} (LT)	*Pna*2$_1$	19	110	13.429(4)	15.317(6)	11.286(3)	2,321.44	4	580.4	[29]
Nb_6I_{11}	Nb_6I_{11} (LT)	*Pna*2$_1$	19	258	13.489(3)	15.324(4)	11.311(2)	2,338.05	4	584.5	[29]
$Nb_6I_{10.5}Br_{0.5}$	Nb_6I_{11} (LT)	*Pna*2$_1$	19	110	13.404(1)	15.287(1)	11.249(1)	2,305.00	4	576.3	[38]
$Nb_6I_{8.7}Br_{2.3}$	Nb_6I_{11} (LT)	*Pna*2$_1$	19	110	13.346(1)	15.064(2)	11.136(1)	2,238.83	4	559.7	[38]
$D_{0.45}Nb_6I_{11}$[a]	Nb_6I_{11} (LT)	*Pna*2$_1$	19/20	120	13.479	15.387	11.294	2,342.39	4	585.6	[39]
DNb_6I_{11}	Nb_6I_{11} (LT)	*Pna*2$_1$	20	295	13.465(7)	15.495(8)	11.328(5)	2,363.48	4	590.9	[42]
HNb_6I_{11}	Nb_6I_{11} (LT)	*Pna*2$_1$	20	216	13.437(2)	15.474(4)	11.303(3)	2,350.17	4	587.5	[29]
$CsNb_6I_{11}$	$CsNb_6I_{11}$	$P6_322$	20	RT	11.007(2)	–	11.894(2)	1,247.95	2	624.0	[9]
Nb_6Cl_{14}	Nb_6Cl_{14}	*Cmca*	16	–	13.494(5)	12.252(5)	11.019(5)	1,821.75	4	455.4	[30]
Ta_6Br_{14}	Nb_6Cl_{14}	*Cmca*	16	293	14.063(4)	13.177(4)	11.570(16)	2,144.02	4	536.0	[43]
Ta_6I_{14}	Nb_6Cl_{14}	*Cmca*	16	–	15.000(5)	14.445(5)	12.505(5)	2,709.52	4	677.4	[44]
Ta_6I_{14}	Nb_6Cl_{14}	*Cmca*	16	293	15.032(4)	14.487(3)	12.518(6)	2,726.02	4	681.5	[45]
$Nb_6Cl_{12}I_2$	$Nb_6Cl_{12}I_2$	$Pa\bar{3}$	16	296	12.578(1)	–	–	1,989.92	4	497.5	[31]
$Nb_6Cl_{10.8}I_{3.2}$	$Nb_6Cl_{12}I_2$	$Pa\bar{3}$	16	296	12.720(17)	–	–	2,058.08	4	514.5	[31]

(continued)

Table 2 (continued)

Compound	Structure type	SG stand.	VEC	T (K)	a (Å)	b (Å)	c (Å)	V (Å^3)	Z	V/Z (Å^3)	Ref.
Nb_6F_{15}	Nb_6F_{15}	$Im\bar{3}m$	15	–	8.19	–	–	549.35	2	274.7	[32]
Nb_6F_{15}	Nb_6F_{15}	$Im\bar{3}m$	15	RT	8.1878(2)	–	–	548.91	2	274.5	[46]
$CsNb_6Cl_8F_7$	$CsNb_6Cl_8F_7$	$Pm\bar{3}m$	16	293	8.2743(3)	–	–	566.49	1	566.5	[20]
$Na_2Nb_6Cl_8F_7(NbF_6)$	$Na_2Nb_6Cl_8F_7$ (NbF_6)	$Pm\bar{3}m$	16	298	8.2005(9)	–	–	551.47	1	551.5	[19]
$Na_2Nb_6Br_4F_{11}(NbF_6)$	$Na_2Nb_6Cl_8F_7$ (NbF_6)	$Pm\bar{3}m$	16	293	8.1765(6)	–	–	546.64	1	546.6	[34]
Ta_6Cl_{15}	Ta_6Cl_{15}	$Ia\bar{3}d$	15	–	20.286(1)	–	–	8,348.13	16	521.8	[33]
Ta_6Cl_{15}	Ta_6Cl_{15}	$Ia\bar{3}d$	15	293	20.326(1)	–	–	8,397.61	16	524.9	[47]
Ta_6Br_{15}	Ta_6Cl_{15}	$Ia\bar{3}d$	15	293	21.309(2)	–	–	9,675.85	16	604.7	[47]
$Nb_6Cl_{12.8}F_{2.2}$	Ta_6Cl_{15}	$Ia\bar{3}d$	15	RT	20.099(1)	–	–	8,119.39	16	507.5	[48]
$Nb_6Cl_{10.6}F_{4.4}$	Ta_6Cl_{15}	$Ia\bar{3}d$	15	RT	19.9700(20)	–	–	7,964.05	16	497.8	[48]
$NaNb_6Cl_{15}$	$NaNb_6Cl_{15}$	$Ia\bar{3}d$	16	293	20.417(2)	–	–	8,510.91	16	531.9	[16]
$LiNb_6Cl_{15}$	$NaNb_6Cl_{15}$	$Ia\bar{3}d$	16	100	20.5550(20)	–	–	8,684.65	16	542.8	[49]
$KNb_6Cl_{10}F_5$	$KNb_6Cl_{10}F_5$	$Ia\bar{3}d$	16	293	19.589(1)	–	–	7,516.87	16	469.8	[20]
$Nb_6Br_8F_7$	$Nb_6Br_8F_7$	$R\bar{3}c$	15	293	9.6373(6)	–	35.415(2)	2,848.58	6	474.8	[34]
$Ta_6Br_{15}(TaBr_6)_{0.86}$	$Ta_6Br_{15}(TaBr_6)_{0.86}$	$R\bar{3}c$	14	293	12.9860(11)	–	33.285(4)	4,861.05	6	810.2	[35]
$InNb_6Cl_{15}$	$InNb_6Cl_{15}$	$Pmma$	16	296	17.866(1)	13.4552(8)	9.2934(8)	2,234.05	4	558.5	[18]
$K_{0.77}Nb_6Cl_{15}$	$InNb_6Cl_{15}$	$Pmma$	16	293	17.8010(20)	13.4143(11)	9.2551(10)	2,210.01	4	552.5	[50]
$RbNb_6Cl_{15}$	$InNb_6Cl_{15}$	$Pmma$	16	293	17.8348(14)	13.4135(9)	9.2142(6)	2,204.29	4	551.1	[50]
$CsNb_6Cl_{15}$	$InNb_6Cl_{15}$	$Pmma$	16	293	17.8948(15)	13.4397(10)	9.2437(11)	2,223.12	4	555.8	[50]

[a]Deuterium deficiency is due to the absence of deuteriation of the inner part of the single-crystal specimen in approximatively equal weight [39]

Table 3 Main interatomic distances (Å) encountered in inorganic niobium and tantalum octahedral cluster halide compounds with three-dimensional cluster frameworks

Compound	VEC	T (K)	$\langle d_{M-M} \rangle$	$\overline{d_{M-M}}$	$\langle d_{M-X^i} \rangle$	$\overline{d_{M-X^i}}$	$\overline{d_{M-X^{i-a}}}$	$\overline{d_{M-X^{a-i}}}$	$\overline{d_{M-X^{a-a}}}$	$\overline{d_{M-X^{a-a-a}}}$	Ref.
Nb_6I_{11}	19	–	2.712–2.936	2.834	2.774–2.939	2.863	–	–	2.942	–	[28]
Nb_6I_{11}	19	298	2.743–2.918	2.851	2.834–2.903	2.867	–	–	2.926	–	[29]
$Nb_6I_{10.5}Br_{0.5}$	19	298	2.751–2.912	2.852	2.829–2.897	2.861	–	–	2.888	–	[38]
$Nb_6I_{8.7}Br_{2.3}$	19	298	2.734–2.899	2.829	2.809–2.879	2.841	–	–	2.852	–	[38]
$D_{0.45}Nb_6I_{11}$	19/20	350	2.773–2.930	2.866	2.838–2.903	2.870	–	–	2.926	–	[39]
HNb_6I_{11}	20	–	2.727–2.936	2.836	2.775–2.945	2.865	–	–	2.945	–	[40]
HNb_6I_{11}	20	347	2.806–2.950	2.886	2.839–2.910	2.870	–	–	2.918	–	[29]
$Mo_{4.7}Nb_{1.3}I_{11}$	23/24	295	2.667–2.716	2.698	2.760–2.820	2.790	–	–	2.932	–	[41]
$Mo_5Nb_1I_{11}$	24	110	2.661–2.714	2.693	2.752–2.810	2.785	–	–	2.919	–	[41]
$Mo_5Nb_1I_{11}$	24	220	2.664–2.712	2.693	2.755–2.815	2.780	–	–	2.926	–	[41]
Nb_6I_{11}	19	110	2.676–2.982	2.852	2.807–2.901	2.863	–	–	2.921	–	[29]
Nb_6I_{11}	19	258	2.698–2.955	2.842	2.814–2.895	2.863	–	–	2.927	–	[29]
$Nb_6I_{10.5}Br_{0.5}$	19	110	2.683–2.973	2.857	2.816–2.892	2.857	–	–	2.911	–	[38]
$Nb_6I_{8.7}Br_{2.3}$	19	110	2.688–2.922	2.832	2.799–2.870	2.833	–	–	NC[a]	–	[38]
$D_{0.45}Nb_6I_{11}$	19/20	120	2.707–2.976	2.871	2.830–2.906	2.869	–	–	2.922	–	[39]
DNb_6I_{11}	20	295	2.742–2.991	2.855	2.537–2.968	2.805	–	–	2.882	–	[42]
HNb_6I_{11}	20	216	2.722–2.987	2.882	2.823–2.930	2.869	–	–	2.916	–	[29]
$CsNb_6I_{11}$	20	RT	2.771–2.941	2.826	2.862–2.918	2.882	–	–	2.981	–	[9]
Nb_6Cl_{14}	16	–	2.889–2.963	2.915	2.351–2.458	2.408	2.471	3.014	2.582	–	[30]
Ta_6Br_{14}	16	293	2.864–2.959	2.897	2.569–2.609	2.585	2.625	3.440	2.839	–	[43]
Ta_6I_{14}	16	–	2.790–3.112	2.899	2.711–2.826	2.764	2.694	4.349	3.110	–	[44]
Ta_6I_{14}	16	293	2.838–3.115	2.927	2.787–2.803	2.795	2.803	4.231	3.105	–	[45]
$Nb_6Cl_{12}I_2$	16	296	2.906–2.928	2.917	2.434–2.486	2.458	–	–	–	3.148	[31]
$Nb_6Cl_{10.8}I_{3.2}$	16	296	2.907–2.933	2.920	2.449–2.760	2.505	–	–	–	3.189	[31]

(continued)

Table 3 (continued)

Compound	VEC	T (K)	$\langle d_{M-M} \rangle$	$\overline{d_{M-M}}$	$\langle d_{M-X^i} \rangle$	$\overline{d_{M-X^i}}$	$\overline{d_{M-X^{i-a}}}$	$\overline{d_{M-X^{a-i}}}$	$\overline{d_{M-X^{a-a}}}$	$\overline{d_{M-X^{a-a-a}}}$	Ref.
Nb_6F_{15}	15	–	2.803	2.803	2.049	2.049	–	–	2.113	–	[32]
Nb_6F_{15}	15	RT	2.794	2.794	2.059	2.059	–	–	2.118	–	[46]
$CsNb_6Cl_8F_7$	16	293	2.861	2.861	2.095–2.461[b]	2.340	–	–	2.114	–	[20]
$Na_2Nb_6Cl_8F_7(NbF_6)$	16	298	2.831	2.831	2.361	2.361	–	–	2.099	–	[19]
$Na_2Nb_6Br_4F_{11}(NbF_6)$	16	293	2.815	2.815	2.070–2.572[b]	2.223	–	–	2.098	–	[34]
Ta_6Cl_{15}	15	–	2.921–2.928	2.925	2.413–2.462	2.434	–	–	2.564	–	[33]
Ta_6Cl_{15}	15	293	2.918–2.919	2.918	2.424–2.447	2.436	–	–	2.599	–	[47]
Ta_6Br_{15}	15	293	2.956–2.959	2.957	2.568–2.586	2.576	–	–	2.804	–	[47]
$Nb_6Cl_{12.77}F_{2.23}$	15	RT	2.924–2.938	2.931	2.362–2.427	2.404	–	–	2.542	–	[48]
$Nb_6Cl_{10.61}F_{4.39}$	15	RT	2.907–2.930	2.918	2.333–2.428	2.387	–	–	2.520	–	[48]
$NaNb_6Cl_{15}$	16	293	2.926–2.936	2.931	2.445–2.459	2.451	–	–	2.609	–	[16]
$LiNb_6Cl_{15}$	16	100	2.908–2.916	2.912	2.433–2.470	2.451	–	–	2.643	–	[49]
$KNb_6Cl_{10}F_5$	16	293	2.830–2.863	2.846	2.029–2.460	2.309	–	–	2.443	–	[20]
$Nb_6Br_8F_7$	15	293	2.853–2.917	2.885	1.952–2.586[b]	2.288	–	–	2.711	–	[34]
$Ta_6Br_{15}(TaBr_6)_{0.86}$	14	293	2.960–2.964	2.962	2.570–2.589	2.579	–	–	2.808	–	[35]
$InNb_6Cl_{15}$[c]	16	296	2.914–2.951 2.907–2.963	2.936 2.936	2.437–2.472 2.444–2.476	2.454 2.456	– –	– –	2.688 2.628	– –	[18]
$K_{0.77}Nb_6Cl_{15}$[c]	16	293	2.918–2.952 2.915–2.964	2.940 2.935	2.433–2.466 2.436–2.472	2.449 2.450	– –	– –	2.674 2.605	– –	[50]
$RbNb_6Cl_{15}$[c]	16	293	2.919–2.946 2.907–2.952	2.934 2.933	2.434–2.468 2.438–2.465	2.451 2.451	– –	– –	2.678 2.598	– –	[50]
$CsNb_6Cl_{15}$[c]	16	293	2.924–2.951 2.913–2.960	2.937 2.939	2.435–2.461 2.436–2.467	2.449 2.449	– –	– –	2.679 2.605	– –	[50]

[a]*NC* not calculated (strong disorder on apical ligand positions, especially Br[a], leading to Nb-Br[a] distances ranging from 2.567 Å to 4.431 Å)
[b]Atomic coordinates of halogen atoms corresponding to the same inner ligands were refined independently
[c]Calculation done independently for cluster A and cluster B

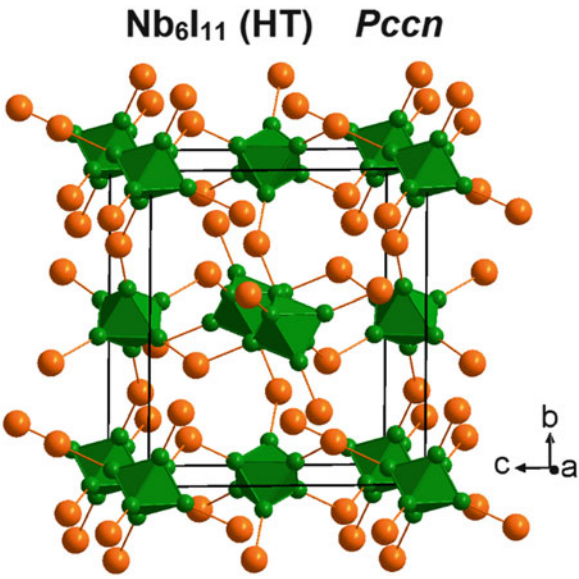

Fig. 3 Crystal structure representation of the high-temperature form of Nb_6I_{11} (space group *Pccn*) highlighting the three-dimensional cluster framework. Inner ligands are omitted for clarity

formula [44, 51]. This hypothesis was confirmed independently by Bateman et al. in 1966 [52] and Simon et al. in 1967 [28] with the resolution of its crystal structure. Nb_6I_{11} crystallizes in the orthorhombic symmetry space group *Pccn* (No. 56) with normalized lattice parameters $a \approx 11.30$ Å, $b \approx 15.31$ Å, and $c \approx 13.56$ Å [28, 52]. Niobium atoms are located on three independent crystallographic sites of general position 8*e*, and iodine atoms are located on five independent 8*e* and one 4*c* crystallographic sites [28]. The structure is built up on four face-capped $[Nb_6I^i_8]^{3+}$ cluster cores per unit cell, which are three-dimensionally bridged two by two by the apical ligands (Fig. 3) leading to the structural formula $[Nb_6I^i_8I^{a\text{-}a}{}_{6/2}]$. Such face-capped cluster units are generally found with molybdenum, tungsten (group 6), and rhenium (group 7), Nb_6I_{11} representing the first compound containing unusual $[M_6X^i_8]^n$ cluster core for the group 5 of transition elements [52].

Nb_6I_{11} is characterized by a second-order structural phase transition at 274 K from the centrosymmetric space group *Pccn* (high-temperature (HT) form) to the non-centrosymmetric one $Pna2_1$ (low-temperature (LT) form) [29]. As the space group $Pna2_1$ is a subgroup of *Pccn* and differs only by the lack of the inversion center, the LT form can be viewed as a continuous deformation of the HT form. Hence, each crystallographic site of general position 8*e* (according to *Pccn* space group) occupied by either niobium or iodine atoms in the HT form splits into two different crystallographic sites of general position 4*a* (according to $Pna2_1$ space group) in the LT form (Fig. 4). It leads for the LT form to the distribution of niobium and iodine atoms on 6 and 11 different 4*a* crystallographic sites, respectively [29]. It should be noted that for the sake of comparison, the published space group was $P2_1cn$ [29] instead of the standardized one $Pna2_1$ (No. 33), allowing keeping equivalent unit cell parameters and orientation of the cluster units for both HT and

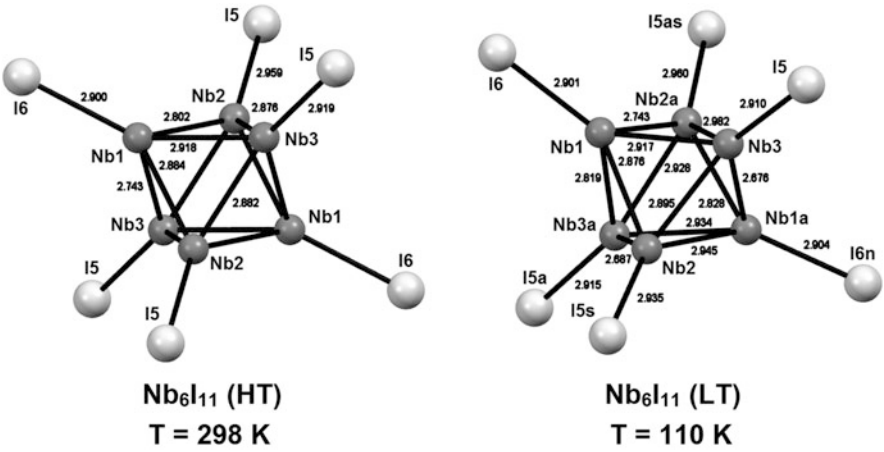

Fig. 4 Representation of the structural transition effect on the distortion of the Nb_6 clusters in the HT form (left) and in the LT form (right) of Nb_6I_{11}. Inner ligands are omitted for clarity. Data are from Ref. [29]

LT forms. This structural phase transition was firstly suggested by large bump in the inverse magnetic susceptibility measurements [28] and then confirmed by specific heat measurements [53, 54] and single-crystal X-ray diffraction [29]. From single-crystal X-ray diffraction, it was shown than both forms evidence a distortion of the Nb_6 clusters (Fig. 4). For the HT form, this distortion is due to the interconnection of the clusters leading to a shift of two opposite metals of the octahedral Nb_6 cluster. It induces that only the inversion center is kept as symmetry element and, consequently, leads to strongly distorted octahedral Nb_6 cluster with Nb-Nb distances ranging between 2.743 Å and 2.918 Å at 298 K (Fig. 4). For the LT form, a distortion component is added which is essentially a twist of 5° at 258 K and 7° at 110 K between the two opposite triangular faces of the Nb_6 octahedron accompanied by a compression along the twist axis [29]. This twist removes the inversion center leading to a non-centrosymmetric structural arrangement and induces a strong distortion of the octahedral Nb_6 cluster with Nb-Nb distances ranging between 2.698 Å and 2.955 Å at 258 K and between 2.676 Å and 2.982 Å at 110 K (Fig. 4).

The $[Nb_6I^i_8]^{3+}$ cluster core shows remarkable magnetic properties in relation with its electron deficiency, only 19 electrons available for 12 cluster metal-metal bonding *d* orbitals (see Sect. 8), and its second-order structural phase transition [28, 53, 54]. Indeed, Nb_6I_{11} exhibits a paramagnetic behavior in agreement with the VEC of 19 with a thermal dependence of the inverse magnetic susceptibility characterized by four different regions (named regions I to IV according to Ref. [54]). Above 274 K (i.e., region IV), Nb_6I_{11} evidences a Curie-Weiss behavior with a quartet ground state ($S = 3/2$) which changes into a doublet ground state ($S = 1/2$) supplemented by a van Vleck paramagnetism contribution between 40 K and 170 K (i.e., region II) [54]. Between these two regions (i.e., region III), the susceptibility of Nb_6I_{11} is unusual and related to a second-order structural phase transition through a spin

crossover transition: the $S = 3/2$ level gradually depopulated due to an increase in the separation between the two states at the expense of the $S = 1/2$ level [54]. From polarized neutron diffraction measurements, it was shown (1) that each Nb_6I_{11} cluster carries three unpaired spins in region IV and only one in region II and (2) that the spin density is predominantly distributed on one of the three pairs of equivalent niobium atoms (centrosymmetrically related) in region IV, while in region II, the spin density is not delocalized over the cluster but rather mainly associated to a niobium site and in a lesser extent to its partner involved in the so-called polarized bond [55]. Finally, the magnetic behavior below 40 K (i.e., region I) is still not well understood as no magnetic ordering is detected down to 2.5 K [54]. For more information see Refs. [53–55].

In parallel to the study of the binary Nb_6I_{11} compound, the H-filled and D-filled analogues were also reported (Table 2). As for its parent compound, a structural phase transition at $T = 324$ K from the centrosymmetric space group *Pccn* to the non-centrosymmetric one $Pna2_1$, as well as similar level crossing mechanism, is observed for HNb_6I_{11} [29, 53, 54]. The HT and LT crystal structures are similar to those of Nb_6I_{11} with the exception that hydrogen atoms are located into the Nb_6 octahedra making these compounds the first examples of centered M_6 octahedral clusters reported in the literature. From neutron powder diffraction results, it was shown that hydrogen/deuterium atoms are located at the center of the Nb_6 octahedra on the 4*a* crystallographic site (according to *Pccn* space group) in the HT form [40], while in the LT form, these interstitial atoms are probably slightly displaced from the center of gravity of the Nb_6 cluster [42]. However, from a single-crystal neutron diffraction study, it was shown that interstitial atoms are located at the centroid of the Nb_6 octahedra in both HT and LT forms [39]. Due to the additional electron coming from hydrogen atom insertion, the $[HNb_6I^i_8]^{3+}$ cluster core in HNb_6I_{11} presents a VEC of 20 explaining the diamagnetic behavior observed at low temperature [40]. Photoelectron spectroscopy data indicated that insertion of hydrogen into Nb_6I_{11} induces an increase of the oxidation state of niobium from ≈1.8 to ≈2.0 [56]. This result could be related with the weak polarization of hydrogen atom by neighboring niobium atoms highlighted by theoretical calculations performed with the self-consistent-field-Xα-scattered-wave (SCF-Xα-SW) method [57]. Structural data and magnetic measurements for both Nb_6I_{11} and HNb_6I_{11} are well explained by a coupled structural and electronic phase transition where degeneracy is reduced through the crossing of electronic levels [29, 53]. On the crystal chemistry point of view, insertion of hydrogen in Nb_6I_{11} leads to a weak increase of the unit cell volume (Table 2) and the Nb-Nb distances (Table 3) whatever the structure [29]. Imoto and Simon indicated that this experimental result is in apparent contradiction with the theoretical increase in the number of bonding electrons expected by the electron transfer from hydrogen atom to metal cluster [29]. However, the distribution of the Nb-Nb distances is narrower in both forms of HNb_6I_{11} compared to those of Nb_6I_{11} [29].

The crystal structure and magnetic influence of a bromine for iodine substitution were evidenced with the study of the $Nb_6I_{11-x}Br_x$ ($0 \leq x \leq 2.7$) series [38]. The authors showed from X-ray diffraction analysis that the unit cell parameters decrease

with the increase of bromine content (Table 2), in agreement with the size difference of bromine and iodine atoms. From single-crystal X-ray diffraction data obtained on $x = 0.5$ and $x = 2.3$ samples at both 298 K and 110 K (Table 2), they established that a preferential substitution of one bridging apical ligand position (i.e., the 4*c* crystallographic site according to *Pccn* space group for the HT form) by bromine atoms first occurs for lower bromine content (i.e., $x = 0.5$), and then for higher bromine content (i.e., $x = 2.3$), bromine atoms are equally distributed on all of the apical ligand positions. Finally, they also showed that the structural phase transition from *Pccn* space group (HT form) to $Pna2_1$ space group (LT form) occurs for all substituted compounds but with a (nonlinear) decrease of the transition temperature with increasing bromine content from 274 K for Nb_6I_{11} to 170 K for $Nb_6I_{8.3}Br_{2.7}$. Concomitantly, a broadening of the transition interval arises from the disorder on apical ligand positions. This influence is also observed through the inverse magnetic susceptibility measurements, where the bump induced by phase transition is less and less pronounced upon the increase of bromine content.

More recently, the crystal structure of two heterometallic iodide compounds ($Mo_{4.7}Nb_{1.3}I_{11}$ and $Mo_5Nb_1I_{11}$, Table 2) was solved by single-crystal X-ray diffraction technique at different temperatures [41]. These compounds crystallize in the Nb_6I_{11}-HT type of structure even at 110 K. Due to very close scattering factors between molybdenum and niobium, the three independent metal atom positions were assumed by the authors to have the same statistical distribution. The ratios were fixed by the chemical composition determined from EDX data for $Mo_{4.7}Nb_{1.3}I_{11}$ and estimated on the basis of the chemical data and similarity of the unit cell parameters for $Mo_5Nb_1I_{11}$ [41]. The authors interpreted the surprising crystal structure modification from Mo_6I_{12} to Nb_6I_{11}-HT for only one niobium to molybdenum atom substitution, by considering the VEC values in Mo_6I_{12}, Nb_6I_{11}, and $Mo_{6-x}Nb_xI_{11}$. Indeed, Nb_6I_{11} is characterized with an electron deficient character of the cluster core (VEC = 19), while Mo_6I_{12} contains the optimal VEC number of 24. The niobium for molybdenum substitution should decrease the VEC number; however, the crystal structure transition from Mo_6I_{12}-type to Nb_6I_{11}-HT implies a transformation of the terminal iodine ligands into bridging atoms resulting to optimal VEC number of 24 for the $[Mo_5Nb_1I^i_8]^{3+}$ cluster core [41]. Nevertheless, electron spin resonance spectrum revealed a broad signal corresponding to one unpaired electron, suggesting also the existence of the $[Mo_4Nb_2I^i_8]^{3+}$ cluster core with VEC number of 23 in the solid solution $Mo_{6-x}Nb_xI_{11}$ ($x = 1$–1.5). Finally, the authors showed that in $Mo_{6-x}Nb_xI_{11}$ (1) the average M-M bond lengths are intermediate between those of the HT form of Nb_6I_{11} and of Mo_6I_{12} and (2) the M-X^i and M-X^a bond lengths are quite similar to those found in Mo_6I_{12} and Nb_6I_{11}, respectively (Table 3) [41].

2.2 $CsNb_6I_{11}$ Type

The crystal structure of $CsNb_6I_{11}$ was reported in 1980 by Imoto and Corbett [9]. This compound crystallizes in the non-centrosymmetric hexagonal symmetry

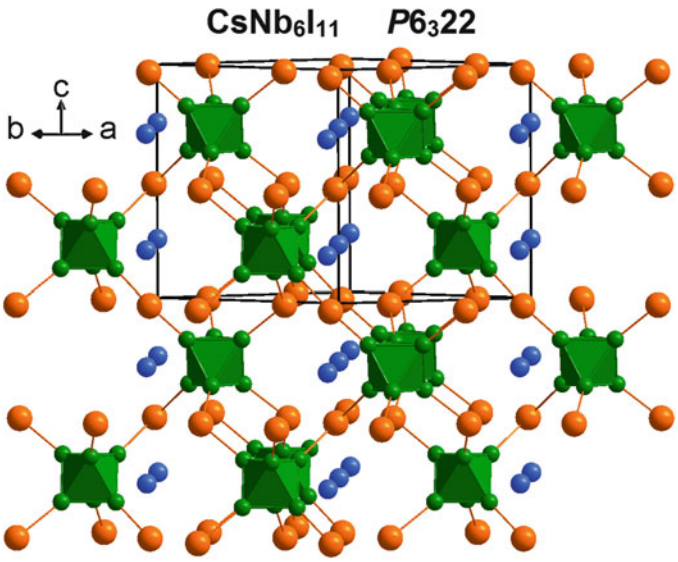

Fig. 5 Crystal structure representation of $CsNb_6I_{11}$ highlighting the three-dimensional cluster framework and the hexagonal close-packed arrangement of the cluster units. Inner ligands are omitted for clarity

space group $P6_322$ (No. 182) with refined cell parameters $a = 11.007(2)$ Å and $c = 11.894(2)$ Å from a Guinier film at room temperature and $a = 11.007(3)$ Å and $c = 11.899(4)$ Å from single-crystal X-ray measurements at the same temperature. Niobium atoms are located on one crystallographic site of general position 12*i*; iodine atoms on three independent crystallographic sites 12*i*, 4*f*, and 6*g*; and cesium atoms on the 2*b* site. The crystal structure consists of a pseudo hexagonal close-packed arrangement along the *c*-axis of distorted face-capped octahedral $[Nb_6I^i_8]^{2+}$ cluster cores (D_{3d} symmetry, VEC = 20) three-dimensionally interconnected by sharing their apical ligands (Fig. 5). This leads, as in Nb_6I_{11}, to a cluster framework of structural formula $[Nb_6I^i_8I^{a\text{-}a}{}_{6/2}]$. Cesium atoms lie in the triangular interstices of the hexagonal cluster layers. The coordination polyhedron of cesium atoms is then formed by six inner iodine ligands at a distance of 4.110(2) Å forming a flattened and twisted trigonal antiprism oriented perpendicularly to the *c*-axis and six apical iodine ligands at a distance of 4.293(1) Å forming an elongated trigonal antiprism along the *c*-axis (Fig. 6).

In $CsNb_6I_{11}$, Nb-Nb distances range from 2.771 Å to 2.941 Å for an average of 2.826 Å, Nb-I^i distances range between 2.862 Å and 2.918 Å for an average of 2.882 Å, and Nb-$I^{a\text{-}a}$ distances are equal to 2.981 Å (Table 3). Existence of short and long Nb-Nb distances arises from the rotation of one metal triangle by 6.1° about the C_3 axis relative to the other [9]. The Nb-Nb and Nb-I^i distances in $CsNb_6I_{11}$ are comparable with those reported for the high-temperature form of Nb_6I_{11} (*Pccn*) (Table 3), indicating that the VEC increase of the cluster core from 19 ($[Nb_6I^i_8]^{3+}$) to 20 ($[Nb_6I^i_8]^{2+}$) does not influence the interatomic distances [9]. On the contrary, the

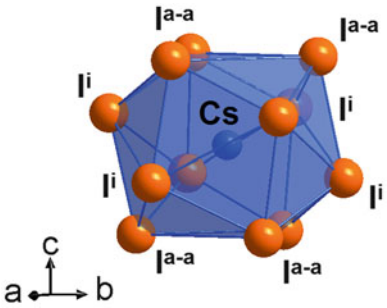

Fig. 6 Representation of the cesium environment in $CsNb_6I_{11}$

Nb-I^a distances are longer in $CsNb_6I_{11}$ than those reported for the high-temperature form of Nb_6I_{11} (Table 3), suggesting that the longer Nb-I^a distances encountered in $CsNb_6I_{11}$ in comparison to those found in Nb_6I_{11} are related to the different cluster unit arrangements as well as ionic interactions between cesium cations and iodine apical ligands in $CsNb_6I_{11}$.

The hydride $CsNb_6I_{11}H_{0.93}$ was reported to be isostructural with its parent compound with unit cell parameters determined from a Guinier film at room temperature ($a = 11.021(1)$ Å and $c = 11.899(2)$ Å) [9]. As for Nb_6I_{11}, insertion of hydrogen into $CsNb_6I_{11}$ leads to a very similar weak increase of the unit cell volume. Consequently, even if the localization of the hydrogen atoms was not determined, it can be assumed that hydrogen atoms are located at the center of the Nb_6 octahedra as shown for Nb_6I_{11} compounds. Finally, the existence of $CsNb_6I_{11}H$, for which the VEC is equal to 21, indicates that hydrogen insertion into Nb_6I_{11} is not simply a result of the presence of an odd number of electrons binding the cluster cage [9].

2.3 *Structural Comparison of Nb_6I_{11} and $CsNb_6I_{11}$*

As previously mentioned, Nb_6I_{11} and $CsNb_6I_{11}$ compounds are characterized by clusters sharing apical ligands leading to the same structural formula $[Nb_6I^i{}_8I^{a\text{-}a}{}_{6/2}]$. However, these compounds evidence different cluster unit arrangements. Indeed, the structure of Nb_6I_{11} may be described as an orthorhombic distortion of a face-centered cube defined by $[Nb_6I^i{}_8I^a{}_3]$ cluster units (Fig. 3), while that of $CsNb_6I_{11}$ consists of a pseudo hexagonal close-packed arrangement of $[Nb_6I^i{}_8I^a{}_3]^-$ cluster units (Fig. 5). The cluster units packing is the result of a compromise between the repulsion between adjacent clusters (electronic effect) and the attraction between cluster units and counter-cations (halogen matrix effect). In $CsNb_6I_{11}$, these two effects coexist, while only the former governs the structure of Nb_6I_{11}. Ionic interactions between cesium cations and iodine apical ligands of the cluster units in $CsNb_6I_{11}$ explain the weak Nb-$I^{a\text{-}a}$-Nb bond angle of 118.41°, leading to short Nb···Nb distances of 5.122 Å (Table 4). On the opposite, the absence of this halogen

Table 4 Nb···Nb distances (Å) and Nb-I$^{a\text{-}a}$-Nb bond angles (°) in $CsNb_6I_{11}$ and Nb_6I_{11}

$CsNb_6I_{11}$ (RT)[a]			
Nb1···Nb1	5.122	Nb1-I3-Nb1	118.41
Nb_6I_{11}-HT ($T = 298$ K)[b]			
Nb1···Nb1	5.629	Nb1-I6-Nb1	152.15
Nb2···Nb3	5.204	Nb2-I5-Nb3	124.59
Nb_6I_{11}-LT ($T = 258$ K)[b]			
Nb1···Nb2	5.635	Nb1-I11-Nb2	151.98
Nb3···Nb5	5.185	Nb3-I9-Nb5	124.18
Nb4···Nb6	5.200	Nb4-I10-Nb6	124.25
Nb_6I_{11}-LT ($T = 110$ K)[b]			
Nb1···Nb2	5.618	Nb1-I11-Nb2	150.78
Nb3···Nb5	5.157	Nb3-I9-Nb5	123.87
Nb4···Nb6	5.178	Nb4-I10-Nb6	123.58

[a]Ref. [9]
[b]Ref. [29]

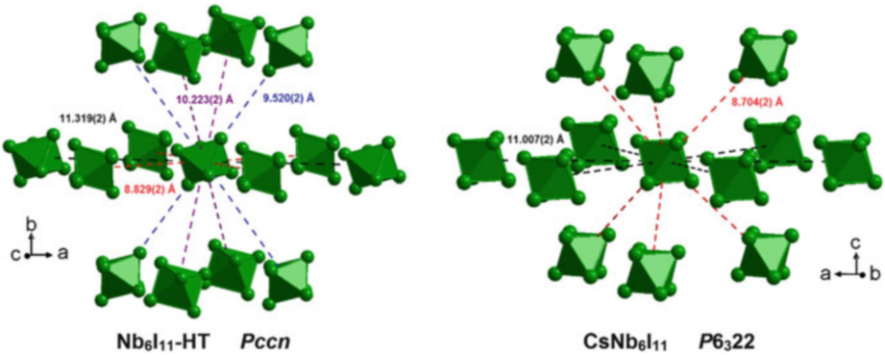

Fig. 7 Representation of the intercluster Nb_6···Nb_6 distances in the high-temperature form of Nb_6I_{11} (left part) and in $CsNb_6I_{11}$ (right part). Distances are calculated from crystal data reported at room temperature in [9, 29], respectively. Cesium and iodine atoms were omitted for clarity

matrix effect in Nb_6I_{11} induces larger Nb-I$^{a\text{-}a}$-Nb bond angles, especially that at ≈152°, leading to longer Nb···Nb distances (Table 4) even if the Nb-I^a distances are shorter in comparison to those encountered in $CsNb_6I_{11}$ (Table 3).

These structural features are also observed through the intercluster distances (i.e., distance between centroids of two adjacent Nb_6 clusters). In $CsNb_6I_{11}$, each Nb_6 cluster is surrounded by six clusters at 11.007(2) Å and by six clusters (three above and three below the hexagonal layer) at 8.704(2) Å (Fig. 7). In Nb_6I_{11}-HT, each Nb_6 cluster is surrounded by four and two clusters in the (*a*,*c*) plane at 8.829(2) Å and 11.319(2) Å, respectively, and by two and two clusters at 9.520(2) Å and 10.223 (2) Å, respectively, both above and below the pseudo hexagonal layer (Fig. 7). The shorter intercluster distances (8.704(2) Å for $CsNb_6I_{11}$, 8.829(2) Å and 9.520(2) Å for Nb_6I_{11}-HT) are observed between Nb_6 clusters bridged by the iodine atoms in apical position. On the opposite, the longer intercluster distances (11.007(2) for

$CsNb_6I_{11}$, 10.223(2) Å and 11.319(2) Å for Nb_6I_{11}-HT) are observed between clusters which are not bridged by apical ligands. The longer intercluster distances in $CsNb_6I_{11}$, observed in the layers where the cesium cations are lying, are intermediate between those measured in Nb_6I_{11}-HT in relation with both steric and electrostatic effects. This observation is coherent with the shorter Nb···Nb distances of adjacent cluster units in $CsNb_6I_{11}$ compared to those in Nb_6I_{11}-HT and confirms the important role of cesium cations to the cluster framework compactness through halogen matrix effect in $CsNb_6I_{11}$.

3 Cluster Frameworks of Structural Formula $[M_6X^i_{10}X^{i\text{-}a}_{2/2}X^{a\text{-}i}_{2/2}X^{a\text{-}a}_{4/2}]$

The preparation of Ta_6Br_{14} and Ta_6I_{14} [58], as well as the crystal structures of Nb_6Cl_{14} [30] and Ta_6I_{14} [44], was reported almost at the same time in 1965. These compounds crystallize in the orthorhombic symmetry normalized space group *Cmca* (No. 64) with lattice parameters $a = 13.494(5)$ Å, $b = 12.252(5)$ Å, and $c = 11.019(5)$ Å for Nb_6Cl_{14} [30] and $a = 15.000(5)$ Å, $b = 14.445(5)$ Å, and $c = 12.505(5)$ Å for Ta_6I_{14} [44] (Table 2). Nb_6Cl_{14} and Ta_6I_{14} were at first published in the non-normalized space group *Bbam*, leading to the redetermination of the crystal structure of Ta_6I_{14} by Artelt and Mayer in 1993 [45]. While the preparation of Ta_6Br_{14} was described in 1965 [58], its crystal structure was reported only in 1995, confirming that this compound is isostructural with Nb_6Cl_{14} and Ta_6I_{14} [43]. Attempts to prepare the isostructural tantalum chloride compound in the same conditions than those used for Ta_6Br_{14} and Ta_6I_{14} led to the formation of Ta_6Cl_{15} [58]. One paper reports about the preparation of Ta_6Cl_{14} from electrochemical reduction of Ta(V) in NaCl-$AlCl_3$ melts [59]; however the chemical composition and crystal structure of the dark green powder product were never confirmed. No publication reports about the existence of the isostructural niobium bromide and iodine compounds. Surprisingly, a temperature independent paramagnetic behavior was reported for Nb_6Cl_{14} and Ta_6I_{14}, though these materials are characterized by an even VEC of 16 [30, 44].

In this type of structure, metal atoms are located on two independent crystallographic sites, one of general position 16*g* and one 8*f*, whereas halogen atoms are located on five independent 8*d*, 8*e*, 8*f*, 16*g*, and 16*g* crystallographic sites. The structure is built up on four edge-bridged $[M_6X^i_{12}]^{2+}$ cluster cores per unit cell. Each cluster is linked to eight neighboring congeners through four apical-apical $X^{a\text{-}a}$, two apical-inner $X^{a\text{-}i}$, and two inner-apical $X^{i\text{-}a}$ bridges (Fig. 8), forming a three-dimensional cluster framework and leading to the structural formula $[M_6X^i_{10}X^{i\text{-}a}_{2/2}X^{a\text{-}i}_{2/2}X^{a\text{-}a}_{4/2}]$. The structure can be viewed as a lozenge arrangement of clusters in the (*a*,*c*) plane linked by the apical-apical $X^{a\text{-}a}$ bridges and stacked along the *b*-axis through the apical-inner $X^{a\text{-}i}$ and inner-apical $X^{i\text{-}a}$ bridges (Fig. 9). In Nb_6Cl_{14}, the apical-inner $X^{a\text{-}i}$ and inner-apical $X^{i\text{-}a}$ bridges lead to four short

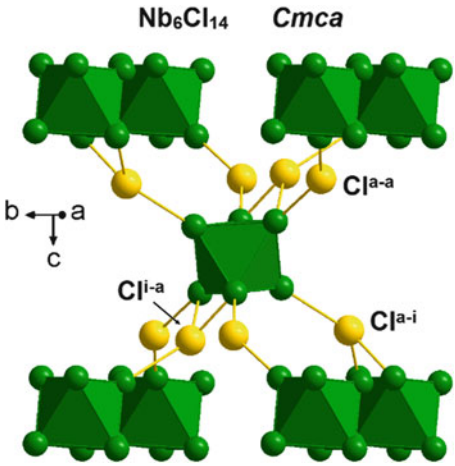

Fig. 8 Crystal structure representation of Nb_6Cl_{14} (space group *Cmca*) highlighting the three-dimensional cluster framework through apical-apical $Cl^{a\text{-}a}$, apical-inner $Cl^{a\text{-}i}$, and inner-apical $Cl^{i\text{-}a}$ bridges

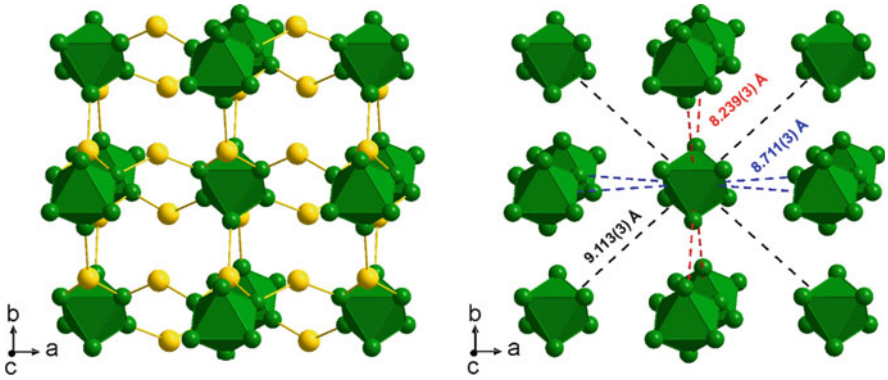

Fig. 9 Representation of the three-dimensional cluster framework (left part) and intercluster $Nb_6\cdots Nb_6$ distances in Nb_6Cl_{14} (right part). Distances are calculated from crystal data reported in [30]

intercluster distances of 8.239(3) Å in the (*b*,*c*) plane and the apical-apical $X^{a\text{-}a}$ bridges to four slightly longer intercluster distances of 8.711(3) Å in the (*a*,*c*) plane (Fig. 9). The environment is completed by four surrounded clusters in the (*a*,*b*) plane not directly linked to the central cluster at intercluster distances of 9.113(3) Å (Fig. 9). Consequently, in Nb_6Cl_{14}, each Nb_6 cluster is surrounded by 12 Nb_6 clusters at relatively close intercluster distances forming a pseudo closed-packed three-dimensional cluster framework. Similar cluster framework is encountered in Ta_6Br_{14} and Ta_6I_{14} compounds with longer intercluster distances in relation with the ionic radius of halogen ligands (Table 5 and Fig. 10). However, the evolution of the

Table 5 $M_6 \cdots M_6$ intercluster distances (Å) in Nb_6Cl_{14}-type structure compounds

Bridging type	Nb_6Cl_{14}[a]	Ta_6Br_{14}[b]	Ta_6I_{14}[c]	Ta_6I_{14}[d]
Direct ($X^{a\text{-}i} \times 2$, $X^{i\text{-}a} \times 2$)	8.239(3)	8.768(6)	9.553(3)	9.573(3)
Direct ($X^{a\text{-}a} \times 4$)	8.711(3)	9.105(6)	9.764(3)	9.781(3)
Indirect ($\times 4$)	9.113(3)	9.640(2)	10.412(3)	10.438(2)

Distances calculated from crystal data reported in: [a]Ref. [30], [b]Ref. [43], [c]Ref. [44], [d]Ref. [45]

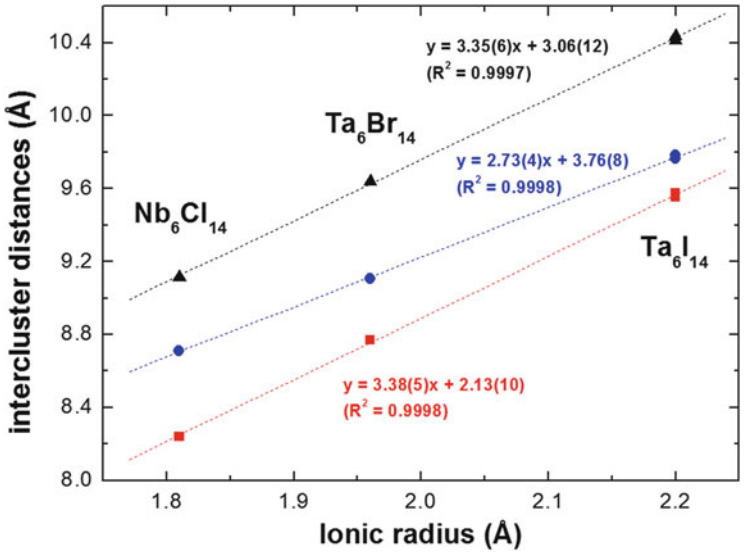

Fig. 10 Evolution of the intercluster distances vs. halogen ionic radius in Nb_6Cl_{14}-type structure compounds. Black triangles correspond to intercluster distances between clusters not directly linked, blue circles correspond to those related to apical-apical $X^{a\text{-}a}$ bridges, and red squares correspond to those related to apical-inner $X^{a\text{-}i}$ and inner-apical $X^{i\text{-}a}$ bridges

intercluster distances as a function of the halogen ionic radius shows some dependence with the type of cluster bridges. Indeed, while the intercluster distances related to surrounding clusters not directly linked (in black in Fig. 10) or linked through apical-inner $X^{a\text{-}i}$ and inner-apical $X^{i\text{-}a}$ bridges (in red in Fig. 10) evolve similarly with the halogen ionic radius, those related to apical-apical $X^{a\text{-}a}$ bridges (in blue in Fig. 10) are not influenced to the same degree with the increase halogen ionic radius. This evolution should be directly related to the ionicity of the M-X bonds, which decreases from X = Cl to X = I, at the expense of a covalent character more and more pronounced.

4 Cluster Frameworks of Structural Formula $[M_6X^i_{12}X^{a\text{-}a\text{-}a}_{6/3}]$

The $Nb_6Cl_{12-x}I_{2+x}$ ($x \leq 2$) compounds, obtained from the reaction of Nb_3Cl_8 and Nb_3I_8 cluster compounds in welded niobium tubes, crystallize in the cubic symmetry space group $Pa\bar{3}$ (No. 205) with lattice parameters a ranging from 12.578(1) Å for $Nb_6Cl_{12}I_2$ to 12.754(1) Å for $Nb_6Cl_{10}I_4$ [31]. Crystal structure resolution, performed for two chemical compositions, i.e., $Nb_6Cl_{12}I_2$ and $Nb_6Cl_{10.8}I_{3.2}$ (Table 2), reveals that, in $Nb_6Cl_{12}I_2$, niobium atoms are located on one crystallographic site of general position 24*d*, chlorine atoms on two independent 24*d* sites, and iodine atoms on an 8*c* crystallographic site. Excess of iodine atoms (i.e., x value) in the $Nb_6Cl_{12-x}I_{2+x}$ ($0 < x \leq 2$) series are located on one of the 24*d* site occupied by chlorine atoms, the second one being fully occupied by chlorine atoms. $Nb_6Cl_{12-x}I_{2+x}$ compounds contain four edge-bridged octahedral niobium clusters per unit cell, connected three by three by iodine atoms in apical position through apical-apical-apical bridges (Fig. 11). This leads to a face-centered cubic three-dimensional arrangement of structural formula $[Nb_6X^i_{12}I^{a\text{-}a\text{-}a}_{6/3}]$ (Fig. 12) closely related to that encountered in Nb_6Cl_{14}-type structure (Fig. 9) compounds via a rotation of the $[Nb_6X^i_{12}]^{2+}$ cluster cores [31]. Consequently, in $Nb_6Cl_{12}I_2$, each Nb_6 cluster is surrounded by 12 Nb_6 clusters at intercluster distances of 8.894(1) Å (Fig. 12). This value, slightly longer than the intercluster distance average encountered in Nb_6Cl_{14} (i.e., 8.688 Å), is due to the presence of two iodine atoms instead of chlorine atoms.

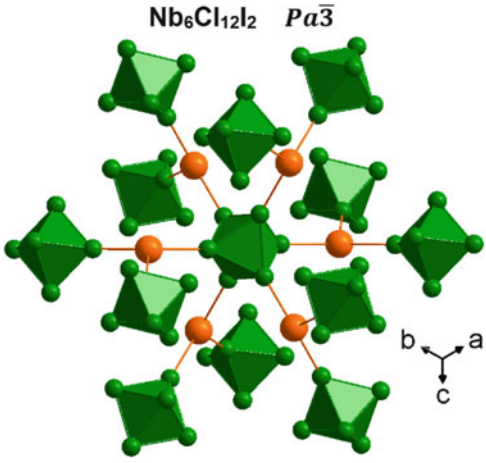

Fig. 11 Crystal structure representation of $Nb_6Cl_{12}I_2$ (space group $Pa\bar{3}$) highlighting the three-dimensional cluster framework through apical-apical $I^{a\text{-}a\text{-}a}$ bridges

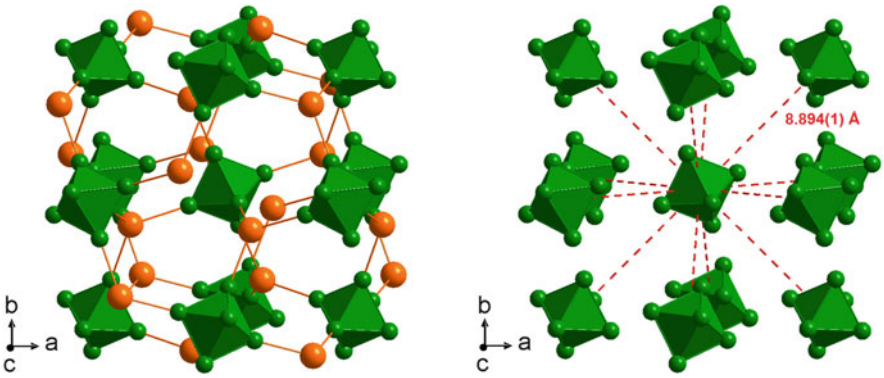

Fig. 12 Representation of the three-dimensional cluster framework (left) and intercluster $Nb_6 \cdots Nb_6$ distances in $Nb_6Cl_{12}I_2$ (right). Distances are calculated from crystal data reported in [31]

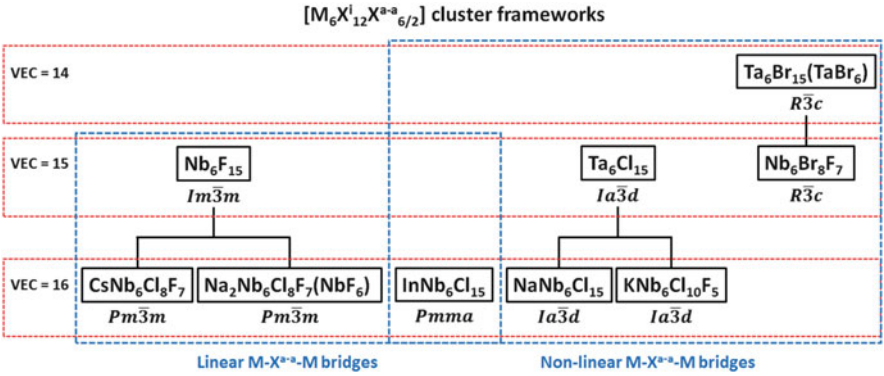

Fig. 13 Classification of the inorganic niobium and tantalum octahedral cluster halide types of structures with three-dimensional frameworks of structural formula $[M_6X^i{}_{12}X^{a\text{-}a}{}_{6/2}]$

5 Cluster Frameworks of Structural Formula $[M_6X^i{}_{12}X^{a\text{-}a}{}_{6/2}]$

Among inorganic niobium and tantalum octahedral cluster halide compounds with three-dimensional frameworks, those characterized by the structural formula $[M_6X^i{}_{12}X^{a\text{-}a}{}_{6/2}]$ form the largest and richest family in term of crystal chemistry and structure types (Fig. 13). This is mainly due to (1) the nature of the apical-apical $M\text{-}X^{a\text{-}a}\text{-}M$ bridges, which can be linear, nonlinear (i.e., bent), or both linear and nonlinear (Fig. 13) and (2) the ability of the cluster frameworks to incorporate cations and/or $(MX_6)^{n-}$ complexes (Fig. 13). This latter point directly influences the VEC of the cluster units which can be stabilized at 14 electrons with incorporation of anion complexes or 16 electrons with incorporation of counter-cations into

15-VEC M_6X_{15} cluster frameworks (Fig. 13). In this section, the crystal structures of cluster compounds of structural formula $[M_6X^i{}_{12}X^{a\text{-}a}{}_{6/2}]$, firstly those related to Nb_6F_{15} (linear M-$X^{a\text{-}a}$-M bridges), secondly those related to Ta_6Cl_{15} (bent M-$X^{a\text{-}a}$-M bridges in cubic structure), thirdly those related to $Nb_6Br_8F_7$ (bent M-$X^{a\text{-}a}$-M bridges in trigonal structure), and finally those related to $InNb_6Cl_{15}$ (both linear and bent M-$X^{a\text{-}a}$-M bridges) will be described.

5.1 Cluster Compounds with Linear M-$X^{a\text{-}a}$-M Bridges

5.1.1 Nb_6F_{15} Type

The crystal structure of Nb_6F_{15} was reported in 1965 by Schäfer et al. [32]. This compound crystallizes in the cubic symmetry (space group $Im\bar{3}m$, No. 229) with lattice parameter $a = 8.19$ Å. Niobium atoms are located on one 12*e* crystallographic site, fluorine atoms in inner position on one 24*h* site, and fluorine atoms in apical position on the 6*b* site [32]. Its crystal structure is formed by the interpenetration of two primitive cubic cluster networks (Fig. 14), related one to the other by a [½, ½, ½] translation. Each primitive network forms a three-dimensional framework through linear apical-apical $F^{a\text{-}a}$ bridges (Fig. 14) and is linked to the second network through $F^i\cdots F^i$ and $F^i\cdots F^a$ halogen bonds of inter-halogen distances of 2.880 Å [46], slightly longer than the sum of the van der Waals radius of fluorine (i.e., 2.70 Å). This leads to a highly compact crystal structure, where each cluster Nb_6F_{15} occupied a volume of 275 $Å^3$ at room temperature. This volume per cluster unit is by far the smallest one among the cluster compounds discussed in this review (Table 2).

The crystal structure of Nb_6F_{15} is characterized by halogen bridging between cluster units leading to the structural formula $[Nb_6F^i{}_{12}F^{a\text{-}a}{}_{6/2}]$ and a VEC of 15, which could cause Curie-Weiss behavior via superexchange interactions [60]. This behavior, related to one unpaired electron per $[Nb_6F^i{}_{12}]^{3+}$ cluster core, was confirmed by magnetic susceptibility, ^{19}F nuclear magnetic resonance, and electron magnetic resonance measurements [46, 60–62]. Below 6 K, Nb_6F_{15} exhibits an

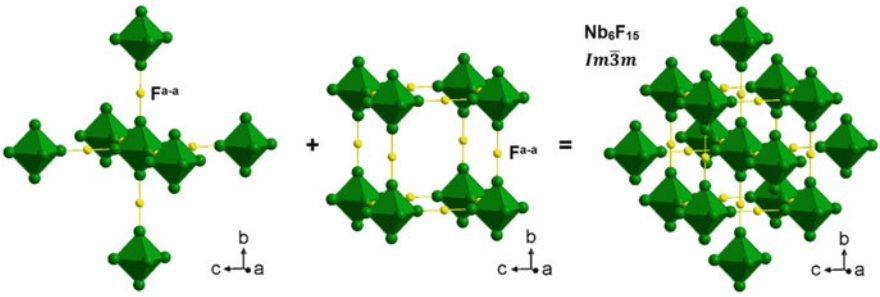

Fig. 14 Crystal structure representation of Nb_6F_{15} (space group $Im\bar{3}m$) highlighting the two interpenetrated primitive cluster networks. Inner ligands are omitted for clarity

antiferromagnetic ordering [46, 61, 62]. From a spin exchange interactions analysis using electronic structure theoretical calculations of extended Hückel type, it was suggested that this antiferromagnetic arrangement is associated to an antiferromagnetic coupling between the two interpenetrating ferromagnetic simple cubic cluster networks [63]. Neutron powder diffraction measurements did not confirm this magnetic structure but rather revealed a decrease of the low-angle background upon cooling [62]. This result is consistent with the emergence of magnetic ordering, which leads to the removal of the paramagnetic scattering contribution to the background, and is a clear signature of the unpaired electron delocalization on the $[Nb_6F^i_{12}]^{3+}$ cluster core [62].

5.1.2 $CsNb_6Cl_8F_7$ Type

$CsNb_6Cl_8F_7$, reported in 2001 by Cordier et al., crystallizes in the cubic symmetry space group $Pm\bar{3}m$ (No. 221) with unit cell parameter $a = 8.2743(3)$ Å [20]. In this structure, niobium atoms are located on one crystallographic site (6*e*), chlorine and fluorine atoms are randomly distributed on one site (12*i*) corresponding to the ligands in inner position, fluorine atoms also fully occupy one site (3*d*) corresponding to the ligands in apical position, and cesium atoms are distributed on six independent sites (6*f*, 12*j*, 24*l*, 24*l*, 24*m*, and 48*n*) all partially occupied. This leads to the refined structural formula $Cs_{1.3(1)}[Nb_6Cl^i_8F^i_4F^{a\text{-}a}_{6/2}]$, where a VEC of 16 is assumed. Its crystal structure can be described as a simple cubic stacking of $[Nb_6Cl^i_8F^i_4F^a_6]$ cluster units linked to six adjacent other ones by linear $F^{a\text{-}a}$ bridges, leading to the $[Nb_6Cl^i_8F^i_4F^{a\text{-}a}_{6/2}]$ structural formula (Fig. 15). This primitive three-dimensional cluster framework can be viewed as a Nb_6F_{15} derivative [20] as

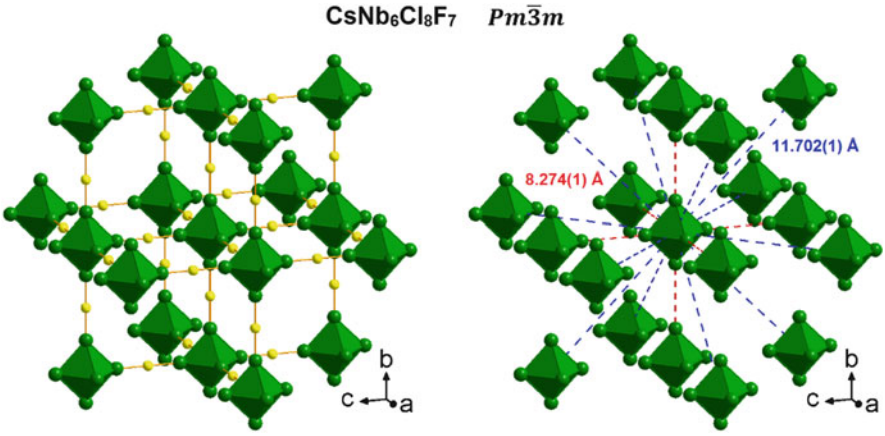

Fig. 15 Representation of the three-dimensional cluster framework (left) and intercluster $Nb_6\cdots Nb_6$ distances (right) in $CsNb_6Cl_8F_7$. Inner ligands are omitted for clarity. Distances are calculated from crystal data reported in [20]

highlighted by only one Nb-Nb distance (i.e., perfectly octahedral cluster), linear $F^{a\text{-}a}$ bridges, and equivalent Nb-$F^{a\text{-}a}$ interatomic distances (2.114 Å for $CsNb_6Cl_8F_7$ compared to 2.113 Å for Nb_6F_{15}, Table 3).

5.1.3 $Na_2Nb_6Cl_8F_7(NbF_6)$ Type

$Na_2Nb_6Cl_8F_7(NbF_6)$ was the first niobium cluster chlorofluoride reported in the literature in 1999 by Cordier and Simon [19]. It crystallizes in the cubic symmetry space group $Pm\bar{3}m$ (No. 221) with unit cell parameter $a = 8.2005(9)$ Å. In this compound, niobium atoms related to the cluster occupy one 6*e* crystallographic site, chlorine and fluorine atoms corresponding to ligands in inner position are randomly distributed on one 12*i* site, while the 3*d* site related to the ligands in apical position is fully occupied by fluorine atoms. Niobium and fluorine atoms related to $(NbF_6)^{n-}$ complexes (see below) occupied the 1*b* and one 6*f* crystallographic sites, respectively. Finally, sodium cations are statistically distributed on one 12*h* crystallographic site with a site occupancy factor (SOF) of 0.156(8). This leads, within the standard deviations, to the structural formula $Na_2[Nb_6Cl^i{}_8F^i{}_4F^{a\text{-}a}{}_{6/2}](NbF_6)$ [19].

The crystal structure of $Na_2Nb_6Cl_8F_7(NbF_6)$ is related to that of Nb_6F_{15}, for which only one cluster network (identical to that encountered in $CsNb_6Cl_8F_7$, Fig. 15) is preserved while the second is replaced by $(NbF_6)^{n-}$ complexes (Fig. 16). Two sodium cations statistically distributed on the faces of the cubic unit cell provide the cohesion of the crystal structure (Fig. 16) and counterbalance the charge of the $(NbF_6)^{n-}$ complex located at the center of the cubic unit cell and eventually that of the cluster [19]. Indeed, the VEC of the cluster should be either 15, if the two sodium cations counterbalance the charge of the $(NbF_6)^{2-}$ complex, or 16 if one sodium cation counterbalances the charge of the $(NbF_6)^{-}$ complex, the second one counterbalancing the charge of the cluster [19].

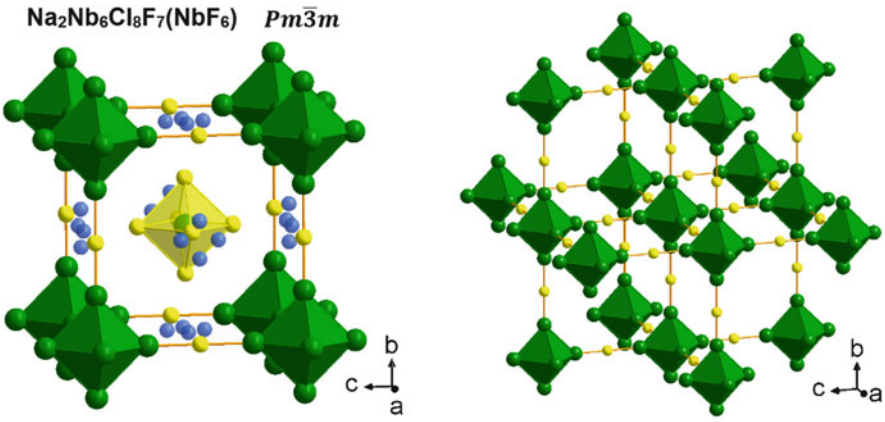

Fig. 16 Representation of the unit cell of $Na_2Nb_6Cl_8F_7(NbF_6)$ (left) and of its three-dimensional cluster framework (right). Inner ligands are omitted for clarity

A second compound was found to be isotypic with $Na_2Nb_6Cl_8F_7(NbF_6)$, namely, $Na_2Nb_6Br_4F_{11}(NbF_6)$ [34]. However, in this case, the atomic coordinates of bromine and fluorine atoms on the inner position were refined independently, while those of chlorine and fluorine were constrained to be the same in $Na_2Nb_6Cl_8F_7(NbF_6)$.

5.1.4 Comparison of Nb_6F_{15}, $CsNb_6Cl_8F_7$, and $Na_2Nb_6Cl_8F_7(NbF_6)$ Cluster Frameworks

In Nb_6F_{15}, the interpenetration of two primitive cubic cluster networks leads to eight very short intercluster distances of 7.09 Å (Table 6). The cluster units separated from these intercluster distances are then not directly linked by halogen bridging but interact through the $F^i\cdots F^i$ and $F^i\cdots F^a$ halogen bonds existing between the two networks. Direct linear apical-apical $F^{a\text{-}a}$ bridges induce six short intercluster distances of 8.19 Å. Finally, the cluster environment is completed by 12 clusters of the same network at intercluster distances of 11.58 Å, which are not directly linked to the central cluster unit.

As previously mentioned, the crystal structures of $CsNb_6Cl_8F_7$ and $Na_2Nb_6Cl_8F_7(NbF_6)$ are related to that of Nb_6F_{15}. However, in the former compounds, only one cluster network is preserved, the second being replaced either by cesium cations or (NbF_6) anionic complexes. This leads to the absence of the eight very short intercluster distances related to the interpenetration of the two primitive cubic cluster networks. Hence, the cluster environment in $CsNb_6Cl_8F_7$ and $Na_2Nb_6Cl_8F_7(NbF_6)$-type structure compounds is formed by six cluster units directly linked through $X^{a\text{-}a}$ bridges and 12 cluster units not directly linked to the central cluster (see, e.g., Fig. 15 and Table 6). The intercluster distances in $CsNb_6Cl_8F_7$ are slightly longer compared to those in Nb_6F_{15} (Table 6). On the contrary, they are equivalent in the $Na_2Nb_6Cl_8F_7(NbF_6)$-type structure compounds (Table 6), despite the fact that partial replacement of fluorine inner ligands either by chlorine (i.e., $Na_2Nb_6Cl_8F_7(NbF_6)$) or by bromine (i.e., $Na_2Nb_6Br_4F_{11}(NbF_6)$) leads to longer $M\text{-}X^i$ interatomic distances (Table 3). This suggests that the size of the cluster core and the electronic effect induced by the repulsion between cluster units

Table 6 $M_6\cdots M_6$ intercluster distances (Å) in Nb_6F_{15}, $CsNb_6Cl_8F_7$ and $Na_2Nb_6Cl_8F_7(NbF_6)$-type structure compounds

Bridging type	Nb_6F_{15}[a]	Nb_6F_{15}[b]	$CsNb_6Cl_8F_7$[c]	$Na_2Nb_6Cl_8F_7(NbF_6)$[d]	$Na_2Nb_6Br_4F_{11}(NbF_6)$[e]
Indirect (×8)	7.093(1)	7.091(1)	–	–	–
Direct (×6)	8.190(1)	8.188(1)	8.274(1)	8.201(1)	8.177(1)
Indirect (×12)	11.582(1)	11.579(1)	11.702(1)	11.597(1)	11.563(1)

Distances calculated from crystal data reported in: [a]Ref. [32], [b]Ref. [46], [c]Ref. [20], [d]Ref. [19], [e]Ref. [34]

and complexes are compensated by halogen matrix effects between sodium cations and cluster units/complexes.

5.2 *Cluster Compounds with Bent M-$X^{a\text{-}a}$-M Bridges in Cubic Structure*

5.2.1 Ta_6Cl_{15} Type

Ta_6Cl_{15} and Ta_6Br_{15} have been reported in 1968 by Bauer and von Schnering to crystallize in the cubic symmetry (space group $Ia\bar{3}d$, No. 230) with lattice parameters $a = 20.286(1)$ Å and 21.290(1) Å, respectively [33]. The crystal structure resolution, performed on single crystal of Ta_6Cl_{15}, indicated that niobium atoms are located on one crystallographic site of general position 96*h*, halogen atoms in inner position are located on two independent 96*h* sites, and halogen atoms in apical position on one 48*g* site [33]. As in Nb_6F_{15}, the crystal structure of Ta_6Cl_{15} is characterized by clusters sharing apical ligands in the three directions (Fig. 17), leading to the same kind of structural formula $[Ta_6Cl^{i}_{12}Cl^{a\text{-}a}_{6/2}]$ but with a different three-dimensional cluster framework arrangement (Fig. 18). Indeed, in Nb_6F_{15} the M-$X^{a\text{-}a}$-M bridges are linear giving two identical independent interpenetrated cluster networks, while in Ta_6Cl_{15} the bridges are bent giving a unique network.

Ta_6I_{15} was also reported in 1968 to crystallize in a cubic unit cell with $a = 11.02$ Å and then was supposed to be isotypic to Nb_6F_{15} [64]. While the crystal structure of Ta_6Br_{15} was confirmed in 1999 by von Schnering et al. [47], that of Ta_6I_{15} is yet unsolved but is probably isotypic to Ta_6Cl_{15}.

Isostructural niobium chloride compound derivatives can be stabilized by the replacement of a small amount of chlorine by fluorine [48]. The crystal structure of two $Nb_6Cl_{15-x}F_x$ chlorofluoride compounds ($x = 2.2$ and 4.4) was studied by single-crystal X-ray diffraction [48]. Their structure is based on $[Nb_6X^{i}_{12}X^{a}_{6}]$ cluster units

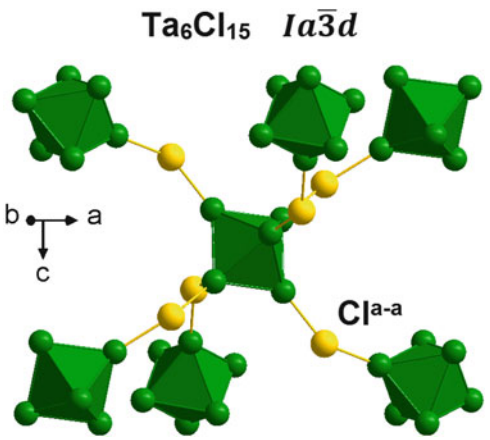

Fig. 17 Crystal structure representation of Ta_6Cl_{15} (space group $Ia\bar{3}d$) highlighting the three-dimensional cluster framework through apical-apical $Cl^{a\text{-}a}$ bridges. Inner ligands are omitted for clarity

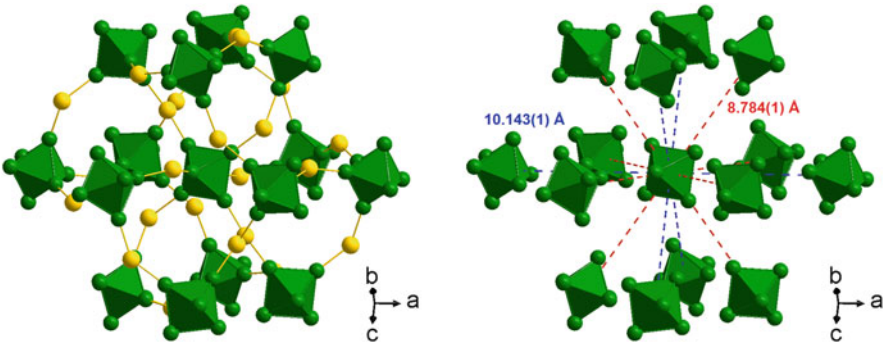

Fig. 18 Representation of the three-dimensional cluster framework (left) and intercluster $Ta_6 \cdots Ta_6$ distances in Ta_6Cl_{15} (right). Inner ligands are omitted for clarity. Distances are calculated from crystal data reported in [33]

sharing apical ligands in which fluorine atoms are randomly distributed on the inner positions but also on the apical positions for $x = 4.4$ [48].

As for Nb_6F_{15}, Ta_6Cl_{15} and Ta_6Br_{15} exhibit a Curie-Weiss behavior in agreement with the VEC of 15 of the $[Ta_6X^i_{12}]^{3+}$ cluster cores [33, 60]. A magnetic behavior is also expected for $Nb_6Cl_{15-x}F_x$ compounds in relation with their VEC of 15 [48], but this was never confirmed experimentally.

5.2.2 $NaNb_6Cl_{15}$ Type

The crystal structure of $NaNb_6Cl_{15}$ was reported in 1995 by Sägebarth et al. [16]. This compound and its isotypic compound, $LiNb_6Cl_{15}$, crystallize in the cubic symmetry space group $Ia\bar{3}d$ (No. 230) with lattice parameter $a = 20.417$ (2) Å at 293 K for $NaNb_6Cl_{15}$ [16] and $a = 20.555(2)$ Å at 100 K for $LiNb_6Cl_{15}$ [49]. The crystal structure of these compounds is characterized by a three-dimensional cluster framework through bent apical-apical $Cl^{a\text{-}a}$ bridges, identical to that encountered in Ta_6Cl_{15} (Figs. 17 and 18), with, however, alkaline cations statistically distributed on an interstitial position partially occupied. Hence, niobium atoms are located on one crystallographic site of general position 96*h*, chlorine atoms in inner position are located on two independent 96*h* sites, chlorine atoms in apical position are located on one 48*g* site, and sodium/lithium atoms are located on one 48*f* site with a SOF of ≈1/3 [16, 49]. Based on bond distances, the alkaline environment can be described as distorted tetrahedral for lithium cations and distorted trigonal-prismatic bicapped for sodium cations [49]. In this type of structure, alkaline atoms are inside linear channels formed by the body-centered $[Nb_6Cl^i_{12}Cl^{a\text{-}a}{}_{6/2}]$ cluster arrangement. These channels are parallel to the [100], [010], and [001] directions and are stacked in fashion that they do not intersect with each other [49].

The stabilization of the Ta_6Cl_{15} three-dimensional cluster framework with $[Nb_6Cl^i_{12}]^{2+}$ cluster core through incorporation of sodium is observed only for the stoichiometric composition $NaNb_6Cl_{15}$, as no range of homogeneity on the sodium site was detected [16]. It indicates that the $NaNb_6Cl_{15}$ crystal structure is stable only for compounds having a VEC of 16, value confirmed by magnetic measurements [16].

$NaNb_6Cl_{15}$ evidences a second-order structural transition around 150 K from the cubic structure with cell parameter $a = 20.364(2)$ Å at 160 K to a tetragonal structure with cell parameters $a = 20.372(6)$ Å and $c = 20.282(2)$ Å at 80 K [16]. The space group of the LT form was reported to probably be $I4_1/acd$ [16] but was never confirmed. No structural transition was reported for $LiNb_6Cl_{15}$. Infrared reflectivity measurements performed on $NaNb_6Cl_{15}$ showed a vanishing of the narrow bands between 50 and 150 cm^{-1} with the increase of the temperature from 100 to 200 K [16]. This is explained by a local order of sodium atoms in the low-temperature crystal structure, while these atoms become mobile above the temperature of the structural transition, suggesting that $NaNb_6Cl_{15}$ is an ionic conductor [16]. This was confirmed by ^{7}Li-NMR measurements [49]. These analyses also evidenced a fast lithium mobility above 170 K in this material [49]. Finally, a study reported on the reversible intercalation of lithium in Ta_6Cl_{15}, leading to the compound $LiTa_6Cl_{15}$, which is mentioned to be structurally and electronically related to $LiNb_6Cl_{15}$ [65].

5.2.3 $KNb_6Cl_{10}F_5$ Type

As for $Nb_6Cl_{15-x}F_x$ [48] and $CsNb_6Cl_8F_7$ [20], $KNb_6Cl_{10}F_5$ was obtained during investigations of fluorine for chlorine substitution in order to increase the interactions between Nb_6 clusters by reducing the steric hindrance of ligands [20]. This latter compound was reported to crystallize in the cubic symmetry space group $Ia\bar{3}d$ (No. 230) with lattice parameter $a = 19.589(1)$ Å at 293 K and a refined formula $K_{1.2(2)}Nb_6Cl_{10}F_5$ assumed to be stoichiometric within the standard deviations [20]. Its crystal structure, derived of the Ta_6Cl_{15}-type of structure, is based on cluster units sharing apical ligands, leading to a three-dimensional cluster framework $[Nb_6X^i_{12}X^{a\text{-}a}_{6/2}]$ with bent bridges. Crystallographic sites corresponding to the ligands positions (two independent 96*h* sites and one 48*g* site) are randomly occupied by chlorine and fluorine atoms. The potassium cations are statistically distributed on two crystallographic sites: 24*d* and 96*h* with SOF of 0.452(24) and 0.08(2), respectively [20]. Despite a complex crystal structure and structural formula, this compound is characterized by a VEC of 16.

5.2.4 Comparison of Ta_6Cl_{15}, $NaNb_6Cl_{15}$, and $KNb_6Cl_{10}F_5$ Cluster Frameworks

In Ta_6Cl_{15}-type structure, each cluster unit is surrounded by eight clusters at short intercluster distances, ranging from 8.647(1) Å for $Nb_6Cl_{10.6}F_{4.4}$ to 9.227

(1) Å for Ta_6Br_{15} (Table 7). Six of these eight cluster units are directly linked to the central cluster through apical-apical M-$X^{a\text{-}a}$-M cluster bridges, while the two remaining cluster units are not directly linked but are located above and below the central cluster on the threefold axis (Fig. 18). The cluster environment is completed by six cluster units, not directly linked to the central cluster (Fig. 18), at longer intercluster distances ranging from 9.985(1) Å for $Nb_6Cl_{10.6}F_{4.4}$ to 10.655(1) Å for Ta_6Br_{15} (Table 7).

The intercluster distances in Ta_6Cl_{15}-type structure compounds evidence a quadratic evolution with the average halogen ionic radius as shown in Fig. 19. This quadratic evolution is directly related to the average M-M, M-X^i, and M-X^a interatomic distances which are slightly shorter and longer when chlorine ligands are partially substituted by fluorine or totally by bromine, respectively (Table 3). This reflects the electronic effect on cluster framework compactness. Moreover, from the quadratic equations, it could be estimated that the minimum intercluster distances should be obtained for an average ionic radius of 1.65/1.66 Å, which corresponds to a chemical composition of $Nb_6Cl_{10}F_5$. This chemical composition,

Table 7 $M_6\cdots M_6$ intercluster distances (Å) in Ta_6Cl_{15}-type structure compounds

Bridging type	$Nb_6Cl_{10.6}F_{4.4}$[a]	$Nb_6Cl_{12.8}F_{2.2}$[a]	Ta_6Cl_{15}[b]	Ta_6Cl_{15}[c]	Ta_6Br_{15}[c]
Direct (×6)	8.647(1)	8.703(1)	8.784(1)	8.801(1)	9.227(1)
Indirect (×2)	8.647(1)	8.703(1)	8.784(1)	8.801(1)	9.227(1)
Indirect (×6)	9.985(1)	10.050(1)	10.143(1)	10.163(1)	10.655(1)

Distances calculated from crystal data reported in: [a]Ref. [48], [b]Ref. [33], [c]Ref. [47]

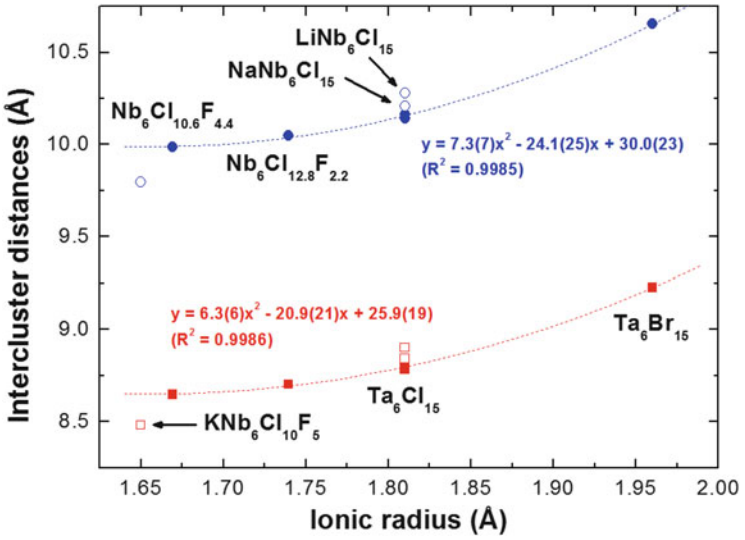

Fig. 19 Evolution of the intercluster distances vs. the average halogen ionic radius in Ta_6Cl_{15}-type, $NaNb_6Cl_{15}$-type, and $KNb_6Cl_{10}F_5$ compounds

Table 8 $M_6 \cdots M_6$ intercluster distances (Å) in $NaNb_6Cl_{15}$-type and $KNb_6Cl_{10}F_5$ compounds

Bridging type	$NaNb_6Cl_{15}$[a]	$LiNb_6Cl_{15}$[b]	$KNb_6Cl_{10}F_5$[c]
Direct (×6)	8.841(1)	8.901(1)	8.482(1)
Indirect (×2)	8.841(1)	8.901(1)	8.482(1)
Indirect (×6)	10.209(1)	10.278(1)	9.795(1)

Distances calculated from crystal data reported in: [a]Ref. [16], [b]Ref. [49], [c]Ref. [20]

close to that reached experimentally with $Nb_6Cl_{10.6}F_{4.4}$, can be considered as a lower limit to the Ta_6Cl_{15}-type of structure stability, explaining the different type of structure for Nb_6F_{15}.

Due to their identical three-dimensional cluster frameworks, the cluster unit environments in $NaNb_6Cl_{15}$ and $KNb_6Cl_{10}F_5$ are related to that encountered in Ta_6Cl_{15}, with eight clusters at short intercluster distances (six directly linked through apical-apical M-$X^{a\text{-}a}$-M cluster bridges and two not directly linked) and six clusters at longer intercluster distances (Table 8). Similarly to Ta_6Cl_{15}-type structure compounds, an electronic effect is observed on the cluster framework compactness. However, this electronic effect is also influenced by halogen matrix effect through electrostatic interactions occurring between the cluster units and the counter-cations. It leads to intercluster distances slightly longer in ternary cluster chlorides $NaNb_6Cl_{15}$ and $LiNb_6Cl_{15}$ (Table 8) than those observed in binary ones (Table 7) and shorter in the pseudo ternary cluster chlorofluoride $KNb_6Cl_{10}F_5$ (Table 8) compared to those expected for the corresponding pseudo binary chlorofluoride cluster compound (Fig. 19).

5.3 *Cluster Compounds with Bent M-$X^{a\text{-}a}$-M Bridges in Trigonal Structure*

5.3.1 $Nb_6Br_8F_7$ Type

$Nb_6Br_8F_7$, reported in 2001 by Cordier et al., crystallizes in the trigonal symmetry space group $R\bar{3}c$ (No. 167) with unit cell parameters $a = 9.6373(6)$ Å and $c = 35.415(2)$ Å [34]. Niobium atoms are located on one 36*f* crystallographic site. Halogen atoms corresponding to inner ligands are located on two independent 36*f* sites, one fully occupied by fluorine atoms and the second statistically occupied by bromine and fluorine atoms with SOF of 0.887(4) and 0.113(4), respectively. Halogen atoms corresponding to apical ligands are located on one 18*e* site fully occupied by bromine atoms [34]. The crystal structure of $Nb_6Br_8F_7$ is based on a three-dimensional cluster framework through bent apical-apical $Br^{a\text{-}a}$ bridges (Fig. 20), leading to the structural formula $[Nb_6Br^{i}{}_5F^{i}{}_7Br^{a\text{-}a}{}_{6/2}]$. The nonlinearity of the bridges leads to a new kind of cluster arrangement among the M_6X_{15} compounds of VEC 15 and is explained by the destabilization of a hypothetical cubic structure due to the

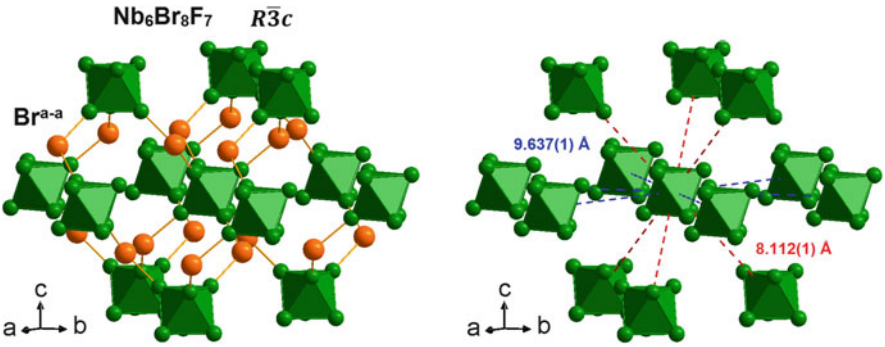

Fig. 20 Representation of the three-dimensional cluster framework (left) and intercluster $Nb_6 \cdots Nb_6$ distances (right) in $Nb_6Br_8F_7$. Inner ligands are omitted for clarity. Distances are calculated from crystal data reported in [34]

presence of a large interstitial void, which is partially filled by bromide apical ligands in the rhombohedral structure [34].

5.3.2 $Ta_6Br_{15}(TaBr_6)$ Type

$Ta_6Br_{15}(TaBr_6)_{0.86}$, formerly known as the elusive "$TaBr_3$", was reported in 2010 by Habermehl et al. [35]. This cluster compound crystallizes in the trigonal symmetry space group $R\bar{3}c$ (No. 167) with unit cell parameters $a = 12.9860(11)$ Å and $c = 33.285(4)$ Å [35]. Tantalum atoms arising from the cluster are located on one 36*f* crystallographic site, bromine atoms corresponding to inner ligands are located on two independent 36*f* sites, and bromine atoms corresponding to apical ligands are located on one 18*e* site. Tantalum and bromine atoms arising from the $TaBr_6$ complex occupied the 6*a* site and one 36*f* site, respectively, both with SOF of 0.861(13) [35]. Tantalum in the $(TaBr_6)$ complex is assumed to be pentavalent, suggesting that $Ta_6Br_{15}(TaBr_6)_{0.86}$ should be a salt formed by the association of $(TaBr_6)^{0.86-}$ complexes and $[Ta_6Br_{15}]^{0.86+}$ cluster units [35]. Hence, for a full occupation of the interstitial sites by $TaBr_6$ complexes, a VEC of 14 is expected for the $[Ta_6Br^{i}_{12}]^{4+}$ cluster core [35].

The crystal structure of $Ta_6Br_{15}(TaBr_6)_{0.86}$ is strongly related to that of $Nb_6Br_8F_7$ through identical three-dimensional cluster framework based on bent apical-apical $Br^{a\text{-}a}$ bridges, in which interstitial cuboctahedral sites are partially filled by $(TaBr_6)$ complexes (Fig. 21). These complexes form a three-dimensional network similar to that of the cluster units. Hence, the crystal structure of $Ta_6Br_{15}(TaBr_6)_{0.86}$ is formed by the interpenetration of clusters and complexes networks, related one to each other by a [2/3, 1/3, 1/12] translation (Fig. 21).

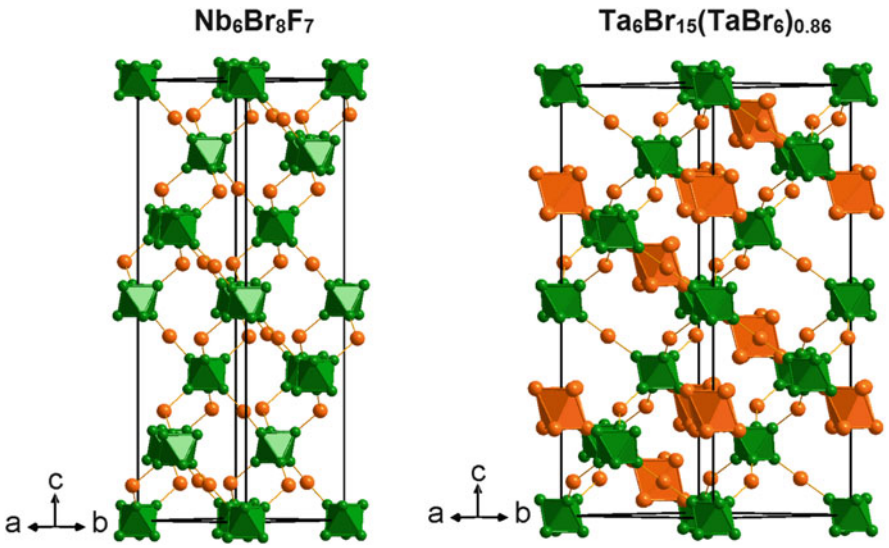

Fig. 21 Representation of the unit cell of $Nb_6Br_8F_7$ (left) and $Ta_6Br_{15}(TaBr_6)_{0.86}$ (right) highlighting the similarity of three-dimensional cluster frameworks. Inner ligands are omitted for clarity

5.3.3 Comparison of $Nb_6Br_8F_7$ and $Ta_6Br_{15}(TaBr_6)_{0.86}$ Cluster Frameworks

As previously mentioned, the crystal structures of $Nb_6Br_8F_7$ and $Ta_6Br_{15}(TaBr_6)_{0.86}$ evidence similar three-dimensional cluster networks characterized by bent apical-apical M-$Br^{a\text{-}a}$-M bridges (Fig. 21). The shorter intercluster distances are found between cluster linked by apical-apical $Br^{a\text{-}a}$ bridges along the *c*-axis, while the longer intercluster distances (corresponding to *a* parameter) are located in the (*a*,*b*) plane between clusters not directly linked by apical-apical bridges (Figs. 20 and 22; Table 9). The crystal structure of $Ta_6Br_{15}(TaBr_6)_{0.86}$ is also characterized by a second network made of $TaBr_6$ complexes, interpenetrated with that of the clusters via a [2/3, 1/3, 1/12] translation (Fig. 21). This leads to an increase of the intercluster $Ta_6\cdots Ta_6$ distances (Table 9) in relation with higher Ta-$Br^{a\text{-}a}$-Ta angles (141.3°) compared to the Nb-$Br^{a\text{-}a}$-Br angles (117.2°) encountered in $Nb_6Br_8F_7$. This increase of intercluster distances is more important between clusters located in the (*a*,*b*) plane and forming an hexagonal plane (+35%), compared to clusters directly linked to the central cluster and located above and below this hexagonal plane (+15%). While, the increase of intercluster distances in the (*a*,*b*) plane is directly related to the *a* parameter expansion (from $Nb_6Br_8F_7$ to $Ta_6Br_{15}(TaBr_6)_{0.86}$) via interpenetration of the two networks, that along the *c*-axis is in apparent contradiction with the *c* parameter contraction of 6% (Table 2). This reveals a large anisotropy of the electronic and halogen matrix effects between $(TaBr_6)^{n-}$ complexes and $[Ta_6Br_{15}]^{n+}$ cluster units in $Ta_6Br_{15}(TaBr_6)_{0.86}$. The former is predominant in the (*a*,*b*) plane and the latter along the *c*-axis.

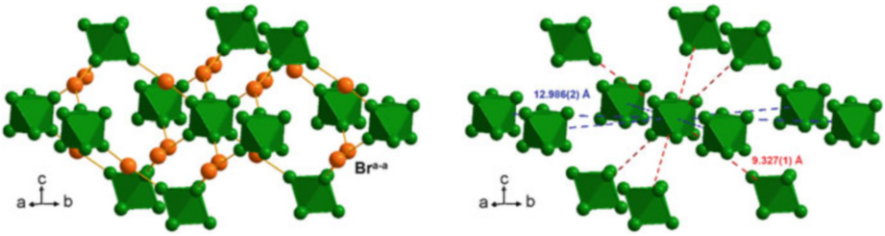

Fig. 22 Representation of the three-dimensional cluster framework (left) and intercluster $Ta_6 \cdots Ta_6$ distances (right) in $Ta_6Br_{15}(TaBr_6)_{0.86}$. Inner ligands are omitted for clarity. Distances are calculated from crystal data reported in [35]

Table 9 $M_6 \cdots M_6$ intercluster distances (Å) in $Nb_6Br_8F_7$ and $Ta_6Br_{15}(TaBr_6)_{0.86}$ compounds

Bridging type	$Nb_6Br_8F_7$[a]	$Ta_6Br_{15}(TaBr_6)_{0.86}$[b]
Direct (×6)	8.112(1)	9.327(1)
Indirect (×6)	9.637(1)	12.986(2)

Distances calculated from crystal data reported in: [a]Ref. [34], [b]Ref. [35]

5.4 *Cluster Compounds with Both Linear and Bent M-$X^{a\text{-}a}$-M Bridges*

The crystal structure of $InNb_6Cl_{15}$ was first reported by Womelsdorf et al. in 1997 to crystallize in the orthorhombic symmetry space group *Pmma* (No. 51) with unit cell parameters $a = 17.866(1)$ Å, $b = 13.4552(8)$ Å, and $c = 9.2934(8)$ Å [18]. Its crystal structure is based on two kinds of Nb_6Cl_{15} cluster units (named cluster A and cluster B) sharing apical ligands. Clusters A form zigzag chains along the *a*-axis through bent apical-apical $Cl^{a\text{-}a}$ bridges, and clusters B form linear chains along the *c*-axis through linear apical-apical $Cl^{a\text{-}a}$ bridges (Fig. 23). These chains, perpendicular to each other, are connected along the *b*-axis through bent apical-apical $Cl^{a\text{-}a}$ bridges. This leads to a three-dimensional cluster framework of structural formula $[Nb_6Cl^{i}{}_{12}Cl^{a\text{-}a}{}_{6/2}]$, which can be viewed as the interpenetration of two cluster networks formed by clusters A and B, respectively, linked to each other by bent apical-apical $Cl^{a\text{-}a}$ bridges along the *b*-axis. Indium atoms are located in tetrahedral cavities formed by two clusters A and two clusters B. The coordination polyhedron of indium atoms is then formed by eight inner chlorine ligands at distances between 3.229(2) and 3.400(2) Å and two apical chlorine ligands at distances of 3.301(1) and 3.430(1) Å, forming a distorted bicapped cubic geometry (Fig. 24). Monovalent indium cations counterbalance the charge of the $[Nb_6Cl_{15}]^-$ cluster units, which are characterized by a VEC of 16. Niobium atoms are located on five independent crystallographic sites (4*j* and 8*l* for cluster A; 2*e*, 2*e*, and 8*l* for cluster B), chlorine atoms on inner positions are on eight independent sites (4*h*, 4*j*, 8*l*, and 8*l* for cluster A; 4*i*, 4*k*, 8*l*, and 8*l* for cluster B), chlorine atoms on apical positions are on three independent sites (2*f* for cluster A; 2*e* for cluster B; 8*l* for chlorine atoms common to cluster A and B), and indium atoms are on one 4*k* site [18].

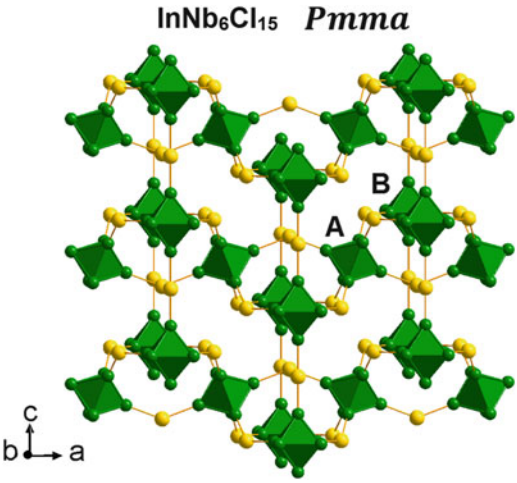

Fig. 23 Representation of the three-dimensional cluster framework encountered in $InNb_6Cl_{15}$. Inner ligands and indium atoms are omitted for clarity

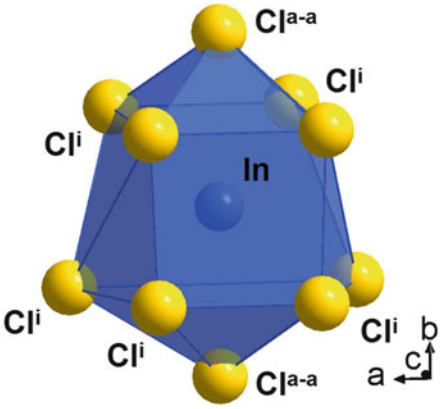

Fig. 24 Representation of the indium environment in $InNb_6Cl_{15}$

The crystal structure of isotypic $K_{0.77}Nb_6Cl_{15}$, $RbNb_6Cl_{15}$, and $CsNb_6Cl_{15}$ compounds was also studied by single-crystal X-ray diffraction [50], while that of $TlNb_6Cl_{15}$ was assigned from powder X-ray diffraction data [18]. However, in contrast to the crystal structure of $InNb_6Cl_{15}$ where the cationic 4*k* site is totally filled, that in $K_{0.77}Nb_6Cl_{15}$ is partially filled with a SOF of 0.768(5), while alkaline atoms in $RbNb_6Cl_{15}$ and $CsNb_6Cl_{15}$ are highly disordered with a statistically distribution on five and four crystallographic sites, respectively.

In $InNb_6Cl_{15}$-type structure compounds, the average Nb-Nb and Nb-Cl^i interatomic distances are equivalent for clusters A and B (Table 3), even if the cluster core is more distorted in the latter than in the former. On the contrary, the average Nb-$Cl^{a\text{-}a}$ interatomic distances are non-equivalent with a systematic higher value for cluster A compared to cluster B (Table 3). This is related to longer Nb-$Cl^{a\text{-}a}$ interatomic distances in the zigzag chains than those encountered in the linear chains.

In $InNb_6Cl_{15}$ short intercluster distances of 8.651(1), 8.933(1), and 9.293(1) Å are encountered between cluster A and cluster B along the *b*-axis through bent apical-apical Nb-$Cl^{a\text{-}a}$-Nb bridges (132.2°), between clusters A along the *a*-axis through bent apical-apical bridges (138.3°), and between clusters B along the *c*-axis through linear apical-apical bridges (180°), respectively (Fig. 25). Due to the interpenetration of the two cluster networks, short intercluster distances of 9.293(1) Å are also observed along the *c*-axis between clusters A, even if these clusters are not directly linked by apical-apical Nb-$Cl^{a\text{-}a}$-Nb bridges (Fig. 25). Finally, the cluster environments of both clusters B and A are completed by surrounded clusters B at intercluster distances of 9.452(1) and 10.176(1) Å, respectively (Fig. 25). The intercluster distances are influenced by the nature of the cation but do not modify the aforementioned description (Table 10). However, due to cation disordering or partial occupation of the cation site, it is not possible to determine the influence of the cation size on the intercluster distances and on the halogen matrix effect in the $InNb_6Cl_{15}$-type structure compounds.

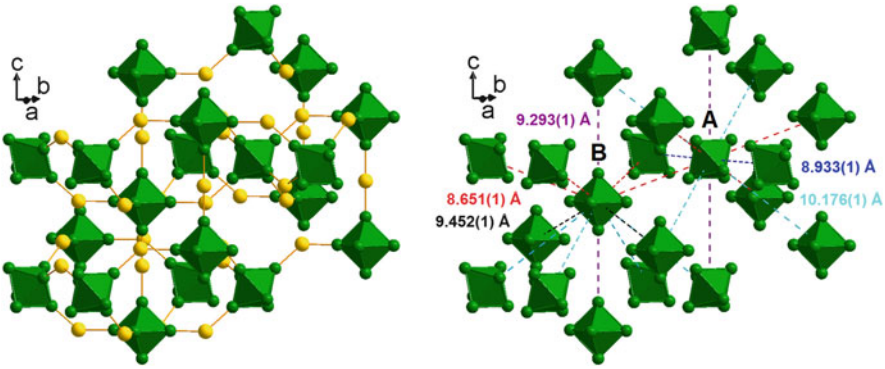

Fig. 25 Representation of the three-dimensional cluster framework (left) and intercluster $Nb_6\cdots Nb_6$ distances (right) in $InNb_6Cl_{15}$. Inner ligands and indium atoms are omitted for clarity. Distances are calculated from crystal data reported in [18]

Table 10 $Nb_6\cdots Nb_6$ intercluster distances (Å) in $InNb_6Cl_{15}$-type structure compounds

Bridging type	$InNb_6Cl_{15}$ [a]	$K_{0.77}Nb_6Cl_{15}$ [b]	$RbNb_6Cl_{15}$ [b]	$CsNb_6Cl_{15}$ [b]
Direct A-B (×4)	8.651(1)	8.634(1)	8.666(1)	8.708(1)
Direct A-A (×2)	8.933(1)	8.901(1)	8.917(1)	8.947(1)
Direct B-B (×2)	9.293(1)	9.255(1)	9.214(1)	9.244(2)
Indirect A-A (×2)	9.293(1)	9.255(1)	9.214(1)	9.244(2)
Indirect B-B (×2)	9.452(1)	9.396(1)	9.351(1)	9.350(1)
Indirect A-B (×4)	10.176(1)	10.119(1)	10.051(1)	10.046(1)

Distances calculated from crystal data reported in: [a]Ref. [18], [b]Ref. [50]

6 Interatomic Distances in Inorganic Nb_6 and Ta_6 Cluster Halide Compounds with Three-Dimensional Frameworks

6.1 Cluster Units Based on Face-Capped $M_6X^i_8X^a_6$ Building Blocks

First, among cluster units based on face-capped $M_6X^i_8X^a_6$ building blocks, those arising from $Mo_{5-x}Nb_{1+x}I_{11}$ compounds must be considered separately from the others. Indeed, these cluster units are generally characterized by a VEC of 24, leading to very short M-M ($\overline{d_{M-M}} = 2.695$ Å) and M-X^i ($\overline{d_{M-I^i}} = 2.785$ Å) interatomic distances compared to those encountered in cluster units characterized by a VEC of 19 or 20 (Table 3). On the opposite, the M-$X^{a\text{-}a}$ interatomic distances are similar to those found in the other iodides (Table 3), indicating that VEC value influences only the $[M_6X^i_8]$ cluster core.

Second, the structural transition from the HT to LT forms occurring in Nb_6I_{11} and derivative compounds with VEC of 19 (excluding $Nb_6I_{8.7}Br_{2.3}$ due to strong disorder on apical positions, especially Br^a, leading to Nb-Br^a distances ranging from 2.567 Å to 4.431 Å) does not influence drastically the interatomic distances: $\overline{d_{M-M}} = 2.846$ Å, $\overline{d_{M-X^i}} = 2.864$ Å, and $\overline{d_{M-X^{a-a}}} = 2.919$ Å for the HT form compounds and $\overline{d_{M-M}} = 2.850$ Å, $\overline{d_{M-X^i}} = 2.861$ Å, and $\overline{d_{M-X^{a-a}}} = 2.920$ Å for the LT form compounds (Table 3).

Finally, as already mentioned, hydrogen/deuterium atom insertion into Nb_6I_{11} leads to a weak increase of the Nb-Nb distances regardless of the structural form and a narrower distribution of them (Table 3).

6.2 Cluster Units Based on Edge-Bridged $M_6X^i_{12}X^a_6$ Building Blocks

In cluster units based on edge-bridged $M_6X^i_{12}X^a_6$ building blocks, it should be noted that the M-M interatomic distances are mainly influenced by the halogen matrix effect. This effect is particularly important when fluorine atoms occupy (partially or totally) the inner positions, leading to the shortest M-M distances, as exemplified by average M-M distances of 2.794–2.803 Å in Nb_6F_{15} or 2.815 Å in $Na_2Nb_6Br_4F_{11}(NbF_6)$, while in Ta_6Cl_{15} and Ta_6Br_{15}, the average M-M distances are 2.918–2.925 Å and 2.957 Å, respectively (Table 3).

In this family of compounds, the halogen matrix effect on M-X^i and M-$X^{a\text{-}a}$ interatomic distances is also predominant. This is highlighted by the linear evolutions of the average M-X^i (Fig. 26) and M-$X^{a\text{-}a}$ (Fig. 27) interatomic distances with the average X^i and X^a ionic radius, respectively. This leads to short M-X^i and M-$X^{a\text{-}a}$ distances of 2.049–2.059 Å and 2.113–2.118 Å, respectively, in Nb_6F_{15} to long M-X^i and M-$X^{a\text{-}a}$ distances of 2.764–2.795 Å and 3.105–3.110 Å, respectively, in Ta_6I_{14} (Table 3). It should be noted that the number of clusters (i.e., 2 or 3) shared by

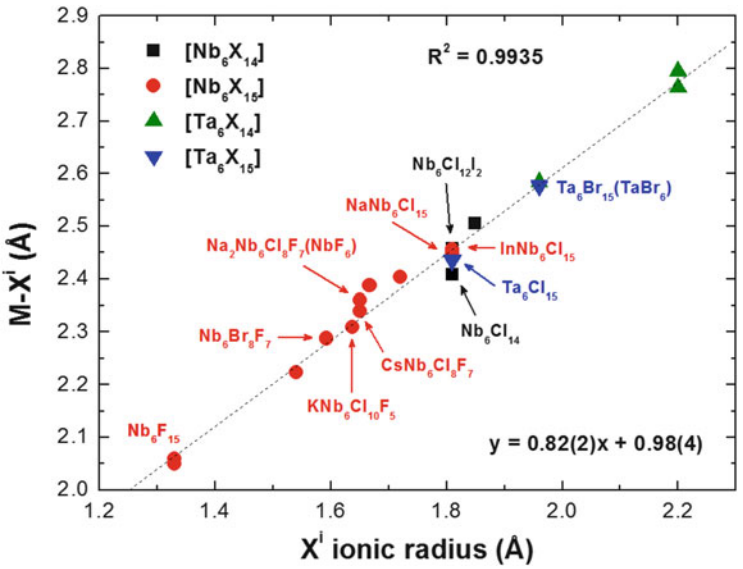

Fig. 26 Evolution of the average M-X^i interatomic distances vs. the average X^i ionic radius in cluster units based on edge-bridged $M_6X^i_{12}X^a_6$ building blocks

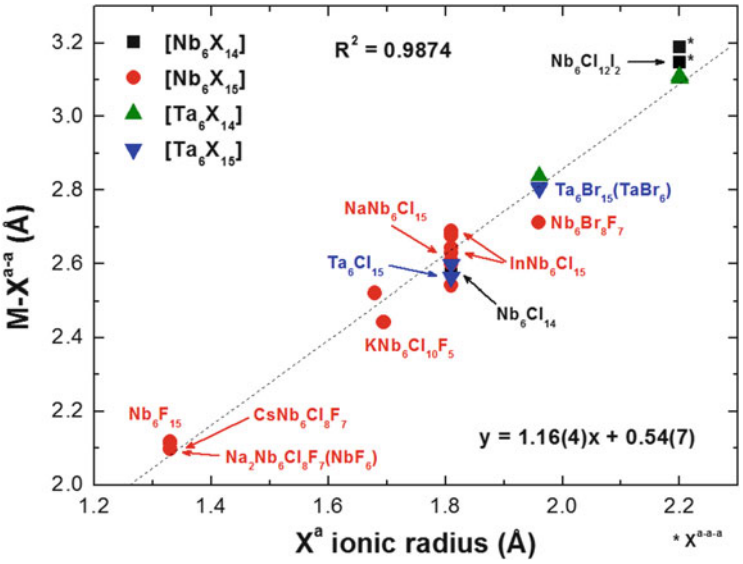

Fig. 27 Evolution of the average M-$X^{a\text{-}a}$ interatomic distances vs. the average X^a ionic radius in cluster units based on edge-bridged $M_6X^i_{12}X^a_6$ building blocks

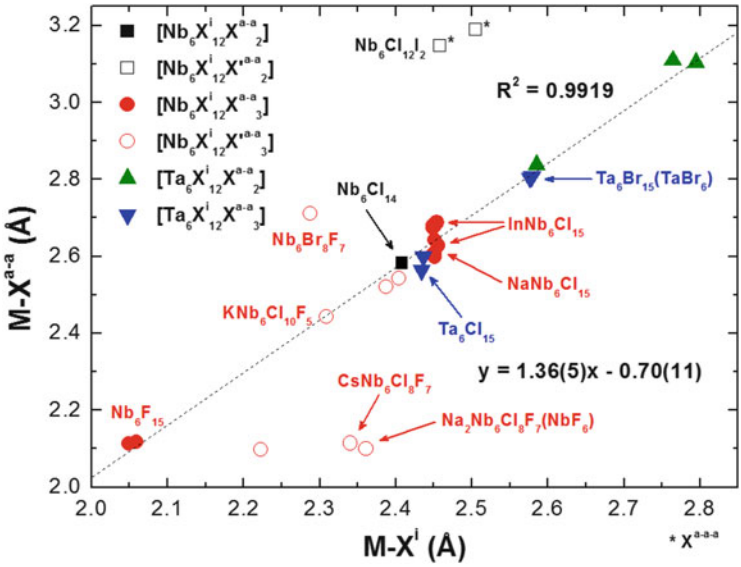

Fig. 28 Evolution of the average M-$X^{a\text{-}a}$ interatomic distances vs. the average M-X^{i} interatomic distances in cluster units based on edge-bridged $M_6X^{i}_{12}X^{a}_{6}$ building blocks

iodine atoms in apical position presents a weak influence on the M-$X^{a\text{-}a}$/M-$X^{a\text{-}a\text{-}a}$ distances (Fig. 27).

Due to the linear evolution of the average M-X^{i} and M-$X^{a\text{-}a}$ distances with the average X^{i} and X^{a} ionic radius, a linear evolution between average M-X^{i} and M-$X^{a\text{-}a}$ distances is also observed when both X^{i} and X^{a} correspond to the same halogen atoms (Fig. 28). On the contrary, for a different nature of inner and apical ligands, a deviation to this linear tendency is expected as exemplified with $Nb_6Br_8F_7$ for which inner and apical positions are occupied by fluorine/bromine and bromine atoms, respectively, or $CsNb_6Cl_8F_7$ for which inner and apical positions are occupied by fluorine/chlorine and fluorine atoms, respectively (Fig. 28).

7 Structural Relationships Between Crystal Structures Based on Hexagonal, Cubic, and Trigonal Symmetry

In Fig. 29 are represented the different cluster arrangements along threefold axes encountered in crystal structures of three-dimensional cluster frameworks with hexagonal (i.e., along the [001] direction), cubic (i.e., along the [111] direction), and trigonal (i.e., along the [001] direction) symmetries. One common structural feature encountered in these types of structures represented in Fig. 29 is that niobium/tantalum atoms are located on only one crystallographic site, which is not

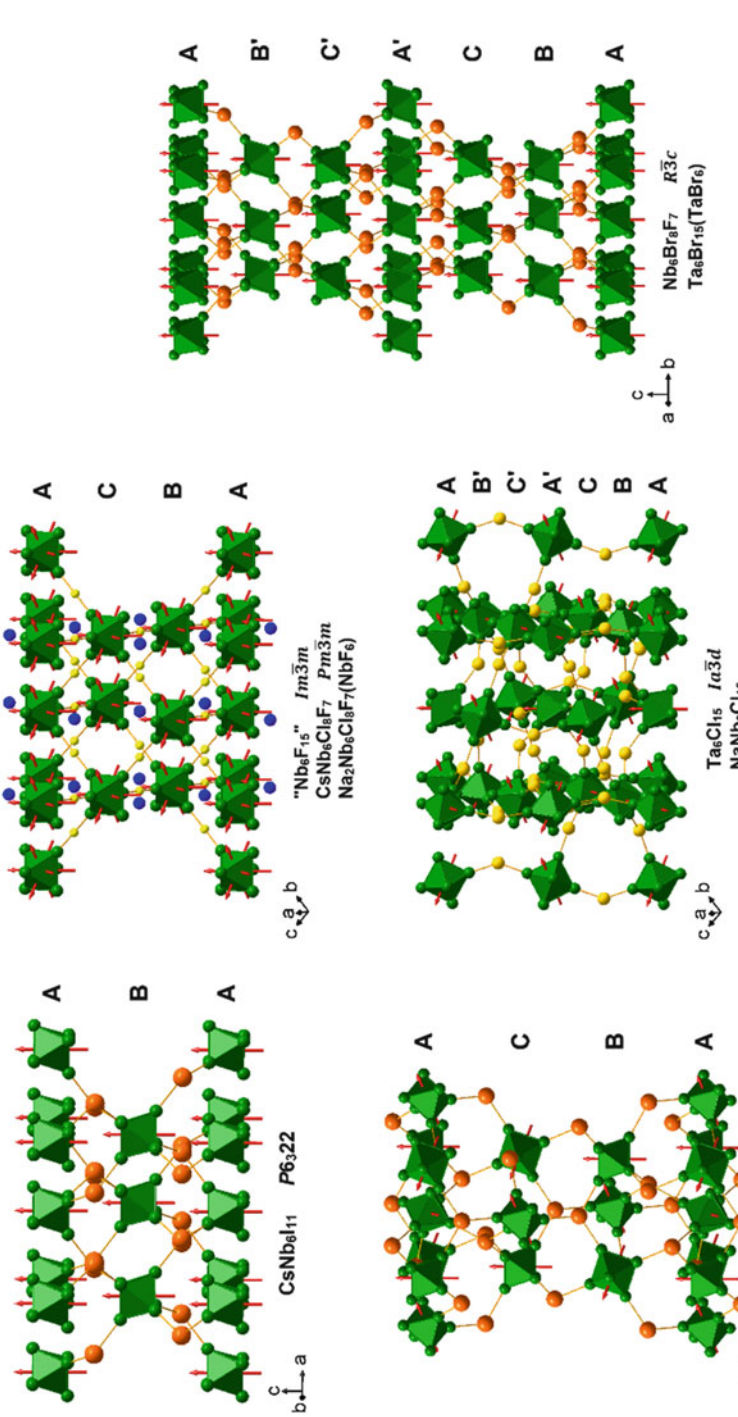

Fig. 29 Cluster arrangements along threefold axes encountered in crystal structures of three-dimensional cluster frameworks with hexagonal (i.e., along the [001] direction), cubic (i.e., along the [111] direction), and trigonal (i.e., along the [001] direction) symmetries. Threefold axes are represented by red arrows. Blue spheres represent either the centroid of the clusters arising from the second cluster framework in Nb_6F_{15} or the centroid of the cesium cations distribution/(NbF_6) complexes in $CsNb_6Cl_8F_7/Na_2Nb_6Cl_8F_7(NbF_6)$

the case for the other structure types discussed in this review. A second common structural feature is related to the fact that the clusters are located on threefold axes. This leads at least to six identical M-M interatomic distances, which are related to the cluster faces perpendicular to the threefold axes. This is also true for $CsNb_6I_{11}$ even if the crystal structure is non-centrosymmetric (Table 1).

These crystal structures can be described by the stacking of hexagonal layers of clusters, which are separated from another by layers of apical ligands (Fig. 29). Due to the existence of only one threefold axis direction in hexagonal and trigonal symmetry structures (i.e., along the [001] direction), the clusters arising from one layer are all oriented in the same direction. This is also the case for Nb_6F_{15}, $CsNb_6Cl_8F_7$, and $Na_2Nb_6Cl_8F_7(NbF_6)$-type structure compounds due to the fact that the centroid of the clusters is at the intersection of the threefold axes along the [111], [$\bar{1}$11], [1$\bar{1}$1], and [11$\bar{1}$] directions (Fig. 29). On the contrary, in the other cubic symmetry structure types (i.e., $Nb_6Cl_{12}I_2$, Ta_6Cl_{15}, $NaNb_6Cl_{15}$, and $KNb_6Cl_{10}F_5$), the clusters are located on only one threefold axis, leading to four different orientations of the clusters in the same layer (Fig. 29).

The crystal structure of $CsNb_6I_{11}$ is characterized by the stacking along the *c*-axis of two cluster layers, denoted A and B in Fig. 29, leading to a pseudo hexagonal close-packed arrangement of cluster units. The cluster layers are separated from another by bent apical-apical bridges. The clusters arising from layer A are related to clusters of layer B by a rotation of 180° induced by the sixfold screw axis 6_3.

The crystal structure of Nb_6F_{15} is characterized by the interpenetration of two cluster frameworks, each forming a pseudo cubic close-packed arrangement "A-B-C" of cluster units oriented in the same direction (Fig. 29), and related one to the other by a [½, ½, ½] translation (Fig. 14). The cluster layers arising from the same framework are separated by linear apical-apical bridges. The crystal structure of $CsNb_6Cl_8F_7$ and $Na_2Nb_6Cl_8F_7(NbF_6)$ is characterized by only one pseudo cubic close-packed arrangement "A-B-C" of cluster units, the second being replaced by cesium cations and (NbF_6) complexes, respectively. As in Nb_6F_{15}, the cluster layers arising from this arrangement are separated to the others by linear apical-apical bridges. For the sake of clarity, the crystal structure representation of these compounds, shown in Fig. 29, highlights only the cluster layer stacking common to the three types of structures, the blue spheres representing either the centroid of the clusters arising from the second framework or the centroid of the cesium cations distribution/(NbF_6) complexes. As in $CsNb_6Cl_8F_7$ and $Na_2Nb_6Cl_8F_7(NbF_6)$, the crystal structure of $Nb_6Cl_{12}I_2$ is also characterized by a pseudo cubic close-packed arrangement "A-B-C" of cluster units (Fig. 29). However in the latter structure, the clusters are oriented in four different directions, and the cluster layers are separated one to the others by bent apical-apical-apical bridges.

The crystal structures of $Nb_6Br_8F_7$ and $Ta_6Br_{15}(TaBr_6)$ are characterized by a cluster layer stacking "A-B-C-A′-C′-B′" along the *c*-axis, where the cluster layers are separated one to the others by bent apical-apical bridges similar to those encountered in $CsNb_6I_{11}$ (Fig. 29). The crystal structures of Ta_6Cl_{15}, $NaNb_6Cl_{15}$, and $KNb_6Cl_{10}F_5$ are also characterized by a cluster layer stacking "A-B-C-A′-C′-B′" but with a higher degree of interpenetration (Fig. 29). These structures can be viewed

as pseudo cubic derivatives close-packed arrangement of cluster units. However, in Ta_6Cl_{15}, $NaNb_6Cl_{15}$, and $KNb_6Cl_{10}F_5$, the cubic symmetry induces four different orientations of the clusters in the same layer, while in $Nb_6Br_8F_7$ and $Ta_6Br_{15}(TaBr_6)$, the clusters show the same orientation inside the layers. Moreover, in Ta_6Cl_{15}, $NaNb_6Cl_{15}$, and $KNb_6Cl_{10}F_5$ structures, bent apical-apical bridges are located between but also inside the cluster layers, leading to an enlargement and a shortening of the structure perpendicularly and in parallel to the stacking direction, respectively, compared to trigonal structures (Fig. 29).

8 Electronic Structure of Niobium and Tantalum Octahedral Cluster Halide Compounds

Face-capped and edge-bridged octahedral clusters, with the general formula $M_6X^i{}_8X^a{}_6$ and $M_6X^i{}_{12}X^a{}_6$, respectively (Fig. 1), are among the oldest prototypes of inorganic cluster chemistry [66]. Over the years, these octahedral clusters have been the subject of considerable theoretical studies carried out at different levels of theory (mostly extended Hückel (EH) and density functional theory (DFT)) [67–84]. Results converge overall to a bonding picture where the M-M bonding is based essentially on the interaction of metal *d* orbitals, a situation notably different from the bonding picture for most transition-metal carbonyl clusters [74, 85]. The bonding in both types of cluster has been described initially in terms of localized two-center or three-center bonds in $M_6X^i{}_8X^a{}_6$ and $M_6X^i{}_{12}X^a{}_6$, respectively [68]. In this description, five hybrid orbitals at each metal atom are directed toward the five ligands, which are arranged in a square-pyramidal fashion (Fig. 1). The remaining four hybrid orbitals per vertex point along the edges for $M_6X^i{}_{12}X^a{}_6$ and into the faces for $M_6X^i{}_8X^a{}_6$. Later on, a delocalized molecular orbital model has been developed providing additional insights into the structural and electronic properties of these clusters [67, 69, 70, 75]. Qualitative molecular orbital diagrams of face-capped and edge-bridged octahedral clusters $M_6X^i{}_8X^a{}_6$ and $M_6X^i{}_{12}X^a{}_6$ are shown in Fig. 30 to illustrate similarities and differences in their electronic structures [79]. In summary, the electronic structure of face-capped $M_6X^i{}_8X^a{}_6$ clusters shows 12 M-M bonding molecular orbitals (MOs) energetically separated from antibonding ones. That of edge-bridged $M_6X^i{}_{12}X^a{}_6$ clusters exhibits only 8 M-M bonding MOs. Consequently, full occupation of these M-M bonding MOs leads to stable VEC of 24 and 16 metal electrons for face-capped $M_6X^i{}_8X^a{}_6$ and edge-bridged $M_6X^i{}_{12}X^a{}_6$ clusters, respectively (Fig. 30). These two different "magic" numbers differ due to the different number and structural distribution of the X^i ligands. Indeed, when the ligands are face-capped, the metal electrons occupy the regions along the M-M bonds to avoid electron-electron repulsion. Similarly, when the ligands are edge-bridged, the metal electrons occupy the regions of metal triangle faces [79]. All theoretical calculations indicate that the highest occupied molecular orbitals (HOMO), e_g for $M_6X^i{}_8X^a{}_6$ and a_{2u} for $M_6X^i{}_{12}X^a{}_6$, are somewhat energetically separated from the other occupied

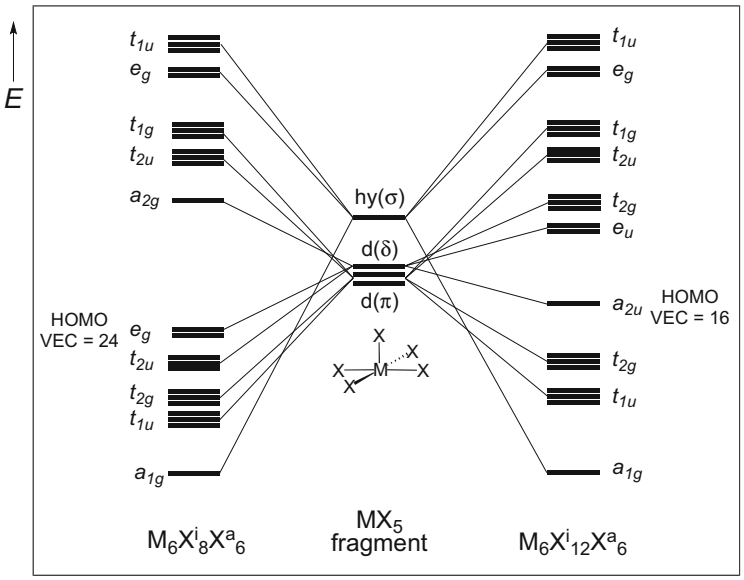

Fig. 30 Qualitative molecular orbital interaction diagrams for face-capped $M_6X^i_8X^a_6$ (left) and edge-bridged $M_6X^i_{12}X^a_6$ (right) octahedral clusters

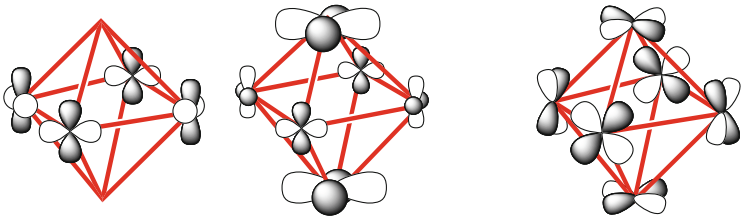

Fig. 31 Qualitative sketch of the e_g and a_{2u} HOMOs of 24-electron face-capped $M_6X^i_8X^a_6$ (left) and 16-electron edge-bridged $M_6X^i_{12}X^a_6$ (right) clusters, respectively

bonding MOs (Fig. 30). This is due to their peculiar nodal properties. In the former, the e_g orbitals are weakly M-M bonding, being of local δ symmetry with respect to an axis extending from M to the neighbor X^a atom as shown in Fig. 31 [73]. In the latter, the a_{2u} orbital is also of δ symmetry and consequently weakly M-M bonding (Fig. 31) and moreover is M-X^i antibonding [81]. This peculiar situation confers exceptional "redox" properties to these face-capped and edge-bridged octahedral clusters and related properties (paramagnetism, conductivity, superconductivity, optics, etc.), explaining the sustained interest in these compounds. A great advantage of the delocalized bonding picture described above is that it can equally well describe $M_6X^i_{12}X^a_6$ and $M_6X^i_8X^a_6$ clusters with variable VEC. For example, $KLuNb_6Cl_{18}$ has a VEC of 16 filling all the M-M bonding MOs of an edge-bridged octahedron, and the Nb-Nb bond lengths are 2.91–2.92 Å [12]. The existence of the

structurally related $LuNb_6Cl_{18}$ compound (VEC of 15) can be associated with the partial depopulation of the a_{2u} MO. The Nb-Nb bond lengths are 2.95–2.96 Å, confirming the weakly bonding nature of the HOMO, and the compound is paramagnetic [12], confirming that the HOMO is singly degenerate.

8.1 Variable VEC of Nb_6I_{11} and Derivatives

As just said, because of the weakly M-M bonding character of the e_g orbital in face-capped octahedral $M_6X^i{}_8X^a{}_6$ clusters, the VEC can rather easily be lowered from 24 to 20. This is the case of the "Chevrel phases" $PbMo_6S_8$, for instance [86], amply discussed in Chevrel-Phases: Genesis and Developments of this volume, which contain 22-electron $[Mo_6S^i{}_8]^{2-}$ motifs, rendering this compound superconductor [87]. Being largely encountered for group 6 and 7 transition elements, face-capped octahedral $M_6X^i{}_8X^a{}_6$ are observed with group 5 metals only for electron-deficient Nb_6I_{11} and derivatives (Tables 1, 2 and 3). With 20 electrons per motif $[Nb_6I^i{}_8I^a{}_3]^-$ in $CsNb_6I_{11}$ [9], the e_g orbital is fully depopulated. More puzzling is the drastically electron deficient 19-electron $[Nb_6I^i{}_8I^a{}_3]$ unit in the paramagnetic Nb_6I_{11} compound [28, 54]. Indeed, the low value of VEC = 19 is the reason for a reversible incorporation of a hydrogen atom into the cluster center.

8.2 Electronic Structure of Edge-Bridged $M_6X^i{}_{12}X^a{}_6$ Clusters

Examination of Tables 1, 2, and 3 indicates that the same relatively regular octahedral architectural unit is observed in all edge-bridged inorganic niobium and tantalum octahedral cluster halide compounds, regardless of the VEC which can vary from 14 to 16. There is, however, some significant lengthening of the M-M distances and some shortening of the M-X^a and M-X^i bond lengths, respectively, with the diminution of the electron count from 16 to 15 or 14. This is the case, for instance, for the structurally related 16-electron $KLuNb_6Cl_{18}$ and 15-electron $LuNb_6Cl_{18}$ compounds just mentioned above due to the partial depopulation of the a_{2u} HOMO in the latter [12].

It is clear that the conceptual ease of describing the structure of inorganic niobium and tantalum octahedral cluster halide compounds with the isolated "molecular" method of construction outlined above obscures the effect of intercluster contacts. As shown above, clusters can pack in different ways generating a plethora of zero- to three-dimensional solid-state structures (Table 1). We may wonder if the various features of intercluster connection and/or the variability in positioning and stoichiometry with regard to the intercalated counterions can influence the VEC of the $M_6X^i{}_{12}X^a{}_6$ motifs. It seems not much looking at Table 1 where most of $M_6X^i{}_{12}X^a{}_6$ clusters possess a VEC = 16, regardless of the dimensionality of the solid-state compounds. Indeed, because of the rather large separations between the $M_6X^i{}_{12}X^a{}_6$

motifs encountered in this kind of compound, it would be difficult to imagine that the energy bands in the solid-state structures, which can be thought of as consisting of a broadening version of the cluster MOs depicted in Fig. 30, would be so perturbed as to modify the electronic properties expected from the "isolated" clusters. This suspicion has not been directly confirmed for inorganic niobium and tantalum octahedral cluster halide compounds since no periodic theoretical calculations have been performed so far to the best of our knowledge. On the other hand, this has been confirmed using periodic EH-tight binding [88] and DFT [89] calculations for related octahedral niobium cluster-based solid-state oxyhalides such as $RbNb_6Cl_{12}O_2$ which contains 15-electron $[Nb_6Cl^i_{10}O^i_1Cl^a_2O^a_1]^-$ units and related compounds [36]. The electronic density of states (DOS) in these species shows narrow peaks that indicate weak intercluster three-dimensional interactions in the compound.

9 Summary

In this review we have surveyed the development of crystal and bonding chemistry of face-capped and edge-bridged inorganic niobium and tantalum octahedral cluster halide compounds, over a long period, from its origin to most recent work, with a particular emphasis on those showing three-dimensional cluster frameworks. Structure and bonding are intimately linked to the valence electron concentration, i.e., the number of electrons that held the octahedral architecture. Apart from Nb_6I_{11} and derivatives, which show electron-deficient face-capped $M_6X^i_8X^a_6$ units, compounds containing edge-bridged $M_6X^i_{12}X^a_6$ motifs are the most largely encountered. Closed-shell compounds with a valence electron concentration of 16 are predominant, although a few 15-electron open-shell magnetic compounds or even 14-electron closed-shell species have also been reported.

Particularly interesting from a structural point of view is the fashion in which these face-capped and edge-bridged clusters "pack" in crystals. The astonishing diversity of structural types, which are observed, is mainly due to the flexibility of the halogen ligands to coordinate in various manners to metal atoms. This is highlighted with the fact that fluorine ligands in apical positions favor the formation of linear bridges between building blocks, whereas they are bent for other halogens, or the predominant halogen matrix effect on $M\text{-}X^i$ and $M\text{-}X^{a\text{-}a}$ interatomic distances. Moreover, considering the ionic nature of the $M\text{-}X^a$ bonds compared to the $M\text{-}X^i$ ones, it turns out that all these structures can be described by the stacking of layers of $\{M_6X^i_{12}\}^{n+}$ or $\{M_6X^i_8\}^{n+}$ cluster cores separated by layers of apical ligands $\{X^a\}^-$. The nature of the clusters orientation arising from one layer influences the degree of ordering/disordering of the apical ligands in their corresponding layers. This is exemplified with hexagonal, trigonal, and cubic structures, where the localization of the cluster units on a threefold axis leads to one or four different orientations of the clusters in the same layer, inducing in the former case a higher degree of ordering of the apical ligands compared to the latter case. Finally, a rigorous structural analysis

of these compounds reveals no close relationship between the valence electron concentration and the variability of the intercluster connections and/or the nature of the counterions. Indeed, the main bonding features of these compounds can be understood from the delocalized bonding picture of isolated "molecular-like" $M_6X^i{}_8X^a{}_6$ or $M_6X^i{}_{12}X^a{}_6$ clusters.

References

1. Cordier S, Hernandez O, Thépot J-Y, Shames AI, Perrin C (2003). Inorg Chem 42:1101–1106
2. Simon A, von Schnering HG (1966). J Less-Common Met 11:31–46
3. Ben Yaich H, Jegaden J-C, Potel M, Sergent M, Rastogi AK, Tournier R (1984). J Less-Common Met 102:9–22
4. Habermehl K, Kleinke H, Meyer G (2010). Z Anorg Allg Chem 636:50–53
5. Cordier S, Gulo F, Roisnel T, Gautier R, Le Guennic B, Halet J-F, Perrin C (2003). Inorg Chem 42:8320–8327
6. Schäfer H, Schnering HG (1964). Angew Chem 76:833–868
7. Vajenine GV, Simon A (1999). Inorg Chem 38:3463–3473
8. Simon A, von Schnering HG, Schäfer H (1968). Z Anorg Allg Chem 361:235–248
9. Imoto H, Corbett JD (1980). Inorg Chem 19:1241–1245
10. Ihmaïne S, Perrin C, Sergent M (1986). C R Acad Sci Paris 303:1293–1298
11. Ihmaïne S, Perrin C, Sergent M (1987). Acta Cryst C 43:813–816
12. Ihmaïne S, Perrin C, Peña O, Sergent M (1988). J Less-Common Met 137:323–332
13. Ihmaïne S, Perrin C, Sergent M (1989). Acta Cryst C 45:705–707
14. Cordier S, Perrin C, Sergent M (1993). Z Anorg Allg Chem 619:621–627
15. Lachgar A, Meyer H-J (1994). J Solid State Chem 110:15–19
16. Sägebarth ME, Simon A, Imoto H, Weppner W, Kliche G (1995). Z Anorg Allg Chem 621:1589–1596
17. Baján B, Meyer H-J (1997). Z Anorg Allg Chem 623:791–795
18. Womelsdorf H, Meyer H-J, Lachgar A (1997). Z Anorg Allg Chem 623:908–912
19. Cordier S, Simon A (1999). Solid State Sci 1:199–209
20. Cordier S, Hernandez O, Perrin C (2001). J Fluor Chem 107:205–214
21. Cordier S, Hernandez O, Perrin C (2002). J Solid State Chem 163:319–324
22. Cordier S, Perrin C (2004). J Solid State Chem 177:1017–1022
23. Lemoine P, Wilmet M, Malaman B, Paofai S, Dumait N, Cordier S (2018). J Solid State Chem 257:72–79
24. Nguyen TKN, Renaud A, Wilmet M, Dumait N, Paofai S, Dierre B, Chen W, Ohashi N, Cordier S, Grasset F, Uchikoshi T (2017). J Mater Chem C 5:10477–10484
25. Renaud A, Wilmet M, Truong TG, Seze M, Lemoine P, Dumait N, Chen W, Saito N, Ohsawa T, Uchikoshi T, Ohashi N, Cordier S, Grasset F (2017). J Mater Chem C 5:8160–8168
26. Chen W, Wilmet M, Truong TG, Dumait N, Cordier S, Matsui Y, Hara T, Takei T, Saito N, Nguyen TKN, Ohsawa T, Ohashi N, Uchikoshi T, Grasset F (2018). Heliyon 4:e00654
27. Prokopuk N, Shriver DF (1998). Chem Mater 10:10–12
28. Simon A, von Schnering HG, Schäfer H (1967). Z Anorg Allg Chem 355:295–310
29. Imoto H, Simon A (1982). Inorg Chem 21:308–319
30. Simon A, Schnering HG, Wöhrle H, Schäfer H (1965). Z Anorg Allg Chem 339:155–170
31. Sägebarth M, Simon A (1990). Z Anorg Allg Chem 587:119–128
32. Schäfer H, Schnering HG, Niehues KJ, Nieder-Vahrenholz HG (1965). J Less-Common Met 9:95–104
33. Bauer D, von Schnering HG (1968). Z Anorg Allg Chem 361:259–276
34. Cordier S, Hernandez O, Perrin C (2001). J Solid State Chem 158:327–333

35. Habermehl K, Mudring A-V, Meyer G (2010). Eur J Inorg Chem:4075–4078
36. Demont A, Prestipino C, Hernandez O, Elkaïm E, Paofai S, Naumov N, Fontaine B, Gautier R, Cordier S (2013). Chem Eur J 19:12711–12719
37. Sperlich E, König J, Weiß DH, Schröder F, Köckerling M (2019). Z Anorg Allg Chem 645:233–241
38. Yoshiasa A, Borrmann H, Simon A (1994). Z Anorg Allg Chem 620:1329–1338
39. Simon A, Stollmaier F, Gregson D, Fuess H (1987). J Chem Soc Dalton Trans:431–434
40. Simon A (1967). Z Anorg Allg Chem 355:311–322
41. Artemkina SB, Naumov NG, Virovets AV, Fedorov VE (2013). Russ J Coord Chem 39:1–5
42. Fitch AN, Barrett SA, Fender BEF, Simon A (1984). J Chem Soc Dalton Trans:501–505
43. Baján B, Meyer H-J (1995). Z Kristallogr 210:607
44. Bauer D, Schnering HG, Schäfer H (1965). J Less-Common Met 8:388–401
45. Artelt HM, Meyer G (1993). Z Kristallogr 206:306–307
46. Knoll R, Sokolovski J, BenHaim Y, Shames AI, Goren SD, Shaked H, Thépot JY, Perrin C, Cordier S (2006). Physica B 381:47–52
47. von Schnering HG, Vu D, Jin SL, Peters K (1999). Z Kristallogr NCS 214:15–16
48. Le Polles L, Cordier S, Perrin C, Sergent M (1999). C R Acad Sci Paris Ser II c 2:661–667
49. Baján B, Balzer G, Meyer H-J (1997). Z Anorg Allg Chem 623:1723–1728
50. Nägele A, Day C, Lachgar A, Meyer H-J (2001). Z Naturforsch B 56:1238–1240
51. Schäfer H, von Schnering HG, Simon A, Giegling D, Bauer D, Siepmann R, Spreckelmeyer B (1966). J Less-Common Met 10:154–155
52. Bateman LR, Blount JF, Dahl LF (1966). J Am Chem Soc 88:1082–1084
53. Finley JJ, Nohl H, Vogel EE, Imoto H, Camley RE, Zevin V, Andersen OK, Simon A (1981). Phys Rev Lett 46:1472–1475
54. Finley JJ, Camley RE, Vogel EE, Zevin V, Gmelin E (1981). Phys Rev B 24:1323–1332
55. Brown PJ, Ziebeck KRA, Simon A, Sägebarth M (1988). J Chem Soc Dalton Trans:111–115
56. Geyer-Lippmann J, Simon A, Stollmaier F (1984). Z Anorg Allg Chem 516:55–66
57. Fritsche H-G, Dübler F, Müller H (1984). Z Anorg Allg Chem 513:46–56
58. Kuhn PJ, McCarley RE (1965). Inorg Chem 4:1482–1486
59. von Barner JH, McCurry LE, Jørgensen CA, Bjerrum NJ, Mamantov G (1992). Inorg Chem 31:1034–1039
60. Converse JG, McCarley RE (1970). Inorg Chem 9:1361–1366
61. MacFarlane WA, Schick-Martin D, Egilmez M, Fan I, Song Q, Chow KH, Cordier S, Perrin C, Goren SD (2009). Physica B 404:622–625
62. Knoll R, Shames A, Goren SD, Shaked H, Cordier S, Perrin C, Hernandez O, Roisnel T, André G, Kremer RK, Simon A (2013). Appl Magn Reson 44:143–151
63. Köhler J, Simon A, Whangbo M-H (2009). Z Anorg Allg Chem 635:2396–2398
64. Bauer D, Schäfer H (1968). J Less-Common Met 14:476
65. Kuhn A, Dill S, Meyer H-J (2005). Z Anorg Allg Chem 631:1565–1567
66. Pauling L (1960) The nature of the chemical bond, 3rd edn. Cornell University Press, Ithaca
67. Cotton FA, Haas RE (1964). Inorg Chem 3:10–17
68. Kettle SFA (1965). Theor Chim Acta 3:211–212
69. Guggenberger LJ, Sleight AW (1969). Inorg Chem 8:2041–2049
70. Bursten BE, Cotton FA, Stanley GG (1980). Isr J Chem 19:132–142
71. Le Beuze A, Makhyoun MA, Lissillour R, Chermette H (1982). J Chem Phys 76:6060–6066
72. Certain D, Le Beuze A, Lissillour R (1983). J Solid State Comm 46:7–10
73. Hughbanks T, Hoffmann R (1983). J Am Chem Soc 105:1150–1162
74. Woolley RG (1985). Inorg Chem 24:3519–3525
75. Johnston RL, Mingos DMP (1986). Inorg Chem 25:1661–1671
76. Mingos DMP, Johnston RL (1987). Struct Bond 68:29–87
77. Mingos DMP, Lin Z (1989). Z Phys D 12:53–59
78. Hughbanks T (1989). Prog Solid State Chem 19:329–372
79. Lin Z, Williams ID (1996). Polyhedron 15:3277–3287

80. Kaltsoyannis N (1997). J Chem Soc Dalton Trans:1–11
81. Ogliaro F, Cordier S, Halet J-F, Perrin C, Saillard J-Y, Sergent M (1998). Inorg Chem 37:6199–6207
82. Ramirez-Tagle R, Arratia-Pérez R (2008). Chem Phys Lett 460:438–441
83. Schott E, Zarate X, Arratia-Pérez R (2012). Polyhedron 36:127–132
84. Kuc A, Heine T, Mineva T (2012). Struct Chem 23:1357–1367
85. Mingos DMP, Wales D (1990) Introduction to cluster chemistry. Prentice-Hall, Englewood Cliffs
86. Chevrel R, Sergent M, Prigent J (1971). J Solid State Chem 3:515–519
87. Matthias BT, Marezio M, Corenzwit E, Cooper AS, Barz HE (1972). Science 175:1465–1466
88. Anokhina EV, Day CS, Meyer H-J, Ströbele M, Kauzlarich SM, Kim H, Whangbo M-H, Lachgar A (2002). J Alloys Compd 338:218–228
89. Fontaine B, Cordier S, Gautier R, Gulo F, Halet J-F, Perić B, Perrin C (2011). New J Chem 35:2245–2252

Index